

## **General Disclaimer**

### **One or more of the Following Statements may affect this Document**

- This document has been reproduced from the best copy furnished by the organizational source. It is being released in the interest of making available as much information as possible.
- This document may contain data, which exceeds the sheet parameters. It was furnished in this condition by the organizational source and is the best copy available.
- This document may contain tone-on-tone or color graphs, charts and/or pictures, which have been reproduced in black and white.
- This document is paginated as submitted by the original source.
- Portions of this document are not fully legible due to the historical nature of some of the material. However, it is the best reproduction available from the original submission.

**NASA CONTRACTOR REPORT 166382**

(NASA-CR-166382) VARIABLE CAMBER ROTOR  
STUDY (Boeing Vertol Co., Philadelphia, Pa.)  
227 p HC A11/MF A01 CSCL 01C

N83-19740

Unclas

G3/05 09174

**Variable Camber Rotor Study**

L. Dadone ✓  
J. Cowan  
F. J. McHugh



**CONTRACT NAS2-10768**  
August 1982

**NASA**

Variable Camber Rotor Study

L. Dadone  
J. Cowan  
F. J. McHugh  
Boeing Vertol Company  
Philadelphia, Pennsylvania

Prepared for  
Ames Research Center  
under Contract NAS2-10768



National Aeronautics and  
Space Administration

**Ames Research Center**  
Moffett Field, California 94035

## TABLE OF CONTENTS

	<u>Page</u>
List of Figures	iv
List of Tables	x
List of Symbols	xi
1.0 Summary	1
2.0 Introduction	7
3.0 Review of Variable Camber Concepts	15
4.0 Variable Camber Modification of Rotor Performance and Loads Analysis Codes	31
5.0 Definition of the Sectional Characteristics of Variable Camber Airfoils	39
6.0 Performance Characteristics of Variable Camber Rotors - Potential Benefits	82
7.0 Mechanical Feasibility	98
8.0 Conclusions and Recommendations	111
9.0 References	128
10.0 Appendices	
(a) Coordinates of the A-1 Airfoil with 35% and 50% Plain T.E. Flaps	
(b) Sectional Characteristics of the A-1 Airfoil with a 35% Plain Flap	
(c) Identification of B-53 Input Variables	

LIST OF FIGURES

<u>Figure No.</u>		<u>Page</u>
(1)	Rotor Environment in Forward Flight	9
(2)	Lift Coefficient and Mach Number Requirements	10
(3)	Comparison of Helicopter Rotor Airfoils	12
(4)	Regions of Variable Camber Deployment in Forward Flight	14
(5)	Effect of Sectional Pitching Moments on Blade Loads	17
(6)	Compressibility Effects on Drag and Pitching Moment Characteristics of Several Helicopter Rotor Sections	18
(7)	Variable Camber Concepts Considered for the A-1 Airfoil	22
(8)	Baseline A-1 Airfoil. Pressure Distribution at $M = 0.4$ , $\alpha = 4^\circ$	23
(9)	A-1 Airfoil, Mod. 1. Overall Camber Change by Upper Surface Modification. Pressure Distribution at $M = 0.4$ , $\alpha = 4^\circ$	24
(10)	A-1 Airfoil, Mod. 2. Trailing Edge Camber Change by Upper Surface Displacement. Pressure Distribution at $M = 0.4$ , $\alpha = 4^\circ$	25
(11)	A-1 Airfoil, Mod. 3. Leading Edge Camber Change by Localized Lower Surface Deflection. Pressure Distribution at $M = 0.4$ , $\alpha = 4^\circ$	26
(12)	A-1 Airfoil, Mod. 4. Leading Edge Camber Variation by Lower Surface Change Distributed over about 1/3 Chord. Pressure Distribution at $M = 0.4$ , $\alpha = 4^\circ$	27
(13)	A-1 Airfoil, Mod. 5. Camber Variation by Increasing Mean-Line Curvature at the Trailing Edge (Rear Loading). Pressure Distribution at $M = 0.4$ , $\alpha = 4^\circ$	28
(14)	A-1 Airfoil, Mod. 6. 35% Plain Trailing Edge Flap Deflected $5.0^\circ$ . Pressure Distribution at $M = 0.4$ , $\alpha = 4^\circ$	29

<u>Figure No.</u>		<u>Page</u>
(15)	A-1 Airfoil, Mod. 7. 50% Plain Trailing Edge Flap, Deflected $5.0^\circ$ . Pressure Distribution at $M = 0.4$ , $\alpha = 4^\circ$	30
(16)	Wake Model in the B-65/B-53 Rotor Performance Analysis	32
(17)	Lift Coefficient Table for the A-1 Airfoil	34
(18)	Drag Coefficient Table for the A-1 Airfoil	35
(19)	Quarter Chord Pitching Moment Coefficient Table for the A-1 Airfoil	36
(20)	High Angle of Attack Data	37
(21)	A-1 Airfoil Contour	42
(22)	Comparison of Measured and Calculated Pitching Moments for the A-1 Airfoil	44
(23)	Evaluation of Maximum Lift Levels from Airfoil Analysis Results	46
(24)	Test/Theory Correlation of Lift and Moment Data for the VR-7 Airfoil	47
(25)	Definition of Suction Loop	50
(26)	Example of Drag Divergence Boundaries	51
(27)	A-1 Airfoil with a 0.35c Plain T.E. Flap	53
(28)	Estimated Maximum Lift Boundaries for the A-1 Airfoil with a 0.35c Plain T.E. Flap	55
(29)	Lift Curve Slope of the A-1 Airfoil with a 0.35c Plain T.E. Flap	57
(30)	Angle of Zero Lift for the A-1 Airfoil with a 0.35c Plain T.E. Flap	58
(31)	Maximum Positive and Negative Lift Boundaries for the A-1 Airfoil with a 0.35c Plain T.E. Flap $\delta_{\text{Flap}} = -5.0^\circ$	59
(32)	Maximum Positive and Negative Lift Boundaries for the A-1 Airfoil with a 0.35c Plain T.E. Flap. $\delta_{\text{Flap}} = 0.0^\circ$	60

<u>Figure No.</u>		<u>Page</u>
(33)	Maximum Positive and Negative Lift Boundaries for the A-1 Airfoil with a 0.35c Plain T.E. Flap. $\delta_{\text{Flap}} = 5.0^\circ$	61
(34)	Maximum Positive and Negative Lift Boundaries for the A-1 Airfoil with a 0.35c Plain T.E. Flap. $\delta_{\text{Flap}} = 10.0^\circ$	62
(35)	Maximum Positive and Negative Lift Boundaries for the A-1 Airfoil with a 0.35c Plain T.E. Flap. $\delta_{\text{Flap}} = 15.0^\circ$	63
(36)	Definition of Drag Tables	64
(37)	Effect of Compressibility on the Pitching Moment about the Aerodynamic Center as Estimated for the A-1 Airfoil with a 0.35c T.E. Flap	65
(38)	Lift/Drag Polars of the A-1 Airfoil with a 0.35c T.E. Flap as Approximated by the Air- foil Tables. $M=0.3$	67
(39)	Lift/Drag Polars of the A-1 Airfoil with a 0.35c T.E. Flap as Approximated by the Air- foil Tables. $M=0.4$	68
(40)	Lift/Drag Polars of the A-1 Airfoil with a 0.35c T.E. Flap as Approximated by the Air- foil Tables. $M=0.5$	69
(41)	Lift/Drag Polars of the A-1 Airfoil with a 0.35c T.E. Flap as Approximated by the Air- foil Tables. $M=0.6$	70
(42)	Lift/Drag Polars of the A-1 Airfoil with a 0.35c T.E. Flap as Approximated by the Air- foil Tables. $M=0.7$	71
(43)	Lift/Drag Polars of the A-1 Airfoil with a 0.35c T.E. Flap as Approximated by the Air- foil Tables. $M=0.8$	72
(44)	A-1 Airfoil with a 0.50c Plain T.E. Flap	74
(45)	Estimated Maximum Lift Boundaries of the A-1 Airfoil with a 0.50c Plain T.E. Flap	75
(46)	Lift Curve Slope of the A-1 Airfoil with a 0.50c Plain T.E. Flap	76

<u>Figure No.</u>		<u>Page</u>
(47)	Angle of Zero Lift of the A-1 Airfoil with a 0.50c Plain T.E. Flap	77
(48)	Maximum Positive and Negative Lift Boundaries for the A-1 Airfoil with a 0.50c Plain T.E. Flap. $\delta_{\text{Flap}} = -5.0^\circ$	78
(49)	Maximum Positive and Negative Lift Boundaries for the A-1 Airfoil with a 0.50c Plain T.E. Flap. $\delta_{\text{Flap}} = -5.0^\circ$	79
(50)	Maximum Positive and Negative Lift Boundaries for the A-1 Airfoil with a 0.50c Plain T.E. Flap. $\delta_{\text{Flap}} = 10.0^\circ$	80
(51)	Effect of Compressibility on the Pitching Moment Coefficients of the A-1 Airfoil with a 0.50c T.E. Flap	81
(52)	Lift Coefficient Variation with Radius and Azimuth for $C_T/\sigma = 0.10$ , $\mu = 0.39$ , $\delta_f = 0$	89
(53)	Comparison of Schedule A16 and Baseline. $C_T/\sigma = 0.06$ , $\mu = 0.39$ , $\bar{x} = 0.048$ (a) Flap Deflection Angle, (b) Horsepower	97
(54)	Blade Tip Twist - Schedule E and Baseline. $C_T/\sigma = 0.06$ , $\mu = 0.39$ , $\bar{x} = 0.048$	99
(55)	Blade Tip Twist - Schedule A1 and Baseline. $C_T/\sigma = 0.09$ , $\mu = 0.5$ , $\bar{x} = 0.046$	100
(56)	Rotor Instantaneous Power Variation - Schedule A1 and Baseline. $C_T/\sigma = 0.09$ , $\mu = 0.5$ , $\bar{x} = 0.046$	101
(57)	Variable Camber Blade, 3-Segment Schedule Characteristics.	103
(58)	Flap Deflection Achieved by Means of Flex- ible Skins at the Flap Hinge.	104
(59)	Example of Dynamic Pressure Environment in Forward Flight.	105
(60)	Example of Local Mach Number Environment in Forward Flight.	106
(61)	Flap Normal Force at the Flap Hinge.	107

<u>Figure No.</u>		<u>Page</u>
(62)	3-Segment Variable Camber Flap Deflection Scheduling.	108
(63)	3-Segment Variable Camber Hinge Moment Loading.	109
(64)	Radial Variation of Hinge Moments for the A-1 Airfoil with a 50% Flap.	110
(65)	3-Segment Variable Camber Mechanical Actuation Systems.	112
(66)	Variable Camber Hydraulic Actuation Systems.	113
(67)	Variable Camber Pneumatic Actuation Systems.	114
(68)	Variable Camber Electric Actuation Systems.	115
(69)	Examples of Variable Camber Deployment.	116
(70)	Flap Deployment Involving Flexible Skins at the Flap Hinge.	117
(71)	Rigid Flap Hinge Arrangement.	118
(72)	Example of Pressure Distributions for a Flap Configuration Utilizing Flexible Skins.	119
(73)	Example of Pressure Distributions for a Flap Configuration Utilizing a Hinge Connecting Rigid Skins.	120
(74)	Rigid versus Flexible Flap Hinge. Comparison of Lift Characteristics.	121
(75)	Rigid versus Flexible Flap Hinge. Comparison of Maximum Local Mach Number Boundaries.	122
(76)	Rigid versus Flexible Flap Hinge. Comparison of Lift/Drag Polars.	123
(77)	Rigid versus Flexible Flap Hinge. Comparison of Pitching Moments.	124

<u>Figure No.</u>		<u>Page</u>
(78)	Rigid versus Flexible Flap Hinge. Comparison of Separation Boundaries.	125
(79)	Approximate Weights of Variable Camber Hardware (28 Ft. Radius Rotor).	126

LIST OF TABLES

<u>Table No.</u>		<u>Page</u>
I	Summary of Variable Camber Configurations	20
II	Coordinates of the A-1 Airfoil	41
III	Estimated Positive Maximum Lift Characteristics of the A-1 Airfoil with a 0.35c Plain T.E. Flap	54
IV	Estimated Negative Maximum Lift Characteristics of the A-1 Airfoil with a 0.35c Plain T.E. Flap	54
V	Estimated Lift Curve Slope Variation with Mach Number for the A-1 Airfoil with a 0.35c Plain T.E. Flap	56
VI	Estimated Effect of Compressibility on the Angle for Zero Lift of the A-1 Airfoil with a 0.35c Plain T.E. Flap	56
VII	Sinusoidal Flap Deployment Schedules	84
VIII	Non-Sinusoidal Flap Deployment Schedules	85
IX	Flight Conditions and Results of B-53 Analyses	93
X	Flight Condition Summary	96

LIST OF SYMBOLS

a	Lift curve slope, Rad $^{-1}$
A	Rotor disc area, $m^2$
b	Number of blades
c	Blade or airfoil chord, m
$C_d$	Blade element drag coefficient, drag/qc
$C_f$	Blade element skin friction coefficient, drag/qc
$C_l$	Blade element lift coefficient, Lift/qc
$C_m$	Blade element pitching moment coefficient about the quarter chord, $\frac{\text{Moment}}{qc^2}$
$C_n$	Blade element normal force coefficient, $\frac{\text{Normal Force}}{qc}$
$C_p$	Pressure coefficient, $(P-P_\infty)/1/2 PV_\infty^2$
$C_T/\sigma$	Rotor thrust coefficient, $T/\sigma\rho AV_T^2$
$C_T'/\sigma$	Rotor lift coefficient, $L/\sigma\rho AV_T^2$
D	Rotor diameter, m
k	Reduced frequency parameter, $\frac{c\Omega}{2V}$
M	Mach Number
P	Rotor power, HP
p	Measured pressure, static when no subscripts are used
q	Dynamic pressure, $1/2\rho V^2$
r	Blade radial station, m
R	Blade radius, m

LIST OF SYMBOLS (Continued)

$R_n$	Reynolds Number based on chord, $\rho V_c/\mu$
$U_p$	Total of velocity components perpendicular to rotor disc plane at a blade station, m/s
$U_t$	Total of Velocity Components in the Plane of the Rotor Disc at a Blade Station, m/s
$V$	Free Stream Velocity m/s
$V_t$	Rotor Tip Speed, m/s
$x$	Blade Element Chordwise Location Measured from Leading Edge, m
$X$	Rotor Propulsive Force
$\bar{X}$	Rotor Propulsive Force Coefficient, $X/qd^2\sigma$
$y$	Blade Element Surface Location Measured Perpendicular to Chord Line, m
$\mu$	Advance Ratio, $V/V_T$
$\alpha$	Blade Element Angle of Attack, Degrees
$\alpha_s$	Rotor Shaft, Angle, Degrees
$\alpha_{TPP}$	Rotor Tip Path Angle $\alpha_s - \beta_{ic}$ , Degrees
$\beta$	Blade Flapping Angle, Degrees
$\beta_{ic}$	Cosine Component of Blade Flapping Angle, Degrees
$\beta_{is}$	Sine Component of Blade Flapping Angle, Degrees
$\delta_F$	Flap Deflection, Degrees
$\delta_o$	Steady Component of Flap Deflection, Degrees
$\delta_{nc}$	$\cos n\psi$ Component of Flap Deflection, Degrees
$\delta_{ns}$	$\sin n\psi$ Component of Flap Deflection, Degrees

LIST OF SYMBOLS (Continued)

$\theta_0$	Blade Collective Pitch at Centerline of Rotation, Degrees
$\theta_{.75R}$	Blade Collective Pitch at 75 Percent Radius, Degrees
$\lambda$	Rotor Inflow Ratio, Degrees
$\rho$	Density of Air, kg/m <sup>3</sup> (Slugs/ft <sup>3</sup> )
$\sigma$	Rotor Solidity, $\frac{bc}{\pi R}$
$\nu$	Kinematic Viscosity, m <sup>2</sup> /sec (ft <sup>2</sup> /sec)
$\psi$	Blade azimuth angle, Degrees
$\Omega$	Rotor speed, Rad/s

Subscripts

ac	aerodynamic center
c/4	for quantities referenced to the quarter chord
c, comp	compressible
c	camber or mean-line
i	"ideal" or design value
inc	incompressible
$\ell$	lower surface, in identification of airfoil coordinates
$\ell$	Local, in reference to flow conditions
L.E.	leading edge
max	maximum value
min	minimum value
o	zero lift condition
sep	separation (flow separation)

LIST OF SYMBOLS (Continued)

t	total
t	thickness distribution
tab	trailing edge tab
T.E.	trailing edge
u	upper surface, in identification of airfoil coordinates
$\infty$	freestream condition

Abbreviations

BSWT	Boeing Supersonic Wind Tunnel
BTWT	Boeing Transonic Wind Tunnel
c.g.	center of gravity

## 1.0 Summary

The potential for the deployment of variable camber concepts on helicopter rotors has been assessed by means of analysis. It was determined that variable camber extended the operating range of helicopters provided that the correct compromise can be obtained between performance/loads gains and mechanical complexity.

As part of this study, a number of variable camber concepts were reviewed on a two-dimensional basis to determine the usefulness of L.E., T.E. and overall camber variation schemes. It was decided that the most powerful method to vary camber was through plain T.E. flaps undergoing relatively small motions ( $-5^\circ$  to  $+15^\circ$ ). The aerodynamic characteristics of the NASA/Ames A-1 airfoil with 35% and 50% plain T.E. flaps were determined by means of current subcritical and transonic airfoil design methods and assembled in airfoil tables directly usable by rotor performance and loads analysis codes.

In order to evaluate the potential benefits to be derived, from variable camber, the B-65 forward flight analysis and C-60 loads analysis were modified to allow the interpolation of the lift, drag and pitching moment characteristics of up to five variable camber levels. The modified codes have been assigned the identification names of B-53 and C-84 respectively.

The present study was limited to variable camber applications outside of the reverse flow circle. Although the deployment of variable camber inside the reverse flow region might offer some benefits, these benefits would be offset by the requirement for relatively large flap deflections and by the significant degree of uncertainty in the evaluation of the reverse flow characteristics.

The definition of variable camber schedules which would result in an improvement in rotor efficiency was unexpectedly difficult. As performance improvement was the primary objective of the current investigation, all efforts were directed to the review of means to improve aerodynamic efficiency, although the mechanical feasibility of rotor blades employing flaps was addressed on a preliminary basis.

The most promising concept reviewed within this study is a configuration with a 35% plain flap to be deployed in an on/off mode near the tip of a blade. The location and extent of these segments has not been optimized as a function of high speed and maximum thrust requirements. Preliminary results show approximately 11% reduction in power is possible at 99 m/s (192 knots,  $\mu = 0.50$ ) and a rotor thrust coefficient ( $C_T/\sigma$ ) of 0.09, as indicated in Figure A. The reduction in rotor power is less than 3% at a  $C_T/\sigma$  of 0.06 and 99 m/s. A sensitivity to forward speed is also illustrated in Figure A.

At 77 m/s ( $m=0.39$ ) there is no reduction in power. The deployment schedule utilized is illustrated in Figure B and provides the greatest power reduction of the schedules examined. Flap deflections of  $-1.43$  degrees to  $-2.62$  degrees were used on a limited portion of the advancing blade. An examination of the rotor characteristics at the 99 m/s operating condition was made to determine the reason for the reduction in power. The azimuthal variation in the power required by an individual blade was determined. Figure C shows a power reduction in the first quadrant, the last half of the second quadrant, and the third quadrant. The largest power saving is in the region where the flaps were deflected. Deflecting the flaps produces a significant change in nose-up section pitching moment and an increase in section drag which should increase power. A nose-up pitching moment causes the blade to unwind, reduce the geometric twist, and have a more positive sectional angle of attack. The elastic twist variation around the azimuth is presented in Figure D and indicates that a large nose-up change in twist occurs in the region where the flaps are deflected. There is a slight decrease in elastic twist in the beginning of the first quadrant, and a big decrease in the first half of the second quadrant.

The 11% reduction in rotor power required, defined in this study, is a result of operating at a lower drag level on the advancing side of the rotor disc. For a given Mach number the lift level at which minimum drag occurs varies with flap deflection angle. The flap deployment schedule used in the 99 m/s operating condition decreased the drag relative to the drag of the undeflected blade. Since flap deployment twists the blade elastically and changes the lift-drag distribution, flap deployment for power reduction cannot be found by any direct and simple procedure. However, since the variation of minimum drag with flap deflection angle is large only in the vicinity of the advancing blade tip, where the Mach number is high, that is where significant power savings can be expected.

The potential demonstrated herein indicates a significant potential for expanding the operating envelope of the helicopter. Further investigation into improving the power saving and defining the improvement in the operational envelope of the helicopter is recommended.

A 10.7% POWER REDUCTION WAS ACHIEVED AT 192 KT,  
BUT NEGLIGIBLE POWER SAVING AT LOWER SPEEDS

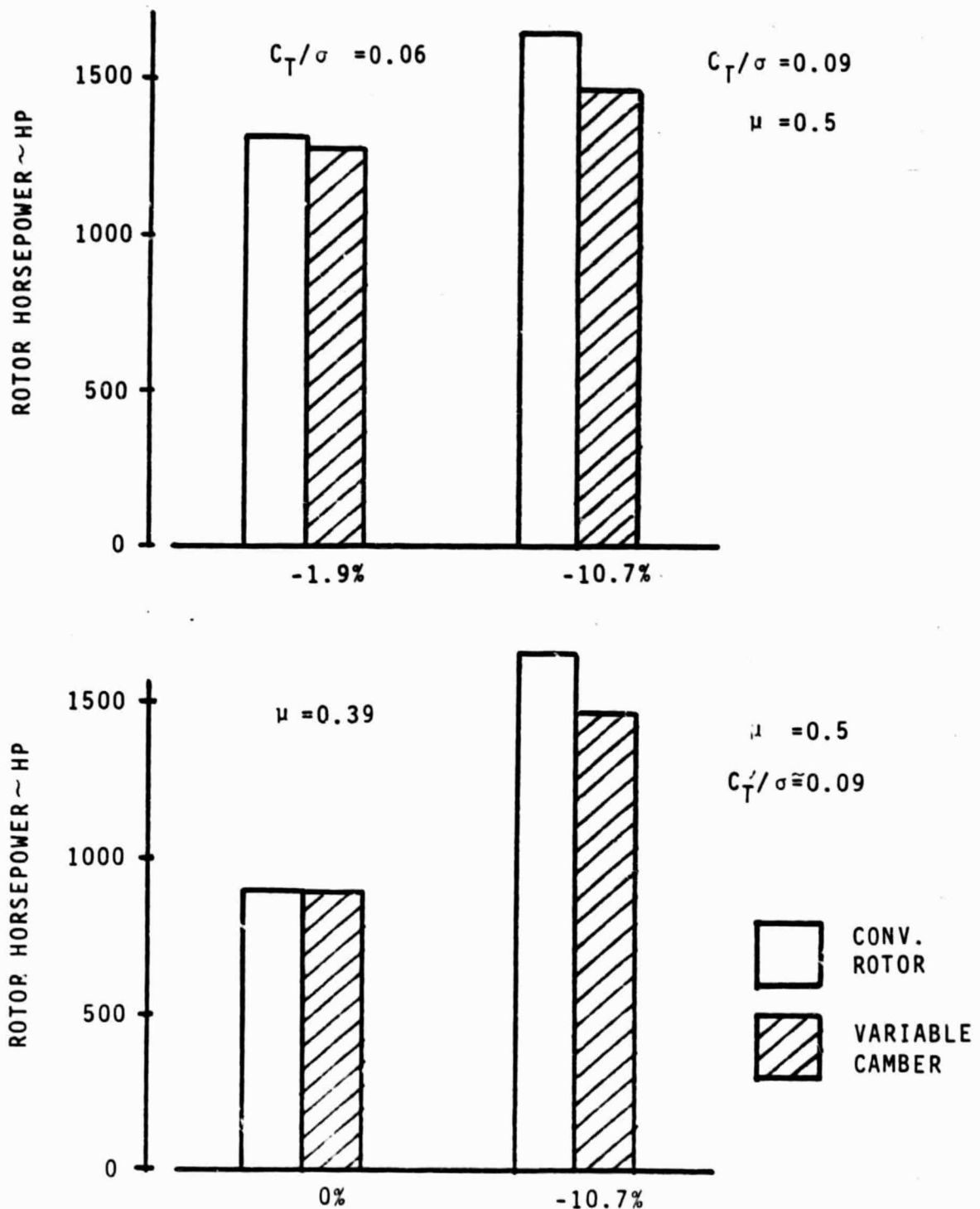


Figure A

# CAMBER SCHEDULE

MU=0.50      192 KTS    ALPHA SHAFT -6.2

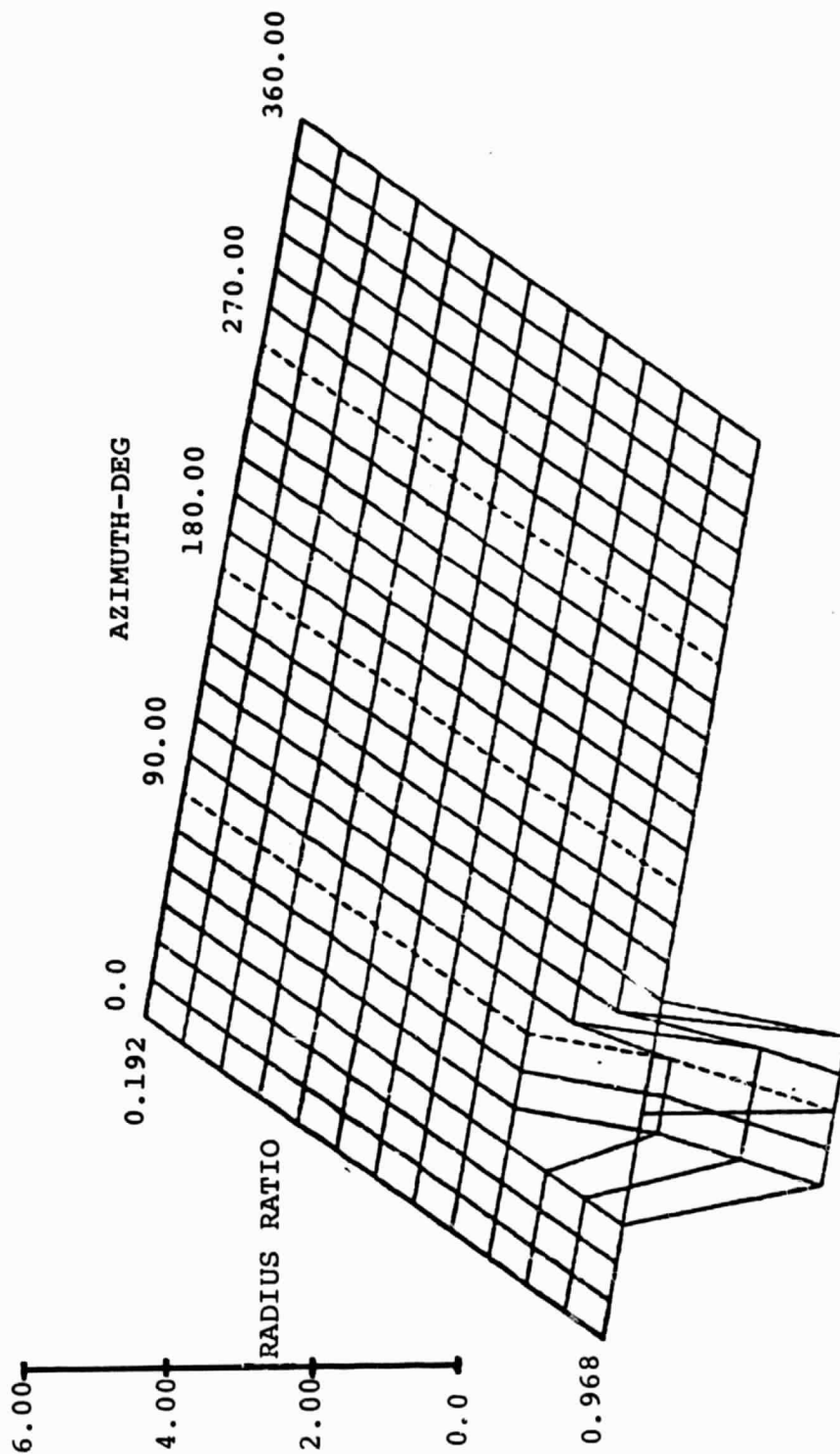


Figure B

# POWER REDUCTION FROM VARIABLE CAMBER DEPLOYMENT

H-34 ROTOR WITH A-1 AIRFOIL  $\mu = 0.5$   
 35% T.E. FLAP (SCHEDULE A)  $C_T'/\sigma = 0.089$   
 $\bar{X} = 0.046$

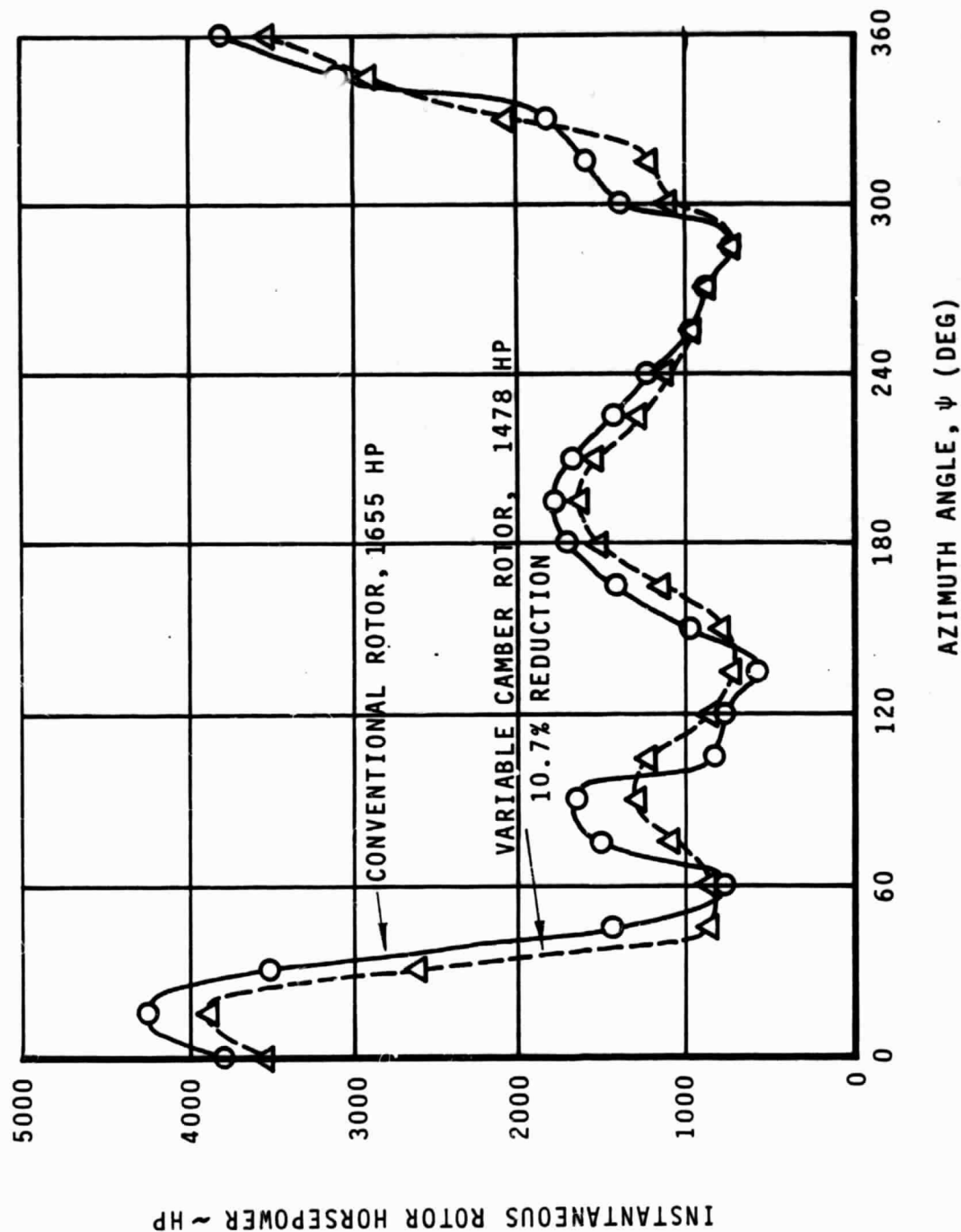


Figure C

# VARIABLE CAMBER PROVIDES THE MEANS TO CONTROL BLADE ELASTIC TWIST

H-34 ROTOR WITH A-1 AIRFOIL  
35% T.E. FLAP (SCHEDULE A)

$\mu = 0.5$   
 $C_T'/\sigma = 0.089$   
 $\bar{X} = 0.046$

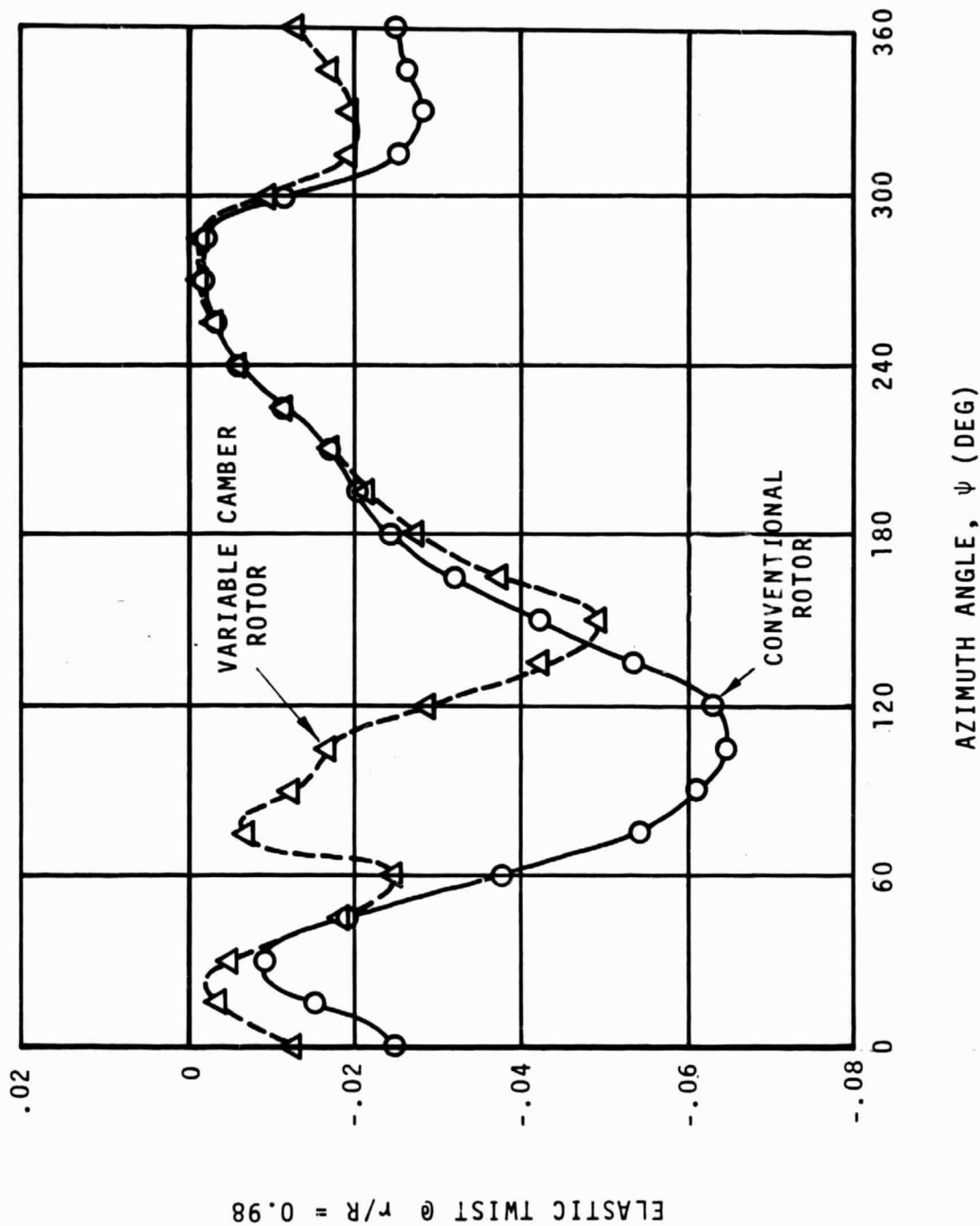


Figure D

## 2.0 Introduction

A "rotor limit" is encountered when a critical level in some measurable parameter is reached and it restricts rotor operation. The limitations related to the degradation in flow over the rotor blades can be categorized as affecting:

- (a) Power requirements,
- (b) Blade and control loads,
- (c) Handling qualities,
- (d) Acoustics.

In forward flight, the limitations attributable to aerodynamic effects are mainly caused by flow separation at high subsonic Mach numbers for low lift levels, and at Mach numbers between  $M = 0.3$  and  $0.5$  for high lift levels. The understanding of these critical regimes is complicated by the presence of substantial spanwise velocity gradients, strong time dependence (unsteady aerodynamics effects), significant three-dimensional effects in the vicinity of the blade tips, and vortex proximity effects.

Although an overall improvement in the aerodynamic characteristic of a rotor will help in all four of the categories listed above, each category is dominated by specific phenomena:

### (a) Power.

Power is function of drag. Improvement in drag is available from two sources:

- (1) Profile drag reduction, which implies operation near  $C_{d_{min}}$  or  $L/D_{max}$ , and below drag divergence.
- (2) Induced-drag reduction, achieved by optimizing the blade loading distributions.

Reduction in the power required by a rotor has been achieved conventionally by combinations of airfoil, twist and planform distribution, although the optimization process is a complex procedure because of conflicting requirements of the various flow regimes necessary for practical helicopter operation.

Rotor optimization through airfoil and planform design deals with the compromise between the advancing and retreating blade flow regimes. As shown in Figure 2, these regimes are quite incompatible and efforts to define viable airfoil sections for helicopter rotor applications have led to the formulation of specialized families of airfoil shapes with characteristics distinctly different from those employed on fixed wings and propellers.

The process of evolution which has led to today's advanced rotors has also dictated the constraints by which rotor sections should be optimized. This process has been described many times, e.g. References 1 to 14. While the quantitative design objectives vary among helicopter manufacturers as a function of rotor system, the sectional optimization for forward flight improvement consistently requires:

- (1) Constraining both low-speed and high-speed pitching moments within prescribed boundaries,
- (2) Restrictions on the minimum acceptable quasi-steady maximum lift levels for Mach numbers between  $M = 0.3$  and  $M = 0.5$ .
- (3) High drag divergence Mach number levels to meet the lift/Mach number requirements along the advancing blade with minimum power and loads penalties.

The requirement for operation at high speeds has recently been the incentive to examine a number of airfoil, planform and twist variations aimed at performance improvement and vibratory load alleviation. It appears now that an optimum conventional rotor should employ some tip planform taper and possibly sweep, in conjunction with optimum twist and airfoils.

This does not rule out the possibility of employing unconventional systems to extend the operating limits and improve the efficiency of helicopter rotors. Unconventional rotor systems have been considered and even tested before. This includes forms of variable camber, such as Kaman's servo-tab system, and rotors employing cyclic blowing. The potential benefits from the deployment of these devices have been assessed as sufficiently significant to justify further research.

With the establishment of large computers and the use of comprehensive computer codes to carry out rotor analysis, it has become feasible to consider a more systematic approach aimed at the analytical assessment of the potential benefits of variable camber on helicopter rotors. At the same time, the methods of 2-D airfoil analysis have progressed to the point that it is possible to evaluate the characteristics of most airfoils with sufficient accuracy to allow a realistic assessment of the potential of variable camber helicopter rotors on the basis of estimated performance and vibratory loads improvements.

#### (b) Rotor loads.

Blade and control loads are mainly the result of growth in pitching moments. As illustrated in Figure 1, there are two areas in the rotor disc from which these pitching moments may arise:

ORIGINAL PAGE 11  
OF POOR QUALITY

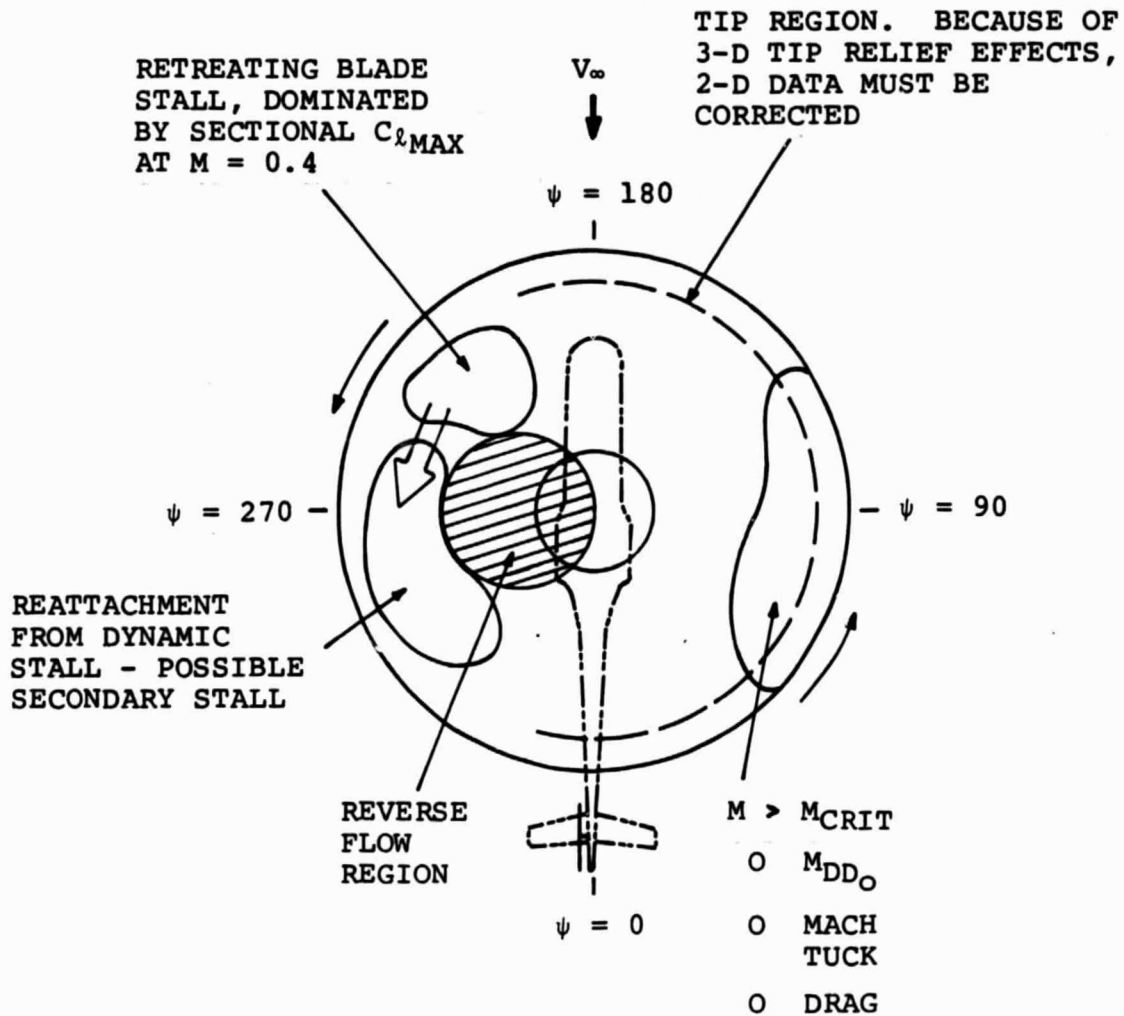


Figure 1 Rotor Environment in Forward Flight.

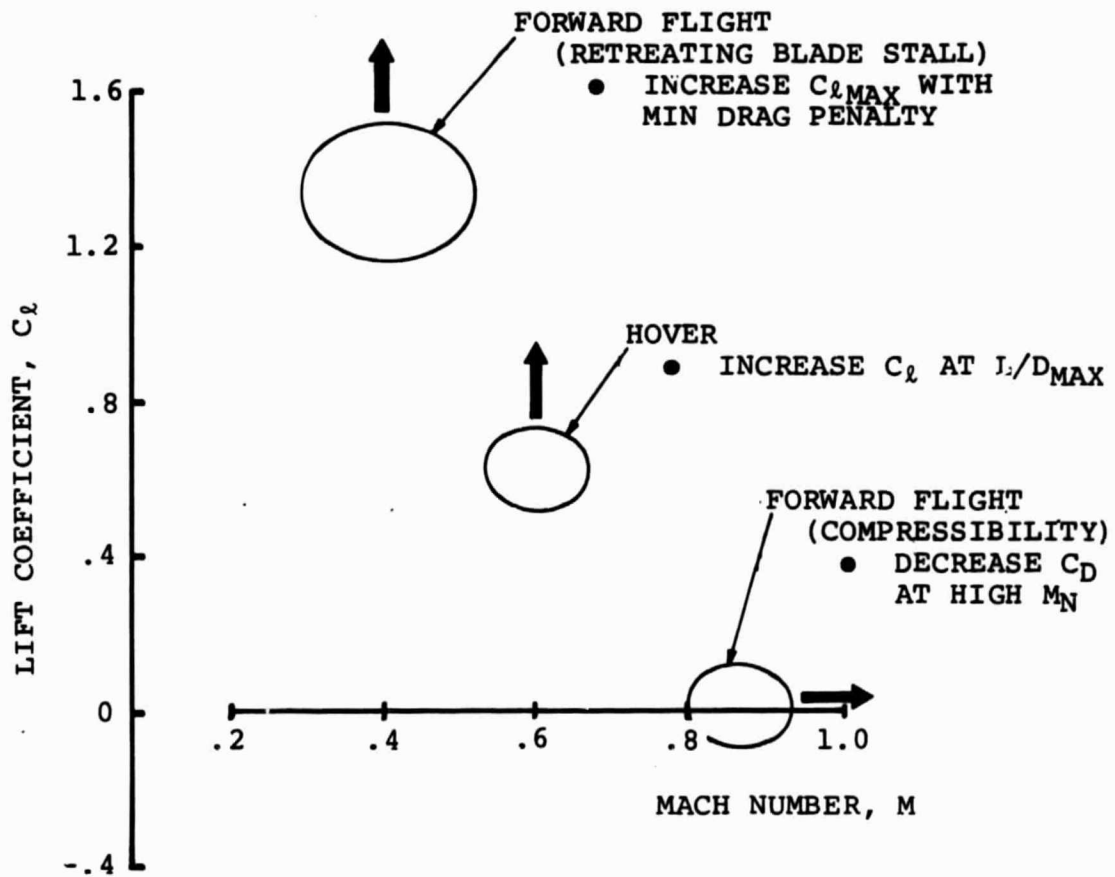


Figure 2 Lift Coefficient and Mach Number Requirements.

- (1) The outboard 30% of the advancing blade,
- (2) Portions of the retreating blade, in the third and fourth quadrant.

(c) Handling Qualities.

The handling qualities of a helicopter cannot be assessed directly through rotor performance and loads analysis, however an extension of the operating envelope of a rotor should result in an extension of the conditions for which local flow separation is delayed and "linear" aerodynamics apply. Typical problems which may be delayed by advanced rotors are the tendency of a rotor to pitch nose down on the advancing blade at high speeds (Mach "tuck", due to large nose-down moments at high Mach numbers) and a degradation in pilot perceived controls above some thrust and speed combinations.

(d) Acoustics.

A reduction in rotor noise will generally follow an improvement in the aerodynamic characteristics of a rotor to the extent that separation, and more significantly shock-induced separation, and sound due to the growth and collapse of local supersonic regions would be reduced. However, the noise due to blade/tip-vortex encounters is more dependent on rotor trim and placement than on the aerodynamic properties of the rotor, making an exception for blade designs which would result in tip vortices with reduced or diffused vorticity.

Sectional Optimization vs Variable Camber

Rotor improvement through airfoil optimization may not have yet been carried out to ultimate limits, but except for instances in which the airfoil requirements are radically novel, the optimization of conventional rotor sections becomes more difficult with each level of improvement. Figure 3 compares the maximum lift and drag divergence boundaries of groups of helicopter rotor airfoils. On the basis of optimization of the maximum lift coefficient at  $M = 0.4$  against the zero lift drag divergence Mach number (within the stated pitching moment restrictions) it would be difficult to significantly exceed the current optimum boundary with conventional airfoils.

The deployment of variable camber on rotor blades can, potentially, provide the means to operate at high lift levels in the Mach number range from  $M = 0.3$  to beyond 0.5, while also providing the means to reduce, or reverse, the camber at high subsonic Mach numbers to maximize the delay in drag rise.

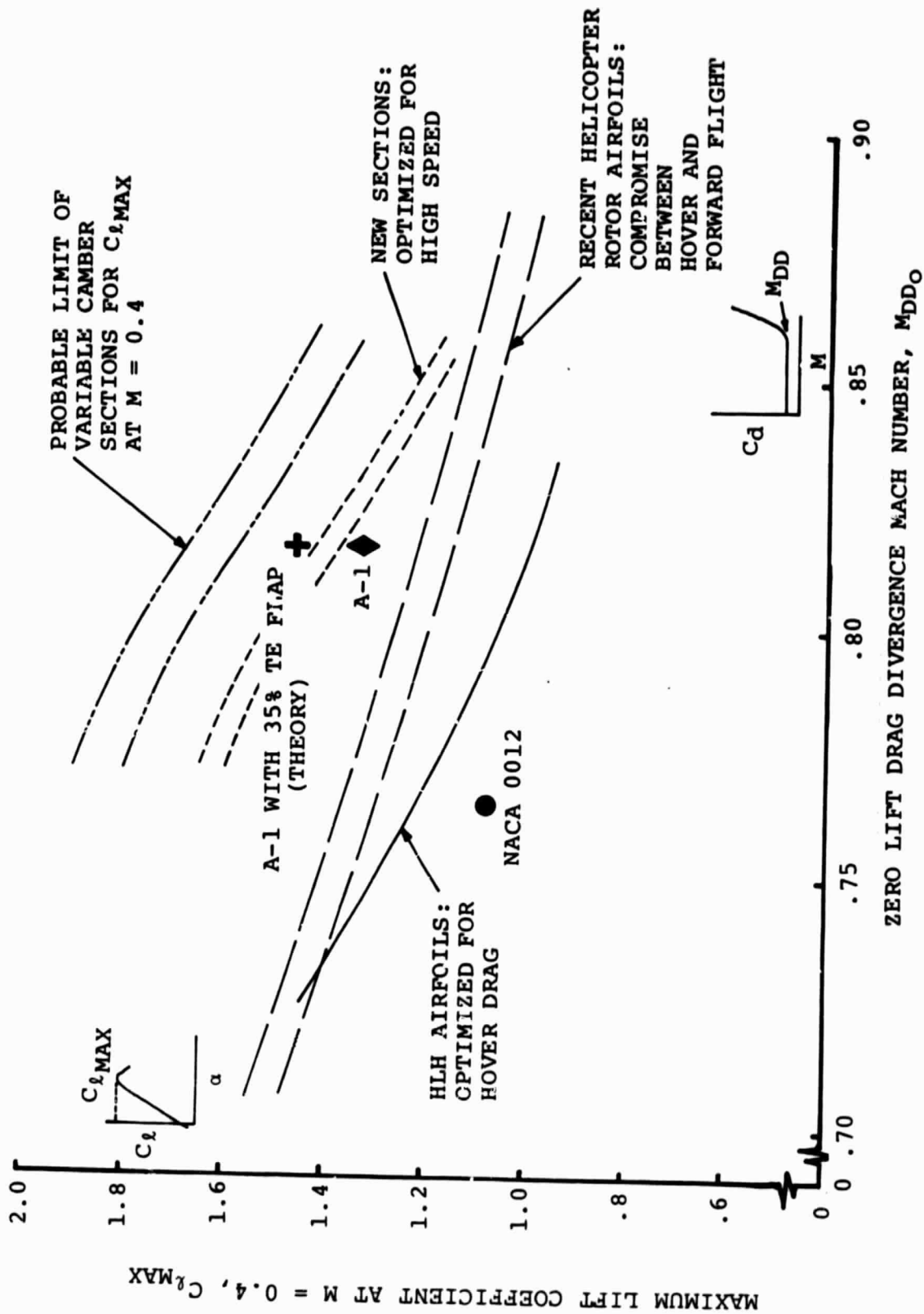


Figure 3 Comparison of Helicopter Rotor Airfoils.

While in principle it may be desirable to delay dynamic stall by extending the quasi-steady maximum lift range, the changes in maximum lift cannot be separated from the pitching moment changes due to camber variation, and an uncoupled extension in maximum lift would be true only for rotor blades which are perfectly stiff in torsion. After elastic effect are accounted for, there may be some advantage in taking a symmetrical or moderately cambered section with very high Mach number penetration and improving by variable camber its maximum lift characteristics as needed to delay dynamic stall. But in fact it appears that variable camber should be mainly used to control the elastic twist of a rotor blade while varying the camber to operate as close as possible to minimum drag. The optimization process should seek to reduce both the profile and the induced drag, through the suppression of extensive separated flow, or the extension of drag divergence of the airfoil sections by deployment of variable camber devices.

On a preliminary basis it appears that variable camber deployment can be separated into three distinct modes of operation, as illustrated in Figure 4:

- (a) High subsonic Mach number deployment, aimed at the delay in growth of drag and pitching moments beyond drag divergence. This would probably involve small camber changes over the outer 20% of span.
- (b) Low to intermediate subsonic Mach number deployment,  $0.3 < M < 0.6$ , taking place over any portion of the blade inboard of  $0.75R$  to  $0.80R$ , aimed at the suppression of dynamic stall through some combination of:
  - o changes in elastic twist (pitching moments)
  - o changes in the angle of zero lift
  - o changes in  $c_{l_{max}}$
- (c) Intermediate Mach number deployment,  $M \approx 0.6$ , near the tip in the fore and aft portions of the rotor disc, as means to generate propulsive force at high advance ratios, beyond conditions for which conventional rotors display a significant degradation in propulsive efficiency.

In any case, the need to minimize mechanical complexity dictates that the extent of blade involving camber be restricted to short spanwise elements.

ORIGINAL PAGE IS  
OF POOR QUALITY

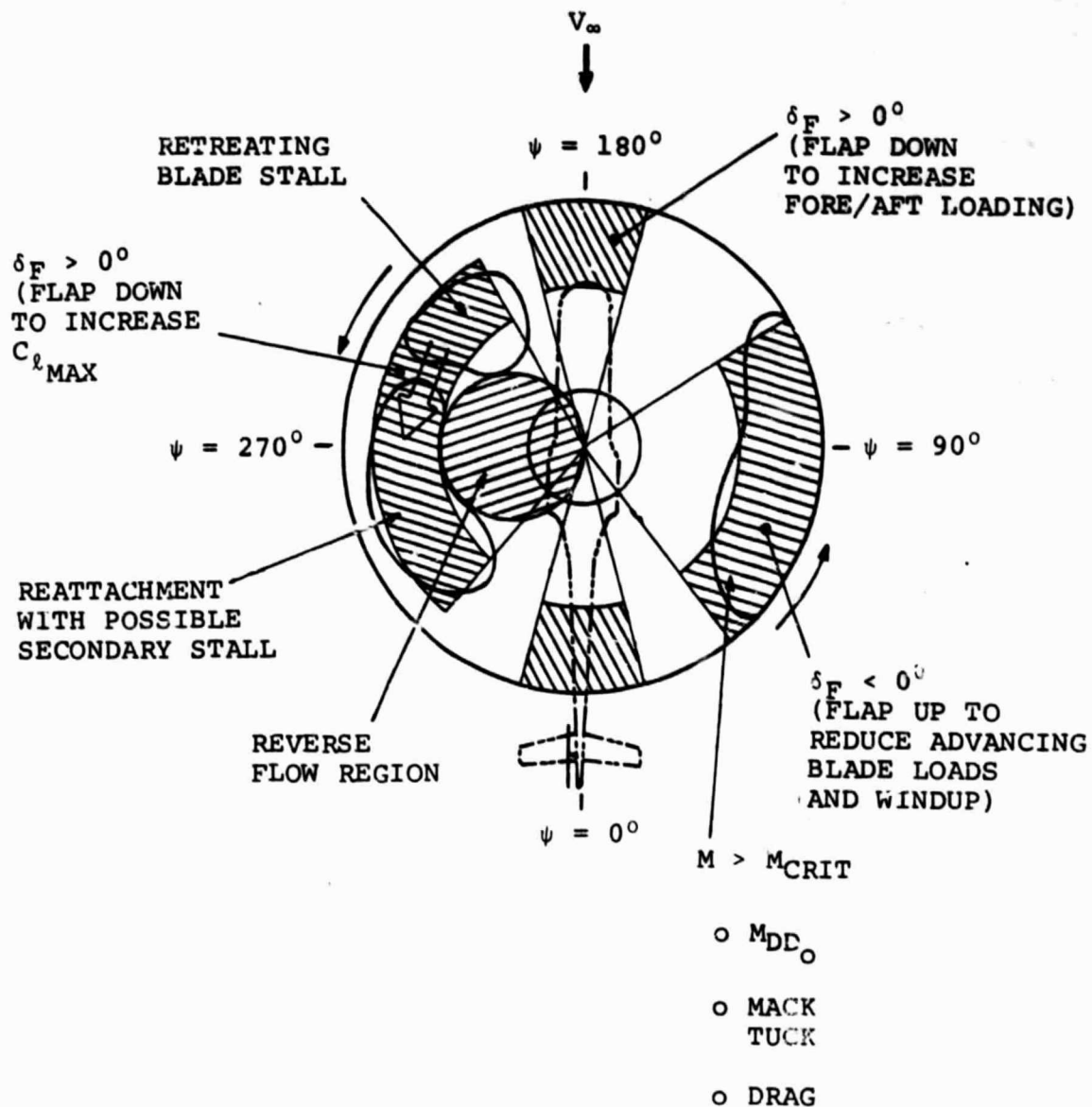


Figure 4 Regions of Variable Camber Deployment in Forward Flight.

From the point of view of azimuthal deployment, variable camber offers these basic alternatives:

- (a) Sinusoidal (cyclic) variation in camber together with conventional cyclic and collective blade pitch.
- (b) Cyclic variable camber entirely replacing conventional cyclic but not blade collective pitch control.
- (c) Combinations of variable-camber cyclic and collective added to conventional blade collective pitch control.
- (d) On/off deployment of variable camber at fixed amplitude and controllable azimuthal extent, or fixed azimuthal extent and variable amplitude, added to conventional cyclic and collective pitch control.

In hover, variable camber might be deployed only to alter the twist in a direction beneficial to performance. Unless camber is to be introduced specifically as the means to improve hover performance, the spanwise and azimuthal distribution of variable camber is likely to be dictated entirely by forward flight requirements.

### 3.0 Review of Variable Camber Concepts

Figure 3 illustrates the advancing/retreating blade potential of a number of airfoils on the basis of the zero lift drag divergence Mach number and of the quasi-steady maximum lift coefficient at  $M = 0.4$ . Rotor optimization on the basis of airfoil characteristics involves:

#### A. Maximum Lift Characteristics.

The delay or suppression of retreating blade stall, which can be related to a delay in static stall at Mach numbers from  $M = 0.3$  to  $M = 0.5$ . In Vertol rotors the key Mach number for dynamic stall delay is  $M = 0.4$ , as borne out by several model rotor tests and confirmed by flight test.

#### B. Drag Divergence.

The delay in drag rise at transonic speeds over a range of positive and negative lift coefficients. Different objectives should be defined as a function of advance ratio, nominal advancing tip Mach number and spanwise location. Any section between  $0.70R$  and  $0.90R$  of the blade span may operate beyond drag divergence as a result of the local lift and Mach number combination, while sections between  $0.90R$  and the tip may be within the drag divergence boundary by virtue of an increase in drag divergence Mach number associated with reduced lift coefficient levels, favorably compounded by the

presence of three-dimensional tip relief effects. In order to simplify the optimization process, the highest priority has been assigned to the drag divergence Mach number at the zero lift level.

#### C. Sectional Pitching Moments.

The attainment of low-speed pitching moment levels about the aerodynamic center within approximately  $-0.01 \leq C_m \leq 0.01$ . Test experience with Vertol rotors dictated the even stricter requirement that low-speed pitching moments be small and positive. Figure 5 illustrates the dependence of blade loads (root torsion) on the level of the low-speed zero-lift pitching moment coefficient, as measured in a Boeing Vertol Wind Tunnel Test, Reference 6.

Additional restrictions limit the growth of pitching moments at high Mach numbers to reduce the advancing blade elastic torsional deflections at high speeds.

Further limitations are imposed to control the relative growth of drag divergence and pitching moment divergence, as illustrated in Figure 6, to make sure that rotor operation would be limited by power rather than by the growth in blade or control loads.

#### D. Hover Performance Requirements.

While drag rise is one of the key elements limiting forward flight performance, hover performance is strongly influenced by the profile drag at Mach numbers from  $M = 0.4$  to  $M = 0.6$ , at lift coefficient levels from  $C_l = 0.4$  to  $C_l = 0.65$ . For design purposes, the lift level  $C_l = 0.6$  at  $M = 0.6$  is recommended to compare the hover drag potential of different rotor airfoils.

The introduction of variable camber alters some of the above sectional requirements. The first restriction to be lifted is on the limits in the combination of high-lift and drag-divergence capability. The second is in the local pitching moment requirements. The third is hover drag, since, in principle, it should be possible to operate with a net local pitch schedule which allows low drag everywhere in the rotor disc.

In fact the emphasis on airfoil characteristics should be reassessed when the freedom in camber level is introduced. The requirement that a rotor section have high Mach number penetration characteristics remains a top priority since the advancing blade still has to operate at high subsonic Mach numbers. However, the variable camber sections should offer some control over the lift levels necessary to maintain every

6 FT. DIA. VR-7/8 ROTOR

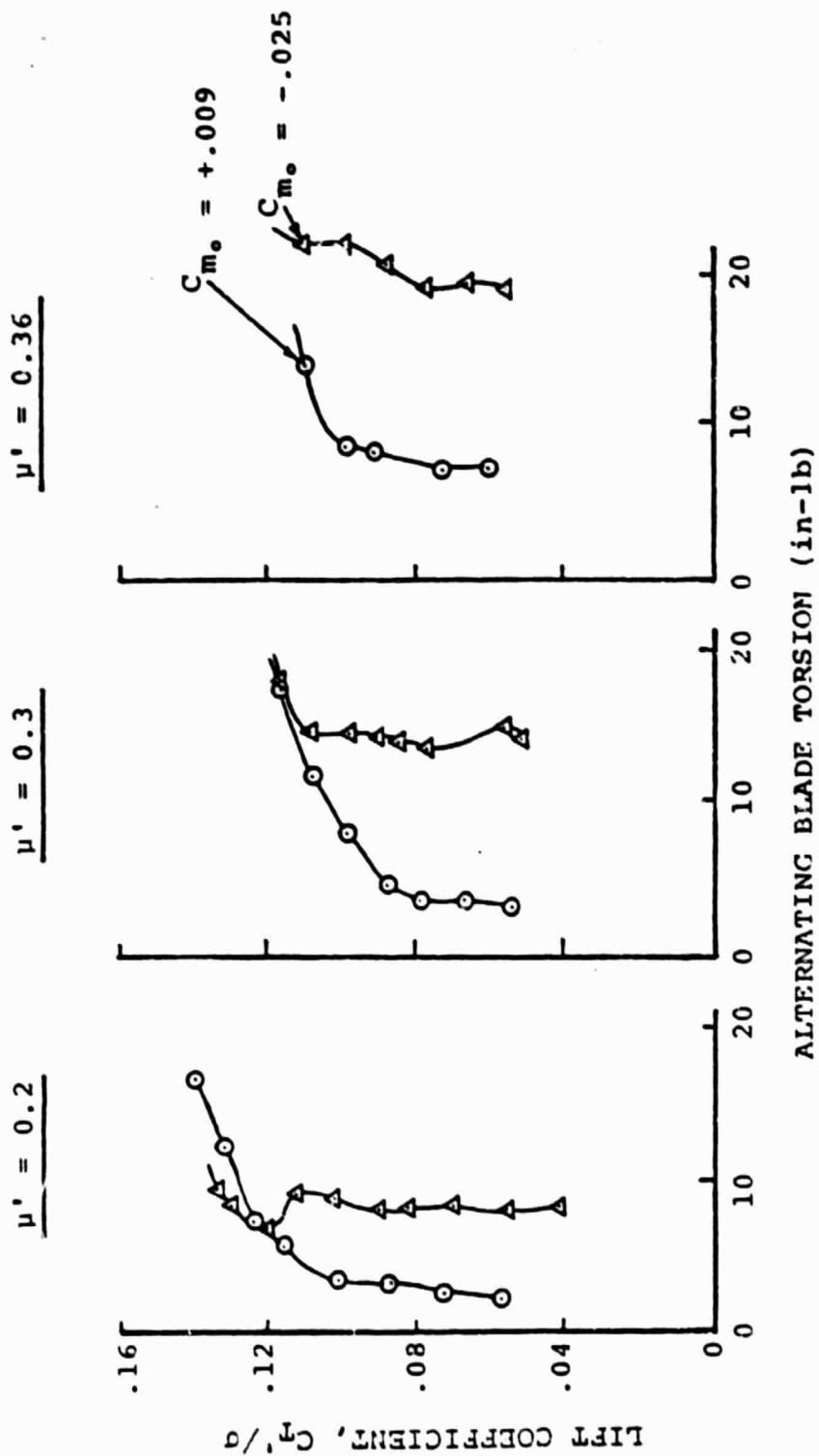


Figure 5 Effect of Sectional Pitching Moments on Blade Loads.

# LOADS AT 90% OF SPAN

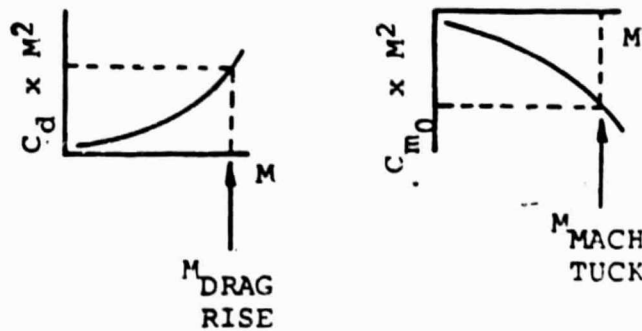
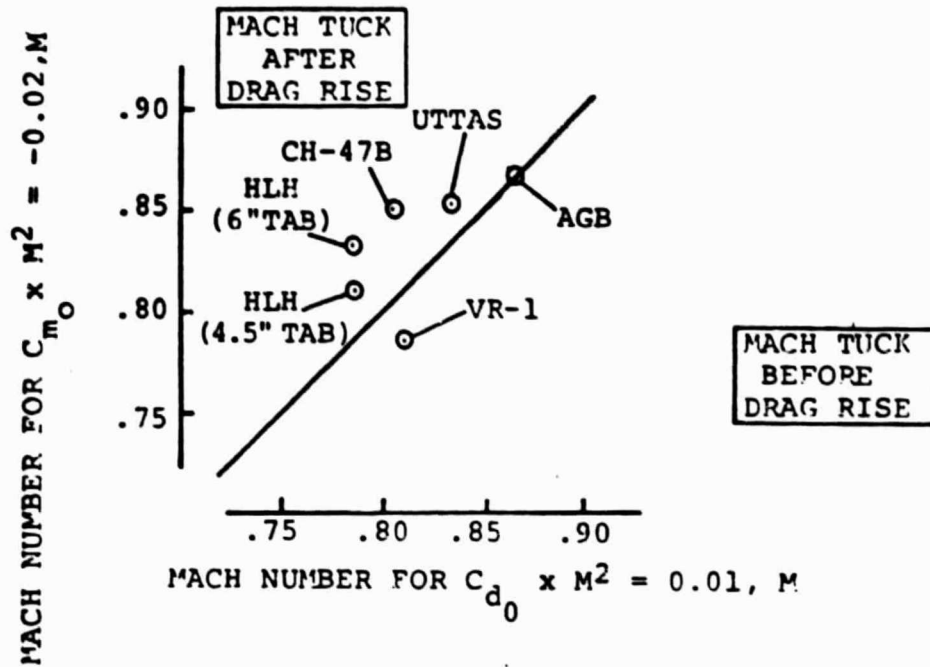


Figure 6 Compressibility Effects on Drag and Pitching Moment Characteristics of Several Helicopter Rotor Sections.

element of the blade at conditions for which drag degradation is minimized while still providing the necessary rotor lift and propulsive forces.

In principle, the requirement that the quasi-steady lift of the basic airfoil section be very high is no longer a design objective because the rotor blade may avoid dynamic stall by 1) a reduction of the angle of attack through elastic twist deflections, or 2) by changes in the angle of zero-lift as a function of camber level, without being dependent on fixed maximum lift characteristics.

The role of unsteady aerodynamics effects remain somewhat uncertain and may have to be quantified more rigorously in the future. In the present formulation all unsteady effects have been modeled on the basis of data from 2-D airfoils undergoing some form of sinusoidal motion (pitching or plunging) at constant Mach number. In the variable camber rotor there are contributions to the shed vorticity from camber changes (e.g. flap motions) which are only in part accounted for by the current formulation since camber variation introduces effects not described by a fixed relationship between angle of attack and lift. Since the variable camber excursions and deployment rates contemplated for this study should be generally small, this lack in correspondence between the quasi-steady lift and angle of attack and any additional shed wake effects attributable to flap motions will be assumed to be negligible.

### 3.1 Review of Possible Configurations

An initial review of two-dimensional variable camber concepts covered leading edge, trailing edge as well as overall camber changes. Table I and Figure 7 summarize the key configurations reviewed. Airfoil contours and representative pressure distributions from Y-39, at  $M = 0.4$  and  $\alpha = 4.0^\circ$  are shown in Figures 8 through 15. The L.E. devices were disappointing because they did not provide any significant change in maximum lift characteristics at the critical  $M = 0.4$  level, they caused small changes in pitching moment, offered little to no relief in drag divergence and would probably be very hard to design and implement. This last difficulty arises from the need to maintain the structural integrity of the blade spar. In the event of significant performance and loads benefits, it would be worthwhile to challenge these design difficulties, but at present there is no indication that such an effort would be worth it.

Subtle changes in overall camber also proved to be hard to justify. For instance, local variations in lower surface contour, as suggested for use on glider wings, yielded sectional performance changes which were not significant within rotor requirements. Some of these concepts, deployed in a

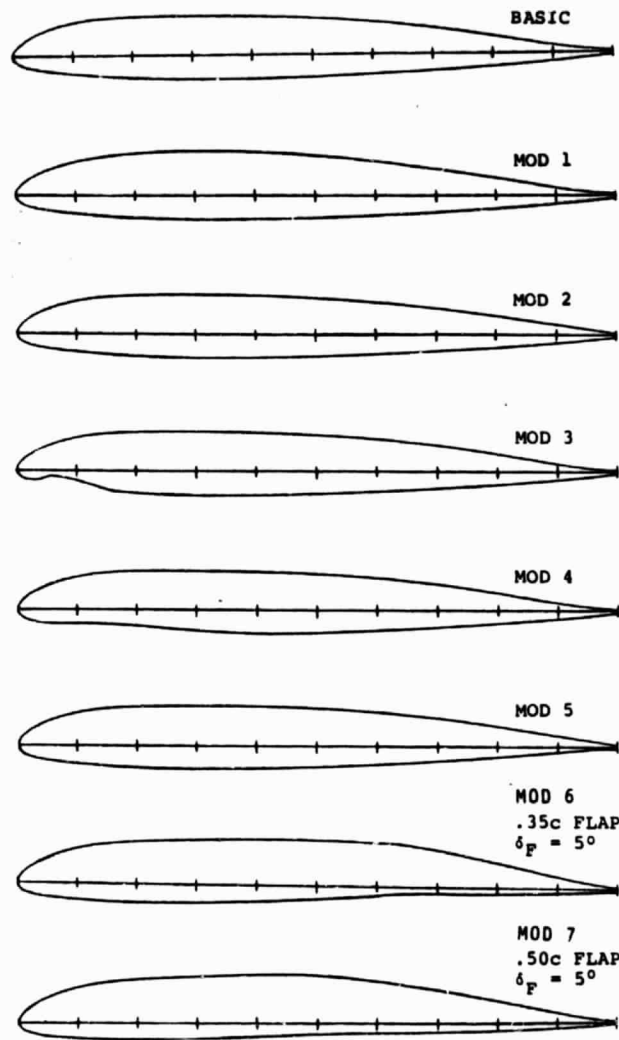
Table I Summary of Variable Camber Configurations

<u>DESIGNATION</u>	<u>DESCRIPTION</u>	<u>REMARKS</u>
Mod. 1	Overall camber change obtained by increasing the upper surface thickness between 0.15c and 0.70c, with a maximum $\Delta y/c = 0.0084$ at $x/c \approx 0.35$ .	This contour variation did not significantly increase the maximum lift at $M=0.4$ , and it caused a small degradation in $M_{DD}$ at low lift levels.
Mod. 2	T.E. thickness increased by filling out the upper surface reflex area between 0.70c and the T.E. Intended to verify the effect of reducing T.E. mean line reflex.	Negligible effect on $C_{lmax}$ and $M_{DD}$ . $0.5^\circ$ shift in the angle for zero lift. Low speed pitching moment coefficient changed from $C_{mo} = +.004$ (baseline) to $C_{mo} = -.0112$ .
Mod. 3	Abrupt lower surface change between the L.E. and 0.20c to simulate the effect of pulling in some portion of the contour.	No change in maximum lift capability at $M = 0.4$ , and adverse effect on drag divergence. Other changes not significant. By current methods the flow at the surface depression cannot be modeled correctly.
Mod. 4	Lower surface change distributed between 0.025c and 0.45c, to simulate the effect of pulling in a substantial portion of the contour and increase the overall camber level.	Small improvement in lifting capability, $C_{lmax}$ , at $M = 0.4$ . Other effects were negligible.
Mod. 5	Altered T.E. Contour to change (reverse) the direction of T.E. loading. Caused the A-1 to become a "rear loaded" airfoil.	7% increase in $C_{lmax}$ at $M = 0.4$ , with significant changes in $C_{mo}$ and $\alpha_o$ . Review of Mod. 5 performance led to plain T.E. flaps (Mods 6 and 7).

Table I Summary of Variable Camber Configurations (continued)

<u>DESIGNATION</u>	<u>DESCRIPTION</u>	<u>REMARKS</u>
Mod. 6	Plain sealed 35% T.E. flap, with flap hinge in area where the basic contour already displays a pronounced change in curvature (at $X/C = 0.65$ ).	Detailed characteristics evaluated for flap angles from $-5^\circ$ to $+15^\circ$ . Usefulness of flap angles beyond $5^\circ$ is questionable.
Mod. 7	Plain, sealed 50% T.E. flap, to investigate large camber effects with small deflections.	Detailed data evaluated for $-5^\circ$ and $+5^\circ$ flap angles.

ORIGINAL PAGE IS  
OF POOR QUALITY



THEORY: Y-39

$C_{LMAX}$ @ $M = 0.4$	$MDD_0$	$C_{mac}$ @ $M = 0.4$	$\alpha_0$ (DEG) @ $M = 0.4$	$C_L$ @ $M = 0.4$ $\alpha = 4.0$
1.30	.818	.004	-.45	.55
1.32	.785	.0012	-.6	.57
1.31	.82	-.0112	-.9	.61
1.31	—	.0083	-.55	.55
1.33	.825	.0062	-.5	.56
1.40	.783	-.0392	-2.1	.75
1.50	.65	-.0583	-4.2	.96
1.50	.625	-.0419	-4.47	1.03

Figure 7 Variable Camber Concepts Considered for the A-1 Airfoil.

ORIGINAL PAGE IS  
OF POOR QUALITY

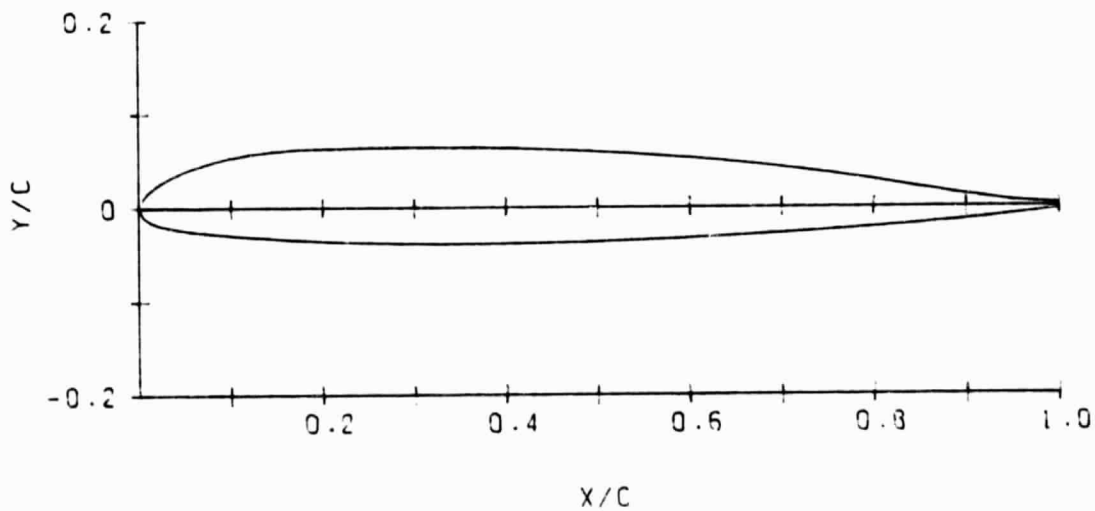
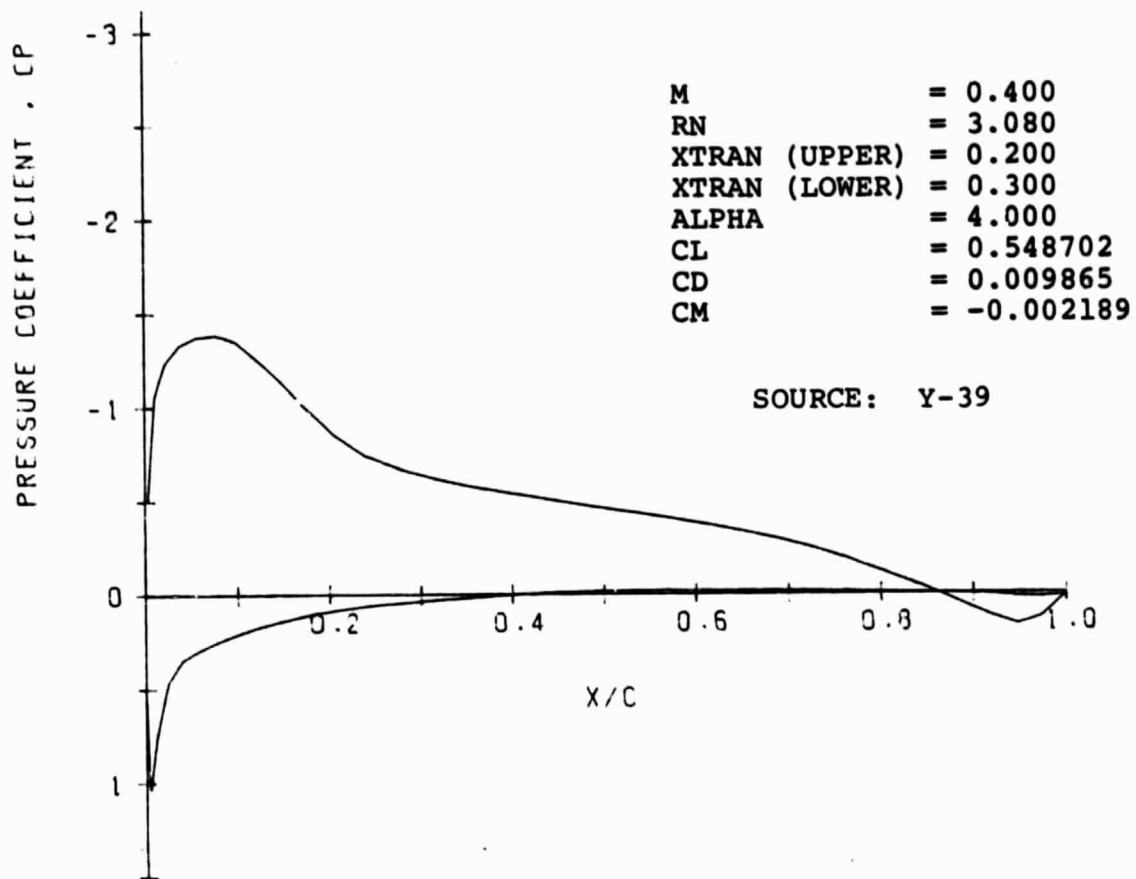


Figure 8 Baseline A-1 Airfoil. Pressure Distribution  
at  $M = 0.4$ ,  $\alpha = 4^\circ$ .

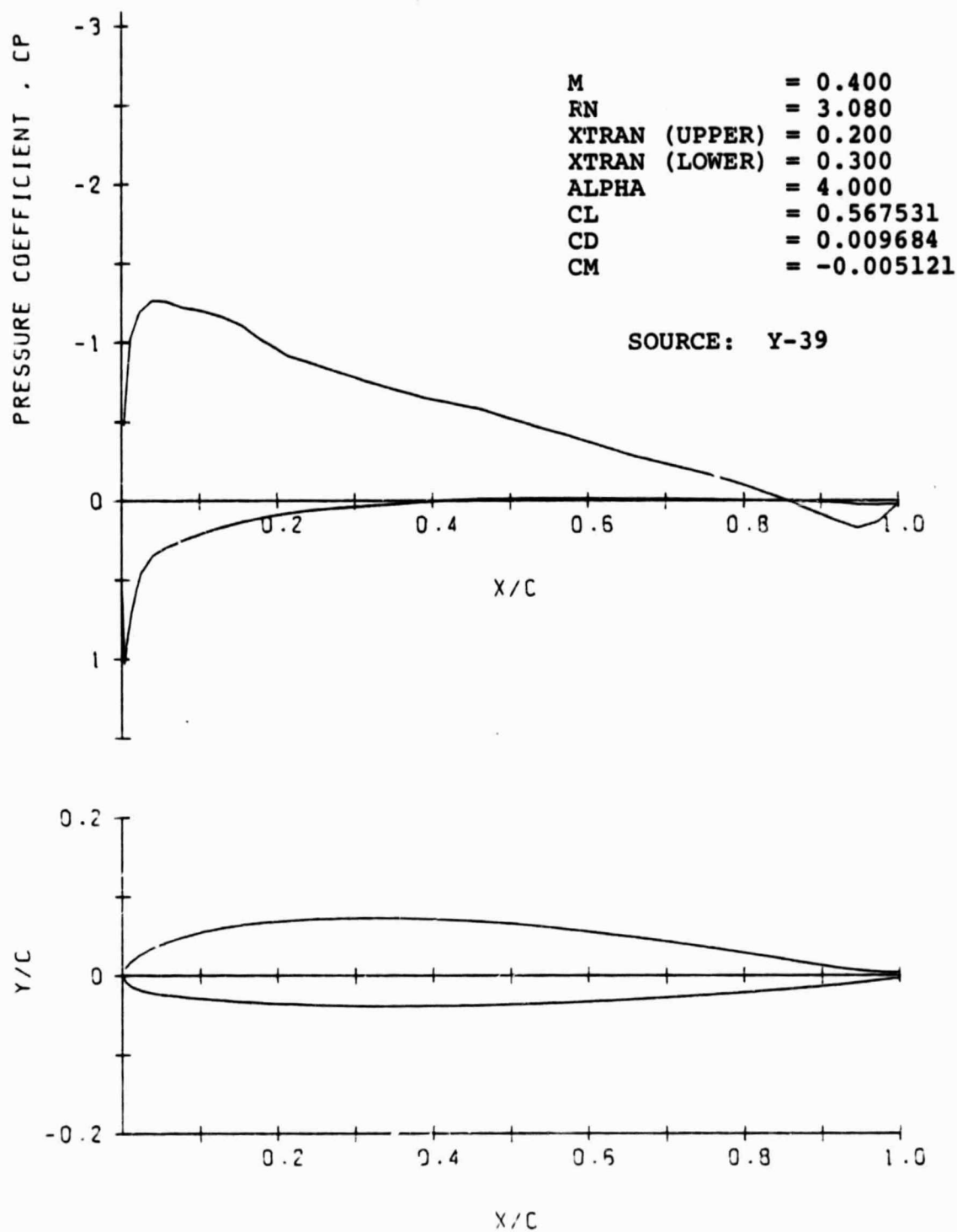


Figure 9 A-1 Airfoil, Mod. 1. Overall Camber Change by Upper Surface Modification. Pressure Distribution at  $M = 0.4$ ,  $\alpha = 4^\circ$ .

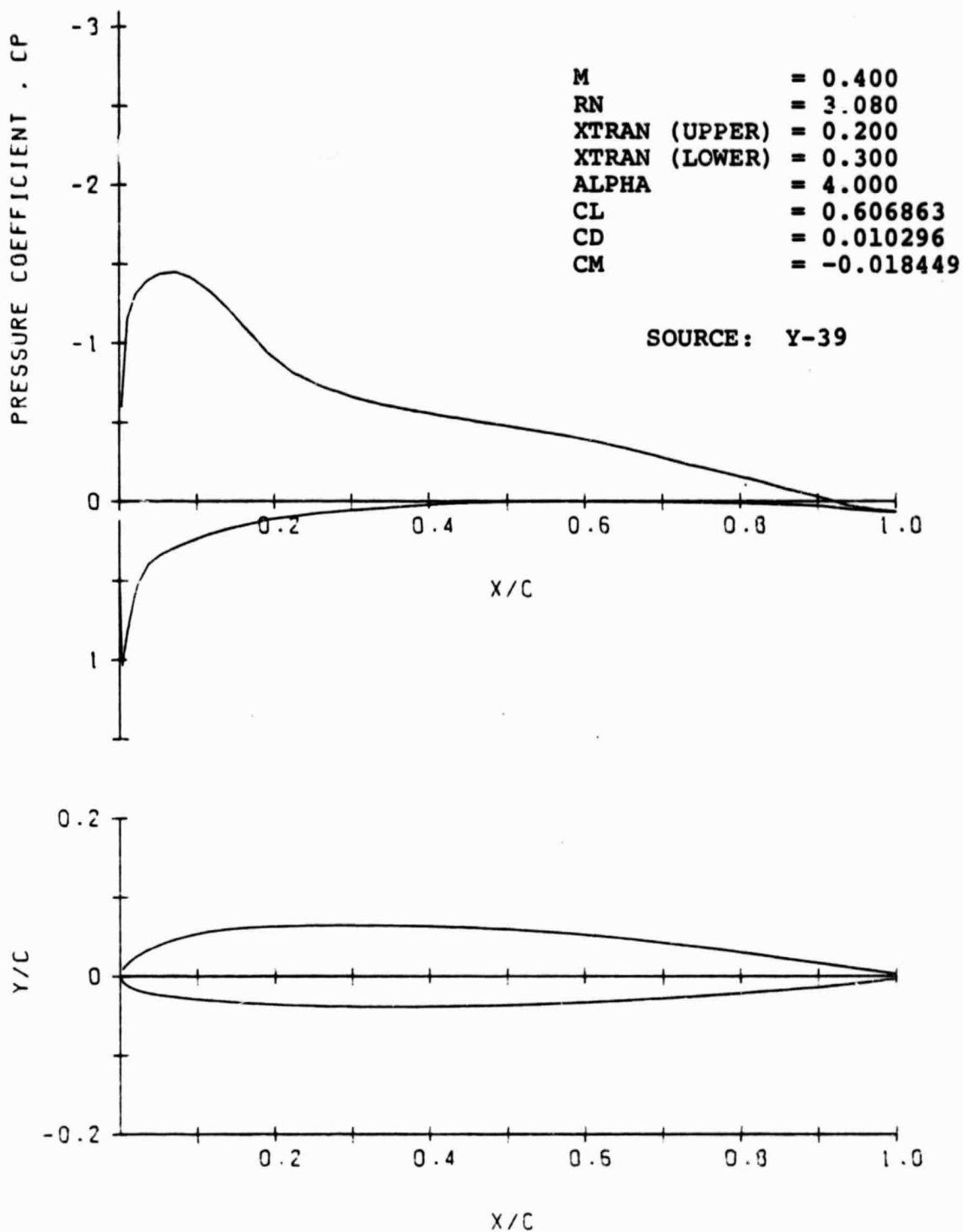


Figure 10 A-1 Airfoil, Mod. 2. Trailing Edge Camber  
 Change by Upper Surface Displacement.  
 Pressure Distribution at  $M = 0.4$ ,  $\alpha = 4^\circ$ .

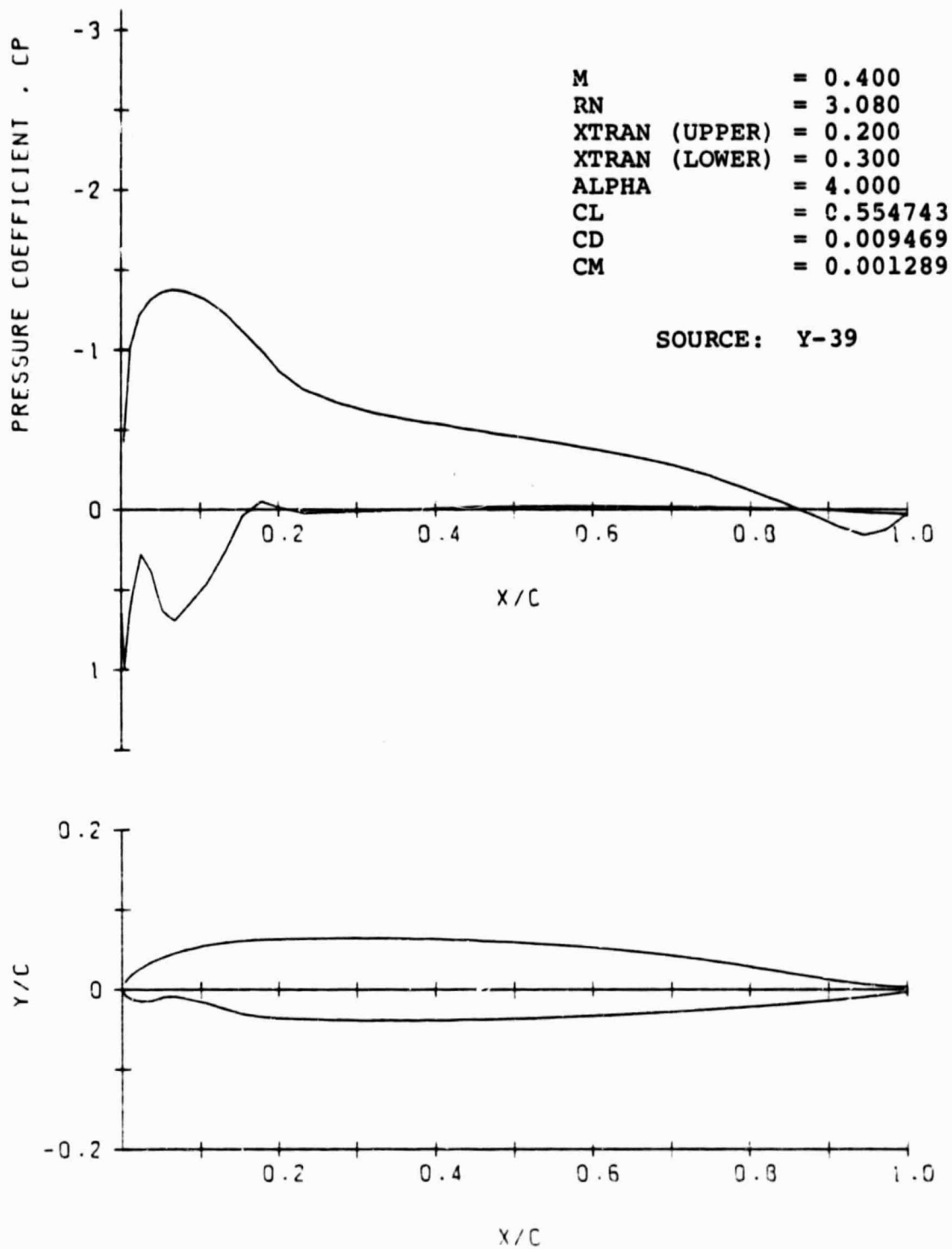


Figure 11 A-1 Airfoil, Mod. 3. Leading Edge Camber  
 Change by Localized Lower Surface Deflection.  
 Pressure Distribution at  $M = 0.4$ ,  $\alpha = 4^\circ$ .

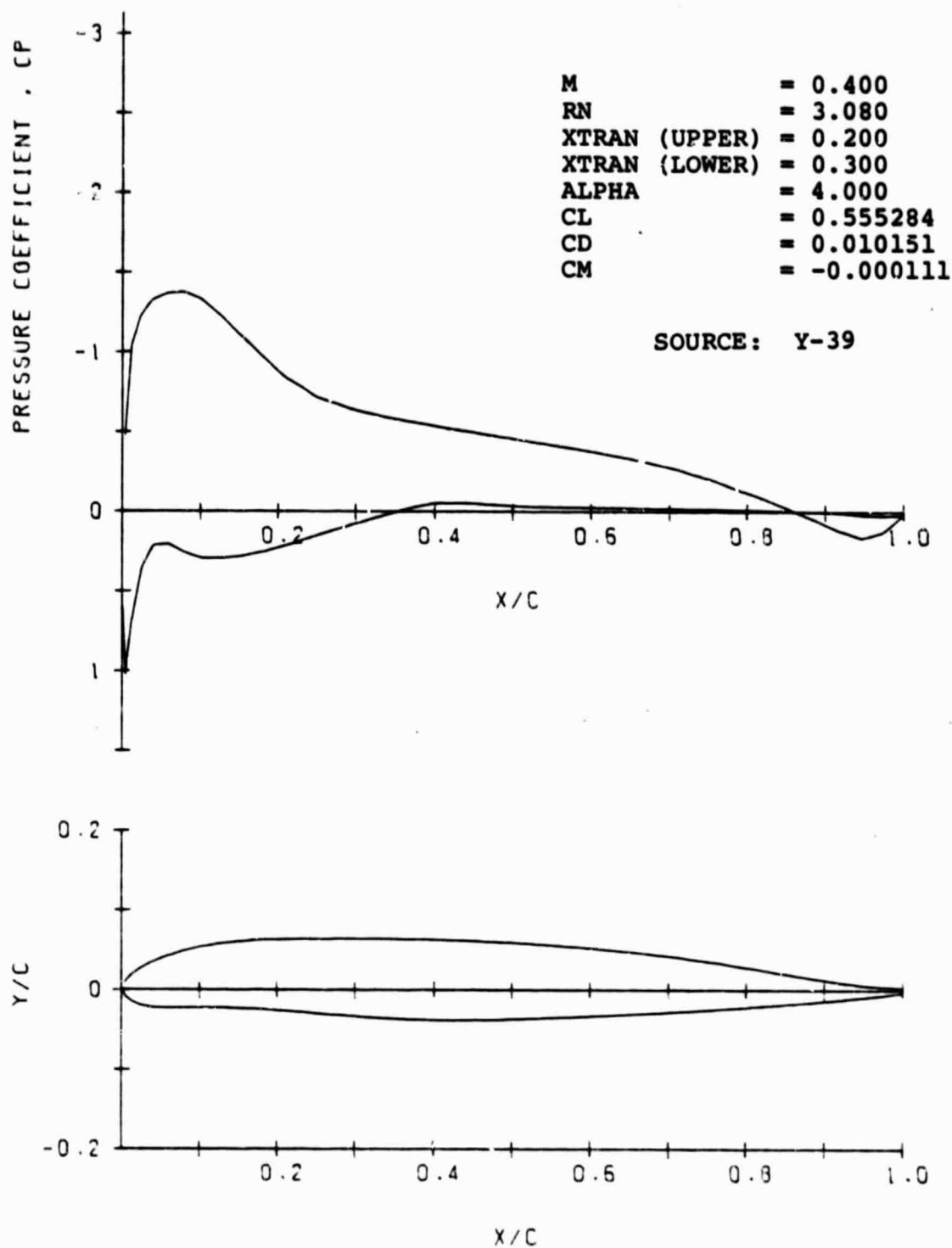


Figure 12 A-1 Airfoil, Mod. 4. Leading Edge Camber Variation by Lower Surface Change Distributed over about 1/3 Chord. Pressure Distribution at  $M = 0.4$ ,  $\alpha = 4^\circ$ .

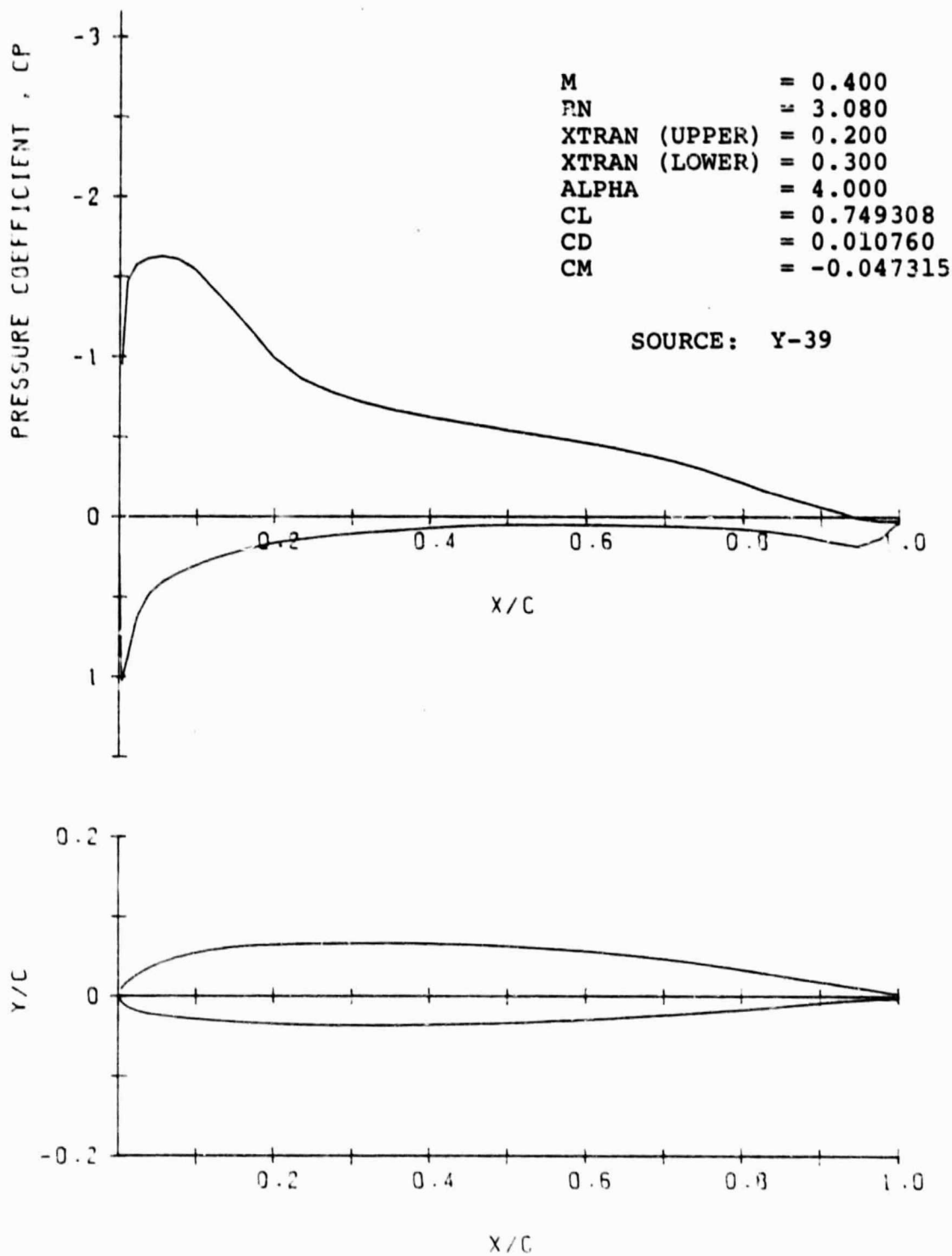


Figure 13 A-1 Airfoil, Mod. 5. Camber Variation by Increasing Mean-Line Curvature at the Trailing Edge (Rear Loading). Pressure Distribution at  $M = 0.4$ ,  $\alpha = 4^\circ$ .

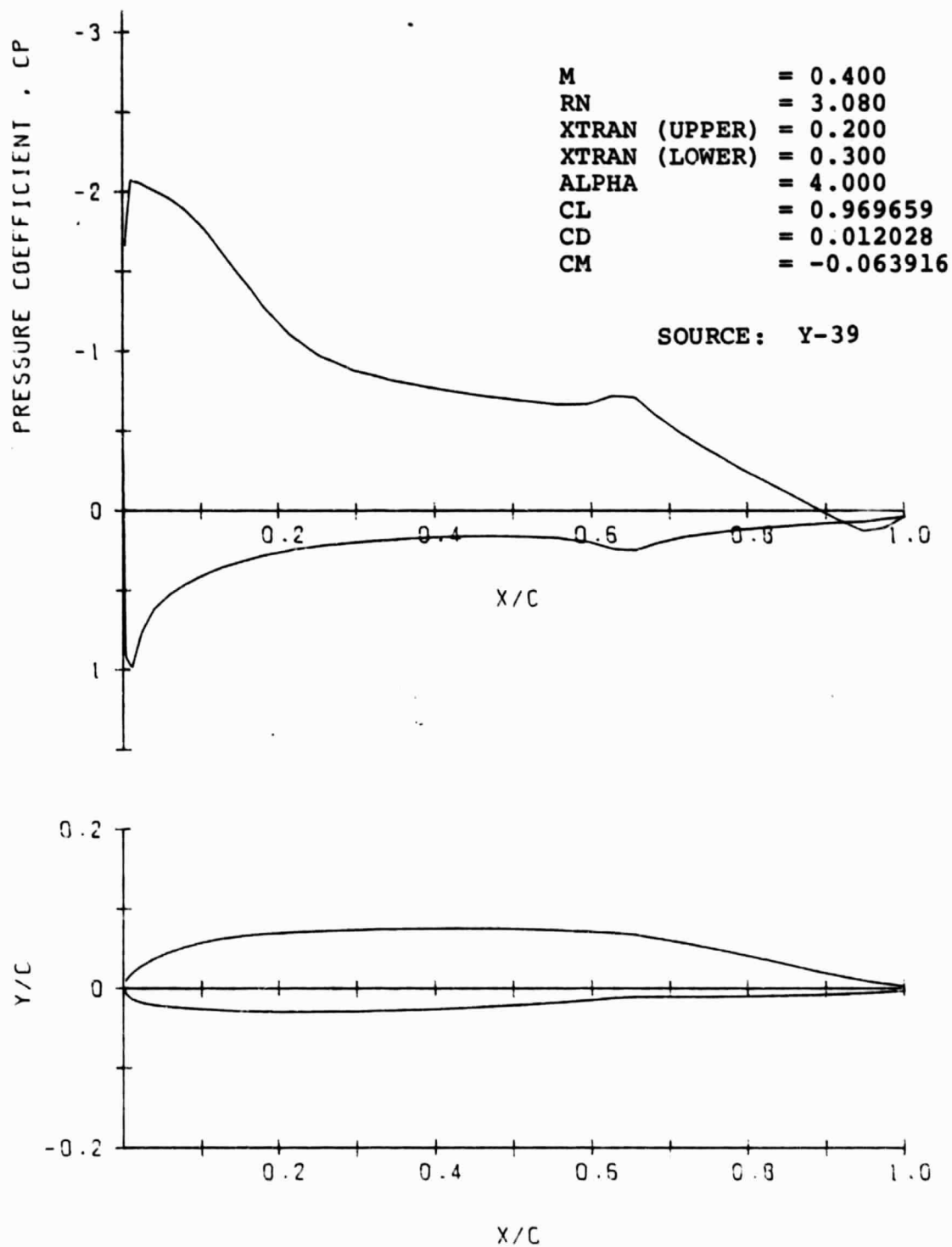


Figure 14 A-1 Airfoil, Mod. 6. 35% Plain Trailing Edge Flap Deflected 5.0°. Pressure Distribution at  $M = 0.4$ ,  $\alpha = 4^\circ$ .

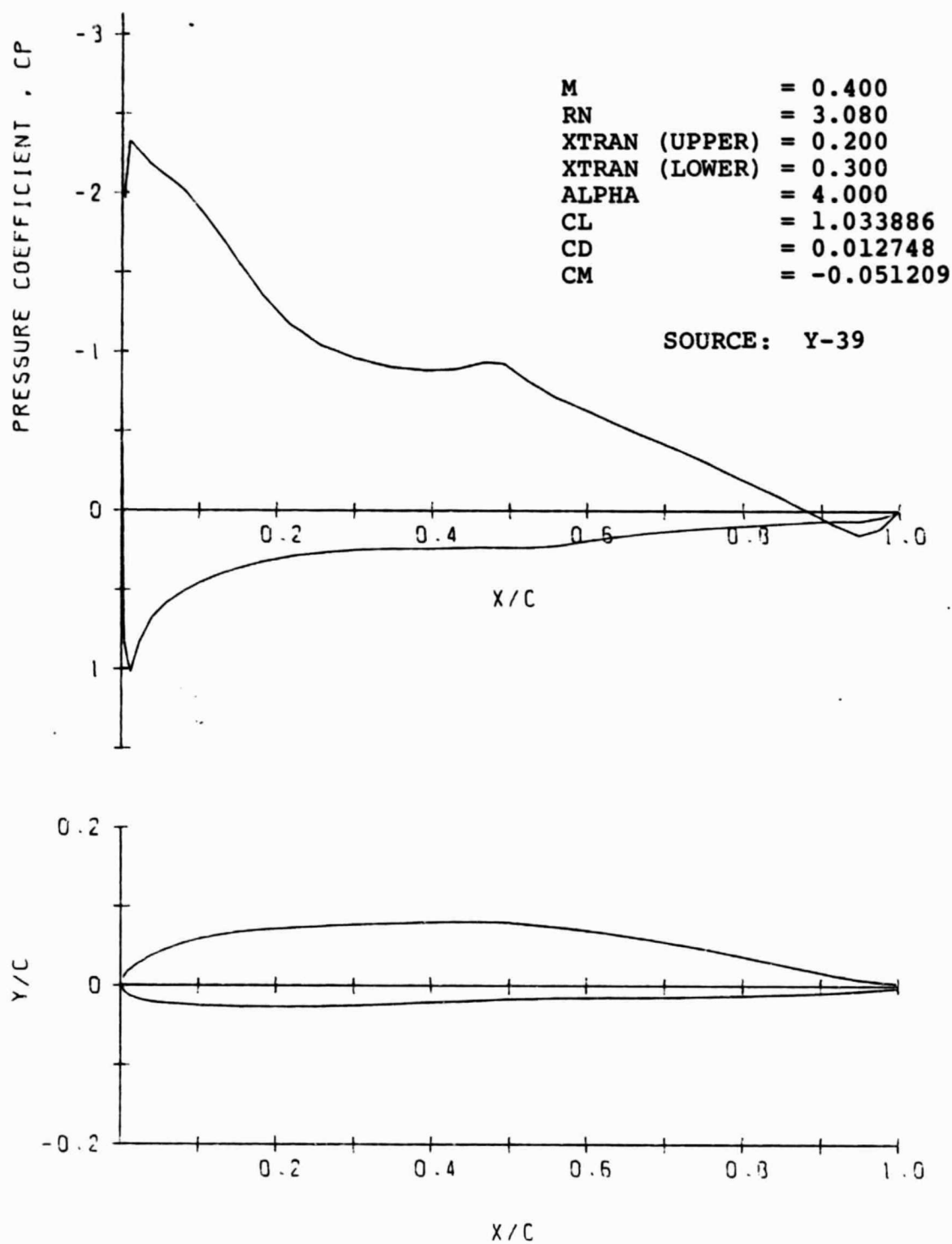


Figure 15 A-1 Airfoil, Mod. 7. 50% Plain Trailing Edge Flap, Deflected  $5.0^\circ$ . Pressure Distribution at  $M = 0.4$ ,  $\alpha = 4^\circ$ .

two-position on/off mode, might turn out to be practical on fixed wing aircraft other than gliders, but cannot be justified for rotor applications at this time.

The most promising concept turned out to be plain, sealed T.E. flaps with relatively small flap angle excursions. Upon 2-D simulation by means of viscous transonic flow methods and subcritical potential flow/boundary layer interaction methods, 35% and 50% plain flaps deployed on the A-1 airfoil proved to be useful in controlling the sectional maximum lift to Mach numbers up to  $M = 0.6$ . The most useful range was within flap angles  $5^\circ$  above and below the neutral position. Useful lift was possible to Mach numbers beyond  $M = 0.8$ , as will be discussed later.

For flap deflections beyond  $5^\circ$  the advantage in flap deployment is restricted to lower Mach numbers, although some useful lift range up to  $M = 0.6$  remains even at the largest flap angles considered ( $15^\circ$ ). In view of the large pitching moments associated with flap deflection it is not likely that, for the flap configurations considered at this time, flap angles much beyond  $5^\circ$  will be practical.

#### 4.0 Variable Camber Modification of Rotor Performance and Loads Analysis Codes

An existing rotor performance analysis, B-65, and an existing loads analysis, C-60, were modified to allow the introduction of variable camber airfoil tables. The basic formulation of B-65 is outlined in Reference 15. The C-60 code is described in Reference 16. As the definition of deployment schedules which would result in a power saving was much harder to accomplish than anticipated, the study was focused on aerodynamic efficiency because loads alleviation alone would not have justified the introduction of a rotor system of this complexity.

##### 4.1 Rotor Performance Analysis, B-65

The variable camber modification of this code has been identified as B-53. The basis for the B-65 and B-53 codes is a model of the wake trailed by each blade, represented by groups of straight vortex segments with linearly varying vorticity from one end to the other of each segment. As illustrated in Figure 16, a root and a tip vortex are rolled up after a fixed azimuthal interval ( $1/8$ th of a revolution) at a radial location which is determined from the instantaneous spanwise blade loading (Betz criteria). The vortex sheet trailed by each blade is modeled by a system of vortices identified as the near-wake, attached to the blade quarter chord line and trailed  $1/24$ th of a revolution ( $\Delta\psi = 15^\circ$ ) and a mid-wake, which extends for two additional time intervals ( $\Delta\psi = 30^\circ$ ) beyond the near-wake.

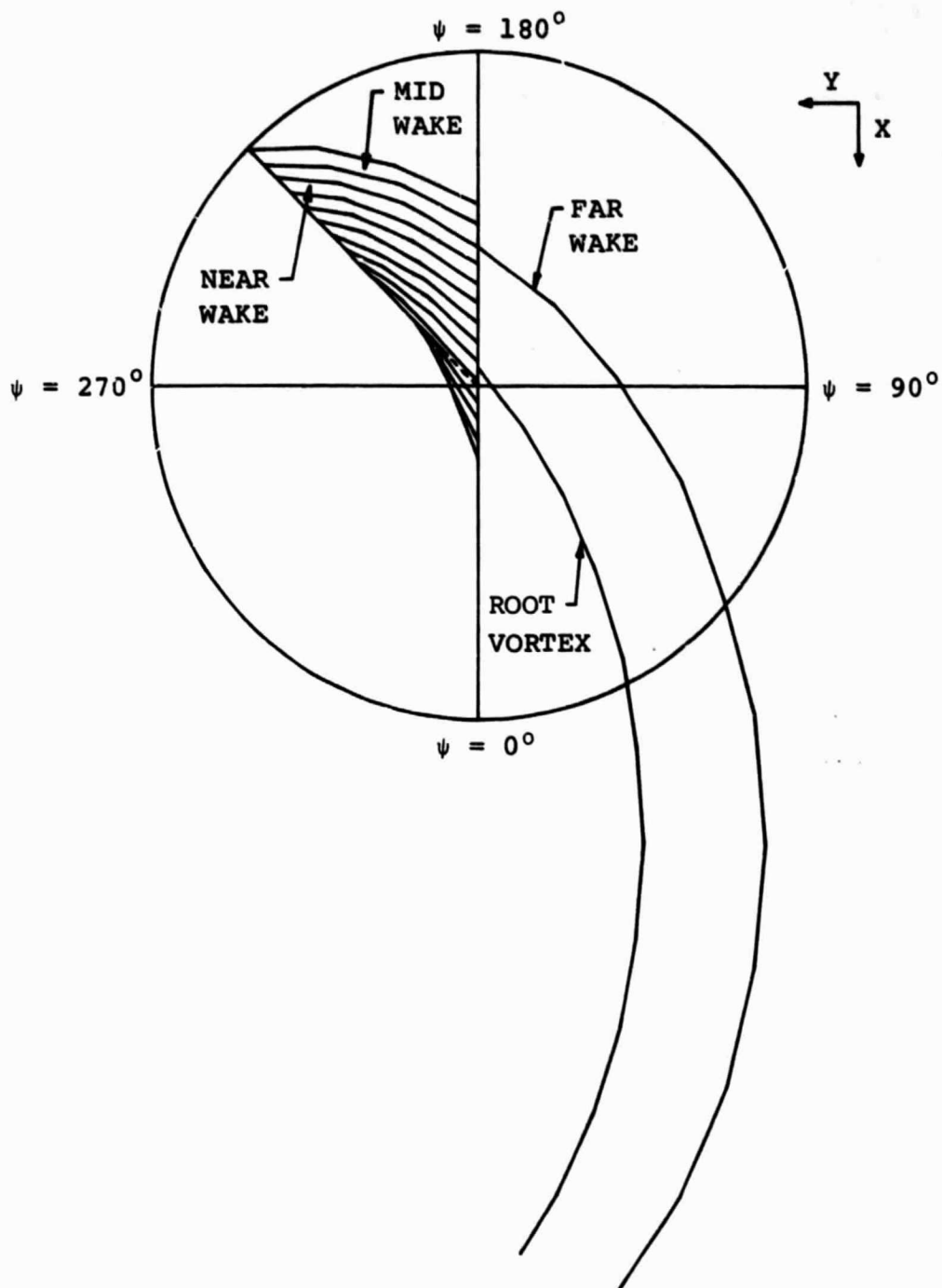


Figure 16 Wake Model in the B-65/B-53 Rotor Performance Analysis.

As the B-65/B-53 codes subdivide a rotor blade into 13 spanwise segments of equal length, from root cutout to tip, the vortex sheet trailed by each blade is represented by 13 horseshoe vortices. Except for the initial "Betz" rollup criteria which set the spanwise location of the tip vortices, the wake model is otherwise rigid, and its displacement is a combination of flight kinematics with a uniform induced downwash velocity.

Blade elastic properties are represented by a modal approach. The aerodynamic formulation, based on a lifting line system, includes an approximation of unsteady aerodynamic effects, dynamic stall delay, radial flow, reverse flow and three-dimensional tip relief effects.

The sectional characteristics are obtained by look-up and interpolation of tables of two-dimensional airfoil data compiled from experimental or analytical sources. The tabulated airfoil characteristics are listed in the following sequence:

- (a) Lift Coefficient,  $C_l$ . Presented as a function of angle of attack at fixed Mach number levels, for angles from  $0^\circ$  to  $20^\circ$ , and from  $-20^\circ$  ( $340^\circ$ ) back to  $0^\circ$  ( $360^\circ$ ), for Mach numbers from  $M = 0.0$  to  $M = 1.0$ , as illustrated in Figure 17. Lift data from  $20^\circ$  to  $340^\circ$  is simulated by equations based on test data for the NACA 0012 airfoil, Reference 14. These equations are independent of Mach number as they are meant to approximate the high-angle-of-attack flow conditions inside the reverse flow circle.
- (b) Drag Coefficient,  $C_d$ . Drag is presented as a function of Mach number, for  $M = 0.0$  to  $M = 1.0$ , at constant angle of attack levels over an angle of attack range which can be specified in the input. An example of drag characteristics is shown in Figure 18. Outside of the specified angle of attack range the drag is approximated by equations independent of Mach number and based on NACA 0012 test data.
- (c) Pitching Moment Coefficient,  $C_{m.25}$ . Pitching moments are tabulated as a function of Mach number, from  $M = 0.0$  to  $M = 1.0$ , for angles of attack from  $0^\circ$  to  $16^\circ$ , and from  $-16^\circ$  ( $344^\circ$ ) to  $0^\circ$  ( $360^\circ$ ). Figure 19 shows an example for the basic A-1 airfoil. Equations based on NACA 0012 data cover the rest of the high angle of attack range.

The lift, drag and pitching moment data at high angles of attack used in all current Boeing Vertol codes are summarized in Figure 20.

In B-53, the variable camber version of B-65, the airfoil table lookup has been expanded to include interpolation on

ORIGINAL PAGE IS  
OF POOR QUALITY

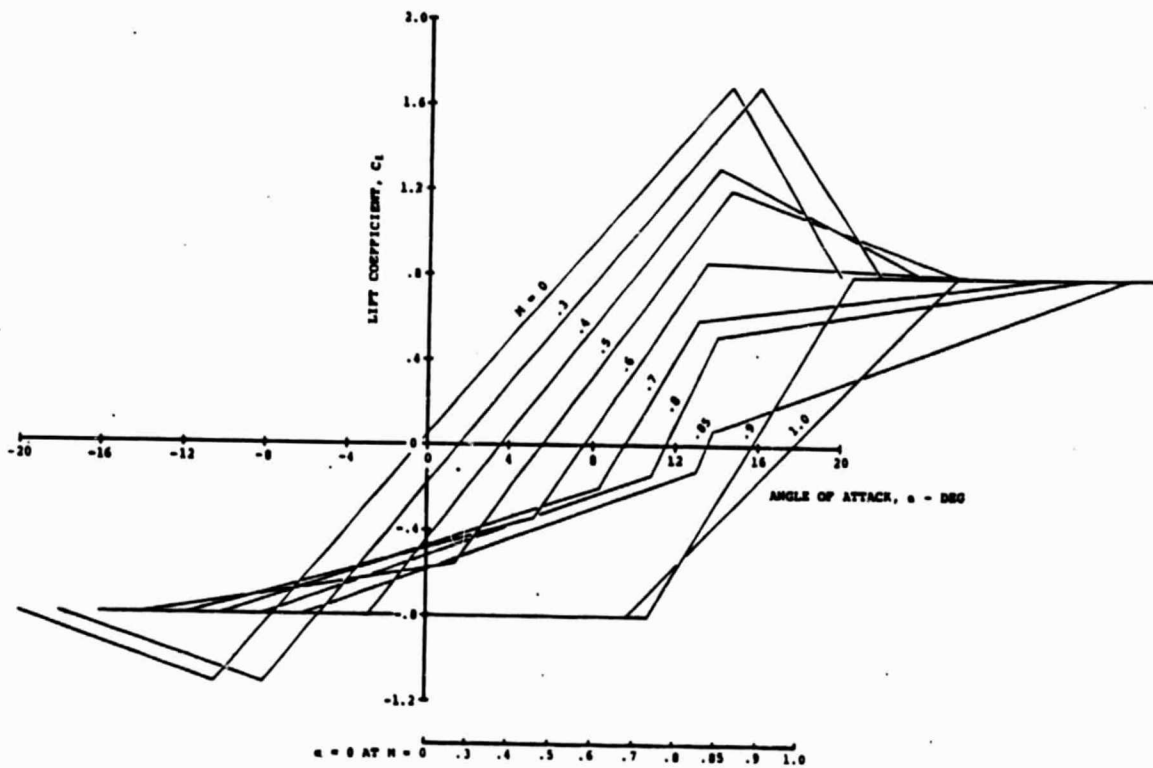


Figure 17 Lift Coefficient Table for the A-1 Airfoil.

ORIGINAL PAGE IS  
OF POOR QUALITY

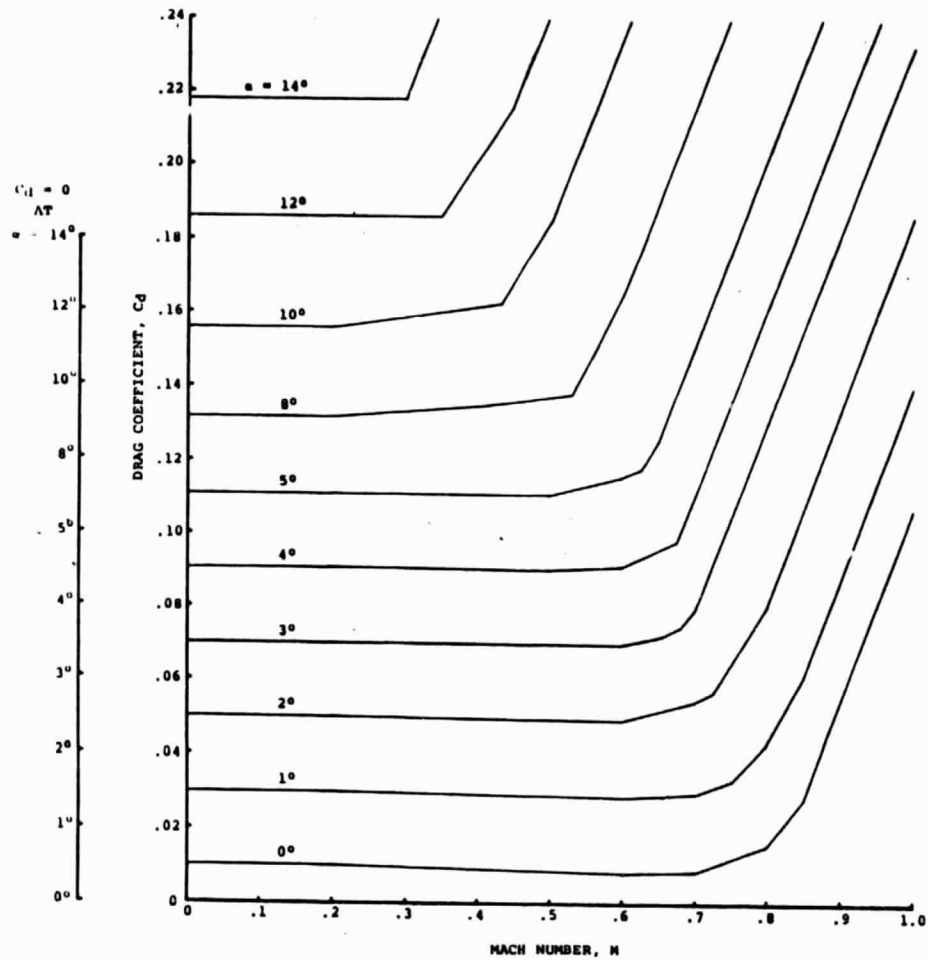


Figure 18 Drag Coefficient Table for the A-1 Airfoil.

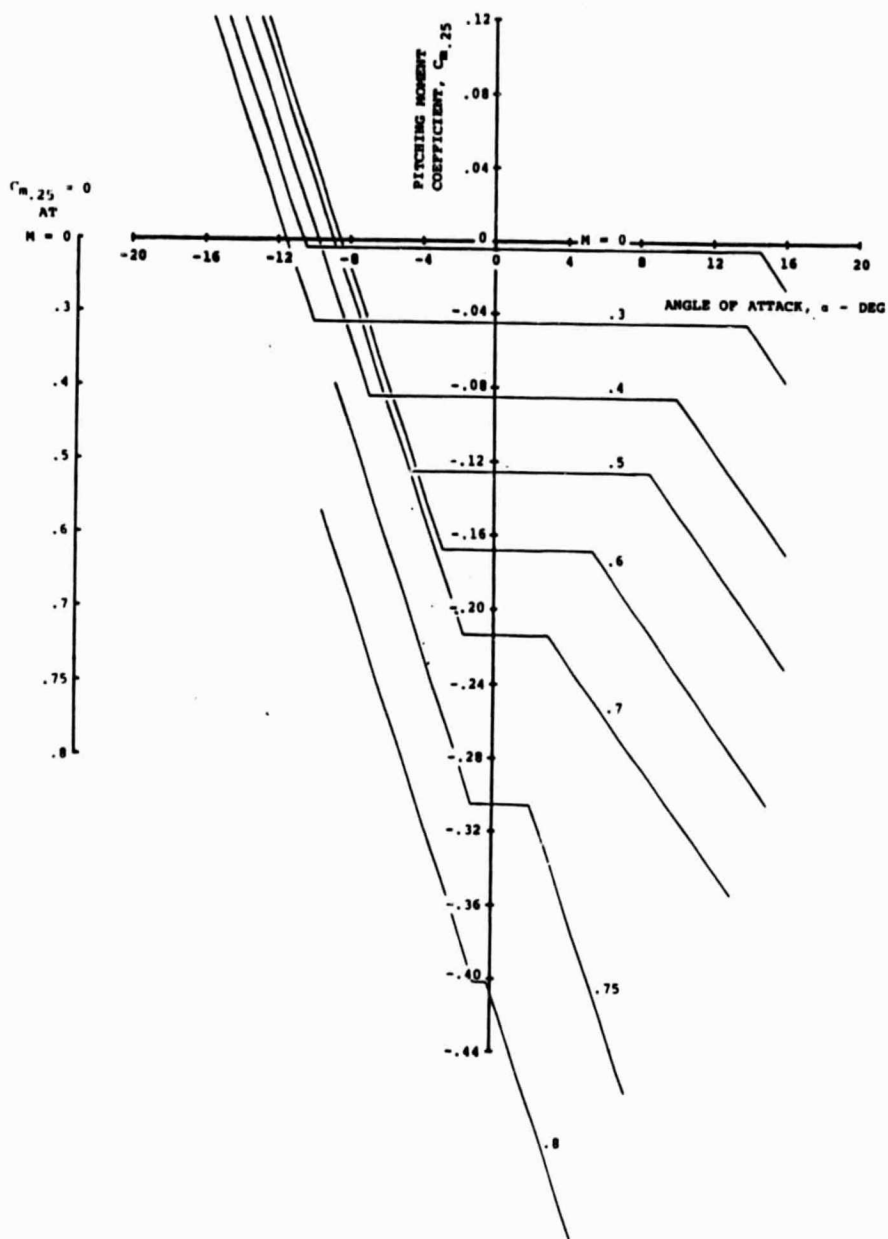


Figure 19 Quarter Chord Pitching Moment Coefficient  
Table for the A-1 Airfoil.

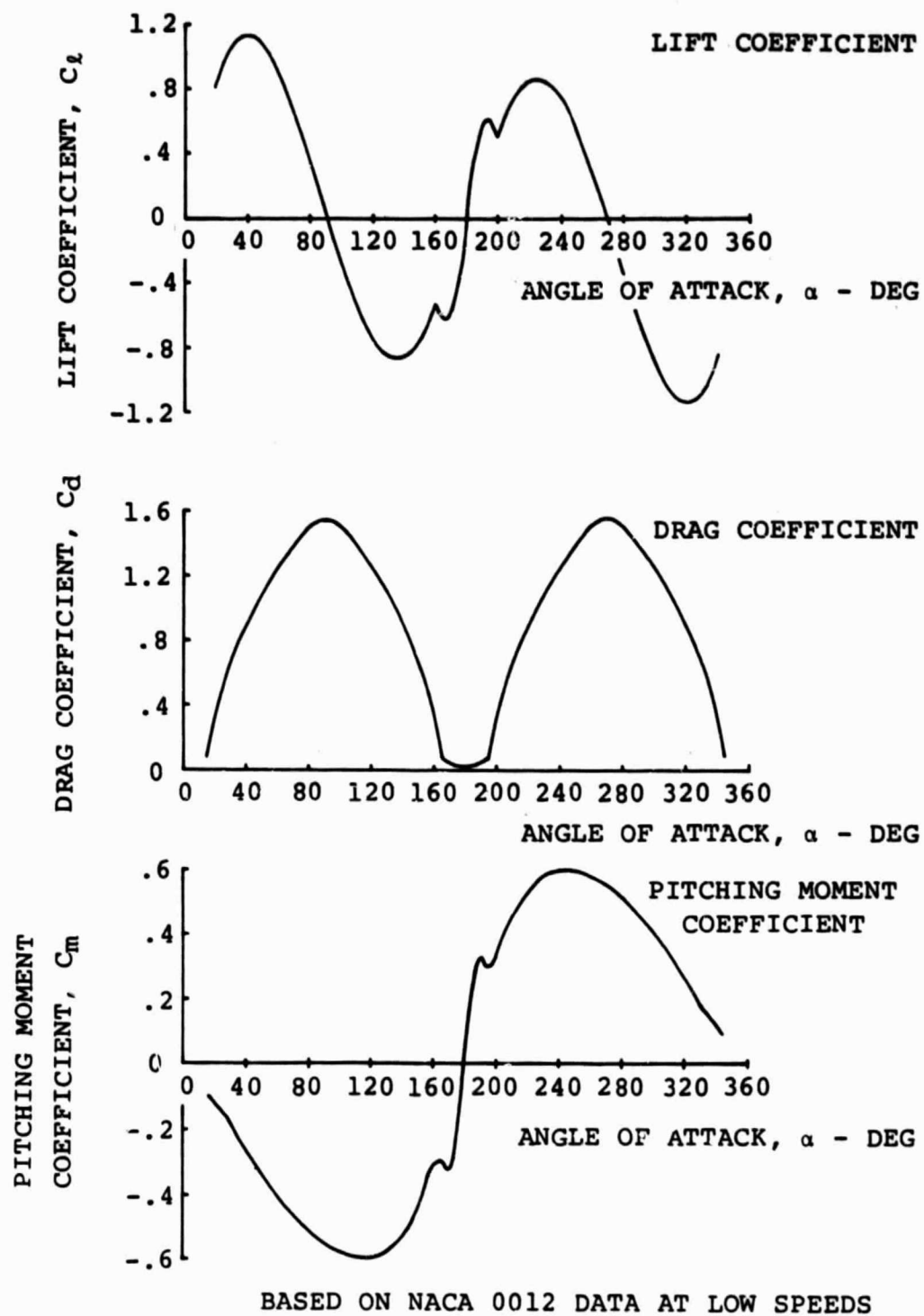


Figure 20 High Angle of Attack Data.

the basis a camber level. This camber level can be expressed in any convenient way: as a percentage of camber, or as a flap deflection angle. Where B-65 has provisions for up to five sets of airfoil tables specified along the span of a rotor blade, with the added dimension of camber level, B-53 can be input with up to 25 sets of tables, encompassing 5 camber levels for each of the 5 radial data stations. The sectional characteristics at each of the 13 computation stations are interpolated from the data stations.

On the assumption that the variable camber devices could be mass balanced about their hinge (as for instance a flap hinge), and that the entire blade section could be locally mass-balanced about the quarter chord, each segment equipped with a variable camber device would then be entirely accounted for by a local increase in mass, from which mode shapes and frequencies can be calculated.

To simplify the modeling of the variable camber distributions, provisions have been made to prescribe independent variable camber levels for each of the (up to) 13 blade panels. At each computation panel, the camber can be prescribed either as a Fourier series consisting of a steady value and up to two harmonics, or as a complete set of values prescribed for each azimuth position. The latter method allows the input of any deployment schedule, including constant level on/off schedules.

By assigning each variable camber segment to one computation panel (1/13th of the span, as measured from the root cutout to the tip) it was possible to provide enough resolution to evaluate complex variable camber schemes without unnecessary complexity in spanwise interpolation.

Another benefit of this approach is that while the current wake model cannot account for any of the secondary rollup of the vortex sheet due to highly localized lift variations, each computation panel will carry its own horseshoe vortex for  $\Delta\psi = 45^\circ$  (i.e. 1/8 of a revolution). It remains to be shown, for variable camber deployed near the tip, that the vorticity due to secondary rollup would not be already rolled up into one main tip vortex by the next blade passage.

The unsteady and radial flow corrections of B-53 are a simplification of the model described by R. Gormont in Reference 17. Transonic 3-D relief corrections for the drag coefficient have been introduced following the procedure outlined by LeNard in References 18 and 19. Lift curve slope corrections to account for tip relief have been worked out by I. Levacic. Tip relief on pitching moments is carried out by relieving the 2-D data at Mach numbers beyond  $M = 0.7$  by  $AR = 1.0$  trends.

#### 4.2 Description of the C-60/C-84 Rotor Load Codes

This analysis has been developed at Boeing Vertol by the Rotor Dynamics Group. A detailed description of C-60 can be found in Reference 16.

C-60, and hence C-84, consist of a lumped-mass representation of a rotor blade including up to 50 masses. The airloads are evaluated on a relatively coarse radial and azimuthal grid from which dense airload distributions can be generated by interpolation and harmonic analysis.

Although C-60 has provisions for a trailed vortex sheet, satisfactory airloads have been calculated by means of induced velocities from the root and tip vortices only.

Without the limitations of the modal approach of R-65/B-53, the C-60/C-84 analysis can evaluate the motions and deflections of a rotor blade in whatever complexity the dynamics and aerodynamics of the problem dictate. Blade and control loads can be then defined and analyzed in detail with the harmonic content.

Although the current C-84 code does not model a variable camber rotor in all its possible structural complexity, it will simulate the key element of the problem and utilize the correct aerodynamic inputs through a multiple table lookup and interpolation procedure analogous to the procedure introduced into B-53. As C-60 has provisions for three sets of basic airfoil tables, with the added dimension of five (5) camber levels C-84 will accept up to fifteen (15) sets of airfoil tables.

#### 5.0 Definition of the Sectional Characteristics of Variable Camber Airfoils

Having decided that plain T.E. flaps were the best choice of variable camber alternative for the current study, as described in Section 3.1, the two-dimensional characteristics of the A-1 airfoil with T.E. flaps were evaluated by means of the following airfoil analysis methods:

- 1) The potential flow boundary/layer interaction code by Stevens, Goradia and Braden, Reference 20, available at Boeing Vertol as code Y-39.
- 2) A modification of the above code by G. Brune, Reference 21.
- 3) The viscous transonic analysis by Bauer, Garabedian, Korn, and Jameson, Reference 22 available at Boeing Vertol as Code A-37.

- 4) The 2-D separated flow analysis by M. Henderson, TEA 456, Reference 23. A similar code by Analytical Methods, Inc. (AMI), Reference 24, is available on Government computing facilities.

### 5.1 Baseline Airfoil (0° Flap Deflection Angle)

The NASA Ames A-1 airfoil, designed and tested by McCroskey and Hicks, Reference 25, was selected as the best candidate for variable camber studies because:

- (a) It is one of the latest advanced airfoils designed for helicopter rotors and it is very close to be as optimized as it is possible within current design constraints.
- (b) It has been designed by means of up-to-date transonic airfoil analysis methods.
- (c) It is well suited for use along the entire span of a rotor blade, i.e. its camber and thickness make it a good compromise both as a tip section and a midspan "working" section.

The coordinates of the A-1 airfoil are shown in Table II. The A-1 contour is shown in Figure 21. Key maximum lift and drag divergence characteristics of the A-1 are compared to other helicopter rotor airfoils in Figure 3.

The lift, drag and pitching moment coefficients of the A-1 have been evaluated by means of the airfoil analysis codes used to evaluate the sectional performance in presence of variable camber modifications. The performance measured in the wind tunnel test of Reference 25 was compared with the performance estimated by means of the airfoil codes. Test and theory were in good agreement at all but a few conditions, but, in order to provide a smooth transition in sectional performance when deploying variable camber, the calculated performance of the basic A-1 contour was not adjusted to the test levels. Empirical adjustments between test and theory would be generally small, and they would not contribute to the validity of the assessment of the usefulness of variable camber.

In terms of test/theory correlation the biggest discrepancy is in the level of  $C_{l_{max}}$  was at  $M = 0.3$ , where the measurements yielded a value of  $C_{l_{max}} = 1.33$  and the analysis  $C_{l_{max}} = 1.69$ . At  $M = 0.4$ , however, the agreement is good,  $C_{l_{max}} = 1.325$  for test vs.  $C_{l_{max}} = 1.30$  for theory, and this is particularly significant because the maximum lift level

ORIGINAL PAGE IS  
OF POOR QUALITY

$x/c$	$y_U/c$	$y_L/c$
0.00000	0.00000	0.00000
.00020	.00238	-.00223
.00050	.00377	-.00338
.00100	.00541	-.00472
.00200	.00766	-.00651
.00350	.01013	-.00844
.00500	.01214	-.00995
.00650	.01388	-.01120
.00800	.01543	-.01227
.01000	.01732	-.01350
.01250	.01945	-.01482
.01600	.02214	-.01634
.02000	.02490	-.01777
.02500	.02801	-.01922
.03500	.03335	-.02137
.05000	.03991	-.02365
.06500	.04523	-.02549
.08000	.04961	-.02710
.10000	.05421	-.02902
.12500	.05829	-.03104
.15000	.06098	-.03277
.20000	.06344	-.03551
.25000	.06431	-.03727
.30000	.06446	-.03828
.35000	.06409	-.03866
.40000	.06316	-.03848
.45000	.06154	-.03782
.50000	.05924	-.03665
.55000	.05623	-.03501
.60000	.05249	-.03297
.65000	.04792	-.03056
.70000	.04246	-.02785
.75000	.03600	-.02486
.80000	.02860	-.02153
.85000	.02064	-.01786
.90000	.01260	-.01374
.92500	.00899	-.01144
.95000	.00598	-.00888
.97500	.00392	-.00603
.99000	.00322	-.00421
1.00000	.00299	-.00300

TABLE II- COORDINATES FOR THE A-1 AIRFOIL

6' 3047 2400 100  
YTHA-0 6 1 1



Figure 21 A-1 Airfoil Contour.

at  $M = 0.4$  appears to dominate the retreating blade stall characteristics. At  $M = 0.5$  subcritical airfoil theory ( $C_{l_{\max}} = 1.08$ ) underpredicts the test level ( $C_{l_{\max}} = 1.26$ ), although the use of transonic analysis (A-37) improves the prediction ( $C_{l_{\max}} = 1.2$ ). At Mach numbers above  $M = 0.6$  the "useful" range rather than maximum lift should be emphasized, and the lift limits were set mostly on the basis of local Mach number considerations, whether the solution was obtained from a subcritical or a transonic analysis. The calculated "useful" lift range does not match exactly the maximum lift levels measured in the report of Reference 25.

Another difference between test and theory is in the location of the aerodynamic center. In the test report it was mentioned that the airfoil design predicted a zero lift pitching moment  $C_{m_0}$  within  $\pm 0.01$ , while the test measurements showed  $C_{m_0}$  generally exceeding  $-0.01$ .

Figure 22 compares measured and predicted pitching moments, about the quarter chord for  $M = 0.3$ . The results from the Y-39 analysis show that the aerodynamic center is forward, as evidenced by a positive  $dC_m/d\alpha$ . The results from the A-37 analysis, however, show a negative  $dC_m/d\alpha$  with a characteristic similar to the test data but shifted towards zero  $C_m$ . It should be pointed out that the A-37 transonic analysis does not account for the development of a laminar boundary layer, and that turbulent boundary calculations are started at a prescribed location near the leading edge (in this case at  $0.05c$ ). The Y-39 analysis was run allowing natural transition between the leading edge and  $0.20c$  on the upper surface and  $0.30c$  on the lower. Since the location of the aerodynamic center sometimes is a function of the extent of laminar flow (or phenomenon observed on other airfoils similar to the A-1), it was decided to assume that, for the purposes of the current variable camber study, the aerodynamic center remain at the quarter chord over the entire range of attached flow conditions.

The profile drag levels assumed for the basic A-1 are in general agreement with the measured levels except where the drag would be influenced by laminar flow extending either beyond  $0.20c$  on the upper surface or  $0.30c$  on the lower. Drag "buckets", where present, were faired out.

One last difference between test and theory is in the variations of  $dC_l/d\alpha$  and  $dC_m/d\alpha$  at high angle of attack levels, when approaching  $C_{l_{\max}}$ . While the test data show some changes in lift and pitching moment slope while approaching stall, the A-1 airfoil tables are defined linear in lift and moment from the angle of attack for negative stall to the angle of attack for positive stall, as illustrated in Figure 17. This

ORIGINAL PAGE IS  
OF POOR QUALITY

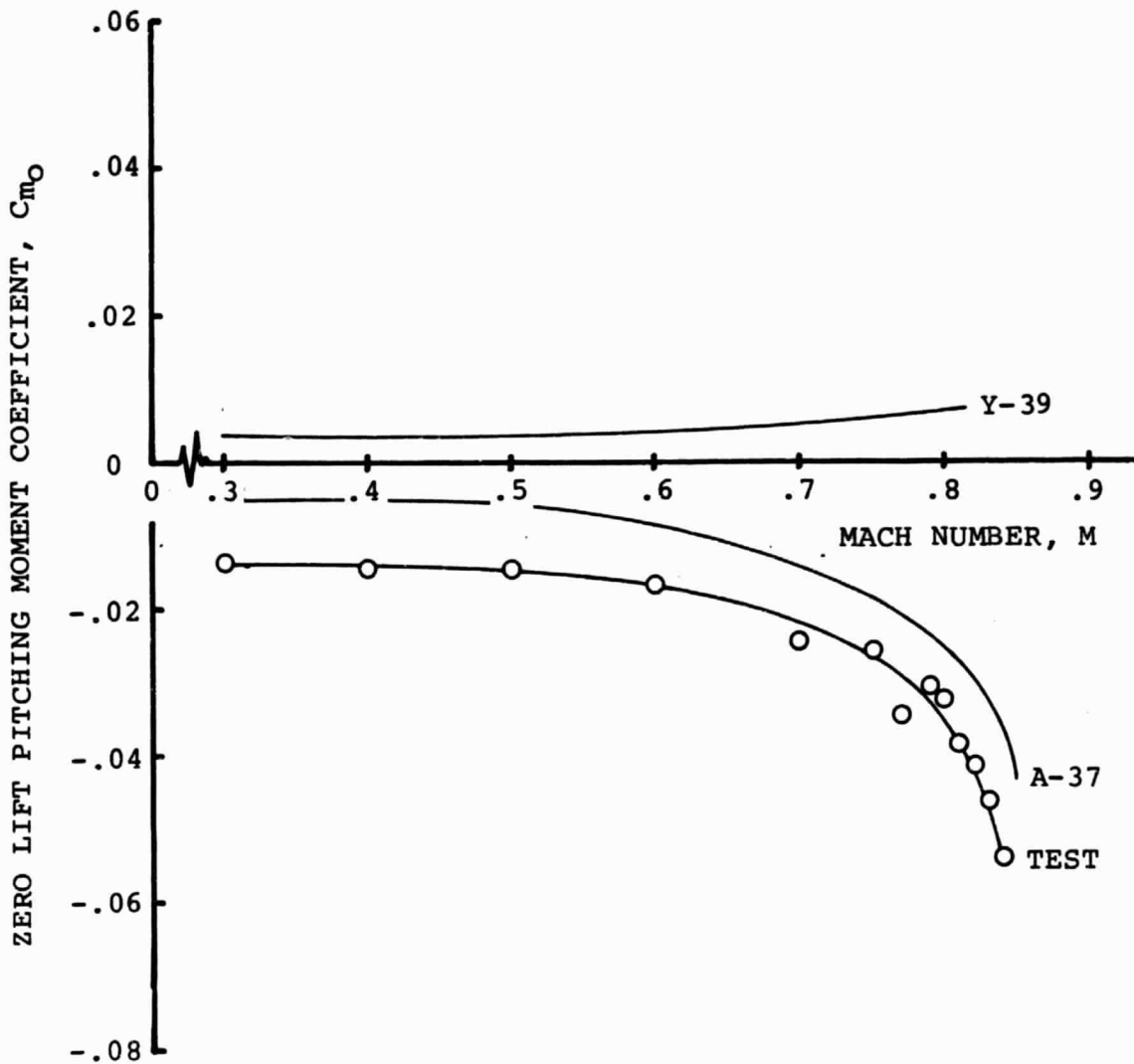


Figure 22 Comparison of Measured and Calculated Pitching Moments for the A-1 Airfoil.

was done to facilitate the definition of sectional characteristics for the flapped configurations and to eliminate a possible source of discontinuities in the rotor performance and loads calculations.

## 5.2 Procedures to Evaluate the Characteristics of the A-1 Airfoil with 0.35C and 0.50C T.E. Flaps

The characteristics of the baseline A-1 section and the A-1 airfoil with plain, sealed, T.E. flaps were calculated mainly by means of the Y-39 and A-37 codes (Reference 20 and 22). The separated flow analysis of Reference 23 was used extensively at the start of the study, but after the ground rules to formulate the airfoil tables were finalized it became less necessary to evaluate details of the flow separation process. The TEA 456 analysis was then used only to verify specific conditions. Similarly, the TEA 315 code, Reference 21, was used only at selected conditions.

The basis for the prediction of the characteristics of the flapped airfoils is as described in Reference 9. As discussed there in some detail, the key to the prediction of maximum lift at the Mach numbers of interest for helicopter rotor studies is that, above  $M = 0.3$ , the phenomena which precipitate stall take place sufficiently abruptly to allow an estimate of the maximum lift from observation of the conditions leading to stall, without the need for a separated flow model. This balance between viscous and compressible flow effects is particularly true at  $M = 0.4$ . At  $M = 0.3$  viscous effects may be more dominant than at  $M = 0.4$ , with some inaccuracy in  $C_{l_{max}}$  resulting from predictions which do not model the separated flow region. At  $M = 0.5$  the maximum lift prediction should be carried out by means of both subcritical potential flow/boundary layer analysis and viscous transonic flow analysis to verify whether or not there are beneficial transonic flow effects present near the leading edge of the airfoil. The A-1 section does benefit of some of these favourable effects, as demonstrated by a comparison of the A-37 and Y-39 estimates of  $C_{l_{max}}$  (1.20 vs. 1.08), although neither code matches (nor should it be expected to match exactly) the test level ( $C_{l_{max}} = 1.26$ ).

As illustrated in Figures 23 and 24 the range of "useful" lift, whether comparable to a measured maximum lift, or based on the growth of the drag coefficient to some appropriate value, can be assessed by observing when analysis will first detect:

- (a) The attainment of  $M_{local} = 1.4$  anywhere on the surface, or

ORIGINAL PAGE IS  
OF POOR QUALITY

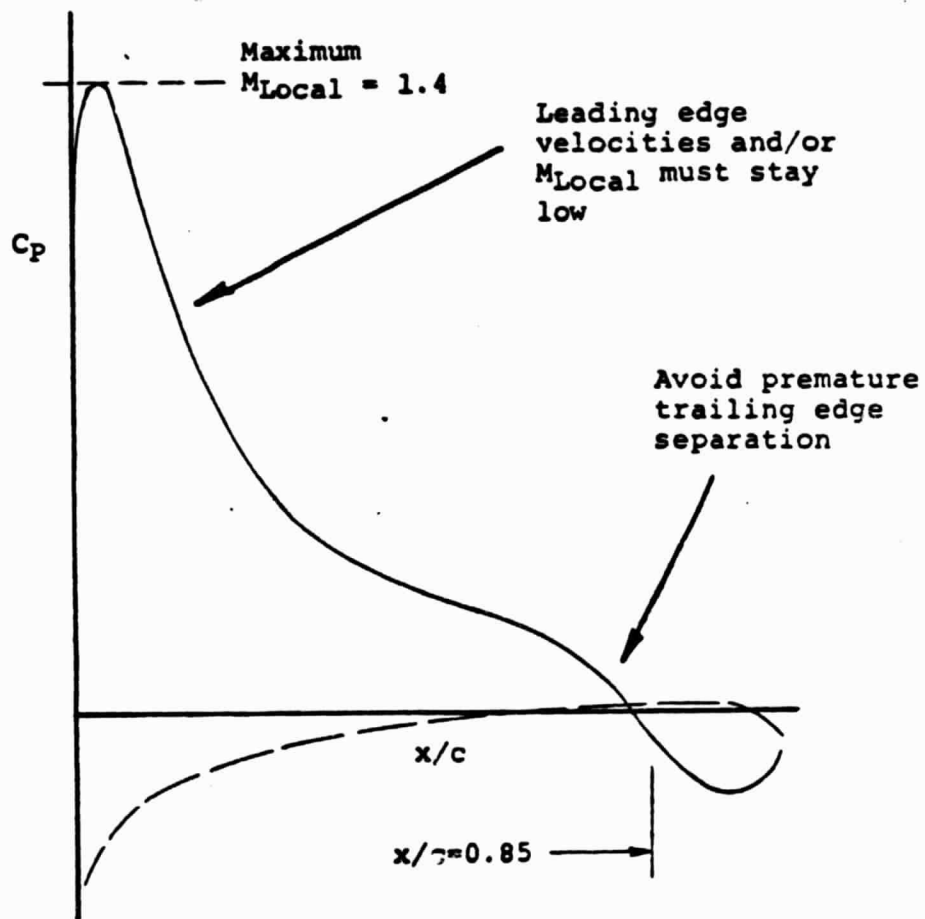


Figure 23 Evaluation of Maximum Lift Levels from Airfoil Analysis Results.

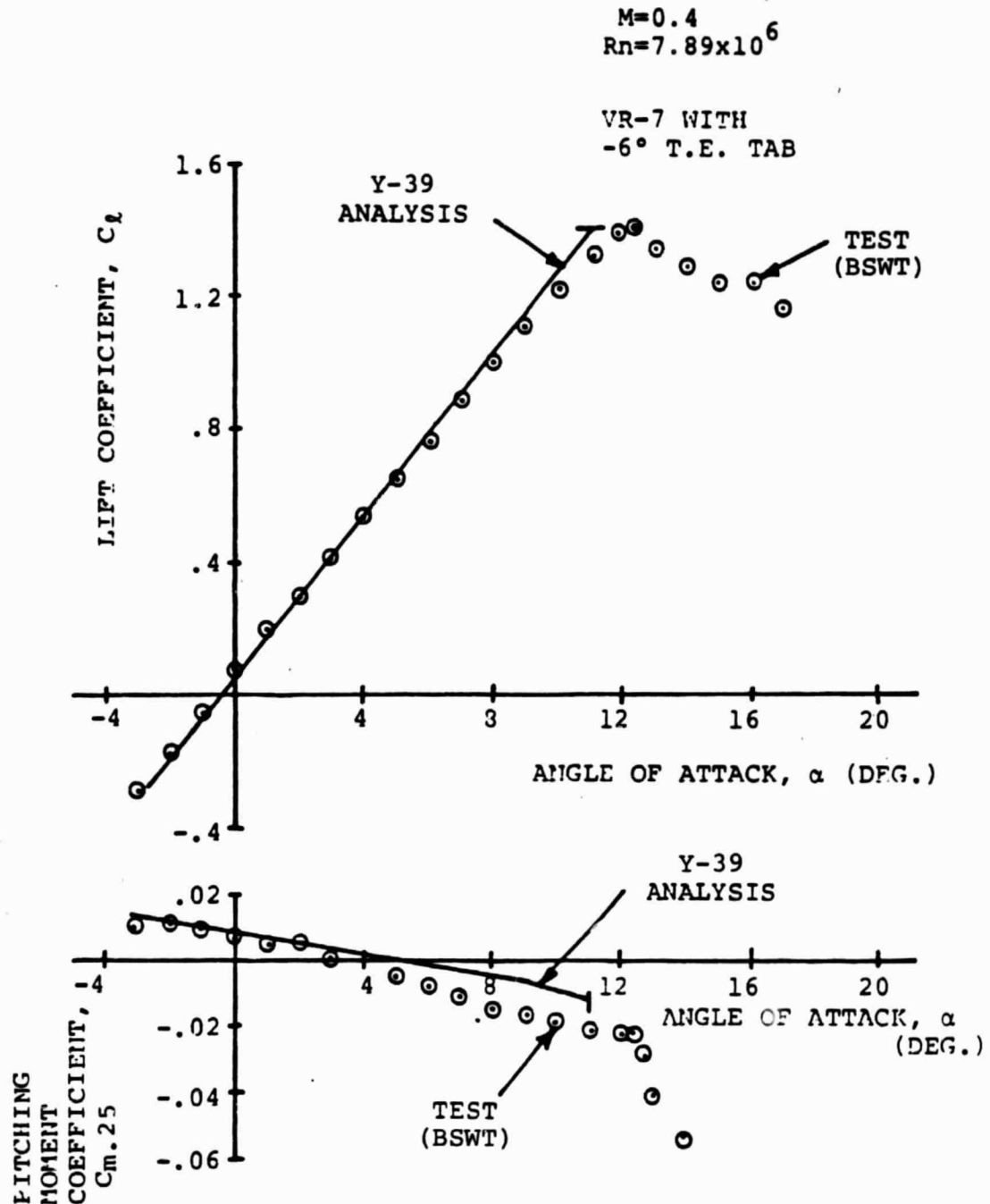


Figure 24 Test/Theory Correlation of Lift and Moment Data for the VR-7 Airfoil.

- (b) The movement of turbulent boundary layer separation point from the trailing edge,  $x/c = 1.0$ , to  $x/c = 0.85$  ( $x/c = 0.90$  with same codes, as determined by calibration with test data).

When  $M_L = 1.4$  is first reached at or near the leading edge of a section, the stall is likely to have a "leading edge" stall character (abrupt, with large static stall hysteresis). Conversely if the maximum lift is limited by T.E. separation the stall can be classified as gradual (T.E. stall or thick airfoil stall).

When studying airfoils with flaps (particularly of the plain type) the local Mach number allowed over the knee of the flap should be restricted to  $M_L \cong 1.0$  or some level below  $M_L = 1.1$ . The limit of  $M_L = 1.4$  is truly applicable only to laminar boundary layers, as observed in the test of Reference 26, and it should not be assumed that, in presence of substantial supersonic flow, the flow would remain attached over the aft half of airfoils, particularly with the destabilizing influence of a flap. This additional restriction was not exercised over the range of conditions examined in this study because  $Cl_{max}$  was always limited either by L.E. velocities or by T.E. separation.

The Mach number for drag divergence,  $M_{DD}$ , is defined by determining the free stream Mach number for which  $dC_d/dM = 0.1$  when Mach number is increased at constant angle of attack (a traditional wind tunnel measurement procedure).  $M_{DD}$  can be evaluated analytically with methods which have been shown to be quite reliable for standard high speed airfoil sections.

These methods are:

- (a) Crest line theory, described in detail in Reference 27,  
(b) The viscous transonic analysis of Reference 22.

Of the two methods, crest line theory is the more cost effective and efficient technique, as long as detailed information on the transonic characteristics of an airfoil are not needed. Crest line theory is based on the observation that the onset of drag rise can be determined from an incompressible and inviscid airfoil solution by calculating the free stream Mach number for which the flow at the "crest" of an airfoil would first become sonic (on the basis of a compressibility correction such as the Karman-Tsien rule). The "crest" of an airfoil is a point on the surface tangent to a line parallel to the remote wind. What crest line theory implies is that when the local supersonic flow extends beyond the crest of an airfoil the pressure drag becomes significant. Reference 27 describes in detail test/theory correlation efforts which lead to the definition of the crest line approach. The

recommended crest Mach number limit is  $M_c = 1.02$ . A further assessment of drag rise effects can be obtained from observation of the incompressible pressure distributions plotted against a skewed coordinate,  $y'/c$  as illustrated in Figure 25. While the significance of the shape of the so-called suction loops is not important in the present study, it is relevant to note that the maximum value of  $y'/c$  corresponds to the crest of the airfoil. In the event that two crests must be considered (upper and lower surface) the crest corresponding to the lower free stream Mach number will set the drag divergence limit.

Once the drag divergence Mach number has been assessed for a given angle of attack, the corresponding incompressible lift coefficient can be corrected to account for compressibility up to such Mach number value. By repeating this process over a range of angles of attack it is possible to estimate the drag divergence boundary at positive as well as negative lift levels, as illustrated in Figure 26. On cambered airfoils the degradation in drag divergence Mach number with lift is more pronounced over the range of negative lifts, although the largest delay in drag divergence generally takes place at a small negative lift level. Test/theory correlation has shown that the analytical drag divergence boundary should be increased by  $\Delta M_{DD} = 0.02$  for better agreement with wind tunnel measurements. This increment was used in evaluating the variable camber airfoils of the present study.

It remains to be demonstrated experimentally to what extent crest line theory is applicable to sections employing a substantial amount of camber or T.E. flaps. However, in the evaluation of the current variable camber configurations the results of crest line theory were utilized only within the "useful" lift range defined by the local Mach number and separation criteria outlined earlier.

As already mentioned in discussing the data for the A-1 airfoil, the Y-39 potential flow/boundary layer interaction predictions were carried out by restricting the transition from laminar to turbulent boundary layer to take place within  $0.20c$  on the upper surface, and within  $0.30c$  on the lower surface. In the A-37 viscous transonic analysis the transition was fixed to  $0.05c$  on both surfaces.

In presence of a limited extent of turbulent boundary layer separation, the drag coefficient calculated in the Y-39 analysis was corrected by an increment based on the drag of truncated airfoils, suggested by Hoerner, Ref. 28. Beyond drag divergence, a fixed rate of change of the drag coefficient with Mach number,  $dC_d/dM = 0.053$  was obtained from a survey of the airfoil data of Reference 14. This rate of change was applied to the drag curves beyond drag divergence to extend the definition of drag to  $M = 1.0$ .

ORIGINAL PAGE IS  
OF POOR QUALITY

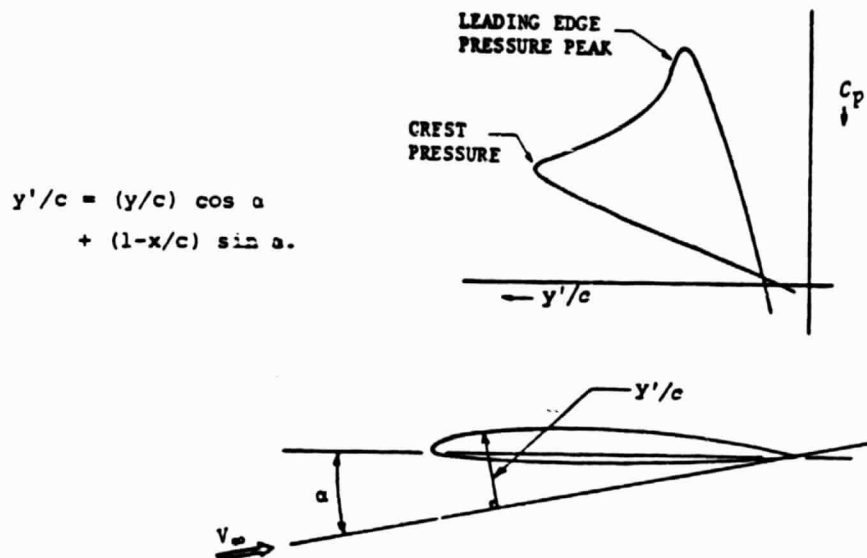


Figure 25 Definition of Suction Loop.

ORIGINAL PAGE IS  
OF POOR QUALITY

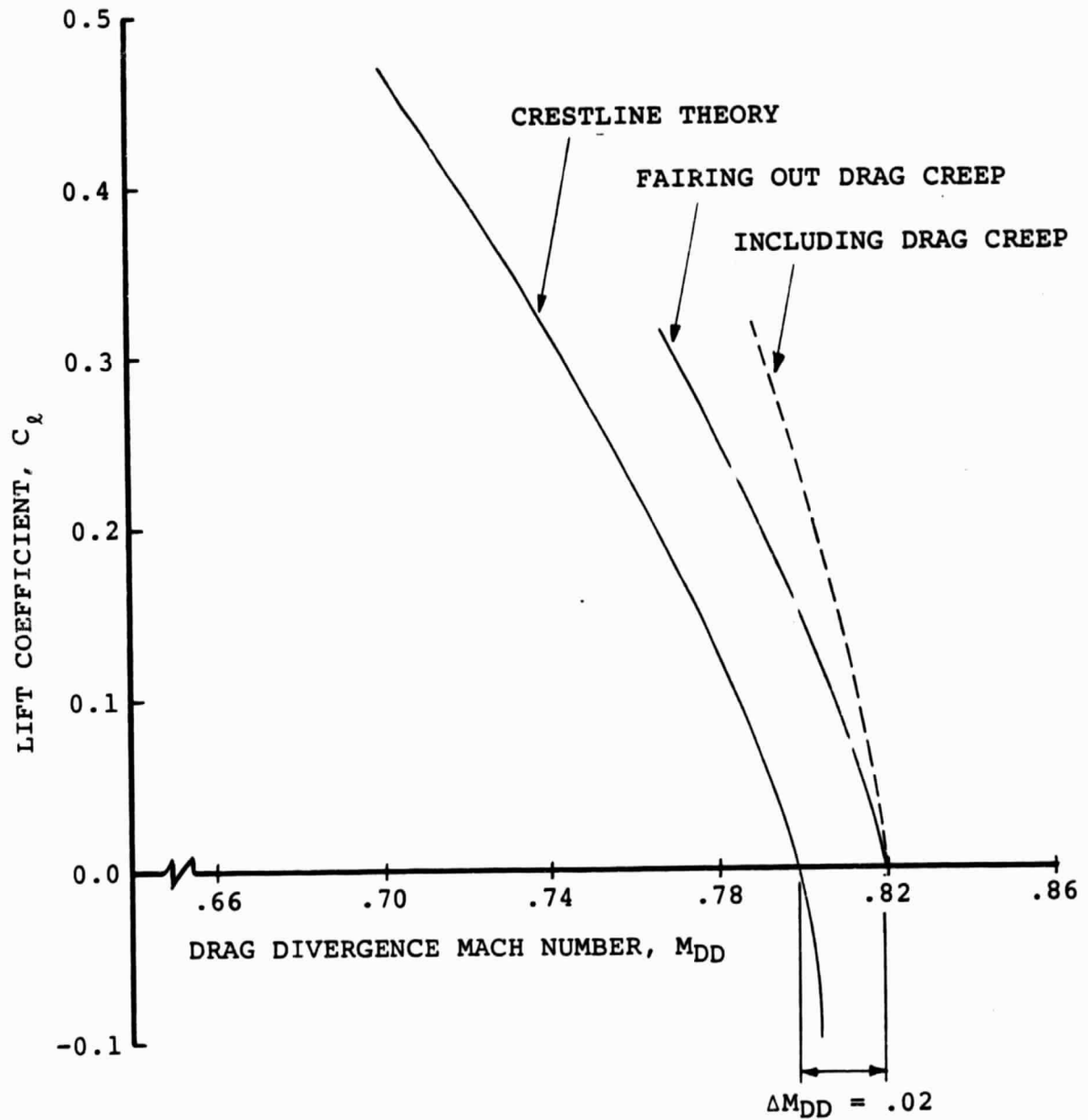


Figure 26 Example of Drag Divergence Boundaries.

### 5.3 Sectional Characteristics of the A-1 Airfoil With a 0.35c T.E. Flap

Figure 27 shows the contours of the A1 airfoil with a 35% plain T.E. flap deflected from  $-5^\circ$  (above the reference chord line) to  $15^\circ$  (below the chordline). The flap excursions were selected to provide a range of variable camber levels which would cover all the applications foreseen at this time. This includes provisions to decamber the airfoil over the advancing blade, and a range of positive camber changes in excess of the level for which an increase in  $C_{l_{max}}$  can be expected at  $M = 0.3$  for possible retreating blade stall alleviation. No special precautions were taken to optimize the contour at the knee of the flap, although if it were assumed that by some flexible skin arrangement the curvature of the flap knee contour could be reduced, some performance improvement would probably result from a delay in turbulent boundary layer separation at the T.E. The contour coordinates are listed in Appendix A.

The estimated maximum lift coefficients for the A-1 airfoil with a 35% chord flap, for each of the flap settings, are summarized in Table III for positive angles of attack and Table IV for negative angles of attack. These boundaries are also summarized and compared in Figure 28. A flap deflection of  $\pm 5^\circ$  results in an increment in  $C_{l_{max}}$  but does not change the trend with Mach Numbers. Deflections of  $10^\circ$  and  $15^\circ$  severely degrade the maximum positive lift capability to values lower than for  $0^\circ$  deflection.

The lift curve slope and the angles of zero lift as a function of Mach number are listed in Tables V and VI, and shown in Figures 29 and 30. The "flap effectiveness" of this configuration, defined as the rate of change of the angle of zero lift with flap deflection angle, is between 0.67 and 0.68. By comparison, the values quoted by Abbott and Von Doenhoff, Reference 29, for a 35% plain flap are 0.65 for the fairing through test data, and 0.71 from thin airfoil theory. Flap deflection has no impact on lift curve slope up to a Mach Number of .65 and reduces the slope with positive deflections beyond  $M = 0.65$ .

Figures 31 through 35 show the maximum positive and negative lift range with the angle of attack distribution for each flap deflection. Superimposed on these figures are the corresponding drag divergence boundaries for each flap deflection angle:  $-5.0^\circ$ ,  $0.0^\circ$ ,  $5.0^\circ$ ,  $10.0^\circ$ , and  $15.0^\circ$ .

The information from Figures 31 through 35 combined with the drag data from the Y-39, A-37 and TEA 456 was used to generate the trends of drag coefficient as a function of Mach number at constant angle of attack, as necessary to prepare the airfoil tables. The procedure is outlined in Figure 36 for drag.

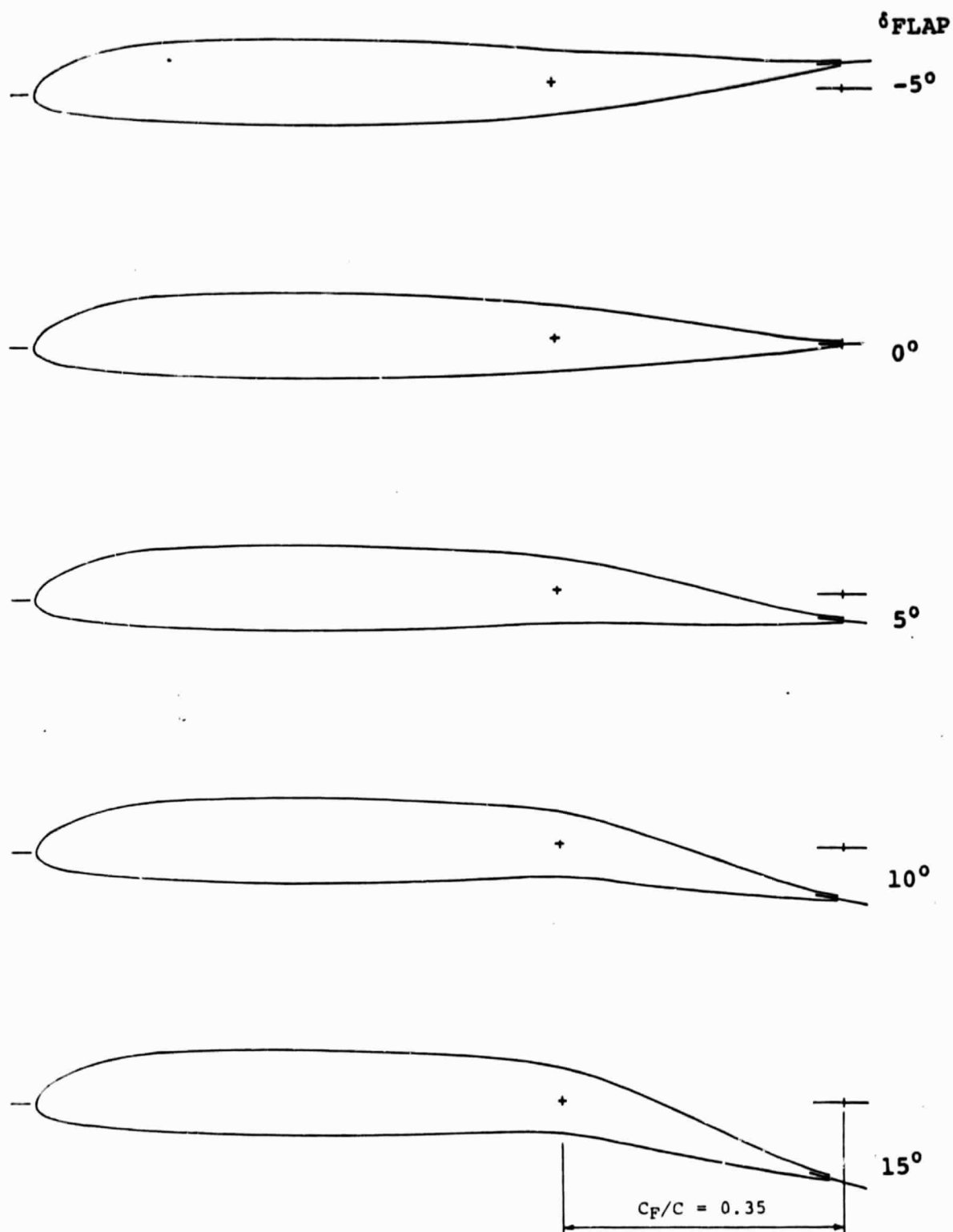


Figure 27 A-1 Airfoil with a 0.35c Plain T.E. Flap.

TABLE III

Estimated Positive Maximum Lift Characteristics of  
the A-1 Airfoil with a 0.35C Plain T.E. Flap

	MAXIMUM LIFT COEFFICIENT, $C_{LMAX}$ AT MACH NUMBER							
$\delta_F$	0.3	0.4	0.5	0.6	0.65	0.7	0.8	0.85
-5°	1.54	1.13	0.99	0.66		0.35	0.21	.14
0°	1.69	1.30	1.2	0.86		0.59	0.51	.075
5°	1.82	1.5	1.41	1.06		0.81	0.54	
10°	1.96	1.31	1.08	0.93	0.6	0.36		
15°	1.4	1.02	.975	.5				

TABLE IV

Estimated Negative Maximum Lift Characteristics of  
the A-1 Airfoil with a 0.35C Plain T.E. Flap

	MAXIMUM NEGATIVE LIFT COEFFICIENT, $C_{LMIN}$ AT MACH NUMBER							
$\delta_F$	0.3	0.4	0.5	0.6	0.7	0.8	0.85	
-5°	-1.34	-.99	-.74	-.52	-.48	-.4	0.01	
0°	-1.12	-.8	-.55	-.34	-.2	-.14	-.2	
5°	-1.0	-.6	-.35	-.10	.07	.15		
10°	-.62	-.42	-.16	.08	.3			
15°	-.54	-.31	.03	0.3				

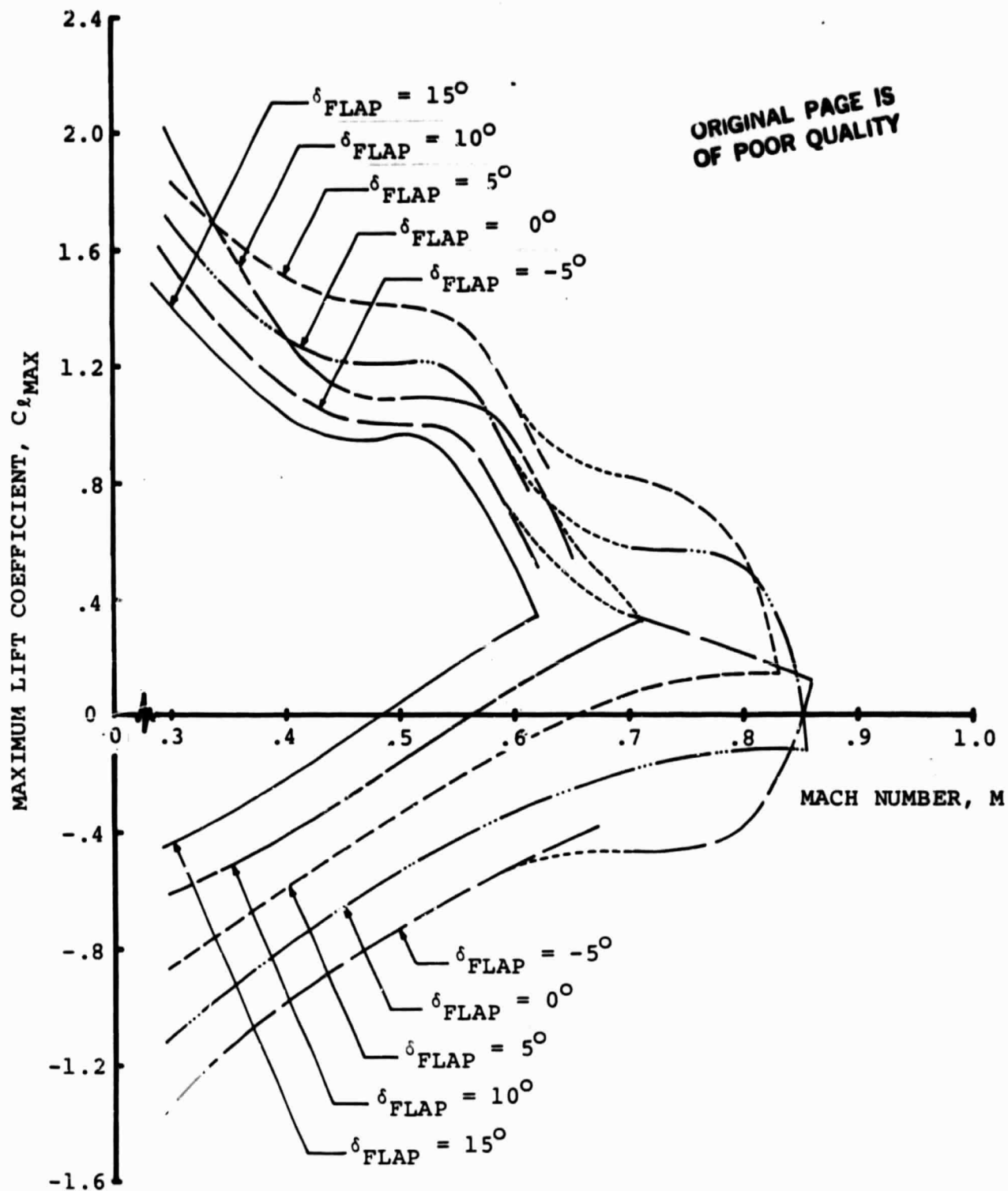


Figure 28 Estimated Maximum Lift Boundaries for the A-1 Airfoil with a 0.35c Plain T.E. Flap.

TABLE V

Estimated Lift Curve Slope Variation with Mach  
Number for the A-1 Airfoil with a 0.35C Plain T.E. Flap

	Lift Curve Slope, $dC_l/d\alpha$ (Deg <sup>-1</sup> ) at Mach Number										
$\delta f$	0.0	0.3	0.4	0.5	0.6	0.7	0.75	0.8	0.85	0.9	1.0
-5	.1127	.1181	.1242	.1328	.1462	.1675		.203	.2198	.1616	.10
0	.1123	.1177	.124	.133	.1465	.166		.2	.214	.164	.10
5	.1120	.1174	.1239	.133	.1468	.1663		.1871	.1903	.166	.10
10	.1122	.1176	.1246	.133	.1466	.166		.18	.172	.148	.10
15	.1120	.1174	.125	.133	.1464	.16	.165	.162	.15	.133	.10

TABLE VI

Estimated Effect of Compressibility on the Angle for  
Zero Lift of the A-1 Airfoil with a 0.35C Plain T.E. Flap

	Angle for Zero Lift, $\alpha_0$ (Deg) at Mach Number										
$\delta F$	0.	.3	.4	.5	.6	.65	.7	.8	.85	.9	1.0
-5	2.97	2.97	2.96	2.95	2.94	2.92	2.92	2.9	3.02	2.69	2.03
0	-.45	-.45	-.44	-.46	-.46		-.47	-.52	-.47	-.41	-.3
5	-3.87	-3.87	-3.87	-3.86	-3.84		-3.9	-3.7	-3.78	-3.32	-2.42
10	-7.26	-7.26	-7.25	-7.22	-7.17	-7.10	-7.04	-7.06	-7.42	-7.81	-8.58
15	-10.59	-10.59	-10.55	-10.49	-10.37		-11.25	-12.1		-13.0	-13.74

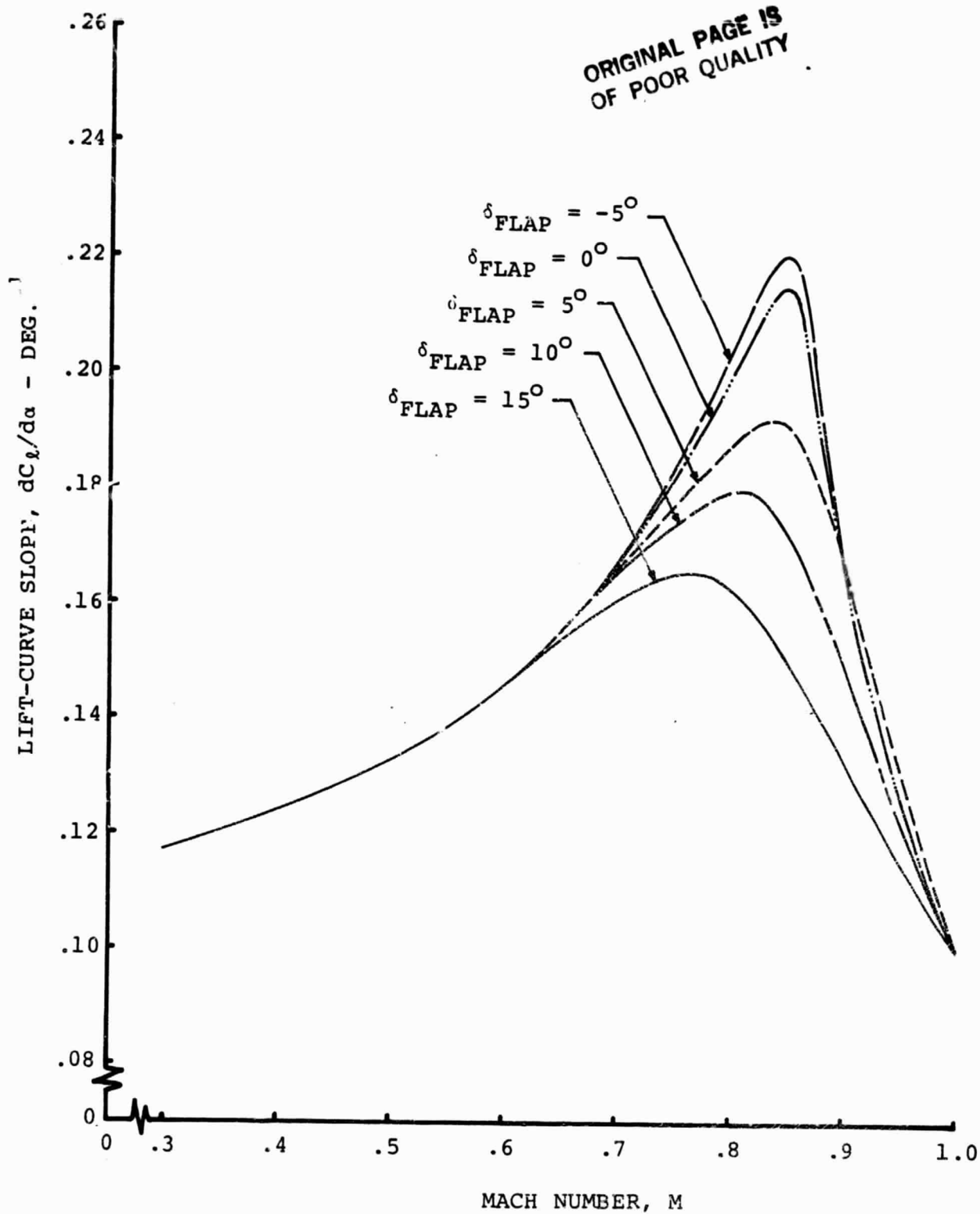


Figure 29 Lift Curve Slope of the A-1 Airfoil with a 0.35c Plain T.E. Flap.

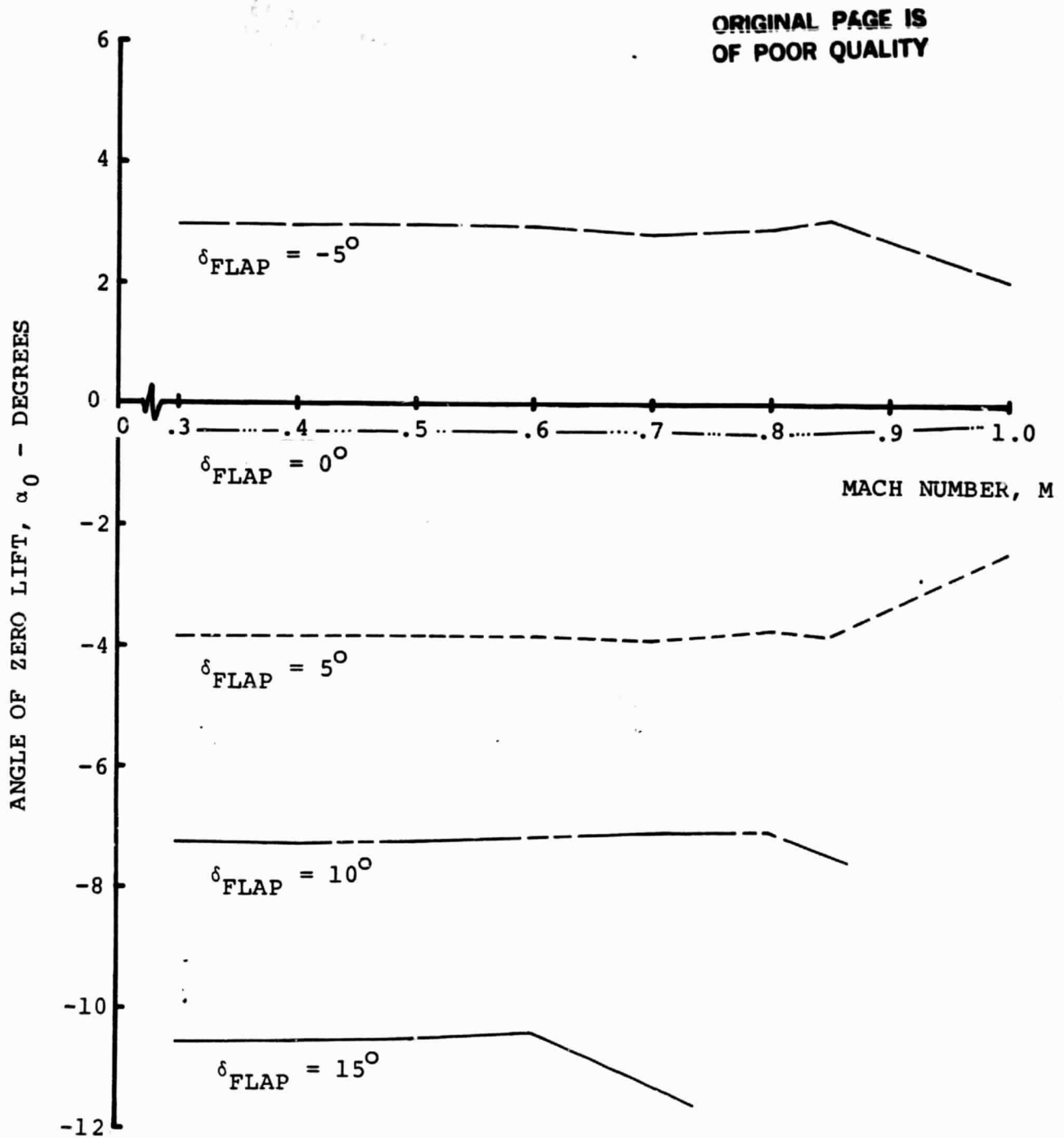


Figure 30 Angle of Zero Lift for the A-1 Airfoil with a 0.35c Plain T.E. Flap

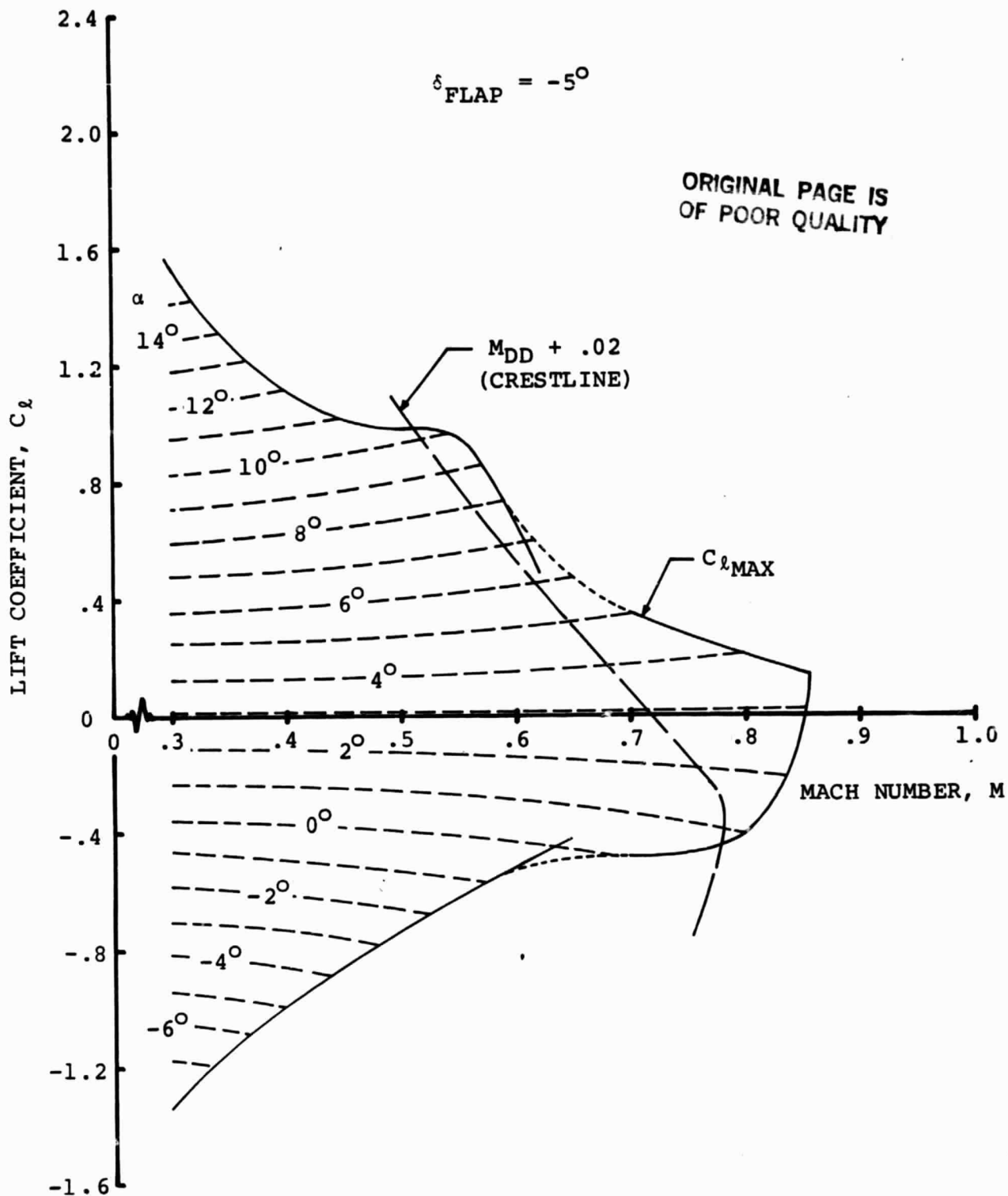


Figure 31 Maximum Positive and Negative Lift Boundaries for the A-1 Airfoil with a 0.35c Plain T.E. Flap.  $\delta_{\text{Flap}} = -5.0^\circ$ .

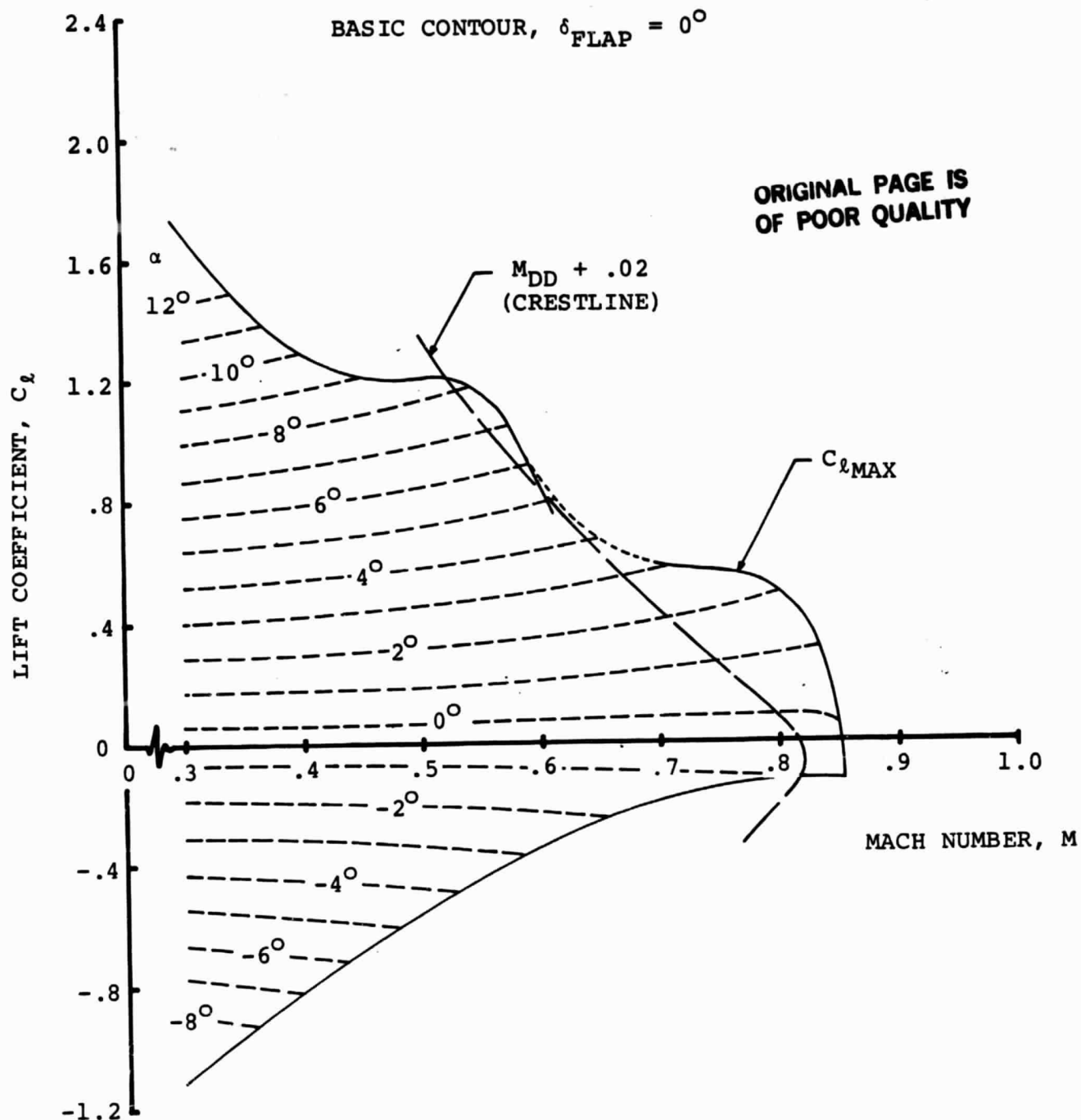


Figure 32 Maximum Positive and Negative Lift Boundaries for the A-1 Airfoil with a 0.35c Plain T.E. Flap.  $\delta_{\text{Flap}} = 0.0^\circ$ .

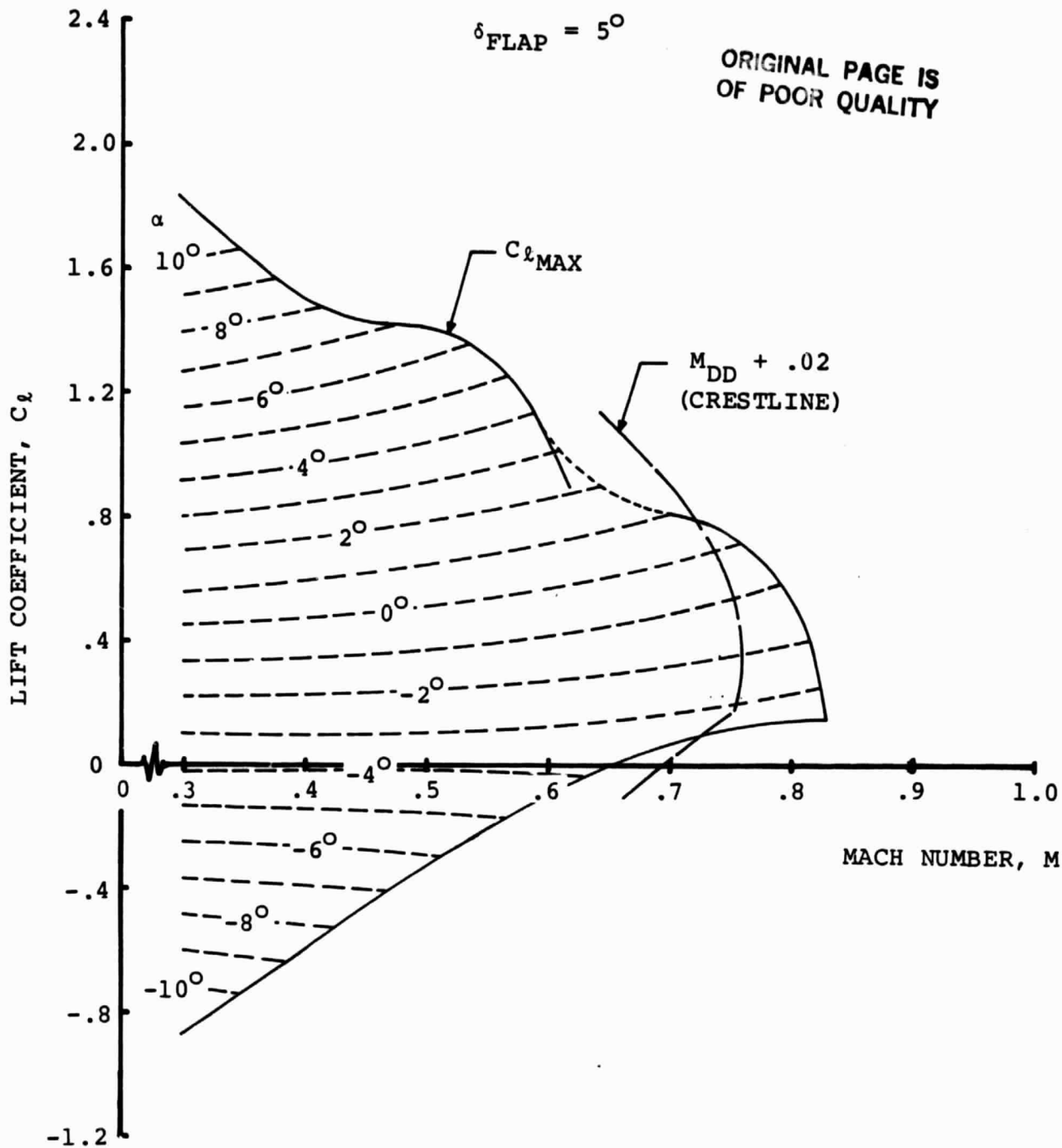


Figure 33 Maximum Positive and Negative Lift Boundaries for the A-1 Airfoil with a 0.35c Plain T.E. Flap.  $\delta_{\text{Flap}} = 5.0^\circ$ .

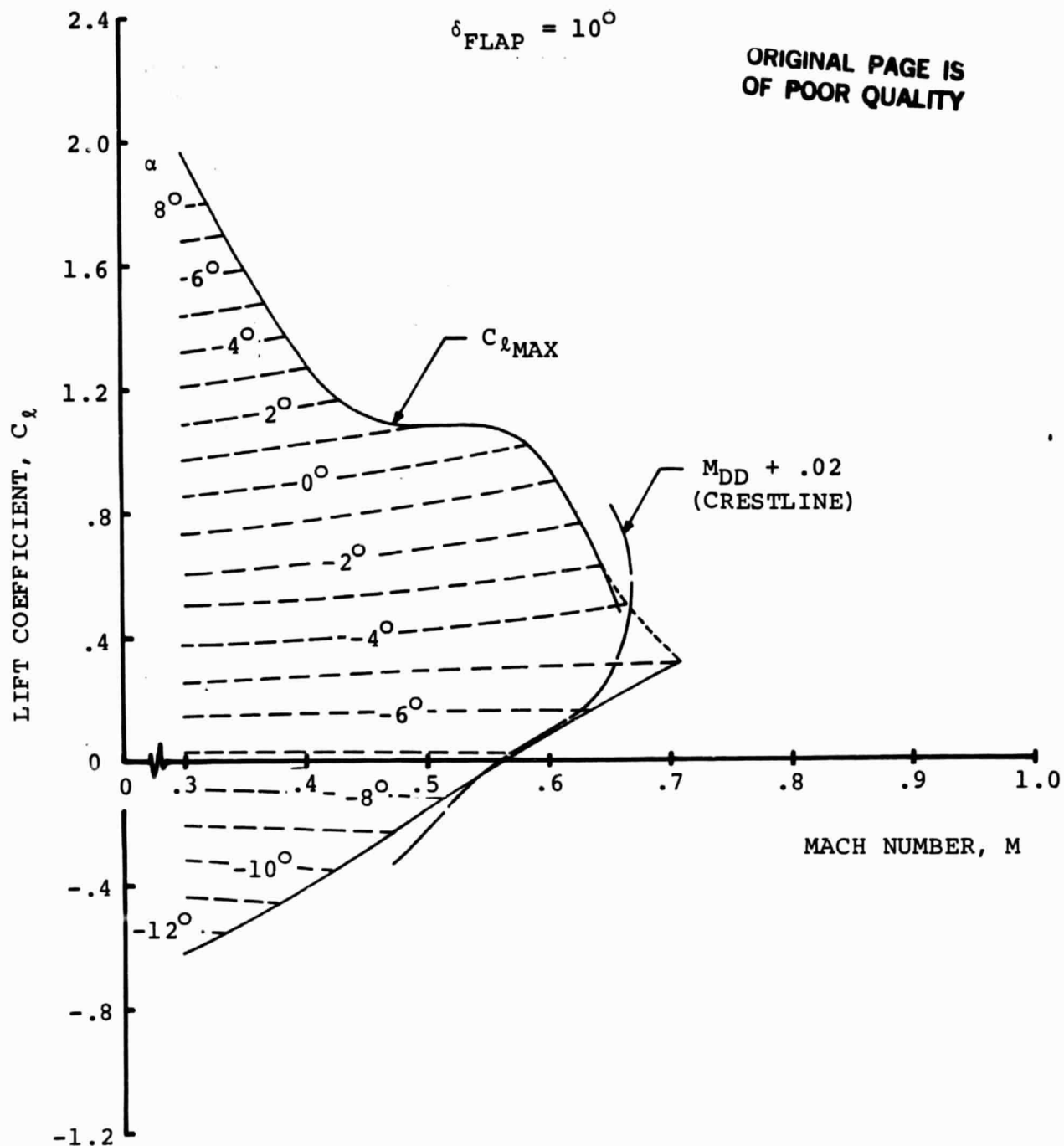


Figure 34 Maximum Positive and Negative Lift Boundaries for the A-1 Airfoil with a 0.35c Plain T.E. Flap.  $\delta_{\text{Flap}} = 10.0^\circ$ .

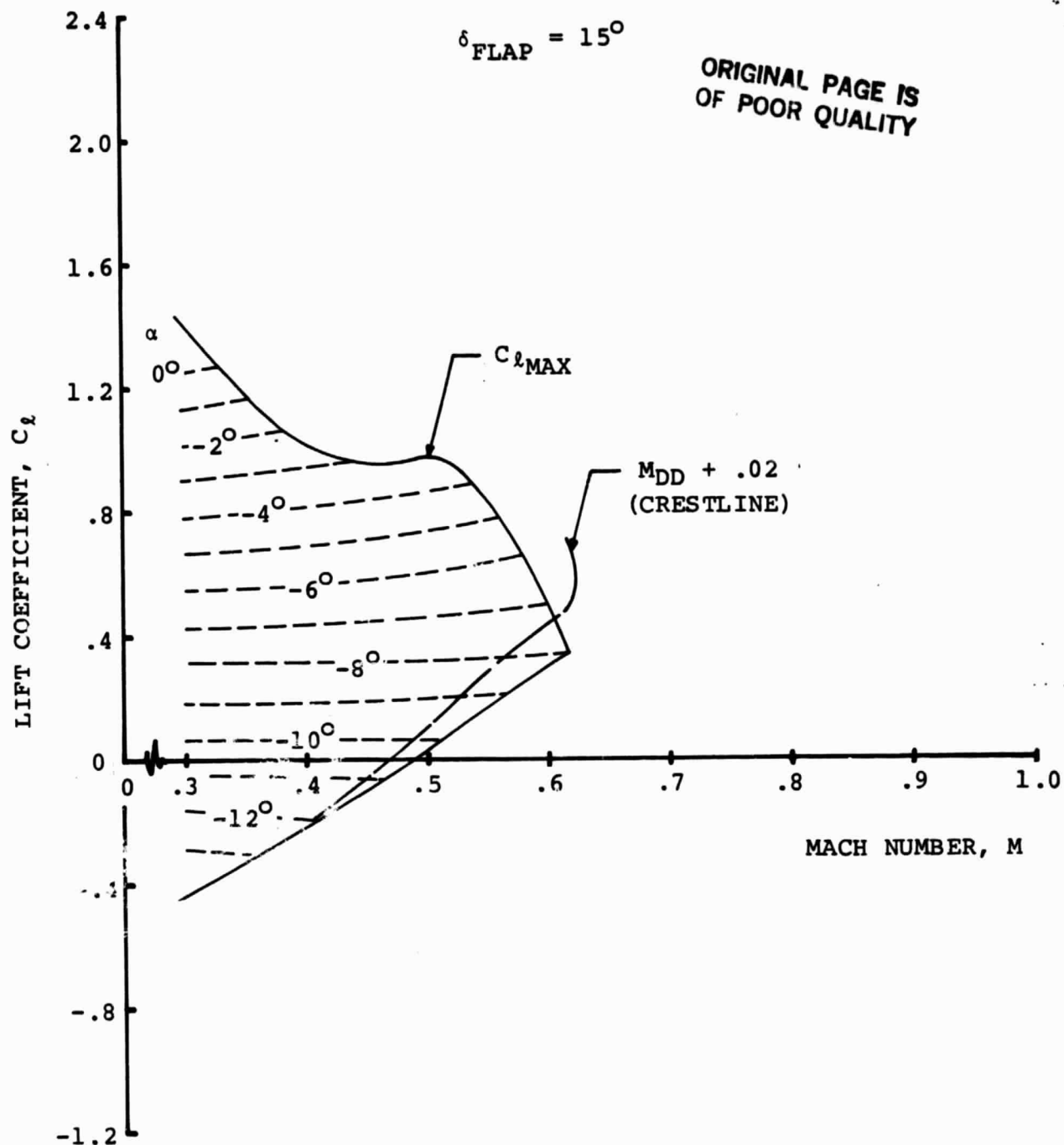


Figure 35 Maximum Positive and Negative Lift Boundaries for the A-1 Airfoil with a 0.35c Plain T.E. Flap.  $\delta_{\text{Flap}} = 15.0^\circ$ .

ORIGINAL PAGE IS  
OF POOR QUALITY

- ① DRAG VALUES FROM ANALYSIS, CORRECTED  
FOR SEPARATION IF NECESSARY. ( $M = 0.3$  TO  $0.6$  OR  $0.7$ )
- ② DRAG EXTRAPOLATED TO  $M = 0$ . FROM LOW  
MACH NUMBER TRENDS.
- ③ AROUND DRAG DIVERGENCE  $dC_d/dM = 0.1$
- ④ BEYOND THE USEFUL LIFT BOUNDARY IT IS  
ASSUMED THAT  $dC_d/dM = 0.53$

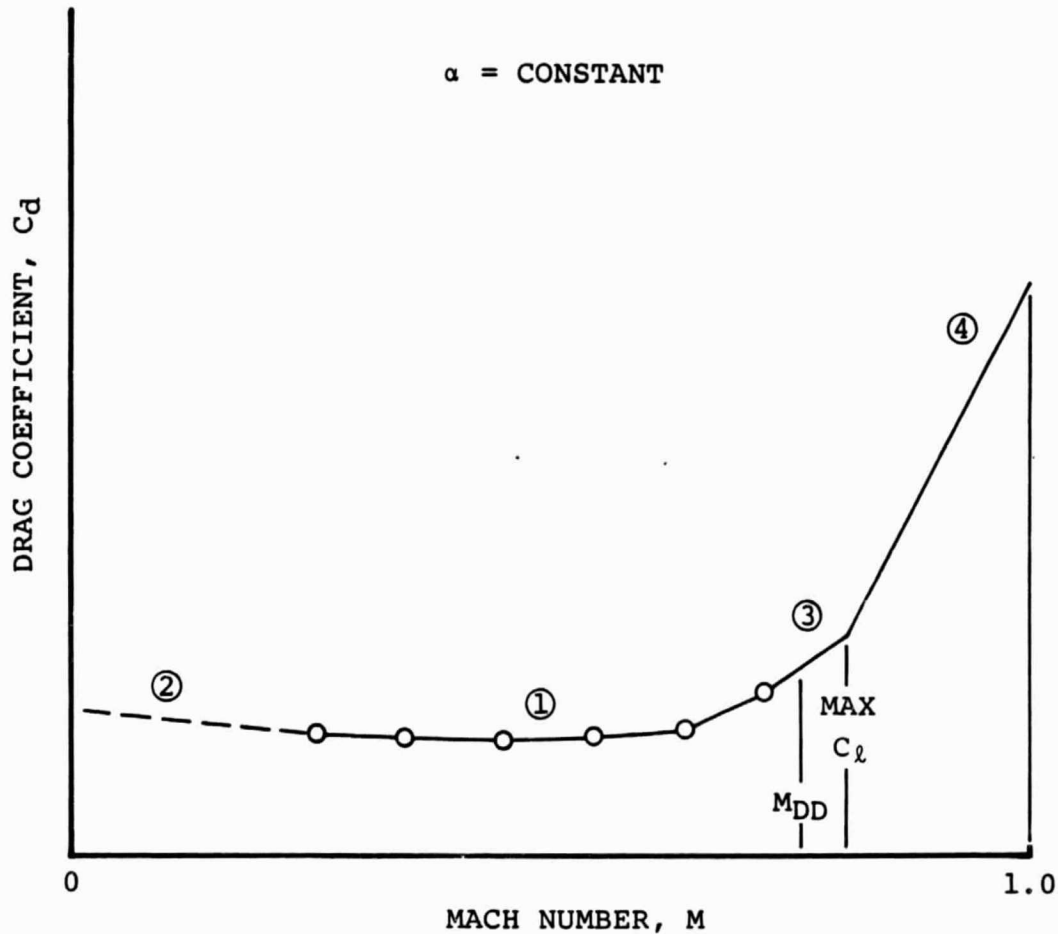


Figure 36 Definition of Drag Tables.

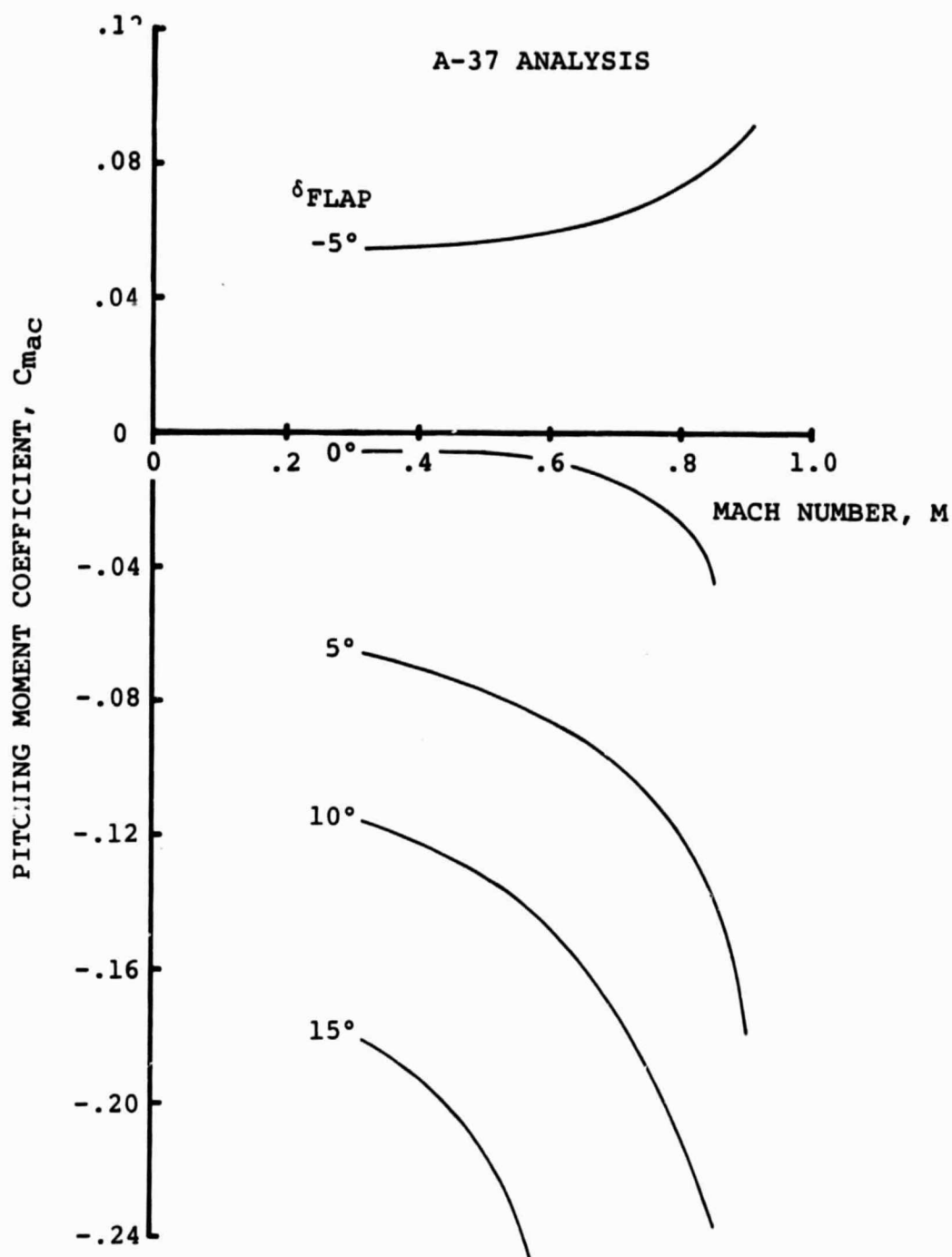


Figure 37 Effect of Compressibility on the Pitching Moment about the Aerodynamic Center as Estimated for the A-1 Airfoil with a 0.35c T.E. Flap

Figure 37 summarizes the calculated effect of compressibility on the pitching moment about the aerodynamic center of the A-1 airfoil with the 0.35c plain T.E. flap. The trends were obtained by means of the viscous transonic analysis A-37. A comparison with thin airfoil theory, Reference 29, shows that  $dC_{m,25}/d\delta_{flap} = -.0112/\text{deg}$ , by Glauert, and between  $-.011/\text{deg}$  and  $-.012/\text{deg}$  from the results of viscous subsonic and transonic analysis A-37 at low speeds ( $M = .3$ ). The effect of flap deflection becomes less linear with flap angle at higher subsonic Mach numbers, but some of these non-linearities could be due to small discrepancies in the contours describing the flap deflections.

Complete plots and tabulated values for the sectional characteristics of the A1 airfoil with the 0.35c plain T.E. flap are presented in Appendix B. The airfoil tables have been defined in the format necessary to carry out performance and loads calculations with the B-53 and C-84 codes. The listings in the Appendix have been interpreted to facilitate the verification of the actual values.

Figures 38 through 43 compare the lift/drag polars of the A-1 section with the T.E. flap set at angles between  $-5.0^\circ$  and  $15.0^\circ$  for Mach Numbers of 0.3 to 0.8. These polars were obtained from the lift and drag coefficients as formulated in the airfoil Table of Appendix B. They illustrate the effect of changes in camber on sectional characteristics. The most striking trend shown by the polars is the difference in growth of the drag between the positive and negative lift ranges.

At negative lift levels the lift is generally limited by leading edge stall, characterized by relatively small changes in drag, while approaching maximum lift from the angles of attack for attached flow followed by an abrupt loss of lift and large growth in drag. This abrupt behaviour is due to very high velocities and large gradients on the lower surface near the leading edge. At high speeds and low lift levels these gradients may cause small amounts of separation with increasing Mach number, a phenomenon often referred to as "drag creep", typical of all cambered sections at some conditions. At a specific Mach number/lift combination drag creep can be reduced or eliminated by recontouring the surface affected to provide a better distributed rate of change in curvature along the surface. Since a rotor blade is likely to encounter negative lift levels only at high subsonic Mach numbers care was exercised in defining the lower branch of the drag polars at Mach numbers above  $M = 0.6$ , at the cost of some approximation at Mach numbers below  $M = 0.6$ . This was done to remain within the size of the existing angle of attack/Mach number matrix.

ORIGINAL PAGE IS  
OF POOR QUALITY

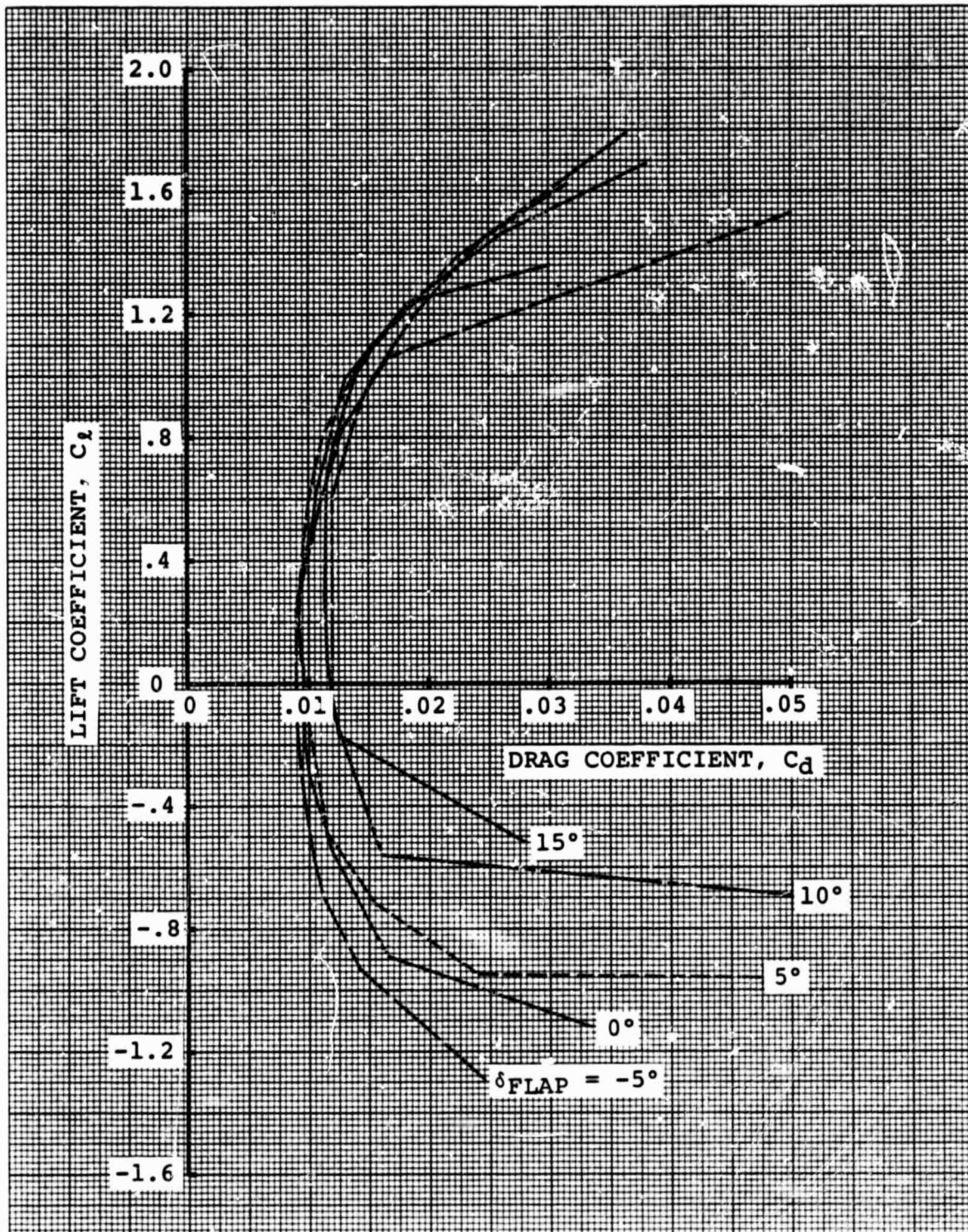


Figure 38 Lift/Drag Polars of the A-1 Airfoil with a 0.35c T.E. Flap as Approximated by the Airfoil Tables.  $M = 0.3$ .

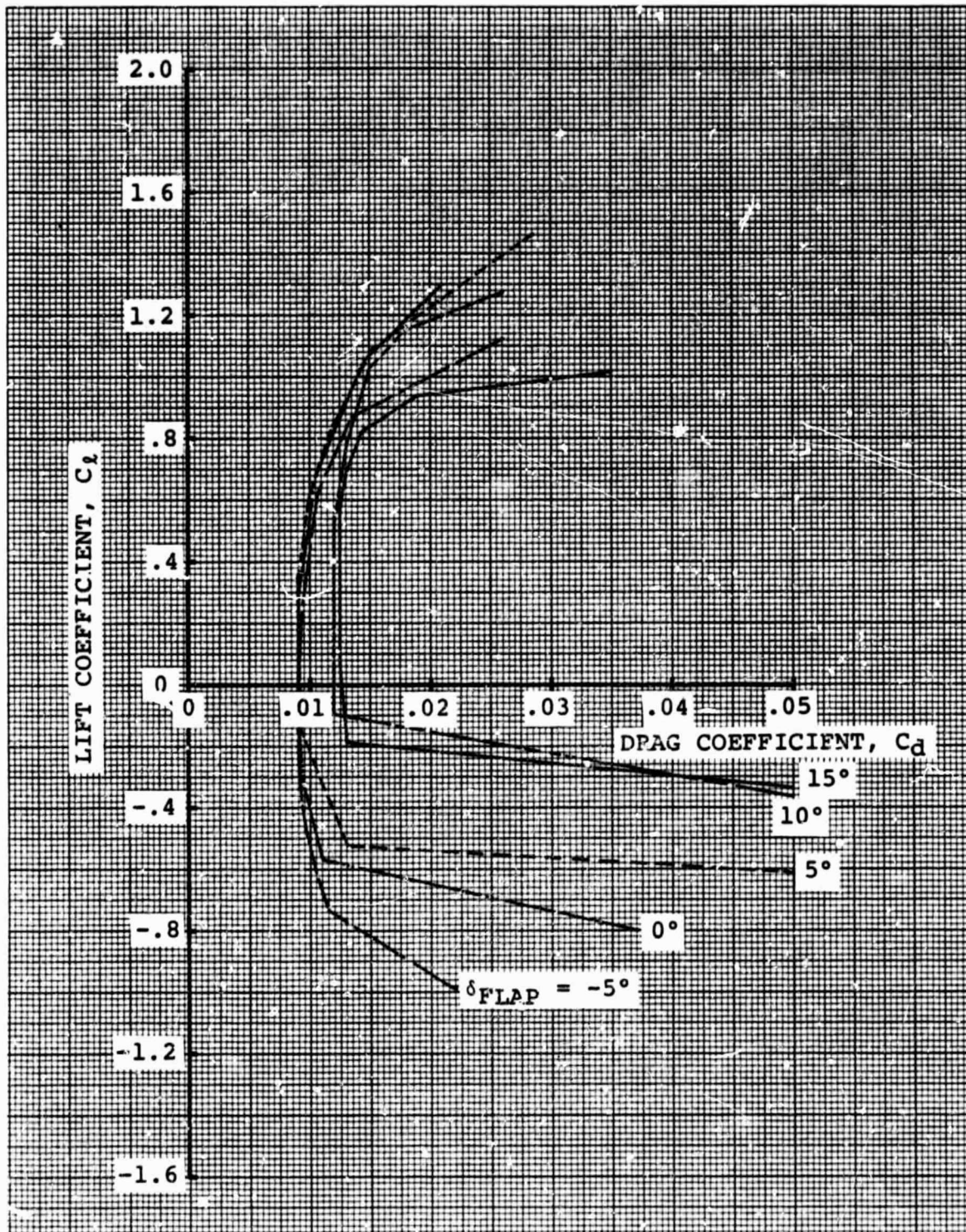


Figure 39 Lift/Drag Polars of the A-1 Airfoil with a 0.35c T.E. Flap as Approximated by the Airfoil Tables.  $M = 0.4$ .

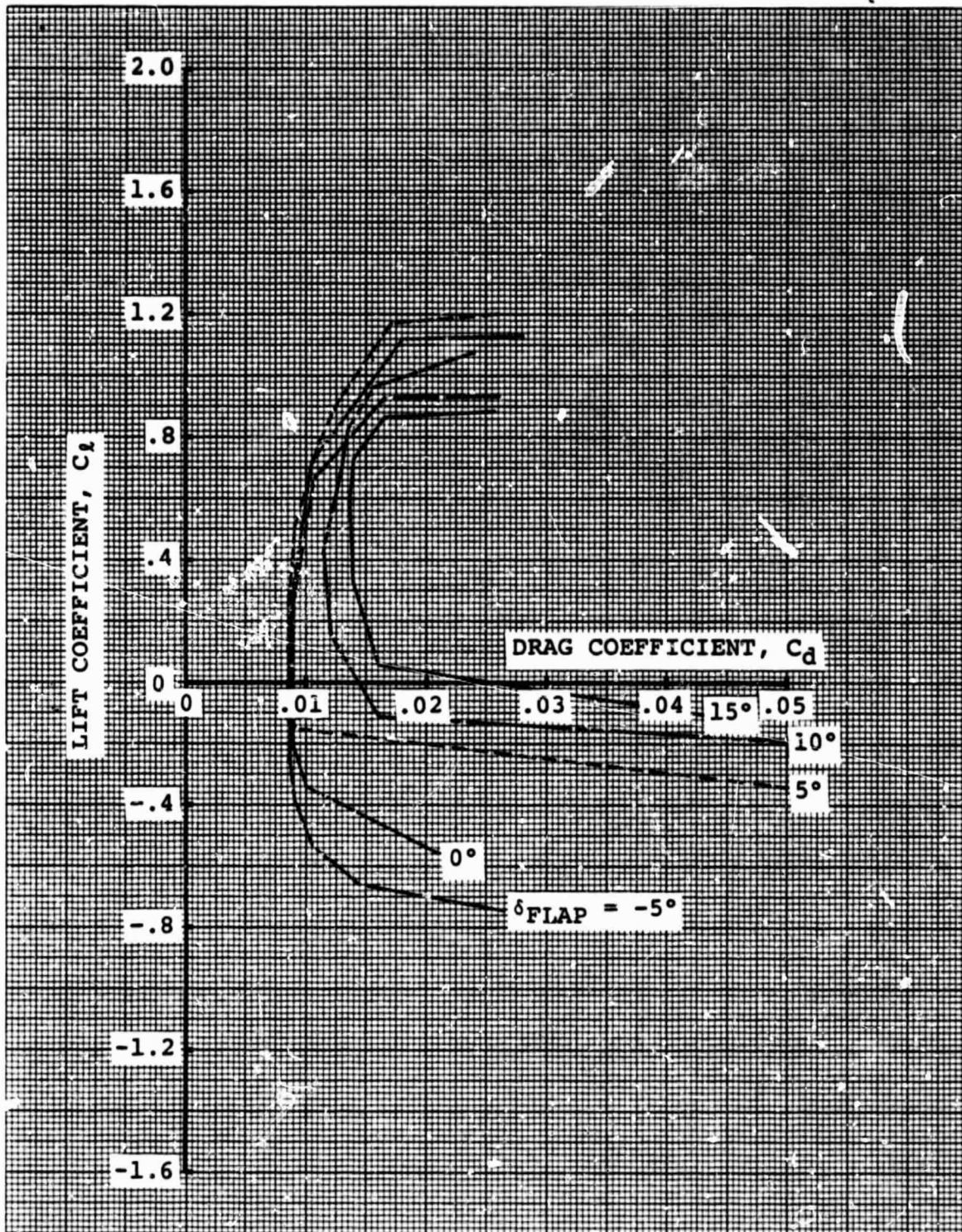


Figure 40 Lift/Drag Polars of the A-1 Airfoil with a 0.35c T.E. Flap as Approximated by the Airfoil Tables.  $M = 0.5$ .

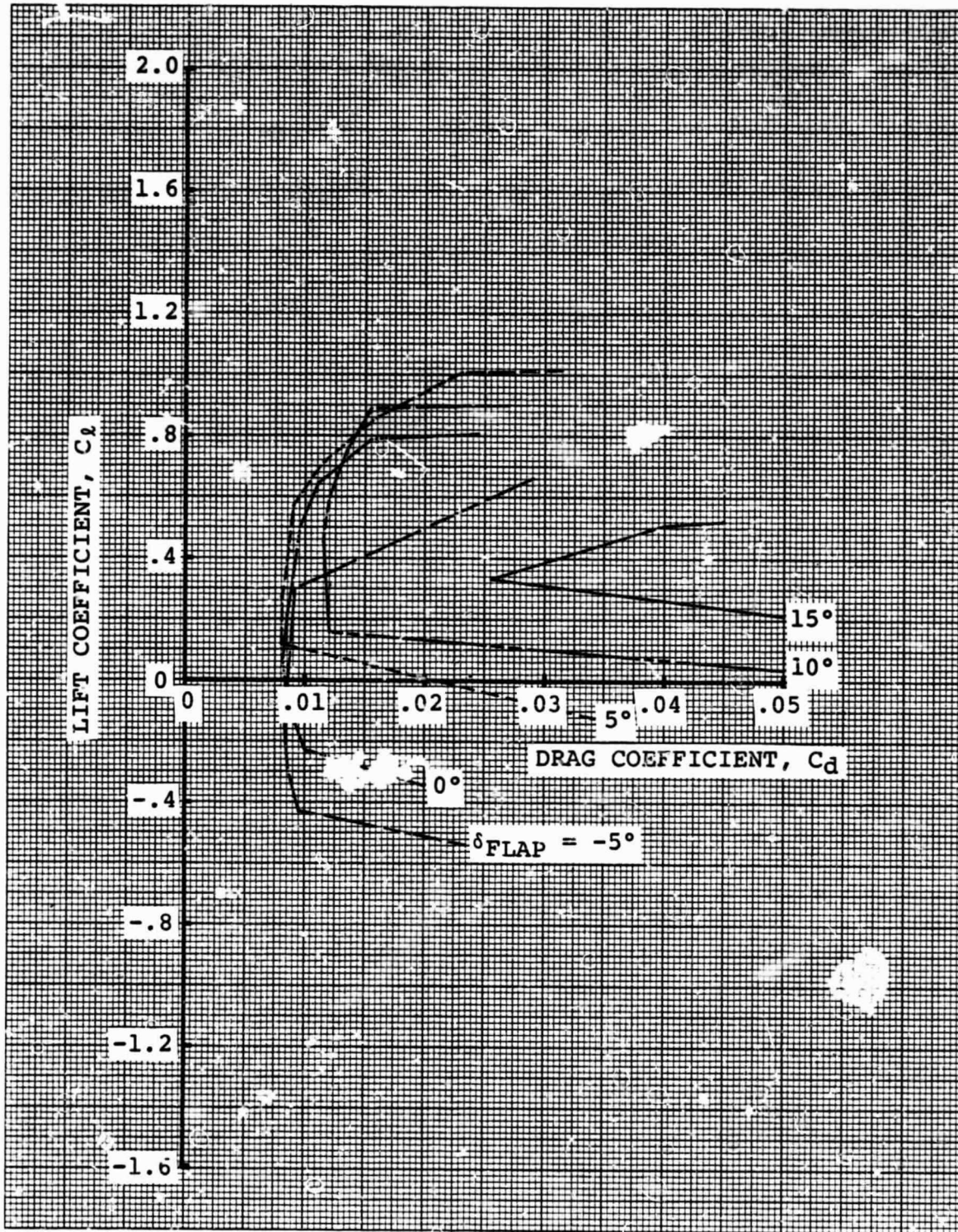


Figure 41 Lift/Drag Polars of the A-1 Airfoil with a 0.35c T.E. Flap as Approximated by the Airfoil Tables.  $M = 0.6$ .

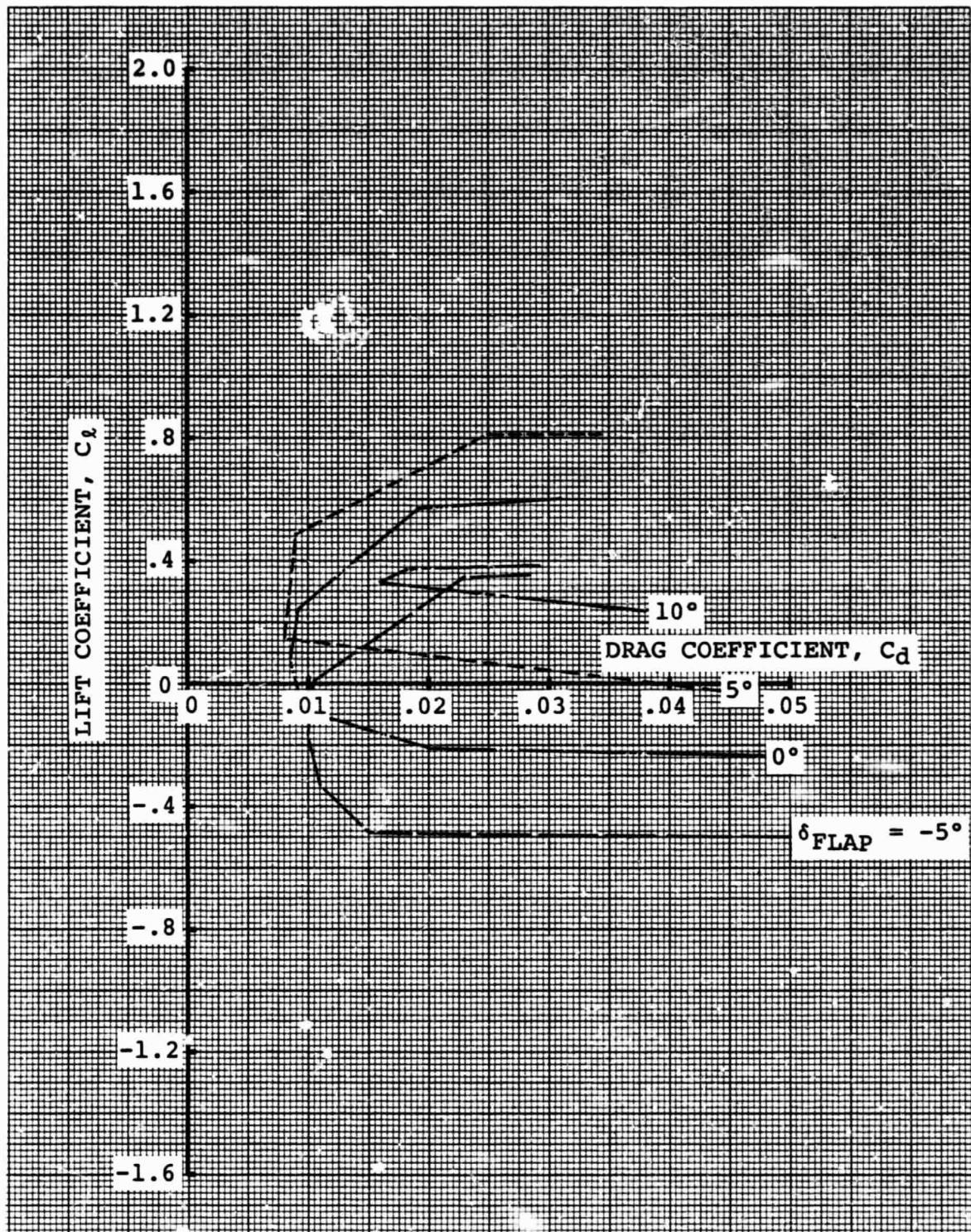


Figure 42 Lift/Drag Polars of the A-1 Airfoil with a 0.35c T.E. Flap as Approximated by the Airfoil Tables.  $M = 0.7$ .

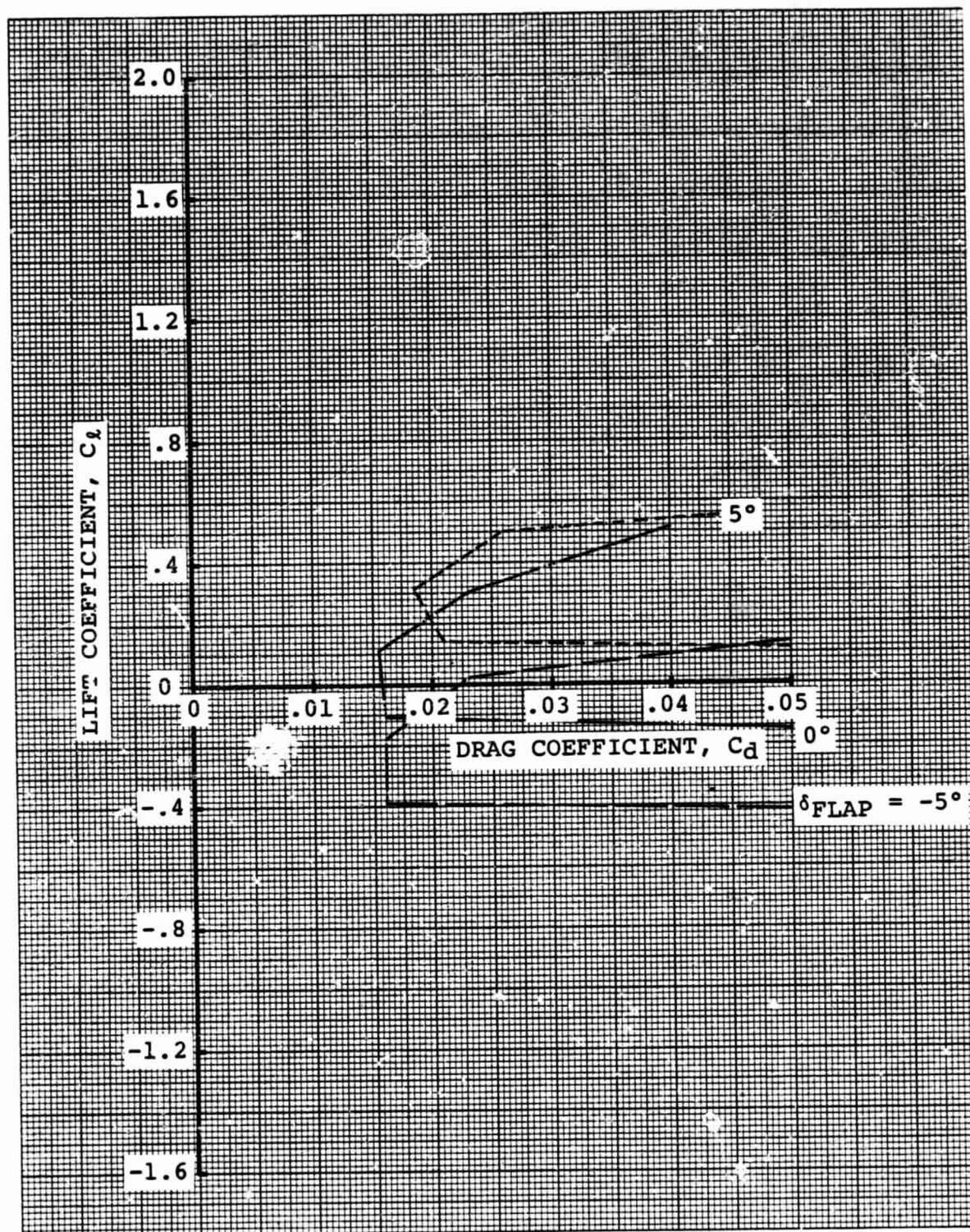


Figure 43 Lift/Drag Polars of the A-1 Airfoil with a 0.35c T.E. Flap as Approximated by the Airfoil Tables.  $M = 0.8$ .

At positive lift levels the maximum lift capability of an airfoil can be limited by either leading edge velocities or by trailing edge separation, but, as flaps are deployed, small regions of separation at the trailing edge are virtually unavoidable even at lift levels well below maximum lift. While a small amount of separation will not compromise the maximum lift capability, the associated increase in drag appears to reduce the advantages of flap deployment near positive  $(L/D)_{\max}$  at Mach numbers below  $M = 0.6$ . This implies that, while the flaps offer a definite stall delay potential, there seems to be little advantage in changing camber to minimize profile drag below  $M = 0.6$ .

The growth of the profile drag with lift near  $(L/D)_{\max}$ , shown in Figures 38 through 43, was estimated by airfoil analysis with the base drag corrections described in Section 5.2. In absence of directly applicable test evidence there is no reason to assume more optimistic lift/drag polars at this time, but this is one of the issues for which two-dimensional test verification is necessary before the benefits of variable camber can be assessed more rigorously.

#### 5.4 Sectional Characteristics of the A-1 Airfoil with a 0.50c T.E. Flap

Figure 44 illustrates the contours of the A-1 airfoil with a 50% T.E. flap. Although contours were defined for flap angles ranging from  $-5^\circ$  to  $+15^\circ$ ; detailed calculations have been carried out only to  $\delta_{\text{flap}} = 10^\circ$ . Contour coordinates are listed in Appendix A. The estimated maximum positive and negative ranges of useful lift as a function of Mach number for flap angles from  $-5^\circ$  to  $+10^\circ$  are compared in Figure 45. The lift curve slopes and angles of zero lift are shown in Figures 46 and 47.

Figures 48, 49 and 50, respectively summarize the lift characteristics for  $-5^\circ$ ,  $5^\circ$  and  $10^\circ$  flap deflection angles. The  $0^\circ$  flap condition is the same as for the 0.35c flap, shown in Figures 32. Figures 48, 49 and 50 show the maximum positive and negative lift ranges, the drag divergence boundaries and angle of attack levels for the 0.50 flap configuration. Figure 51 summarizes the effect of flap deflection on the pitching moment about the aerodynamic center. As a result of difficulties in demonstrating that the 35% plain flap could be used to improve the performance of a "variable camber" rotor, the airfoil tables for the 50% plain flap were not completed, although all the information necessary to do so is available and shown in Figures 45 through 51.

ORIGINAL PAGE IS  
OF POOR QUALITY

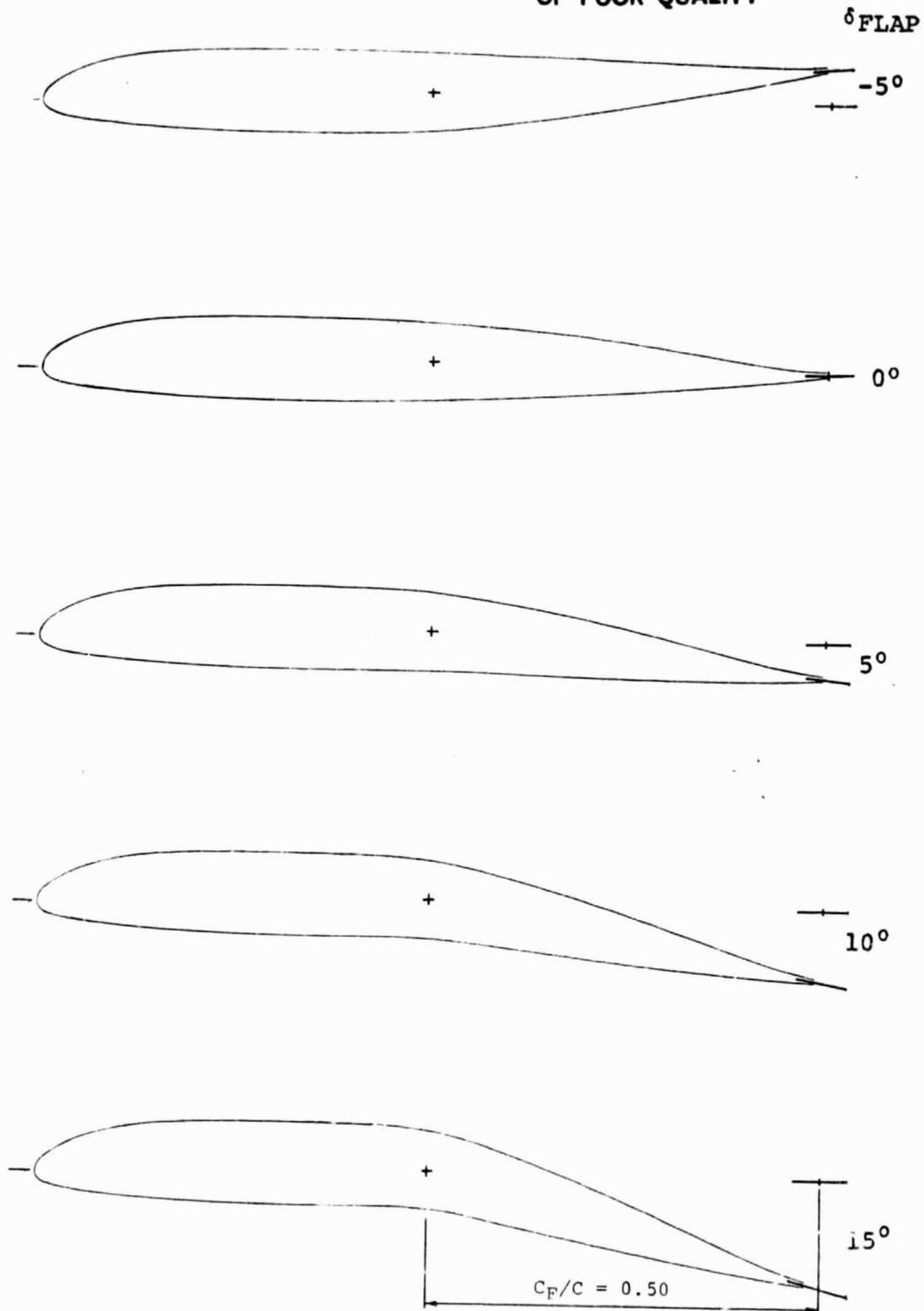


Figure 44 A-1 Airfoil with a 0.50c Plain T.E. Flap.

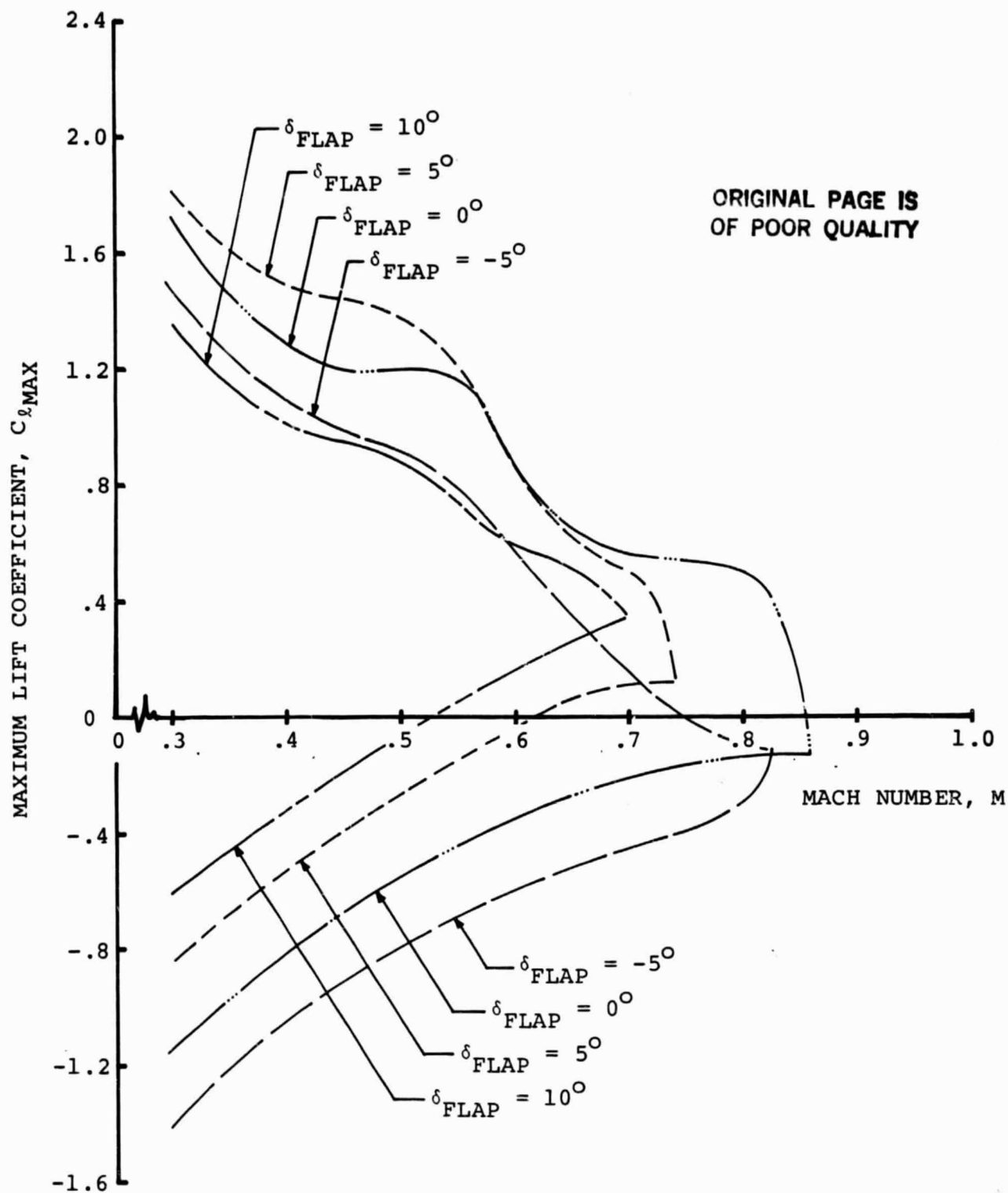


Figure 45 Estimated Maximum Lift Boundaries of the A-1 Airfoil with a 0.50c Plain T.E. Flap.

ORIGINAL PAGE IS  
OF POOR QUALITY

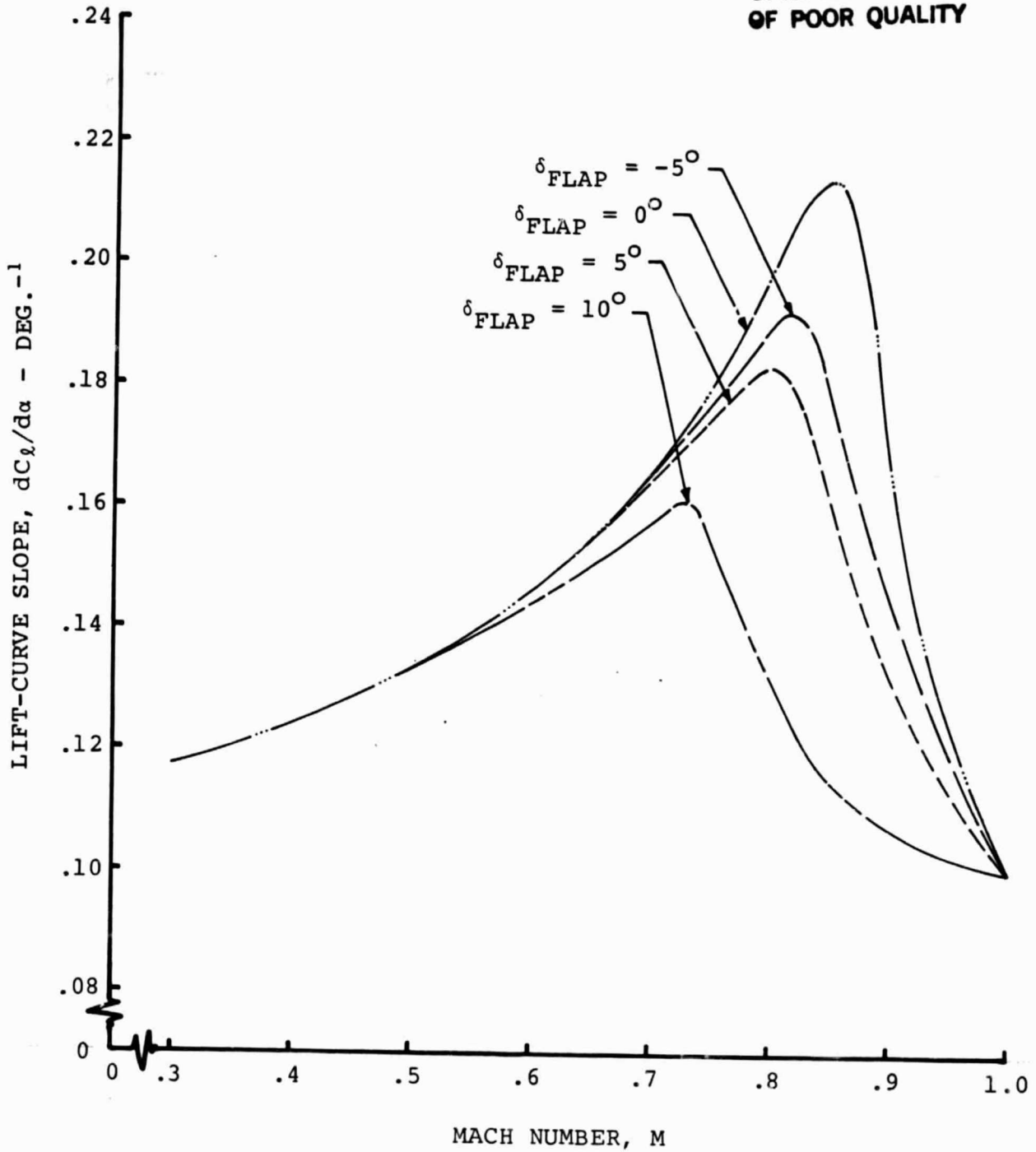


Figure 46 Lift Curve Slope of the A-1 Airfoil with a 0.50c Plain T.E. Flap.

ORIGINAL PAGE 13  
OF POOR QUALITY

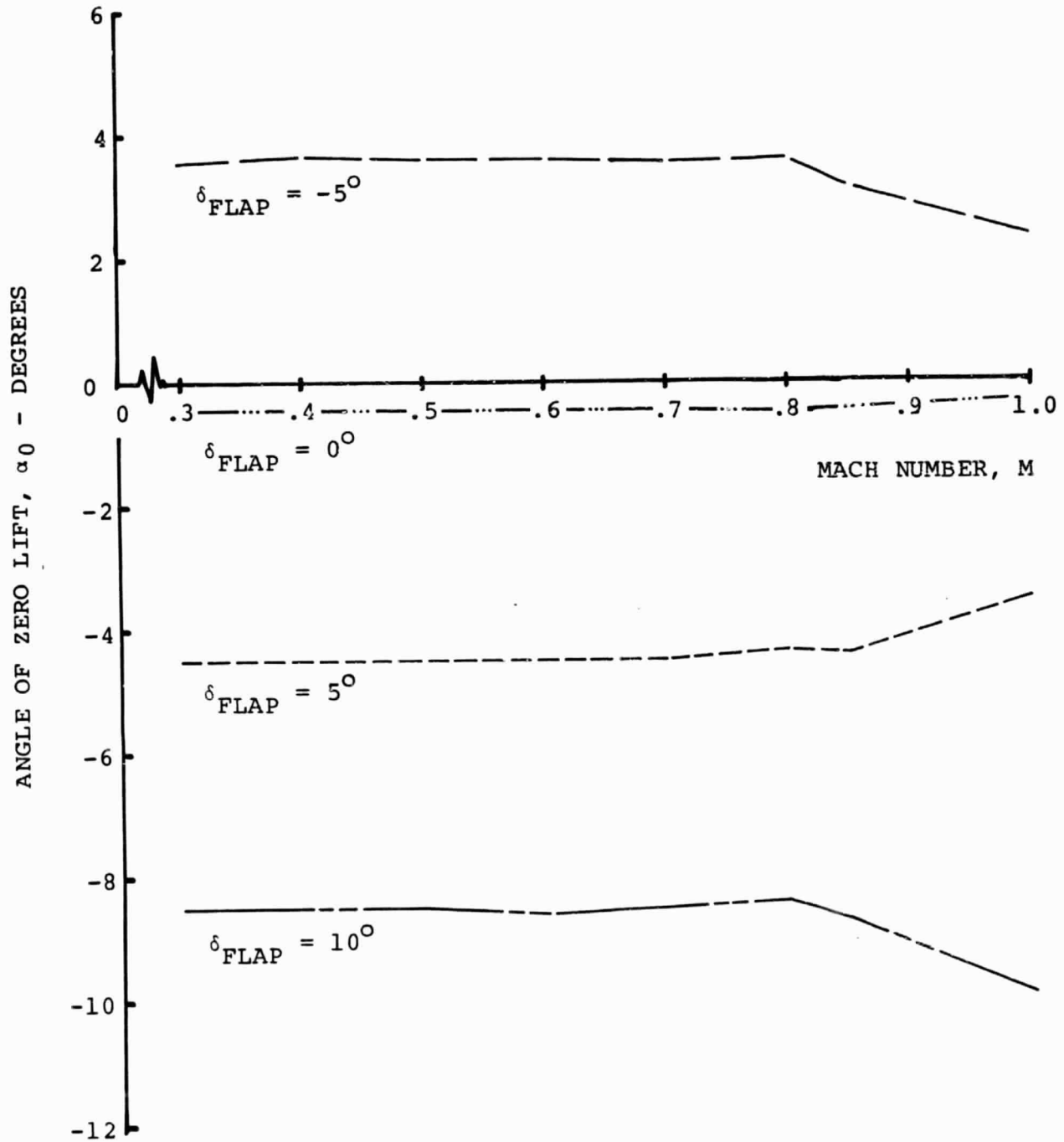


Figure 47 Angle of Zero Lift of the A-1 Airfoil with a  
0.50c Plain T.E. Flap.

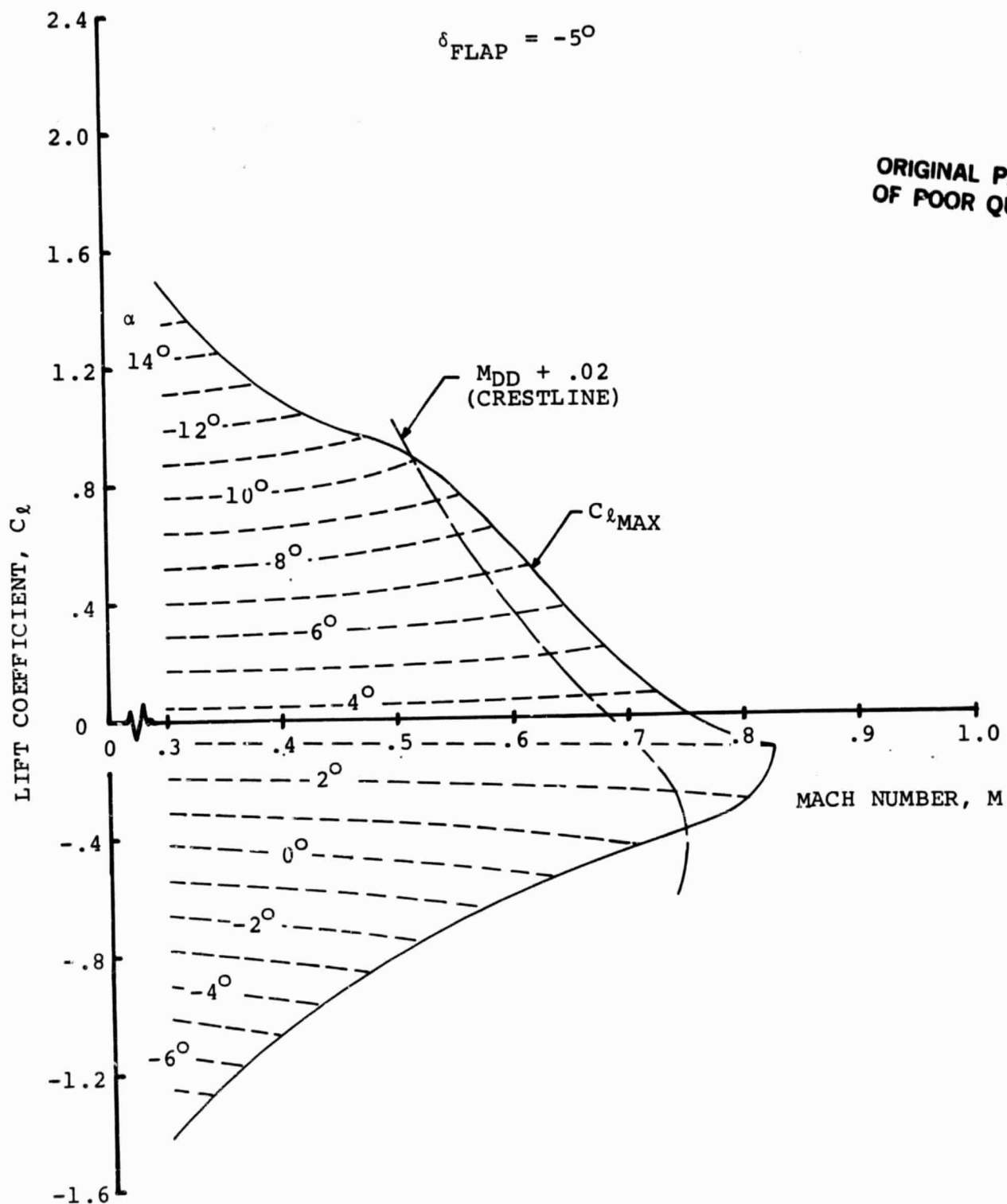


Figure 48 Maximum Positive and Negative Lift Boundaries for the A-1 Airfoil with a 0.50c Plain T.E. Flap.  $\delta_{\text{Flap}} = -5.0^{\circ}$ .

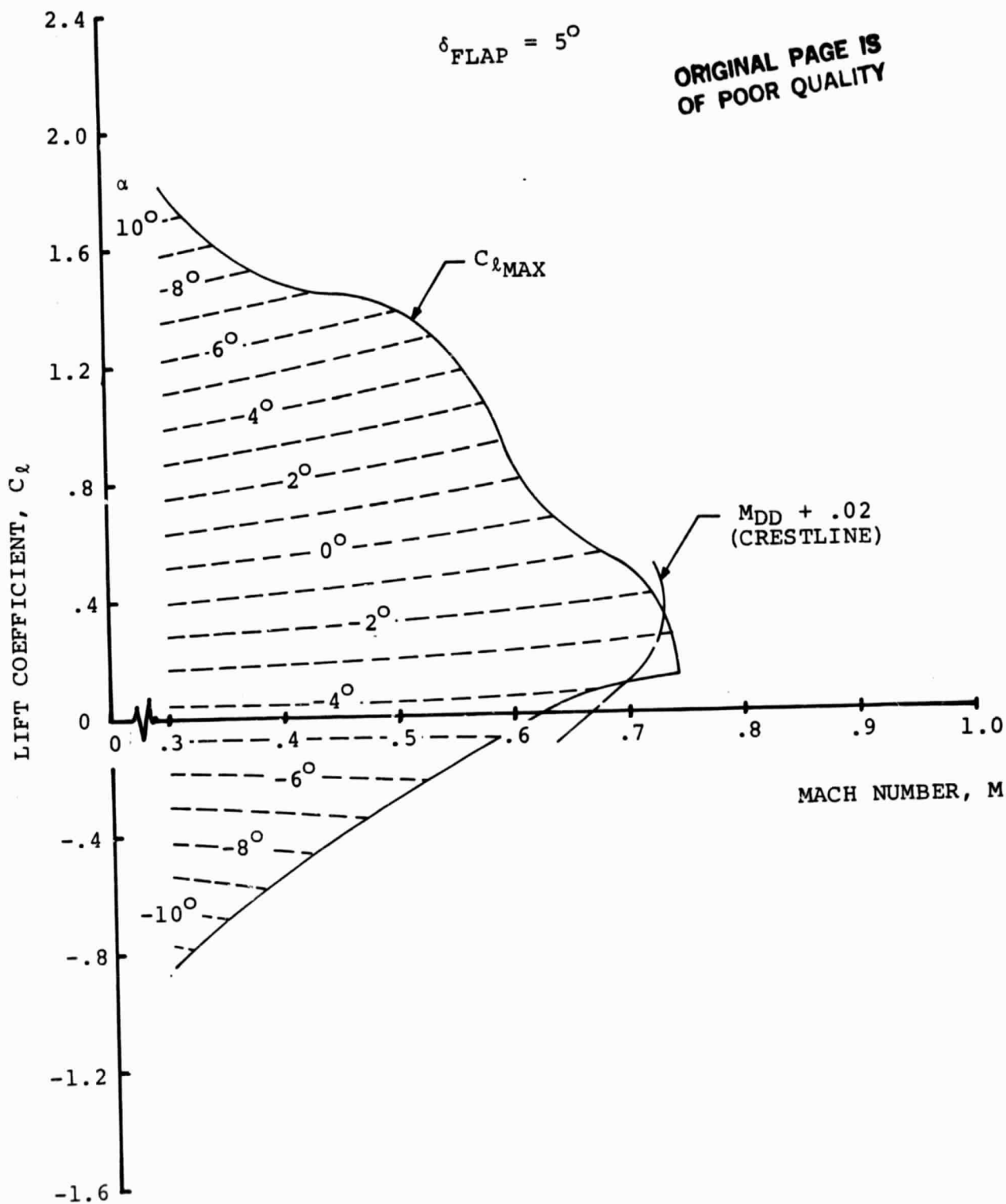


Figure 49 Maximum Positive and Negative Lift Boundaries for the A-1 Airfoil with a 0.50c Plain T.E. Flap.  $\delta_{\text{Flap}} = 5.0^\circ$ .

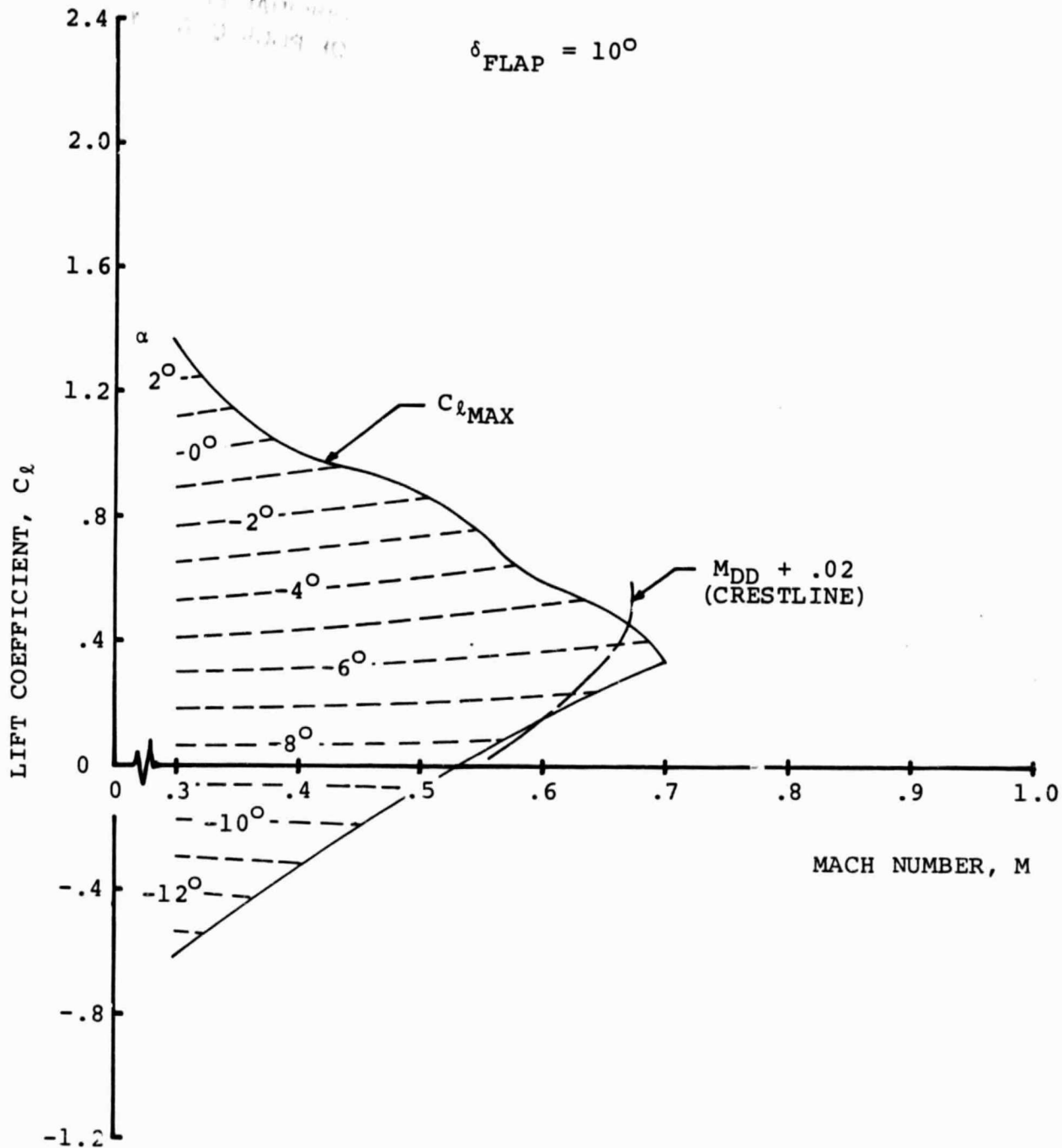


Figure 50 Maximum Positive and Negative Lift Boundaries for the A-1 Airfoil with a 0.50c Plain T.E. Flap.  $\delta_{Flap} = 10.0^\circ$ .

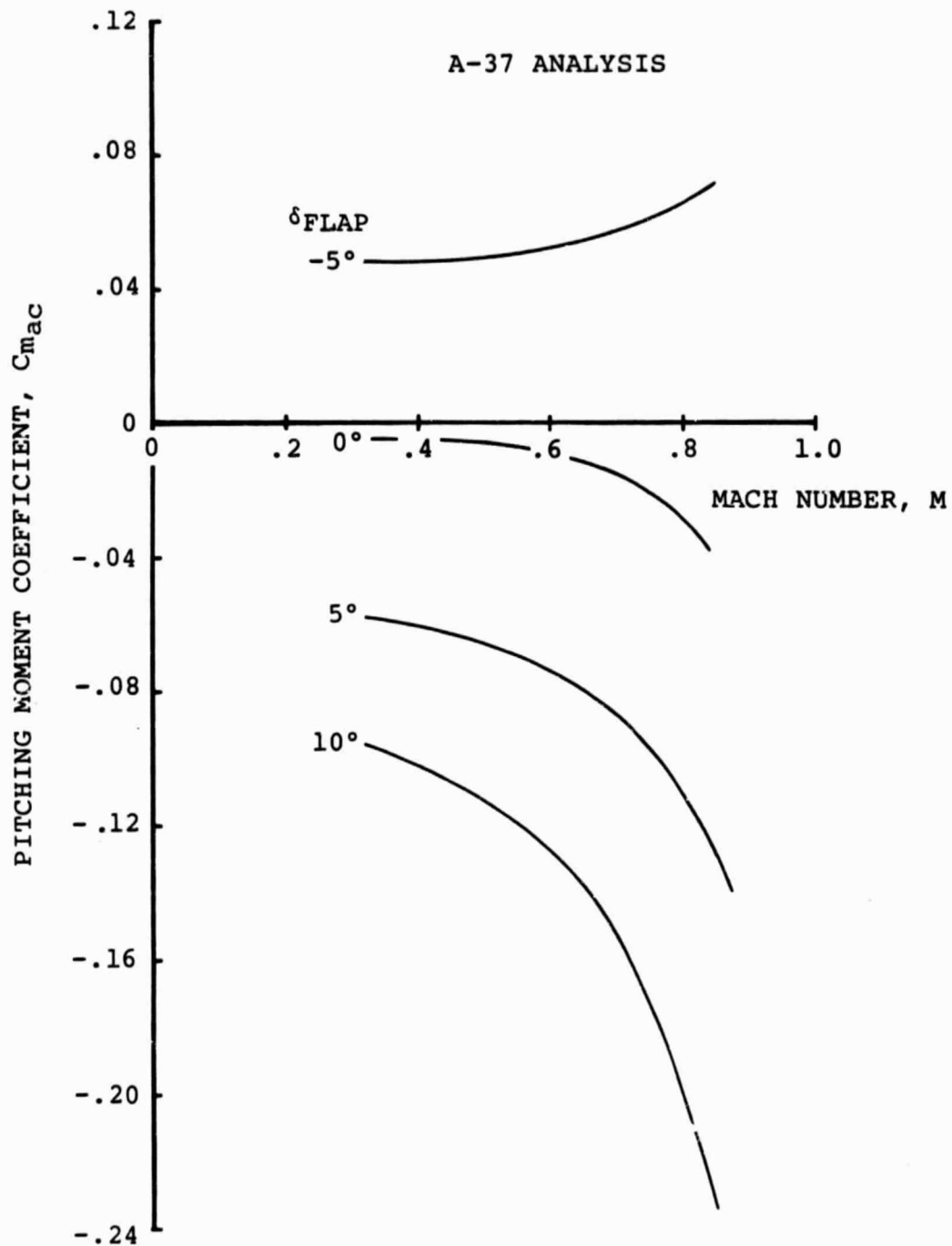


Figure 51 Effect of Compressibility on the Pitching Moment Coefficients of the A-1 Airfoil with a 0.50c T.E. Flap.

## 6.0 Performance Characteristics of Variable Camber Rotors - Potential Benefits

The B-53 rotor performance analysis computer program with variable camber (deployable flap) capability was used to define the potential available from the variable camber rotor. This program predicts performance and limited blade deflections for each flight condition examined.

The analysis of the performance characteristics and potential benefits will address the change in rotor power with flap deflection. An examination of the cause for any change in performance was made by determining the azimuthal and radial variation in power as well as the blade elastic wind-up.

The blade elastic wind-up effects will be confined entirely to the variation of maximum blade tip elastic twist variation with flap deflection. It is implied that a reduction in blade elastic wind-up would result in decreased root torsion and pitch link loads.

The variable camber configuration used in all of the B-53 runs is Mod. 6, the 35% chord flap, from Table I. The single airfoil section was used from cutout to tip.

The blade planform and structural properties used in all of the B-53 runs corresponded to an H-34 rotor blade. This blade was chosen because it is representative of a blade with a large amount of wind tunnel and flight test data for performance, loads and blade pressures. Many of the inputs for program B-53 were taken or derived from Reference 29.

The flight conditions used in predicting performance and elastic effects are shown in Table X. The conditions, such as tip speed and air density, which are not shown in Table X are kept constant throughout the entire study.

The program B-53 modeled flap deflection variations in two ways. One way was a short Fourier series which modeled flap deflection variation as a steady value plus two harmonics in the azimuth angle at each of 13 radial locations.

Flap deflection schedules were defined by the following equation:

$$\delta_F(r, \psi) = \delta_0(r) + \sum_{n=1}^2 (\delta_{nc}(r) \cos n\psi + \delta_{ns}(r) \sin n\psi)$$

where  $\delta_F(r, \psi)$  is the flap deflection at radius  $r$  and azimuth  $\psi$ . The flap deflections were thus controlled by 5 input values ( $\delta_0, \delta_{1c}, \delta_{1s}, \delta_{2c}, \delta_{2s}$ ) at each of the 13 radial flap locations.

In Table VII the various combinations of  $\delta_F$  and the radial locations at which the flaps were deflected are displayed. The flight conditions were  $\mu = 0.39$ ,  $C_T/\sigma = 0.056$ , and  $\bar{X} = 0.044$ . None of the 11 cases shown in Table VII showed any saving at all in power with respect to the baseline case of no flap deflection and the same flight conditions.

The other way of modeling flap deflection variation consisted of designating the actual flap deflections at each radial location and each of 24 azimuthal locations.

The deployment schedules obtained by designating in program B-53 azimuthal and radial flap deflection variations are shown in Table VIII. In this table, only the radial and azimuthal locations where flaps are actually deflected are shown. The radial locations are nondimensionalized by blade radius. The azimuth angles  $\psi$  are in degrees. The flap deflections are in degrees (flap down positive).

### 6.1 Performance Characteristics and Potential Benefits

With a view toward decreasing the average rotor power, the non-sinusoidal flap deflection schedules were determined in two ways. The most common way was to deploy the flaps with systematic radial and azimuthal variation of the deflection angle. Some of these variations are shown in Table VIII.

The other way in which deployment schedules were chosen was based on the decrease of the local profile drag coefficient. An output of program B-53 was used to determine regions of high local drag coefficient by radius and azimuth. The method consisted of determining  $C_{\ell}$  and Mach Number as a function of  $r/R$  and  $\psi$  from the B-53 output. Examples of this output are shown in Figure 52. Having both  $C_{\ell}$  and  $M$  in hand for a particular  $r/R$  and  $\psi$ , one can refer to the drag polars for the given  $M$  (interpolation between polars may be required here) and find  $\delta_F$  for minimum drag. Flaps were then deployed such that the drag coefficient at the original lift coefficient and Mach number was lower than it was for the blade section without a deployed flap. Since the moment coefficient change associated with flap deflection caused the blade to twist and thus change the original angle of attack and lift coefficient, this process was necessarily iterative.

	FULL SPAN	INBOARD HALF	OUTBOARD HALF
$2 \sin \psi$	X		
$-2 \sin \psi$	X	X	X
$-4 \sin \psi$	X	X	X
$-2 \cos \psi$	X	X	X
$-4 \cos \psi$			X

Table VII Sinusoidal Flap Deployment Schedules

ORIGINAL PAGE IS  
OF POOR QUALITY

BLADE AZIMUTH POSITION,  $\gamma$  - DEG.

BLADE RADIAL STA,  $r/R$

.77 .84 .90 .97

60		-1.43	-2.05	-2.62
75		-1.43	-2.05	-2.62
90		-1.43	-2.05	-2.62
105			-2.05	-2.62
120				-2.62

SCHEDULE A1

60			-2.05	-2.62
75			-2.05	-2.62
90			-2.05	-2.62
105			-2.05	-2.62
120				-2.62

SCHEDULE A3

30				
45				
60			-1.5	-1.7
75		-3.0	-4.0	-4.0
90		-1.0	-1.0	-1.5
105			-1.6	-2.0
120				-1.0
135				

SCHEDULE A5

30				-1.5
45			-1.2	
60		-1.7	-2.0	-1.7
75		-1.6	-2.1	-2.8
90		-1.5	-2.1	-2.6
105		-1.5	-1.3	-2.1
120			-1.0	-1.5

SCHEDULE A7

60		-2.1	-2.8	-3.5
75		-2.1	-2.8	-3.5
90		-2.1	-2.8	-3.5
105			-2.8	-3.5
120				-3.5

SCHEDULE A9

75				-1.0
90				

SCHEDULE A11

75				-2.0
----	--	--	--	------

SCHEDULE A13

75	-2.0			
90				
105				
120				
135				
150				
165				

SCHEDULE A15

BLADE RADIAL STA,  $r/R$

.77 .84 .90 .97

	-1.573	-2.255	-2.882
	-1.573	-2.255	-2.882
	-1.573	-2.255	-2.882
		-2.255	-2.882
			-2.882

SCHEDULE A2

			-1.8
	-2.0	-2.0	-2.0
	-1.7	-2.0	-2.0
		-1.2	-1.5
			-1.5

SCHEDULE A4

			-1.5
		-1.5	-1.0
	-1.5	-1.0	-1.5
	-1.0	-1.5	-2.0
	-1.5	-2.0	-2.0
	-1.5	-1.0	-1.5
		-1.5	-1.0
			-1.5

SCHEDULE A6

			-1.5
		-1.2	
	-1.7	-2.0	-2.7
	-1.6	-2.1	-2.8
	-1.5	-2.1	-2.6
	-1.5	-1.5	-2.5
		-1.5	-2.1

SCHEDULE A8

			.8

SCHEDULE A10

			-1.0

SCHEDULE A12

	-2.0		
--	------	--	--

SCHEDULE A14

-2.0	-2.0	-2.0	-2.0
-2.0	-2.0	-2.0	-2.0
-2.0	-2.0	-2.0	-2.0
-2.0	-2.0	-2.0	-2.0
-2.0	-2.0	-2.0	-2.0
-2.0	-2.0	-2.0	-2.0

SCHEDULE A16

Table VIII Non-Sinusoidal Flap Deployment Schedule

OF POOR QUALITY  
ORIGINAL PAGE IS

BLADE RADIAL STA., r/R

**.71    .77    .84    .90    .97**

SCHEDULE B1

BLADE RADIAL STA. F/R

.71 .77 .84 .90

SCHEDULE B2

**SCHEDULE 83**

**SCHEDULE BA**

**SCHEDULE B5**

**SCHEDULE B6**

SCHEDULE C1

**SCHEDULE C2**

**SCHEDULE C3**

**SCHEDULE C**

SCHEDULE D

**SCHEDULE B**

86

ORIGINAL PAGE 15  
OF POOR QUALITY

BLADE AZIMUTH POSITION,  $\psi$  - DEG.

BLADE RADIAL TA.,  $r/R$

.19 .26 .32 .39 .45 .52 .58 .64 .71 .77 .84 .90 .97

0								5.0	5.0	5.0	5.0	5.0	5.0
15								5.0	5.0	5.0	5.0	5.0	5.0
30								5.0	5.0	5.0	5.0	5.0	5.0
45													
60													
75											-1.43	-2.05	-2.62
90											-1.43	-2.05	-2.62
105											-1.43	-2.05	-2.62
120												-2.05	-2.62
135													-2.62
150													
165								5.0	5.0	5.0	5.0	5.0	5.0
180								5.0	5.0	5.0	5.0	5.0	5.0
195								5.0	5.0	5.0	5.0	5.0	5.0
210								5.0	5.0	5.0	5.0	5.0	5.0
225													
240													
255													
270													
285													
300													
315													
330													
345								5.0	5.0	5.0	5.0	5.0	5.0

SCHEDULE F

150	5.0	5.0	5.0										
165													
180													
195													
210													
225													
240													
255													
270													
285													
300													
315													
330	5.0	5.0	5.0										
345													

SCHEDULE G

0	-2.5	-2.5	-2.5		5.0	5.0	2.5	2.5		2.5	5.0	2.5	
15	5.0	5.0	5.0	5.0	3.75	2.5			2.0	2.5	2.5	3.0	2.5
30	5.0	5.0	5.0	2.5									

SCHEDULE H1

330	-3.85	-5.14	-6.43	-7.72	-9.02	-1.031	-1.16	-1.289	-1.418	-1.548	-1.677	-1.806	-1.935
-----	-------	-------	-------	-------	-------	--------	-------	--------	--------	--------	--------	--------	--------

SCHEDULE H2

0	-2.5	-2.5	-2.5		5.0	5.0	2.5	2.5		2.5	5.0	2.5	
15	5.0	5.0	5.0	5.0	3.75	2.5			2.0	2.5	2.5	3.0	2.5
30	5.0	5.0	5.0	2.5									
45	5.0	5.0	2.5										
60	5.0	2.5		-2.0	-2.0								
75	5.0	1.25		2.5	3.7	4.0			1.5	2.5	2.5		-3.7
90	4.0	1.25		2.5	1.25	2.5	5.0	5.0	5.0	2.5	3.7		-4
105	3.0	2.5		1.0	5.0	5.0	5.0	5.0	3.7	2.5	5.0		
120	5.0	2.5	1.25		2.5	5.0	5.0	5.0	.7				
135		5.0	2.5	1.25		2.5	3.7	3.7	.7			2.5	
150		5.0	5.0	4.25	2.5		2.5	4.0	3.7				-2.5
165		5.0	5.0	5.0	5.0	2.5		1.25	2.5	5.0	.7		
180		5.0	5.0	5.0	5.0	5.0	4.0	2.5		2.5	3.7	2.5	

SCHEDULE I

Table VIII (continued)

ORIGINAL PAGE IS  
OF POOR QUALITY

BLADE RADIAL STA., r/R

	.19	.26	.32	.39	.45	.52	.58	.64	.71	.77	.84	.90	.97
0	-2.5	-2.5	-2.5		5.0	5.0	2.5	2.5		2.5	5.0	2.5	
15	5.0	5.0	5.0	5.0	5.0	2.5		1.25	1.25	2.5	2.5	5.0	2.5
30	5.0	5.0	5.0	5.0	1.25		1.25	2.5	2.5	2.5	5.0	5.0	2.5
45	5.0	5.0	2.5			1.25	2.5	2.5	2.5	2.5	2.5	5.0	5.0
60	5.0	2.5				2.5	2.5	1.25		2.5	2.5		
75	5.0	2.5			2.5	2.5							-1.0
90	4.0	2.5		2.5	1.25		5.0					-1.9	-1.9
105	5.0	4.0		2.5	2.5	3.0	2.5						-1.6
120	5.0	5.0	1.25		2.5	3.75	5.0	2.5	1.25	1.0	.65		
135	5.0	5.0	3.0	1.25		2.5	5.0	5.0	3.5	2.5	.5		
150	5.0	5.0	5.0	4.25	2.5		2.5	4.0	5.0	3.7	1.2		
165	5.0	5.0	5.0	5.0	5.0	2.5		1.25	2.5	5.0	3.0		
180	5.0	5.0	5.0	5.0	5.0	5.0	4.0	2.5		2.5	2.5	2.5	
195	5.0	5.0	5.0	5.0	5.0	5.0	5.0	5.0	2.5	1.25	.5	1.25	
210	5.0	5.0	5.0	5.0	5.0	5.0	5.0	5.0	5.0	5.0	1.25		2.0
225	5.0	5.0	5.0	5.0	5.0	5.0	5.0	5.0	5.0	5.0	4.5	2.5	
240	5.0	5.0	5.0	5.0	5.0	5.0	5.0	5.0	5.0	5.0	4.5	4.5	2.5
255	5.0	5.0	5.0	5.0	5.0	5.0	5.0	5.0	5.0	5.0	5.0	5.0	3.0
270	5.0	5.0	5.0	-5.0	-5.0	5.0	5.0	5.0	5.0	5.0	5.0	5.0	4.0
285	5.0	5.0	5.0	-1.0	-3.0	5.0	5.0	5.0	5.0	5.0	5.0	5.0	4.0
300	5.0	5.0	-2.5	-5.0	-5.0	-3.0	5.0	5.0	5.0	5.0	5.0	5.0	5.0
315	5.0	2.5	-5.0	-5.0	-5.0	-4.0	5.0	5.0	5.0	5.0	5.0	2.5	3.0
330	-5.0	-5.0	-5.0	-5.0			4.0	5.0	5.0	5.0	4.0		2.5
345	-5.0	-5.0	-5.0	-3.0		5.0	5.0	5.0	2.5		2.5	2.5	2.5

SCHEDULE J1

	-2.5	-2.5			5.0	5.0	2.5	2.5		2.5	5.0	2.5	
0	-2.5	-2.5			5.0	5.0	2.5	2.5		2.5	5.0	2.5	
15	5.0	5.0		5.0	3.75	2.5			2.0	2.5	2.5	3.0	2.5
30	5.0	5.0	5.0	2.5									
45	5.0	5.0	2.5				-1.7	-2.0	-3.0	-3.7	-2.5		
60	5.0	2.5		-2.0	-2.0			-1.5	-3.2				-3.7
75	5.0	1.25		2.5	3.7	4.0		1.3	2.5	2.5	2.5		
90	4.0	1.25		2.5	1.25	2.5	5.0	5.0	5.0	2.5	3.7	-1.9	
105	5.0	2.5		1.0	5.0	5.0	5.0	5.0	3.7	2.5	5.0		
120	5.0	2.5	1.25		2.5	5.0	5.0	5.0	.7				
135	5.0	5.0	2.5	1.25		2.5	3.7	3.7	.7			2.5	
150	5.0	5.0	5.0	4.25	2.5		2.5	4.0	3.7				-2.5
165	5.0	5.0	5.0	5.0	5.0	2.5		1.25	2.5	5.0	.7		
180	5.0	5.0	5.0	5.0	5.0	5.0	4.0	2.5	2.5	3.7	2.0		
195	5.0	5.0	5.0	5.0	5.0	5.0	5.0	5.0	2.5	1.25	1.0	1.25	
210	5.0	5.0	5.0	5.0	5.0	5.0	5.0	5.0	5.0	3.7	2.5		2.0
225	-5.0	-5.0	5.0	5.0	5.0	5.0	5.0	5.0	5.0	5.0	3.7	1.2	
240	5.0	5.0	-5.0	-3.7	5.0	5.0	5.0	5.0	5.0	5.0	3.7	2.5	
255	5.0	5.0	5.0	-5.0	5.0	5.0	5.0	5.0	5.0	5.0	5.0	5.0	3.7
270	5.0	5.0	5.0	-5.0	-5.0	5.0	5.0	5.0	5.0	5.0	5.0	5.0	3.7
285	5.0	5.0	5.0	-3.7	-5.0	5.0	5.0	5.0	5.0	5.0	5.0	5.0	3.7
300	5.0	5.0	-5.0	-5.0	-5.0	-5.0	5.0	5.0	5.0	5.0	5.0	3.7	2.5
315	5.0		-5.0	-5.0	-5.0	-5.0	5.0	5.0	5.0	5.0	4.5	2.5	
330	-5.0		-5.0	-5.0	-5.0		4.0	5.0	5.0	3.7	2.5		2.5
345	-5.0		-5.0	-1.2	5.0	5.0	4.5	5.0		1.2	2.5	2.5	2.5

SCHEDULE J2

Table VIII (continued)

ORIGINAL PAGE IS  
OF POOR QUALITY

853

$\mu=0.39$  DELTAFLAP=0.0  $C_T/S=0.10$

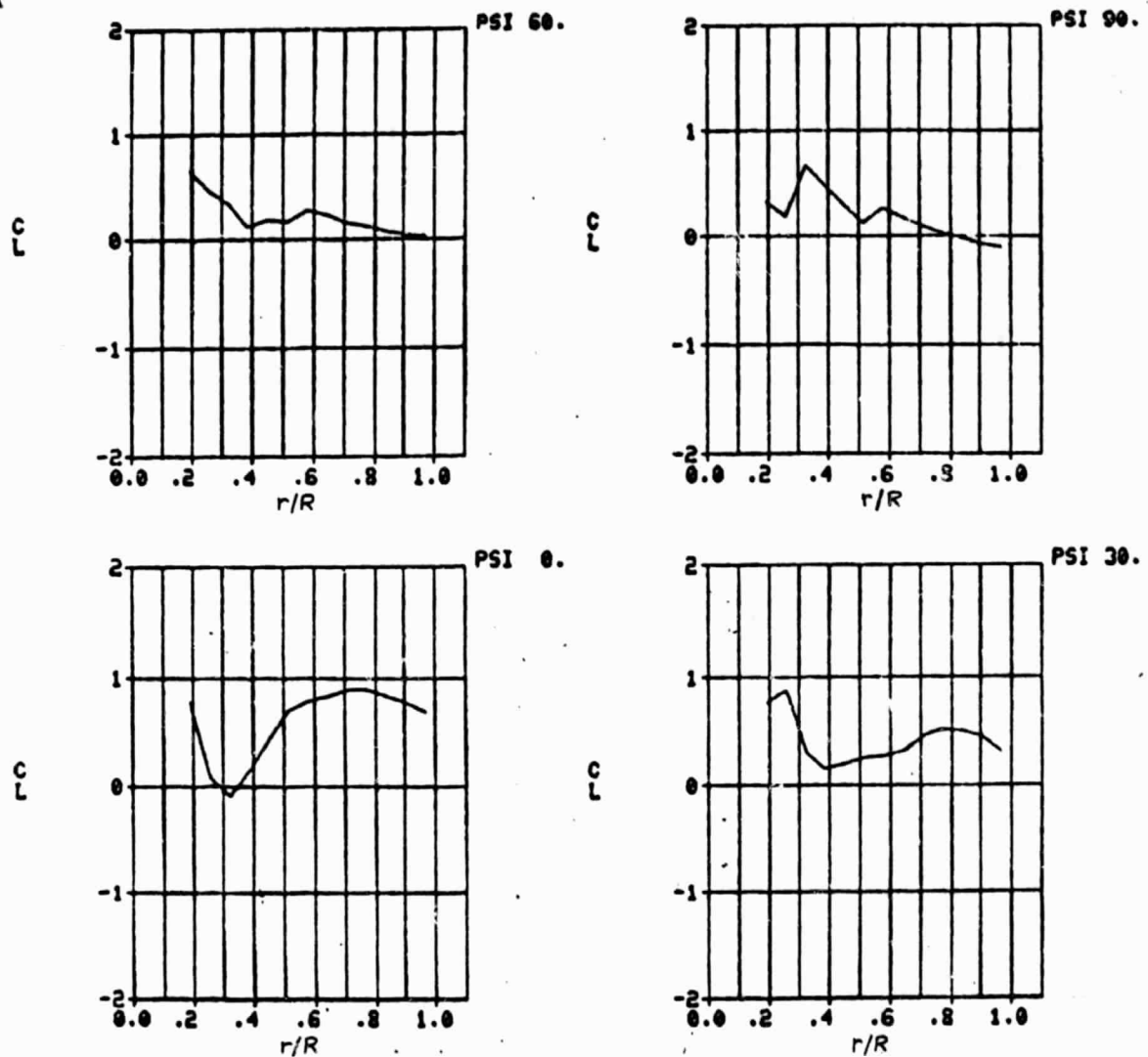


Figure 52 Lift Coefficient Variation with Radius and Azimuth for  $C_T/\sigma = 0.10$ ,  $\mu = 0.39$ ,  $\delta_F = 0$

ORIGINAL PAGE IS  
OF POOR QUALITY

B53

MU=0.39 DELTAFLAP=0.0 CT/S=0.10

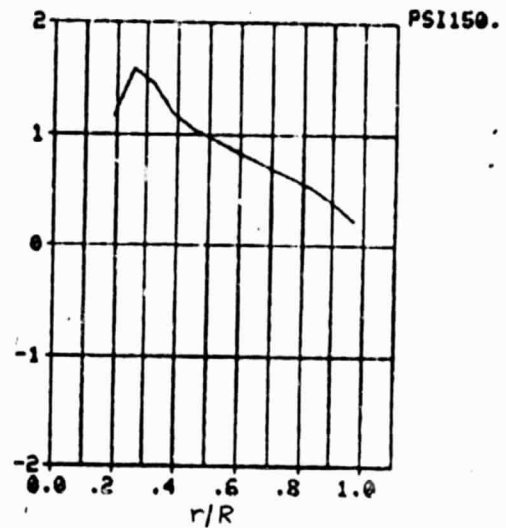
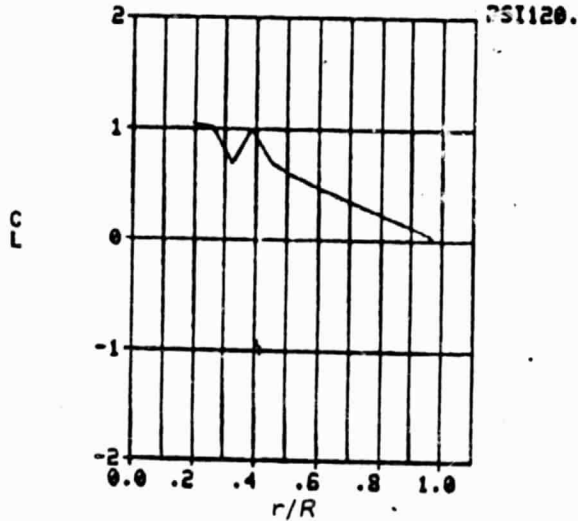
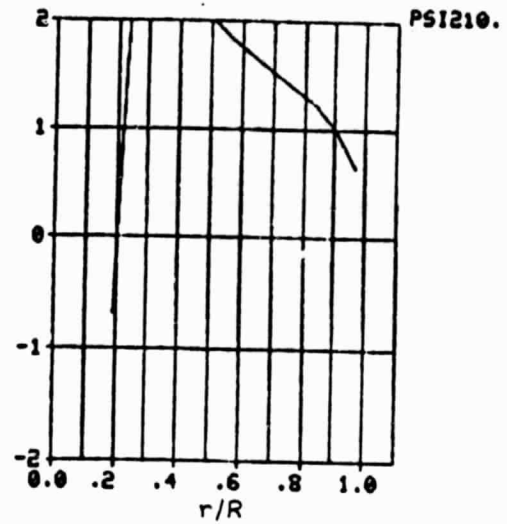
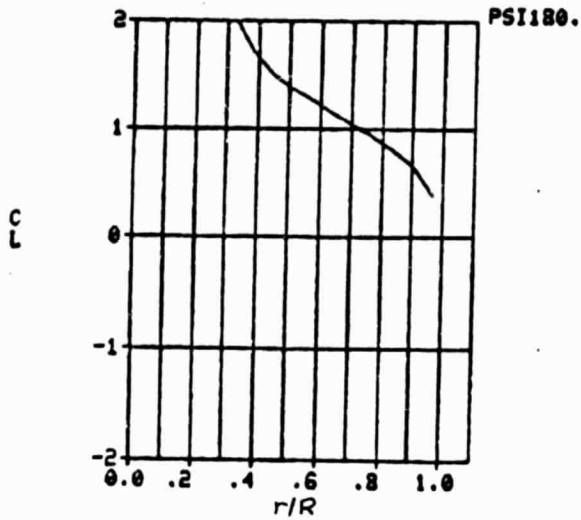


Figure 52 (continued)

ORIGINAL PAGE IS  
OF POOR QUALITY

853

MU=0.39 DELTAFLAP=0.0 CT/S=0.10

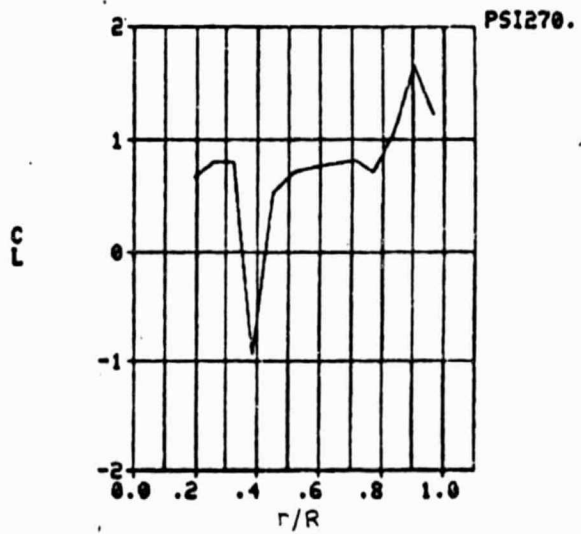
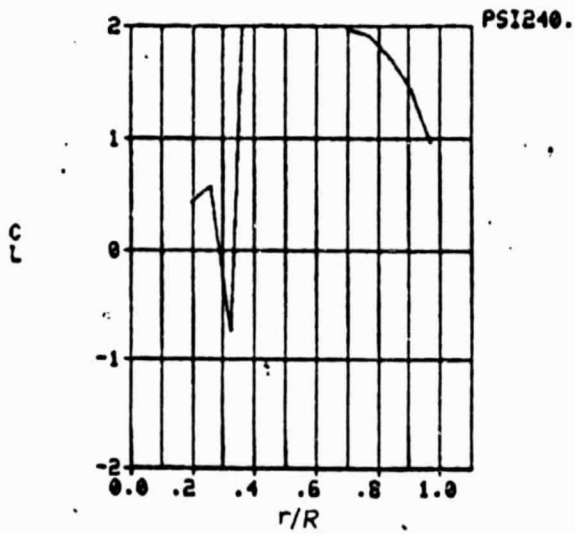
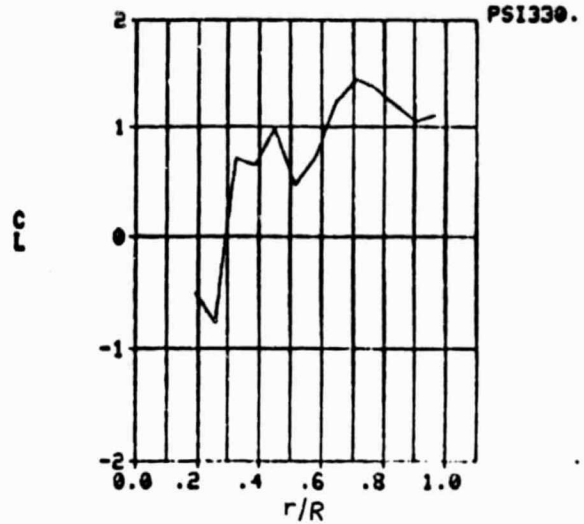
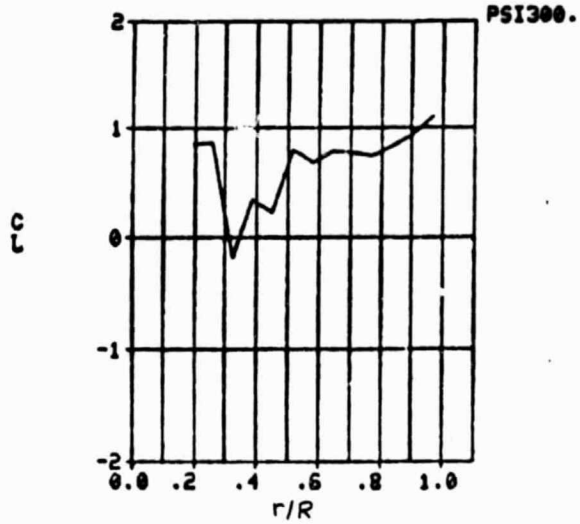


Figure 52 (continued)

The only significant savings in power occurred when the blades were deflected in the vicinity of the advancing blade tip. This is where  $M$  is highest, and only where  $M$  is highest did the minimum  $C_d$  vary greatly with flap deflection.

The various non-sinusoidal flap deflection schedules shown in Table IX are grouped into ten categories. The major categories are designated by the letters A through J, while minor variations in a category are designated by numbers. The general area of the rotor disc where the flap is deflected for each category is shown in the columns of Table IX headed, "Aft Blade", "Advancing Blade", "Front Blade", "Retreating Blade", and "Span".

The columns labeled "Power Savings" in Table IX show the combinations of flight conditions and deflection schedules which resulted in a decrease in average rotor power when compared to a corresponding baseline case of identical flight conditions but no flap deployment. A savings of less than about 3% was not considered significant enough to be considered a positive result. That being the case, only four schedules, A1 through A3 and F, demonstrated an ability to decrease average rotor power, and then only for three sets of flight conditions. Further, Schedules A2, A3 and F differ only slightly from A1. Therefore, only Schedule A1 was used at different flight conditions.

The instantaneous power variation of Schedule A1, under the flight conditions of Table IX (i), is shown in Figure 56.

The decrease of average power shown by Schedule A1 subjected to the flight conditions listed in Table IX (i) was found to be not very sensitive to changes in flap deflection or area of application. Schedules A2, A3 and F are variations in azimuth and radius of Schedule A1. These schedules, as shown in Table IX (i), also produced savings in average power. Tables IX (j) and IX (k) show that small changes in  $\mu$  did not adversely affect the ability of Schedule A1 to decrease rotor power. It should be noted that the analyses in Tables IX (j) and IX (k) were not trimmed completely, but the rotor power in each case was corrected to  $\bar{x} = 0.046$ .

Although a decrease in average power when compared to a baseline case was not expected with Schedule A16, the total excursion from minimum to maximum instantaneous power was. This phenomenon is illustrated in Figure 53. The flight conditions are shown in Table IX (b).

ORIGINAL PAGE IS  
OF POOR QUALITY

NOMINAL FLIGHT CONDITIONS:	$\mu = 0.39$	$C_T/c = 0.06$	$\bar{X} = 0.047$
	$\alpha_g = -6.8^\circ$ (BASELINE)	$C_p/c = 0.0041$ (BASELINE)	

FLAP DEPLOYMENT SCHEDULES									
SCHEDULE NUMBER	AFT BLADE	ADVANCING BLADE	FRONT BLADE	RETREATING BLADE	SPAN	RANGE		$\alpha_g$	POWER SAVINGS
						MIN	MAX		
H1	✓				FULL	-2.5°	5.0°	-4.28°	NO
I	✓	✓	✓		FULL	-3.7°	5.0°	-6.66°	NO
J1	✓	✓	✓		FULL	-5.0°	5.0°	-6.00°	NO
J2	✓	✓	✓	✓	FULL	-5.0°	5.0°	-6.75°	NO

(a)

NOMINAL FLIGHT CONDITIONS:	$\mu = 0.39$	$C_T/c = 0.06$	$\bar{x} = 0.048$							
	$\alpha_g = -6.8^\circ$ (BASELINE)	$C_p/c = 0.0042$ (BASELINE)								
FLAP DEPLOYMENT SCHEDULES										
SCHEDULE NUMBER	AFT BLADE	ADVANCING BLADE	FRONT BLADE	RETREATING BLADE	SPAN	RANGE		$\alpha_g$	POWER SAVINGS	
						MIN	MAX			
A16	✓	✓	✓	✓	TIP	-2.0°	-2.0°	-6.50°	NO	
E (1)		✓			TIP	-1.7°	0.0°	-6.50°	NO	

(1) SCHEDULE E PROVIDED THE LOWEST TIP WINDUP ATTAINED - 5% OF BASELINE VALUE

(b)

NOMINAL FLIGHT CONDITIONS:	$\mu = 0.39$	$C_T/c = 0.10$	$\bar{X} = 0.046$						
	$\alpha_g = -3.0^\circ$ (BASELINE)	$C_D/c = 0.0057$ (BASELINE)							
FLAP DEPLOYMENT SCHEDULES									
SCHEDULE NUMBER	AFT BLADE	ADVANCING BLADE	FRONT BLADE	RETREATING BLADE	SPAN	RANGE		$\alpha_g$	POWER SAVINGS
						MIN	MAX		
H1	✓				FULL	-2.5°	5.0°	-5.12°	NO
I	✓	✓	✓		FULL	-3.7°	5.0°	-4.0°	NO
J1	✓	✓	✓		FULL	-5.0°	5.0°	-3.0°	NO
J2	✓	✓	✓	✓	FULL	-5.0°	5.0°	-3.67°	NO

(c)

NOMINAL FLIGHT CONDITIONS:	$\mu = 0.50$	$C_T/c = 0.06$	$\bar{X} = 0.046$						
	$\alpha_g = -10.21^\circ$ (BASELINE)	$C_p/c = 0.0078$ (BASELINE)							
FLAP DEPLOYMENT SCHEDULE									
SCHEDULE NUMBER	AFT BLADE	ADVANCING BLADE	FRONT BLADE	RETREATING BLADE	JPG-1	RANGE		$\alpha_g$	POWER SAVINGS
						MIN	MAX		
H1	✓				FULL	-2.5°	5.0°	-8.21°	NO

(d)

Table IX Flight Conditions and Results of B-53 Analyses

NOMINAL FLIGHT CONDITIONS:	$\mu = 0.50$	$C_T/\delta = 0.06$	$R = 0.048$						
	$\alpha_s = -10.21^\circ$ (BASELINE)	$C_D/\delta = 0.0079$ (BASELINE)							
FLAP DEPLOYMENT SCHEDULES									
SCHEDULE NUMBER	AFT BLADE	ADVANCING BLADE	FRONT BLADE	RETREATING BLADE	SPAN	RANGE		$\alpha_s$	POWER SAVINGS
						MIN	MAX		
A1		✓			TIP	-2.6°	-1.4°	-9.9°	NO
A4		✓			TIP	-2.0°	-0.8°	-10.21°	NO
A5		✓			TIP	-4.0°	-0.6°	-10.21°	NO
A6		✓			TIP	-2.0°	-0.5°	-10.21°	NO
A7		✓			TIP	-2.8°	-0.2°	-10.21°	NO
A8		✓			TIP	-2.3°	-0.2°	-10.21°	NO
A10		✓			TIP	0.8°	0.8°	-10.21°	NO
A11		✓			TIP	-1.6°	-1.0°	-10.21°	NO
A12		✓			TIP	-1.0°	-1.0°	-10.21°	NO
A13		✓			TIP	-2.0°	-2.0°	-10.21°	NO
A14		✓			TIP	-2.0°	-2.0°	-10.21°	NO
A15		✓			TIP	-2.0°	-2.0°	-10.21°	NO
C6				✓	TIP	5.0°	5.0°	-9.8°	NO
D			✓	✓	TIP	2.0°	2.0°	-10.21°	NO

(e)

NOMINAL FLIGHT CONDITIONS:	$\mu = 0.50$	$C_T/\delta = 0.09$	$\bar{X} = 0.051$							
	$\alpha_s = -7.3^\circ$ (BASELINE)	$C_D/\delta = 0.0097$ (BASELINE)								
FLAP DEPLOYMENT SCHEDULES										
SCHEDULE NUMBER	AFT BLADE	ADVANCING BLADE	FRONT BLADE	RETREATING BLADE	SPAN	RANGE		$\alpha_s$	POWER SAVINGS:	
						MIN	MAX			
A1		✓			TIP	-2.6°	-1.4°	-8.5°	NO	
A9		✓			TIP	-3.5°	-2.1°	-7.8°	N/	
D			✓	✓	TIP	2.0°	2.0°	-6.5°	NO	

(f)

NOMINAL FLIGHT CONDITIONS:		$\mu = 0.39$	$C_T/\delta = 0.10$	$\bar{X} = 0.046$					
		$\alpha_s = -3.05^\circ$ (BASELINE)	$C_D/\delta = 0.0053$ (BASELINE)						
FLAP DEPLOYMENT SCHEDULES									
SCHEDULE NUMBER	AFT BLADE	ADVANCING BLADE	FRONT BLADE	RETREATING BLADE	SPAN	RANGE		$\alpha_s$	POWER SAVINGS
						MIN	MAX		
A1		✓			TIP	-2.6°	-1.4°	-3.0°	NO
B1	✓				TIP	-2.0°	-2.0°	-3.05°	NO
B2	✓				TIP	-5.0°	-2.5°	-3.11°	NO
B3	✓				TIP	-5.0°	3.0°	-3.11°	NO
B4	✓				TIP	2.0°	5.0°	-3.11°	NO
B5	✓				TIP	-5.0°	-2.0°	-3.11°	NO
B6	✓				TIP	-10.0°	6.0°	-3.11°	NO
C1				✓	TIP	1.0°	1.0°	-3.05°	NO
C2				✓	TIP	2.0°	2.0°	-3.05°	NO
G	✓		✓		CUTOUT	5.0°	5.0°	-3.05°	NO
H2	✓				FULL	-1.9°	-0.4°	-3.05°	NO

(1) THESE RESULTS WERE FOUND AFTER B53 MODIFICATION.

(g)

Table IX (continued)

ORIGINAL PAGE 13  
OF POOR QUALITY

NOMINAL FLIGHT CONDITIONS:	$\mu = 0.50$	$C_T/\epsilon = 0.06$	$\bar{X} = 0.046$						
	$\alpha_s = -9.75^\circ$ (BASELINE)	$C_p/\epsilon = 0.0078$ (BASELINE)							
FLAP DEPLOYMENT SCHEDULES									
SCHEDULE NUMBER	AFT BLADE	ADVANCING BLADE	FRONT BLADE	RETRACTING BLADE	SPAN	RANGE		$\alpha_s$	POWER SAVINGS
						MIN	MAX		
A1		✓			TIP	-2.6°	-1.4°	-9.4°	NO
C3				✓	TIP	-2.6°	-5.0°	-9.61°	NO

(1) THESE RESULTS WERE FOUND AFTER B53 MODIFICATION.

(h)

NOMINAL FLIGHT CONDITIONS:		$\mu = 0.50$	$C_T/\epsilon = 0.09$	$\bar{X} = 0.046$					
		$\alpha_s = -6.155^\circ$ (BASELINE)	$C_p/\epsilon = 0.0099$ (BASELINE)						
FLAP DEPLOYMENT SCHEDULES									
SCHEDULE NUMBER	AFT BLADE	ADVANCING BLADE	FRONT BLADE	RETRACTING BLADE	SPAN	RANGE		$\alpha_s$	POWER SAVINGS
						MIN	MAX		
A1		✓			TIP	-2.6°	-1.4°	-6.2°	10.7%
A2		✓			TIP	-2.9°	-1.6°	-6.2°	7.4%
A3		✓			TIP	-2.6°	-2.0°	-6.887°	4.8%
F	✓	✓	✓		INTERIOR	-2.6°	5.0°	-6.0°	15.6%

(1) THESE RESULTS WERE FOUND AFTER B53 MODIFICATION.

(2) THE COMBINATIONS OF FLIGHT CONDITIONS AND FLAP DEPLOYMENT SCHEDULES IN THIS TABLE ARE THE ONLY COMBINATIONS TO RESULT IN A POWER SAVINGS.

(i)

NOMINAL FLIGHT CONDITIONS:	$\mu = 0.474$	$C_T/\epsilon = 0.09$	$\bar{X} = 0.046$						
	$\alpha_s = -6.155^\circ$ (BASELINE)	$C_p/\epsilon = 0.0087$ (BASELINE)							
FLAP DEPLOYMENT SCHEDULES									
SCHEDULE NUMBER	AFT BLADE	ADVANCING BLADE	FRONT BLADE	RETRACTING BLADE	SPAN	RANGE		$\alpha_s$	POWER SAVINGS
						MIN	MAX		
A1		✓			TIP	-2.6°	-1.4°	-6.2°	14.1%

NOMINAL FLIGHT CONDITIONS:	$\mu = 0.526$	$C_T/\epsilon = 0.09$	$\bar{X} = 0.046$						
	$\alpha_s = -6.155^\circ$ (BASELINE)	$C_p/\epsilon = 0.0128$ (BASELINE)							
FLAP DEPLOYMENT SCHEDULES									
SCHEDULE NUMBER	AFT BLADE	ADVANCING BLADE	FRONT BLADE	RETRACTING BLADE	SPAN	RANGE		$K_s$	POWER SAVINGS
						MIN	MAX		
A1		✓			TIP	-2.6°	-1.4°	-6.2°	11.6%

Table IX (continued)

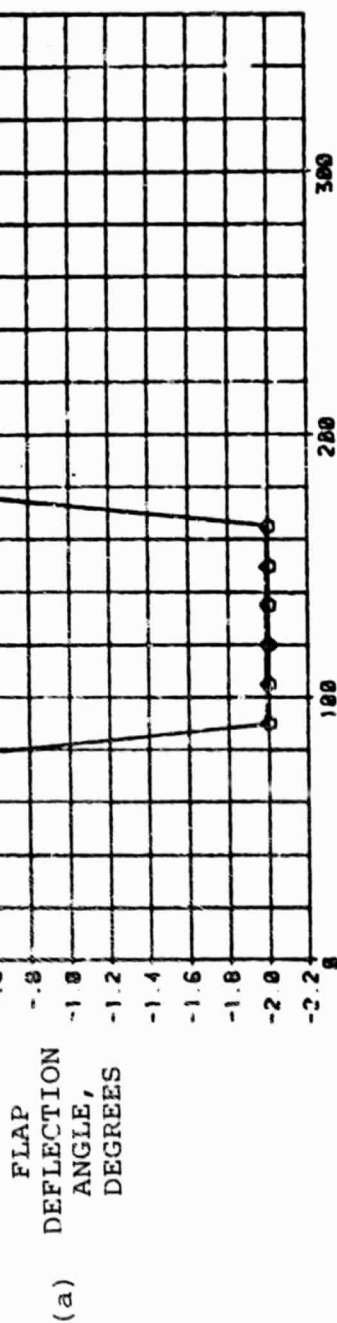
$\mu$	$C_T/\sigma$	$\bar{x}$	$\alpha_s$ (baseline)	$C_p/\sigma$ (baseline)
0.39	0.06	0.047	-6.800	0.0041
0.39	0.06	0.048	-6.800	0.0042
0.39	0.10	0.046	-3.000	0.0057
0.50	0.06	0.046	-10.200	0.0078
0.50	0.06	0.048	-10.200	0.0079
0.50	0.09	0.051	-7.300	0.0097
0.39	0.10	0.046	-3.050	0.0053
0.50	0.06	0.046	-9.750	0.0078
0.50	0.09	0.046	-6.155	0.0099
0.474	0.09	0.046	-6.155	0.0087
0.526	0.09	0.06	-6.155	0.0128

TABLE X. Flight Condition Summary

OF BOOK QUALITY  
ORIGINAL PAGE IS  
21 3049 JAN 1990

NASA AMES A-1 AIRFOIL; H34 ROTOR B53 PROG.  $\mu = 0.39$   $CT = 0.06$   $XBAR = 0.048$

□ BASELINE  
○ SCHEDULE A16



ORIGINAL PAGE IS  
OF POOR QUALITY

□ BASELINE  
○ SCHEDULE A16

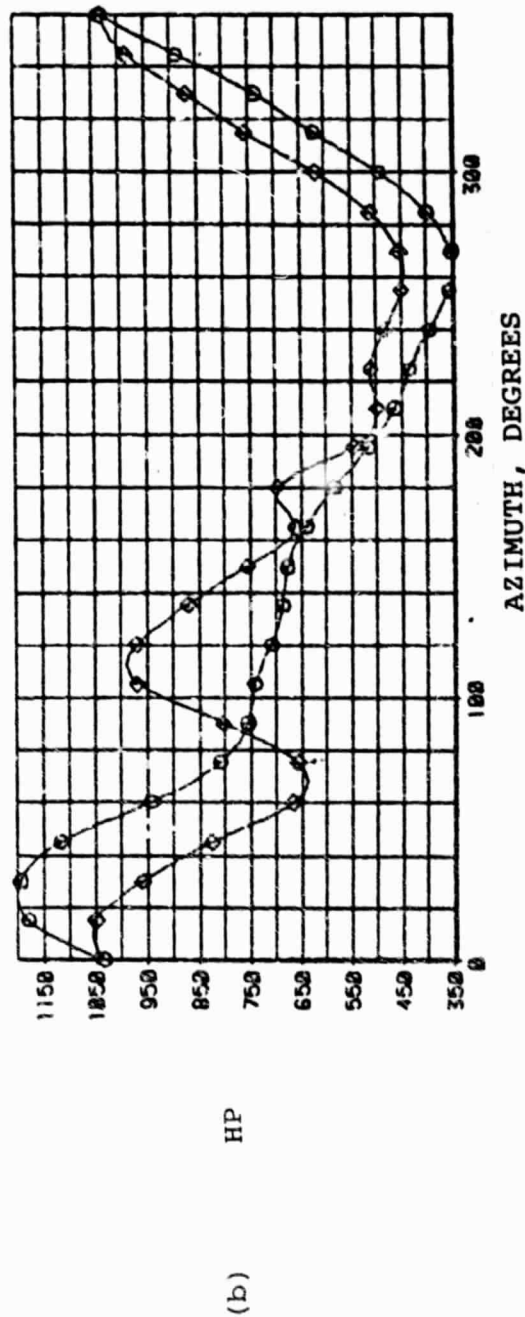


Figure 53 Comparison of Schedule A16 and Baseline.  $C_T/\sigma = 0.06$ ,  $\mu = 0.39$ ,  $\bar{X} = 0.048$ .

(a) FLAP DEFLECTION ANGLE (b) HORSEPOWER

## 6.2 Elastic Effects and Potential Benefits

With a view to decreasing elastic torsional deflections of the rotor blades, the non-sinusoidal flap deflection schedules were determined in two ways. One way was to deploy the flaps with systematic radial and azimuthal variation of the deflection angle. Some of these variations are shown in Table VIII.

Schedule A1, which did provide a decrease in rotor power, also provided a significant decrease in blade tip elastic twist in the azimuthal vicinity of flap deployment as shown in Figure 55. Blade tip twist was reduced only slightly elsewhere on the azimuth. These results were obtained for the flight conditions of Figure 56.

An other attempt to reduce drag on the advancing blade was to define a deployment schedule that would decrease the blade tip elastic twist. The result of this investigation was Schedule E. The flight conditions at which it was used are  $C_T/\sigma = 0.06$ ,  $\bar{X} = 0.047$ , and  $M = 0.39$ . The comparison of blade tip twist between Schedule E and the baseline case with flaps undeflected is shown in Figure 54. As can be seen in Figure 54, Schedule E decreases the maximum absolute value of elastic twist by a factor of about 20. Schedule E did not provide a decrease in average rotor power but did demonstrate the potential for controlling the blade elastic twist to a required level. If a prescribed level of blade elastic twist was defined that would significantly improve rotor performance beyond the reductions in compressibility power demonstrated here, this variable camber concept would provide a powerful means of attaining additional performance benefits.

## 7.0 Mechanical Feasibility

A mechanical feasibility study was started while the candidate variable camber concepts were being evaluated, so that some preliminary assessment could be made of the difficulty involved in deploying the devices under consideration. As the preliminary evaluation showed, all configurations except the trailing edge devices were unsatisfactory due to the unusual lift requirements of helicopter rotors; therefore, the emphasis of the mechanical feasibility study was then focused on trailing edge flaps. The configuration selected for evaluation involved the A-1 airfoil equipped with a 50% plain, sealed flap. The results of the review of 50% flap feasibility are also applicable to the 35% flap.

ORIGINAL PAGE IS  
OF POOR QUALITY

ELASTIC TWIST  
A-1 35% FLAP

● BASELINE  
■ SCHEDULE E

MCDONNELL A-1 AIRFOIL, TWIST AT TIP OF H24 ROTOR  
B33 PROC.  $\mu = 0.39$   $C_T = 0.86$   $X_{BAR} = 0.848$  OUTED SEGMENT

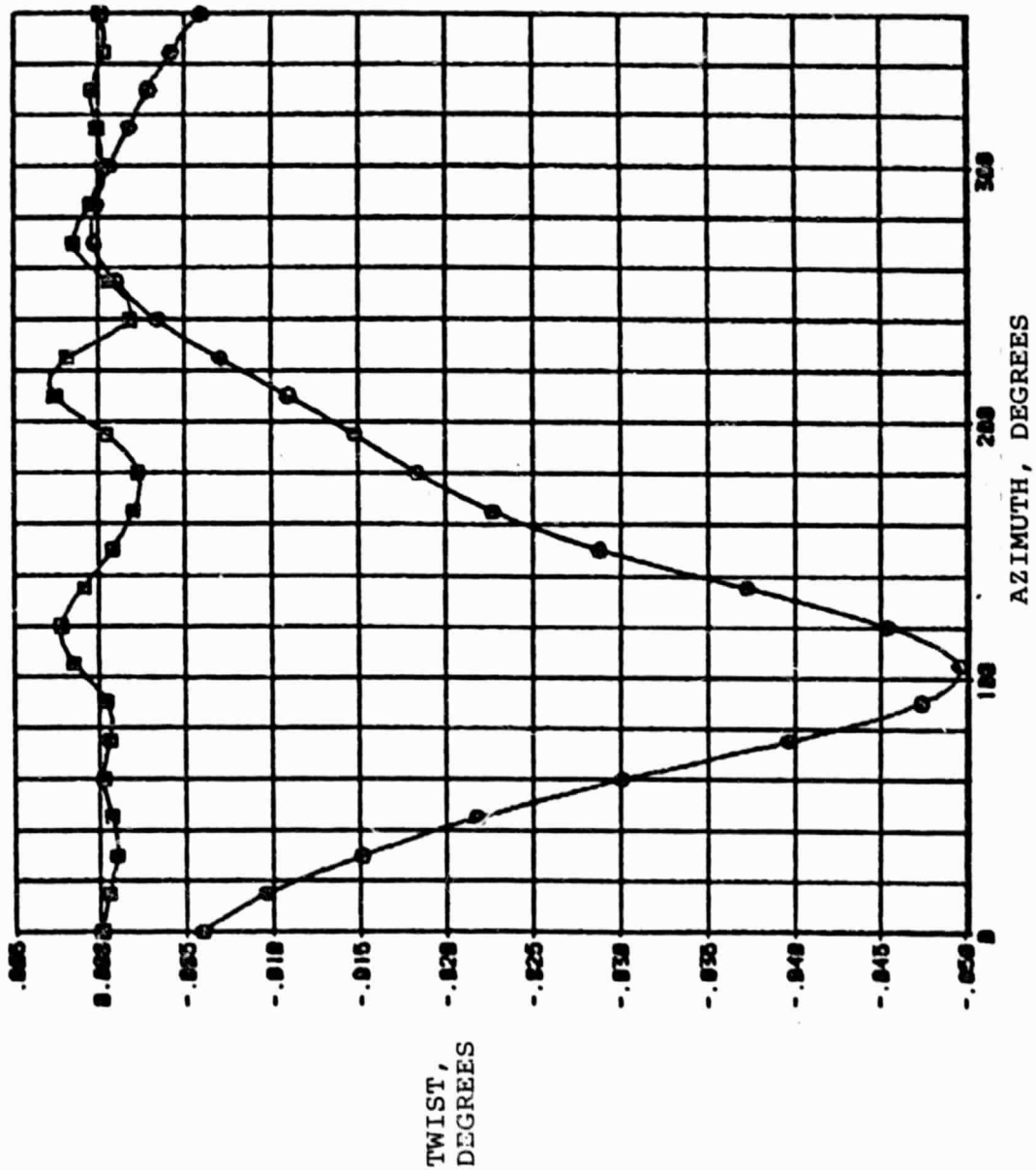


Figure 54 Blade Tip Twist - Schedule E and Baseline.  
 $C_T/\sigma = 0.06$ ,  $\mu = 0.39$ ,  $\bar{X} = 0.048$

ORIGINAL PAGE IS  
OF POOR QUALITY

ORIGINAL PAGE IS  
OF POOR QUALITY

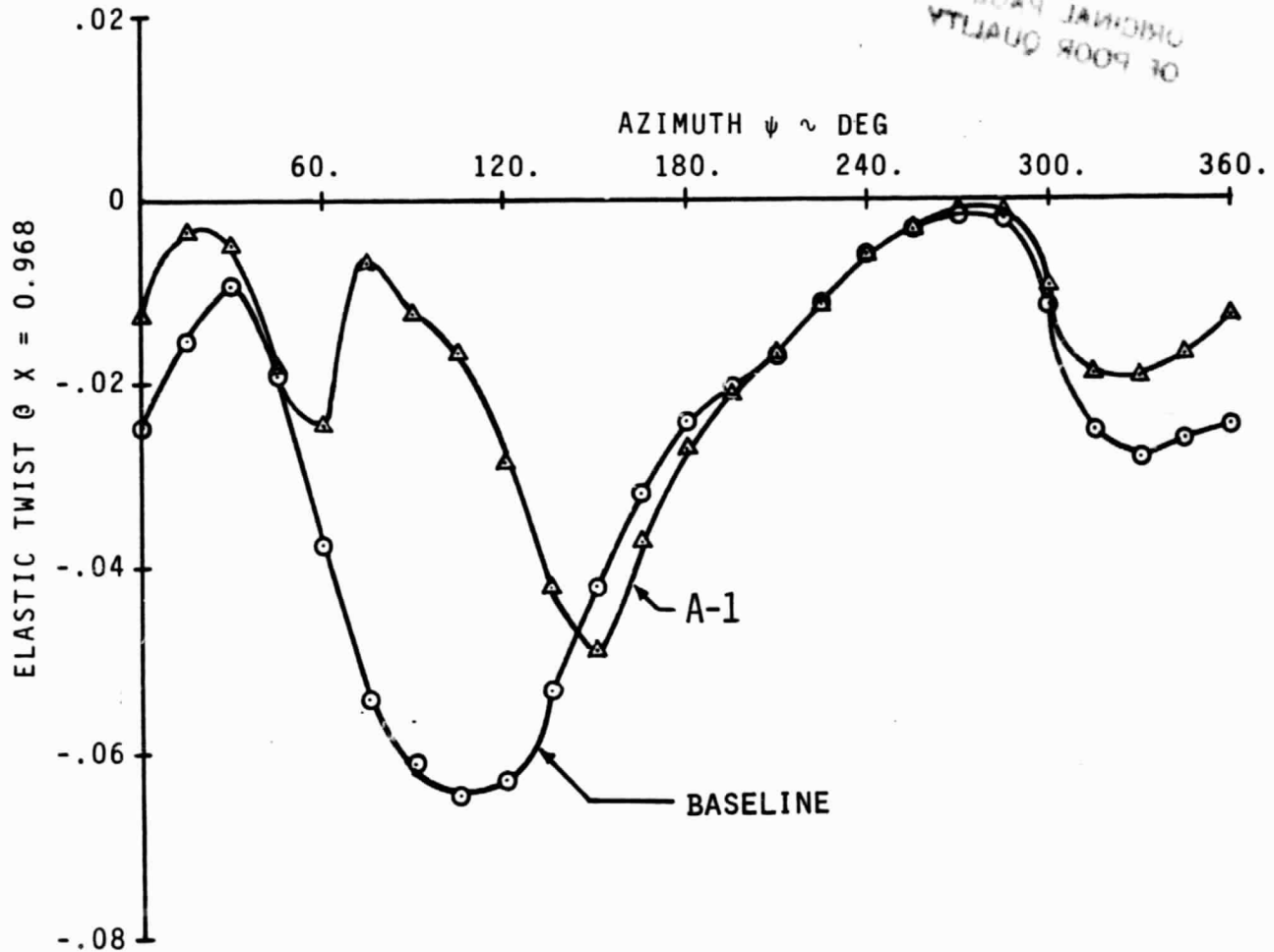


Figure 55 Blade Tip Twist - Schedule A1 and Baseline  
 $C_T/\sigma = 0.09$ ,  $\mu = 0.5$ ,  $\bar{X} = 0.046$

ORIGINAL PAGE IS  
OF POOR QUALITY

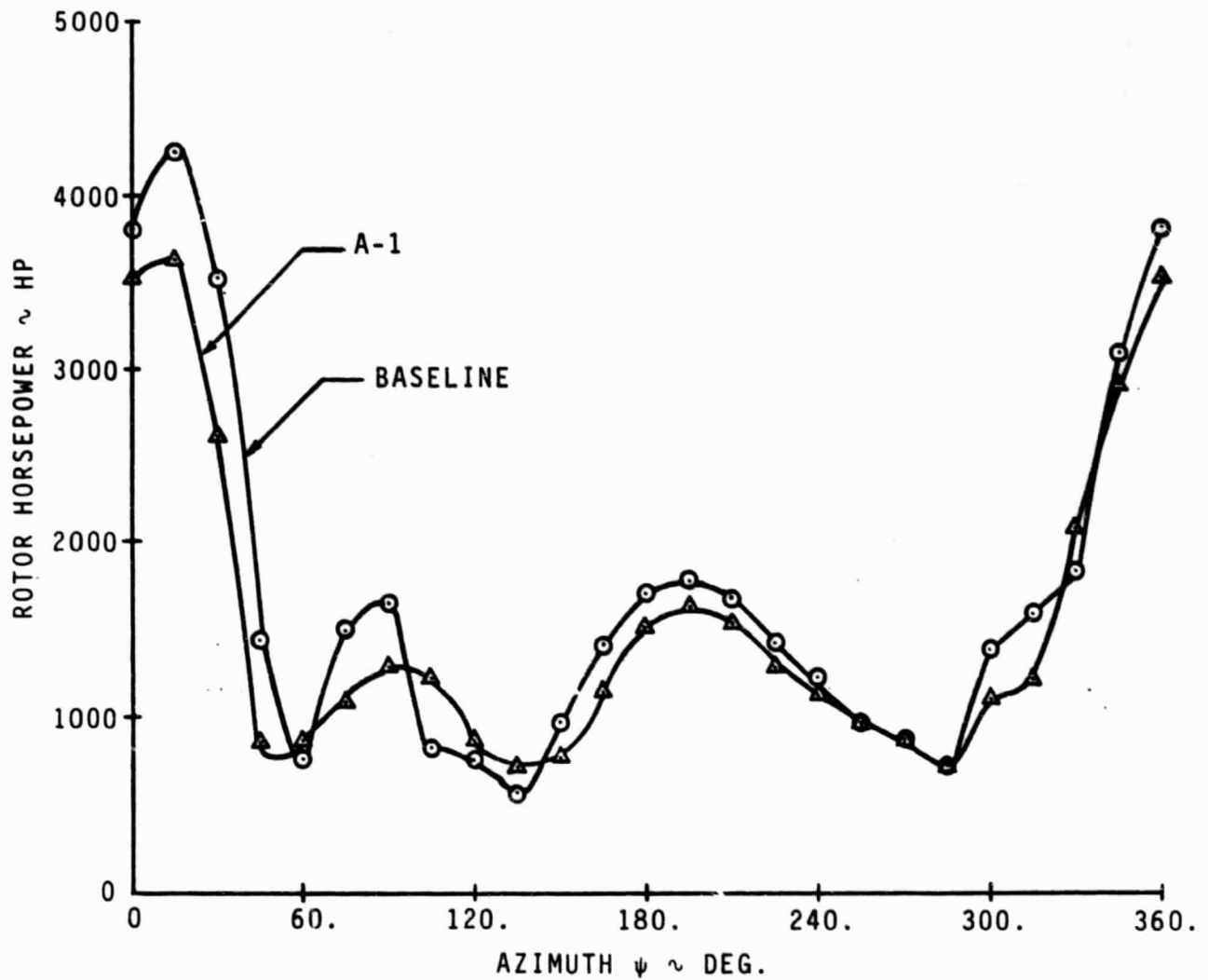


Figure 56 Rotor Instantaneous Power Variation - Schedule A1 and Baseline.  $C_T/\sigma = 0.09$ ,  $\mu = 0.5$

The review of the means to deploy variable camber covered, the following aspects conceptually:

- (a) Spanwise deployment alternatives
- (b) Flap hinge kinematics, rigid vs. flexible skins
- (c) Flap loads and moments, as due to cyclic variations in the local flow environment.
- (d) Means of actuation (mechanical, hydraulic, pneumatic, electric).
- (e) Assessment of weight distribution.

#### 7.1 Example of Flap Deployment Scheme

Figures 57 through 64 illustrate some of the elements to be taken into account when examining the details of variable camber to be deployed on a helicopter rotor. Figure 57 addresses the general features of the flow encountered by the inboard, midspan and outboard segments of a rotor blade. Figure 58 illustrates the probable range of flap deflection angles to be expected in a variable camber blade. Although the 50% flap configuration shown in Figure 58 can be deflected up by  $-5^\circ$ , and down by  $15^\circ$ ; the range of deployment would probably never exceed  $\pm 5^\circ$  because of the very large pitching moments associated with flap deflection, shown earlier in Figure 51.

Figures 59 and 60 show the spanwise and cyclic variation in dynamic pressure and Mach number, respectively, encountered in forward flight at an advance ratio  $\mu = 0.5$ . Figure 61 shows the effect of flap deflection angle on the pressure coefficients integrated from the trailing edge to the flap hinge; i.e. the shear lead at the hinge. The pressures were obtained by means of the airfoil analysis of references 20 and 22, and summarize both the effects of angle of attack and Mach number variation for the A-1 airfoil with a 50% flap. Figure 62 addresses feasible flap deployment alternatives over the three spanwise regions. Depending on the method of actuation, it might be easier to deploy step inputs rather a more complex continuous flap angle variation scheme.

Figure 63 shows the aerodynamic hinge moments to be expected over a 50% at a  $\mu = 0.5$  flight condition. Figure 64 summarizes the spanwise variation in the maximum hinge moment. The loads and moments can be estimated from the Mach number, angle of attack and sectional characteristics calculated by the B-53 analysis. B-53 also provides the blade flapping motions.

ORIGINAL PAGE IS  
OF POOR QUALITY

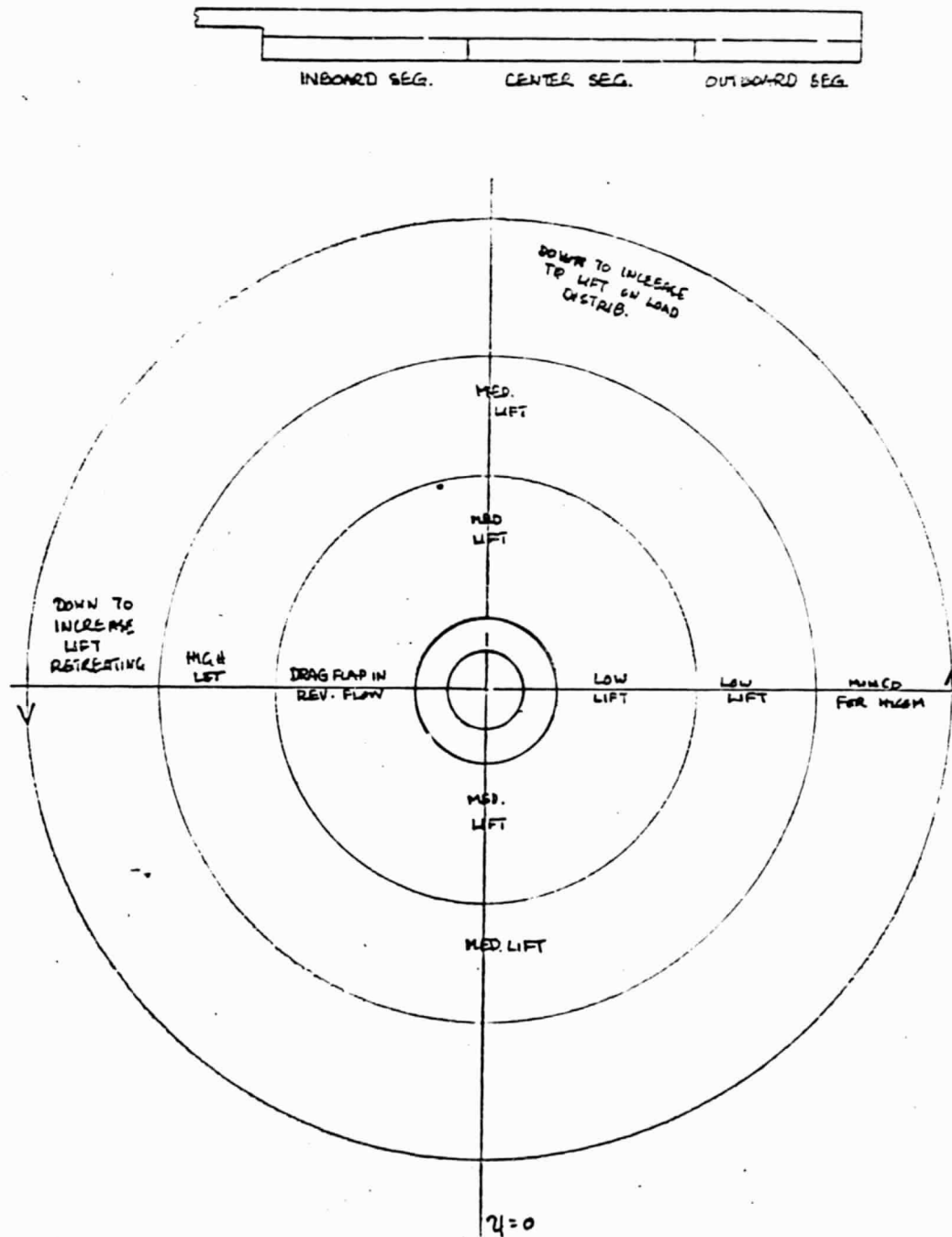


Figure 57 Variable Camber Blade, 3-Segment  
Schedule Characteristics.

ORIGINAL PAGE IS  
OF POOR QUALITY

ORIGINAL PAGE IS  
OF POOR QUALITY

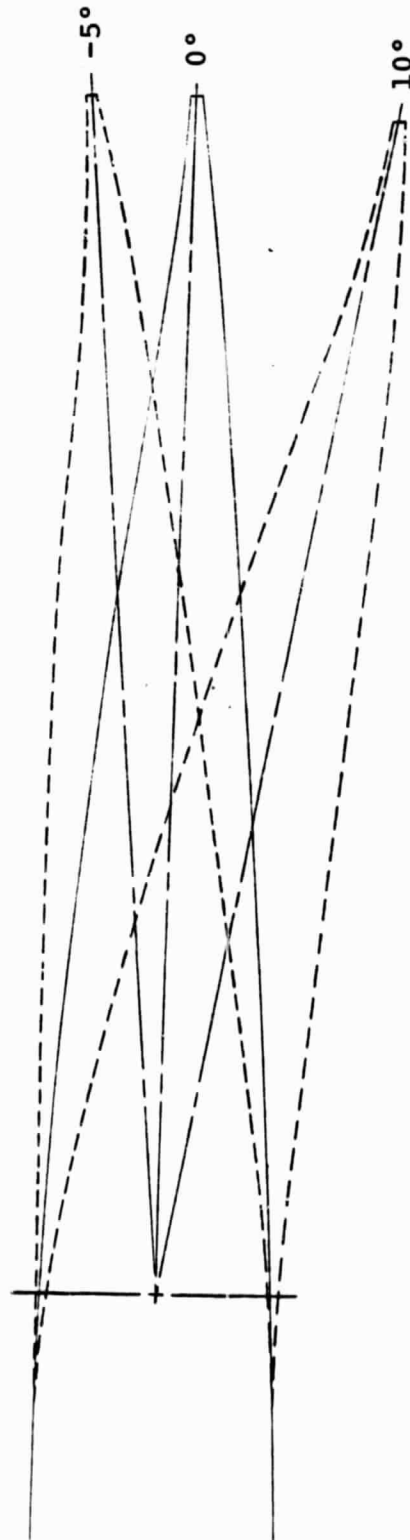


Figure 58 Flap Deflection Achieved by Means of Flexible Skins at the Flap Hinge.

ORIGINAL PAGE IS  
OF POOR QUALITY

DYNAMIC PRESSURE AT VARIOUS ROTOR RADII  
39 FT. DIA ROTOR 225 RPM  $\mu$  8.5

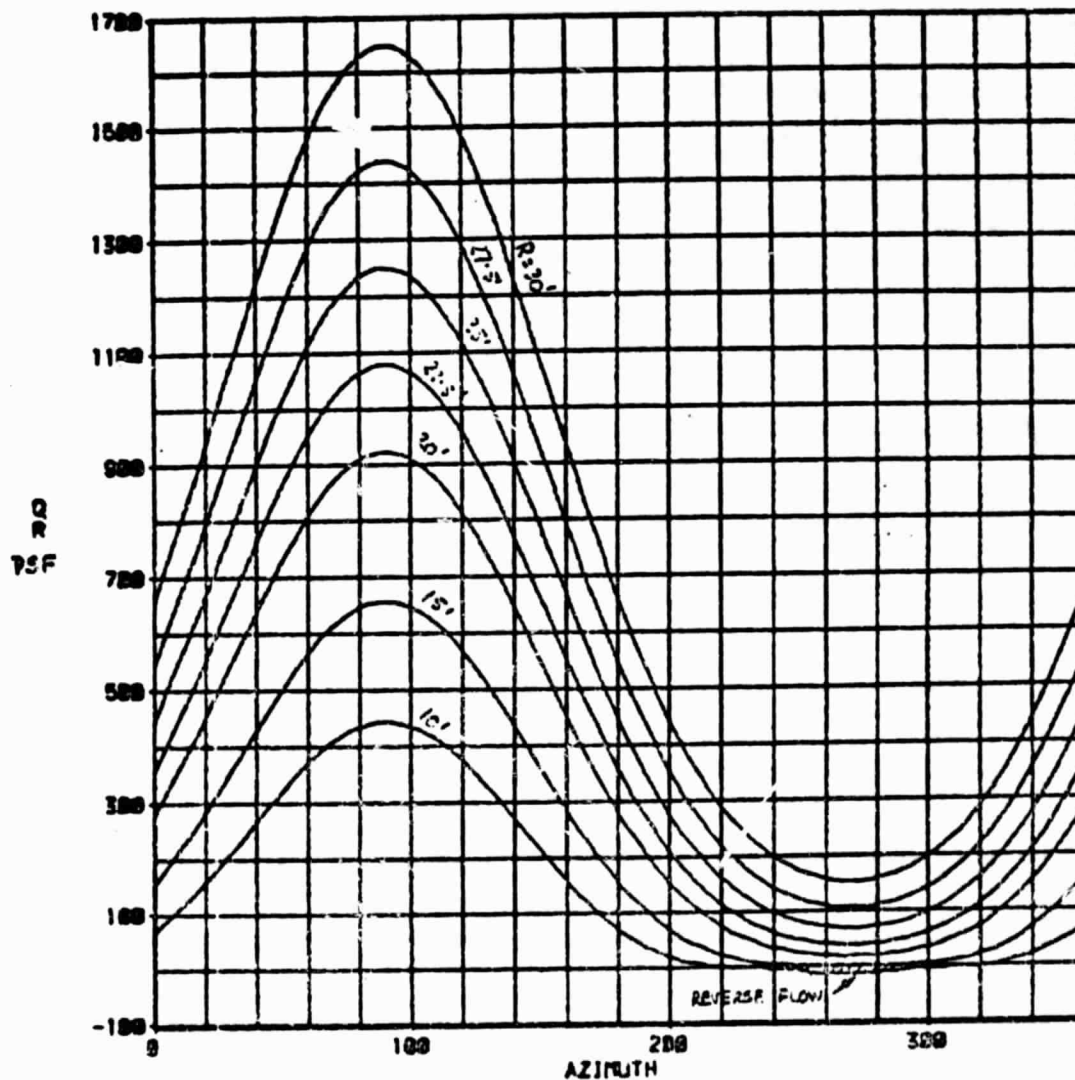


Figure 59 Example of Dynamic Pressure Environment in Forward Flight.

ORIGINAL PAGE IS  
OF POOR QUALITY

LOCAL MACH NO. AT VARIOUS ROTOR RADII  
38 FT. DIA ROTOR 225 RPM MU 0.5

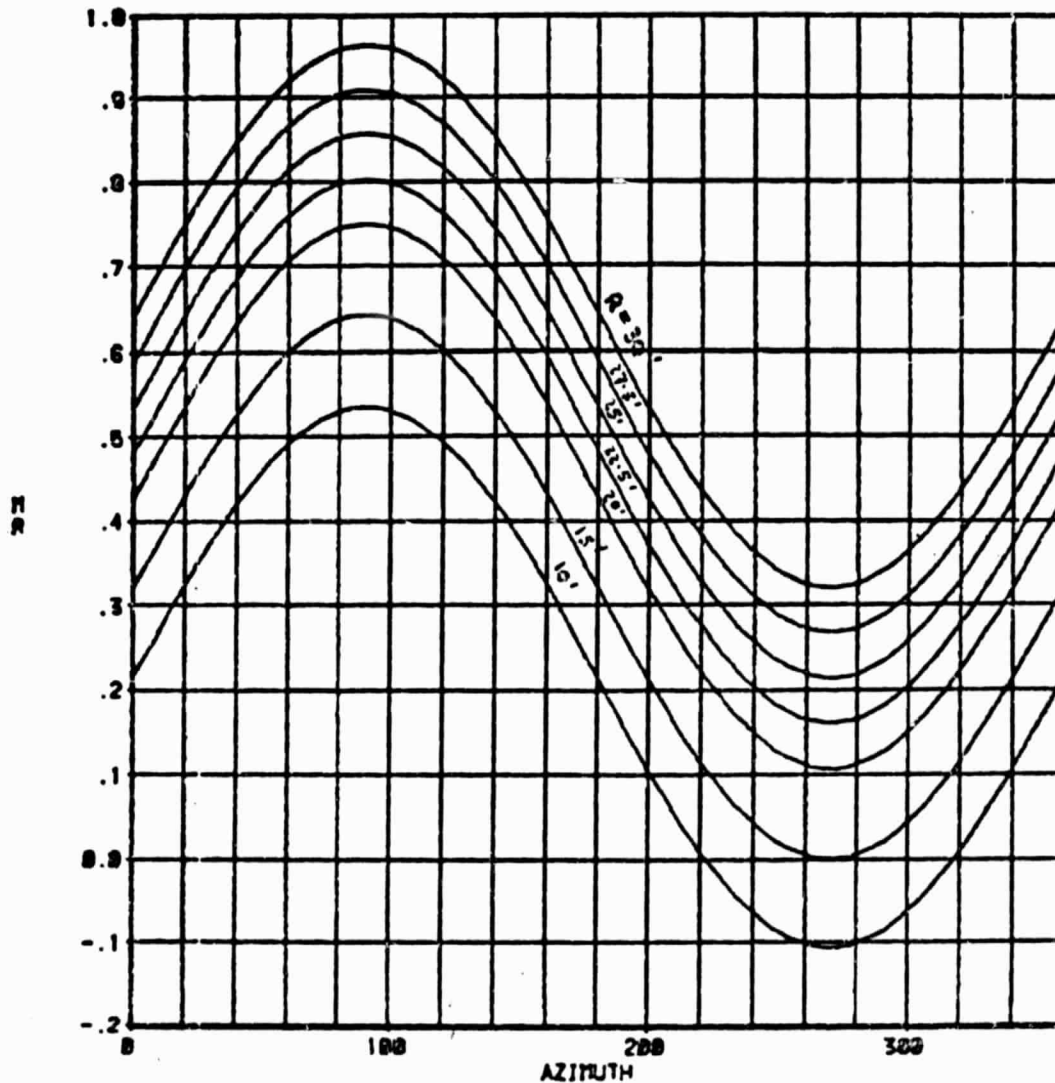


Figure 60 Example of Local Mach Number Environment in Forward Flight.

ORIGINAL PAGE IS  
OF POOR QUALITY

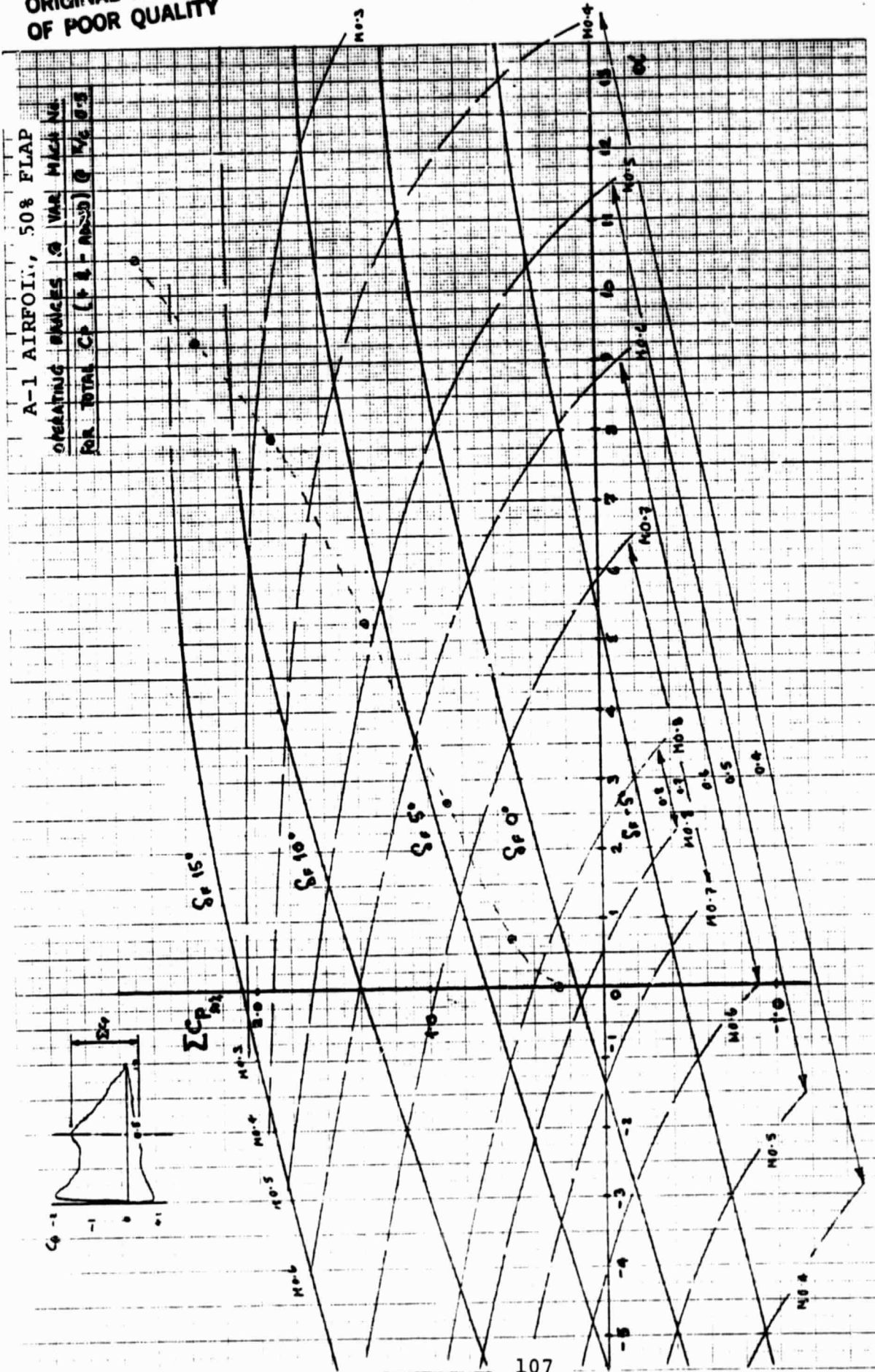
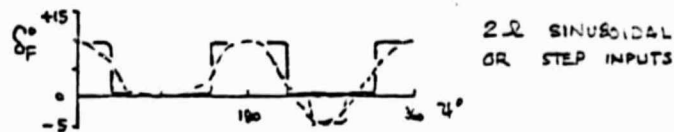


Figure 61 Flap Normal Force at the Flap Hinge.

ORIGINAL PAGE IS  
OF POOR QUALITY

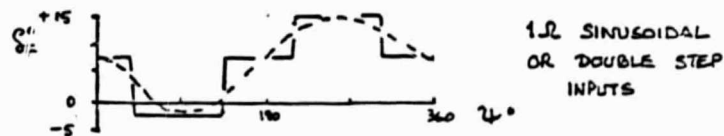
### INBOARD

LOW  $C_L$  ADVANCING ; INCREASING  $C_L$  TO  $180^\circ$  ;  
REDUCE TO HIGH DRAG PROFILE IN REVERSE  
FLOW REGION  $\sim 270^\circ$  ; INCREASING  $C_L$  TO  
 $0^\circ$



### CENTER

LOW  $C_L$  ADVANCING ; INCREASING TO MEDIUM  
VALUE @  $180^\circ$  ; INCREASING TO HIGH VALUE  
RETREATING @  $270^\circ$



### OUTBOARD

MINIMUM  $C_D$  ADVANCING ( $90^\circ$ ) FOR MIN. DRAG  
RISE @ HIGH MACH No. ; INCREASE  $C_L$  @  $180^\circ$   
TO FILL IN LIFT DEFICIT @ TIP DUE TO UNSTEADY AERO;  
INCREASE FOR RETREATING  $270^\circ$

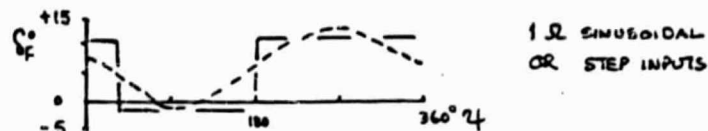


Figure 62 3-Segment Variable Camber Flap  
Deflection Scheduling.

ORIGINAL PAGE IS  
OF POOR QUALITY

VERY APPROXIMATE FROM ESTIMATED DEFLECTIONS  
CH-47 BLADE 2.67' CHORD ; 0.5c FLAP

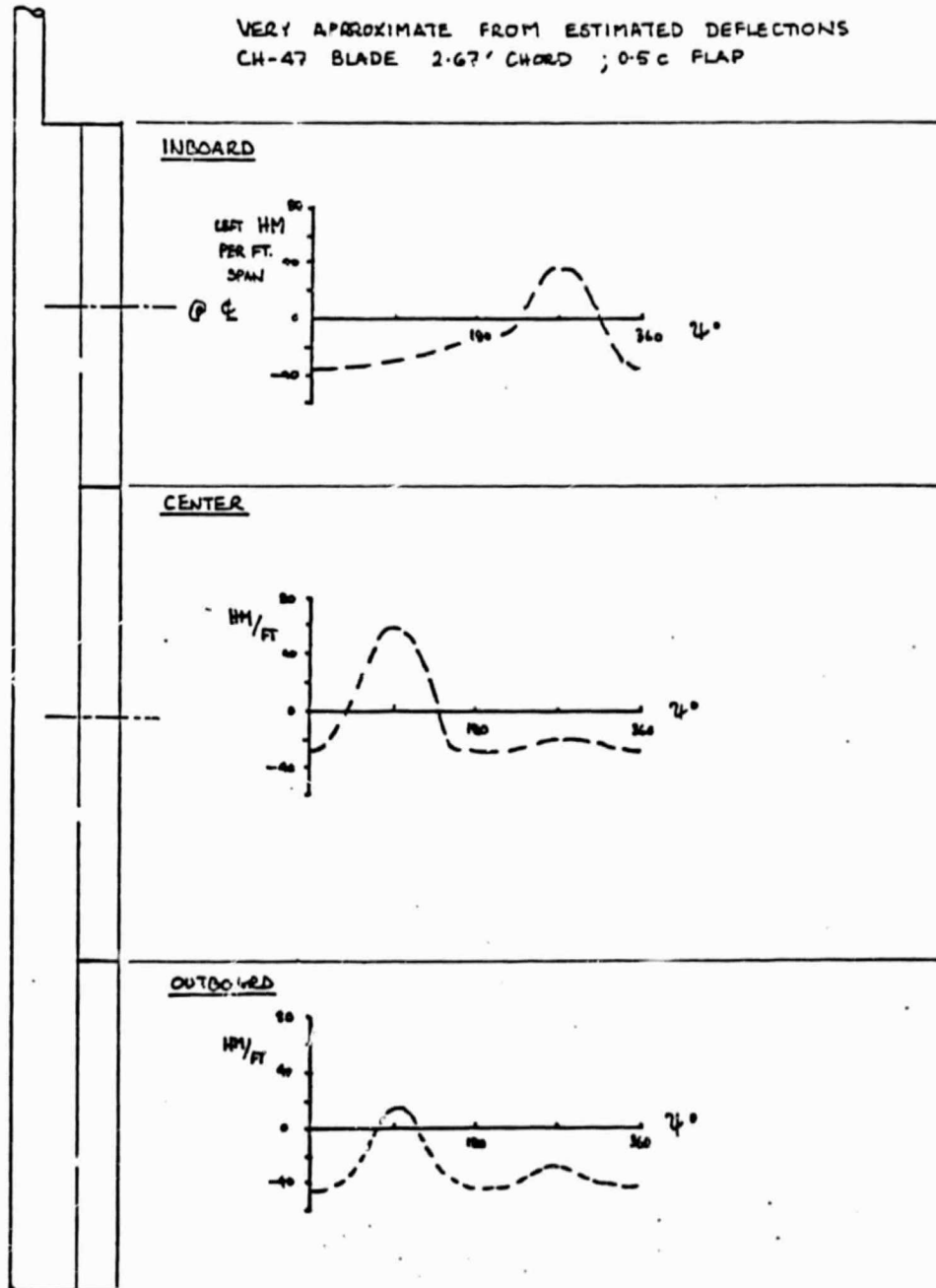


Figure 63 3-Segment Variable Camber Hinge  
Moment Loading.

ORIGINAL PAGE IS  
OF POOR QUALITY

ORIGINAL PAGE IS  
OF POOR QUALITY

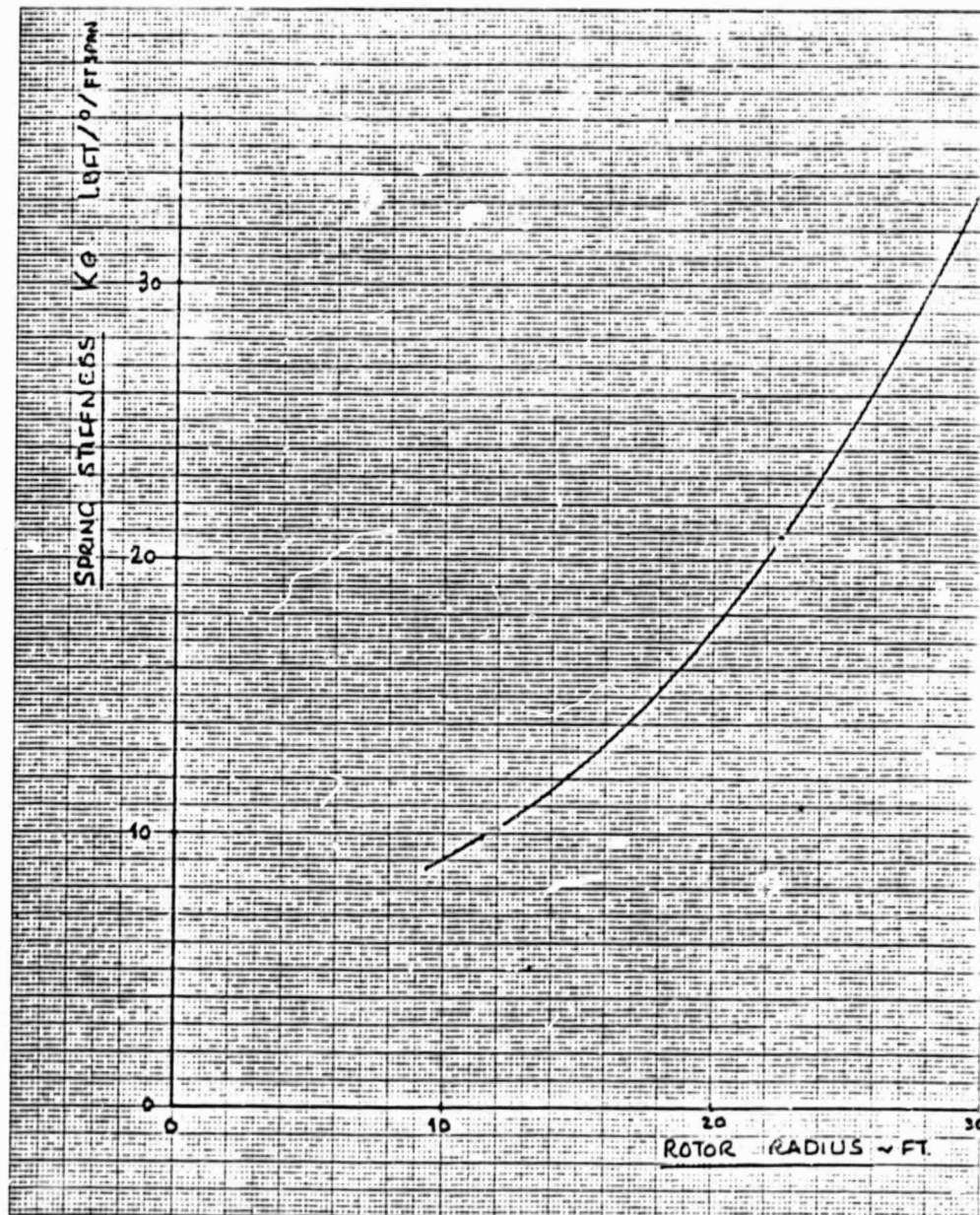


Figure 64 Radial Variation of Hinge Moments for the A-1 Airfoil with a 50% Flap.

## 7.2 Means of Variable Camber Actuation

Figures 65 through 68 address the feasible means to drive variable camber T.E. devices. The methods considered are mechanical, hydraulic, pneumatic and electric. Examples of spanwise deployment are shown in Figure 69.

## 7.3 Hinge Designs

A flexible skin and a rigid skin flap deployment scheme were reviewed in some detail to quantify any potential advantages of one approach over the other. Figures 70 and 71 compare hinge kinematics. Figures 72 and 73 show the effect of hinge contour on the pressure distributions at  $M = 0.4$  for a relatively high lift level ( $\mu = 1.37$ ). A comparison of the pressure distributions points out that, clearly, the flexible skins allow a smoother hinge contour, with potentially substantial benefits in terms of profile drag reduction and/or attainment of higher unseparated lift levels. Figures 74 through 78 compare the Y-39 predictions for the two configurations. Figure 74 shows the variation of the lift coefficient with angle of attack, Figure 75 compares the profile drag coefficients, Figure 76 the lift/drag polars, Figure 77 the pitching moment coefficients, and Figure 78 the calculated turbulent separation boundaries.

## 7.4 Mass Distribution

Figure 79 shows the estimated mass distribution over a blade employing variable camber devices (50% plain flaps) from root to tip. The estimate was carried out for an H-34 blade.

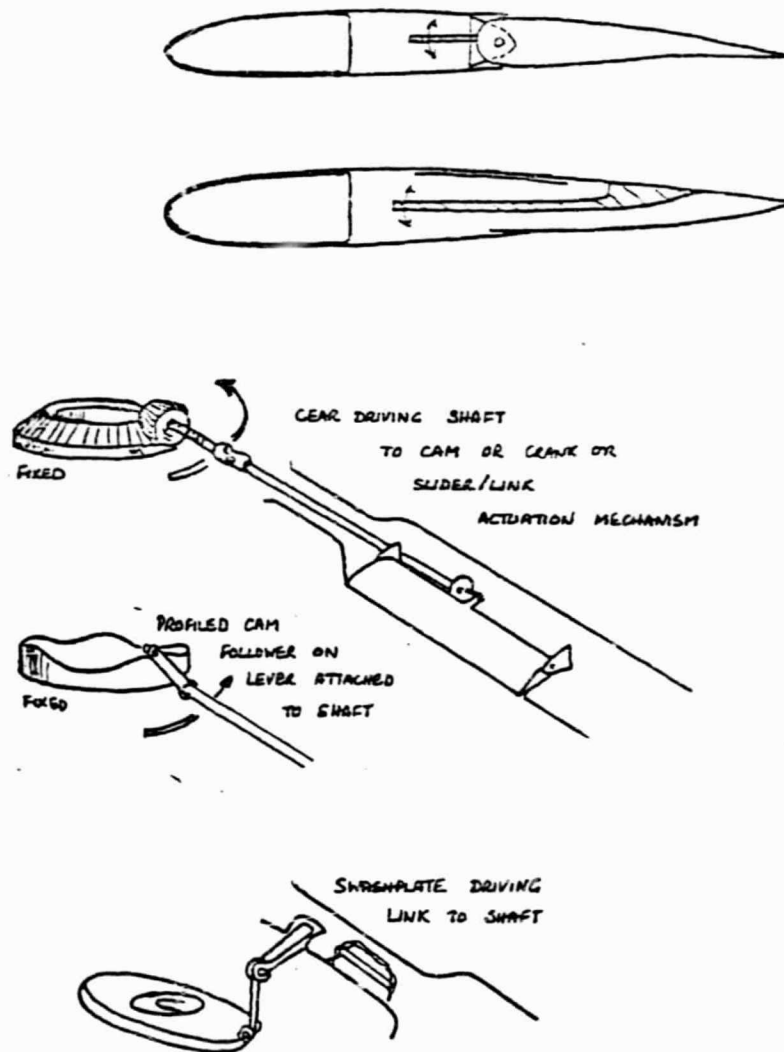
## 8.0 Conclusions and Recommendations

### 8.1 Conclusions Concerning Performance Characteristics and Elastic Effects

The potential benefits in power reduction from using a variable camber rotor requires the flap deployment schedule to be tailored to the flight conditions. This conclusion is based on the fact that Schedule A1 lowered average power considerably for  $\mu \approx 0.50$ ,  $C_T/\sigma = 0.09$ , and  $X = 0.046$  but did not for other flight conditions. These flight conditions contain both high thrust and high advance ratio. Therefore, one can conclude that only in this severe regime can the prospects of finding a power-saving flap deployment schedule be good.

Decreasing blade tip elastic twist by deploying flaps was somewhat easier to accomplish than decreasing average rotor power. Also, the decrease can be striking, as much as a factor of about 20 when compared to a baseline case without flap deflection. However, the power may or may not decrease when the tip twist is lowered.

ORIGINAL PAGE IS  
OF POOR QUALITY



#### ADVANTAGES

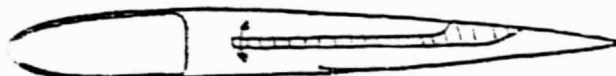
- NO ROTATING HYDRAULICS, PNEUMATICS OR ELECTRICAL SUPPLY
- PRECISE PHASING
- PLENTY OF POWER & ROTOR USED AS FLYWHEEL

#### DISADVANTAGES

- MANY PARTS MAKE UNRELIABLE
- DIFFICULTY OF TAKING SHAFT ACROSS LEAD/LAG & FLAP HINGES
- DIFFICULTY ADJUSTING FOR FLIGHT CONDITIONS
- WEIGHT AFT • NO. OF SEGMENTS LIMIT

Figure 65 3-Segment Variable Camber Mechanical Actuation Systems.

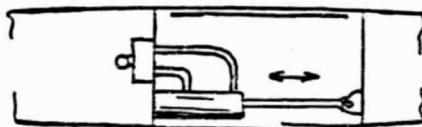
ORIGINAL PAGE 13  
OF POOR QUALITY



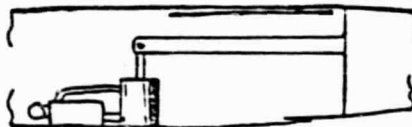
HORIZONTAL CYLINDER, LEVER ACTUATION



HORIZONTAL CYLINDER OVER HINGE



HORIZONTAL CYLINDER OVER SPRING



VERTICAL CYLINDER OVER SPRING

#### • ADVANTAGES

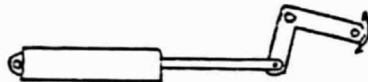
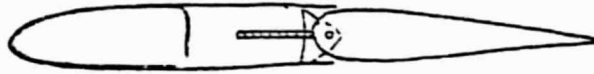
- PLENTY OF POWER
- WEIGHT WELL FWD.
- INFINITE VARIETY FOR SCHED/PHASE
- FEW MOVING PARTS
- HIGH FREQ. RESPONSE

#### • DISADVANTAGES

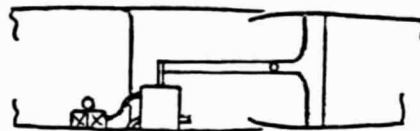
- NEED ROTATING SEAL TO HUB OR PUMP IN BLADE
- PRESSURIZED LINES IN BLADES
- DIFFICULT TO FAIL-SAFE FOR HARDOVER CONDITIONS
- DIFFICULT TO SERVICE
- VALVING AFFECTED BY C.F.

Figure 66 Variable Camber Hydraulic Actuation Systems.

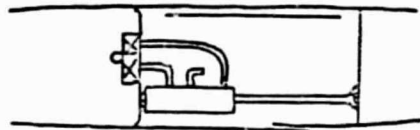
ORIGINAL PAGE IS  
OF POOR QUALITY



HORIZONTAL ACTUATOR & LINK



VERTICAL CYLINDER WITH VENT



HORIZONTAL CYLINDER OVER SPRING



SPRING BELLONS OR BOURDON TUBE

• ADVANTAGES

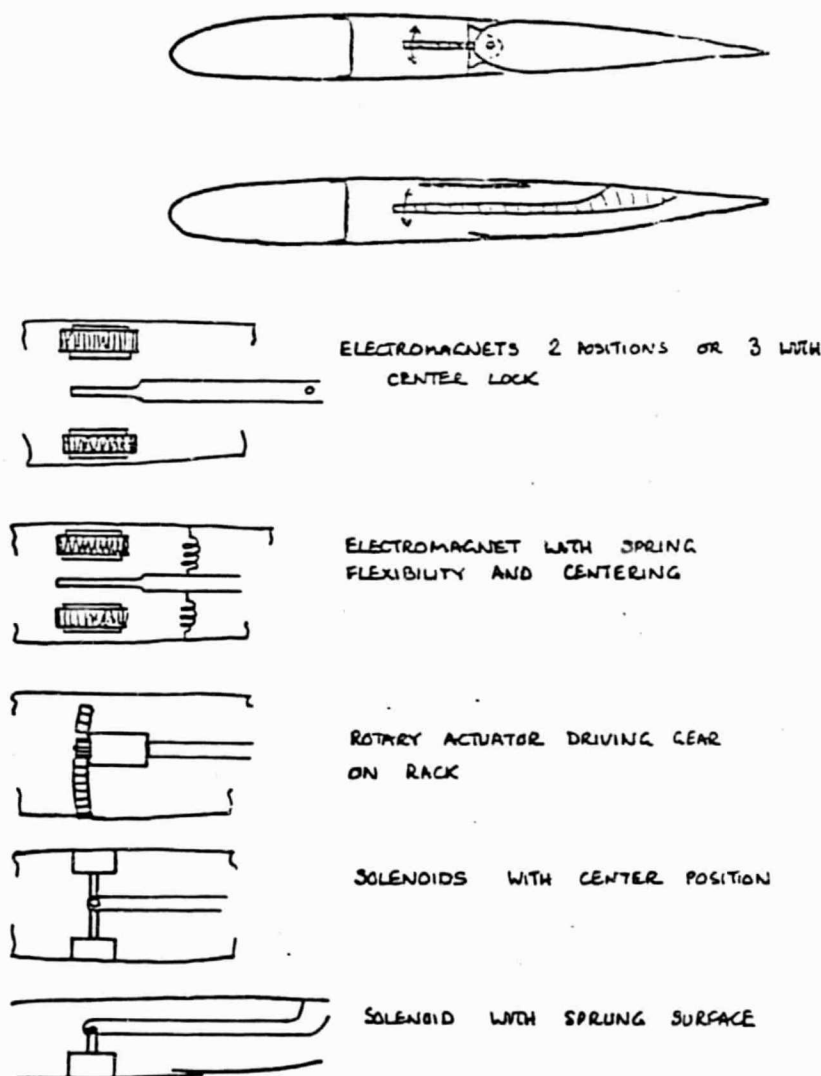
- LIGHTER THAN HYDRAULICS
- SPAR. CAN BE USED AS PLENUM

• DISADVANTAGES

- SLOWER RESPONSE EXCEPT @ HIGH PRESSURE
- NEEDS ROTATING SEAL OR PUMP IN BLADE
- VALVING MAY BE AFFECTED BY C.F.

Figure 67 Variable Camber Pneumatic Actuation Systems.

ORIGINAL PAGE IS  
OF POOR QUALITY



#### ADVANTAGES

- ONLY WIRING DOWN BLADE
- INFINITELY VARIABLE FREQ. & PHASING
- EASILY ACCESSIBLE
- NO GF SENSITIVE COMPONENTS

#### DISADVANTAGES

- HIGH WEIGHT AND POWER REQ.
- STEP INPUTS ONLY

Figure 68 Variable Camber Electric Actuation  
Systems.

ORIGINAL PAGE IS  
OF POOR QUALITY

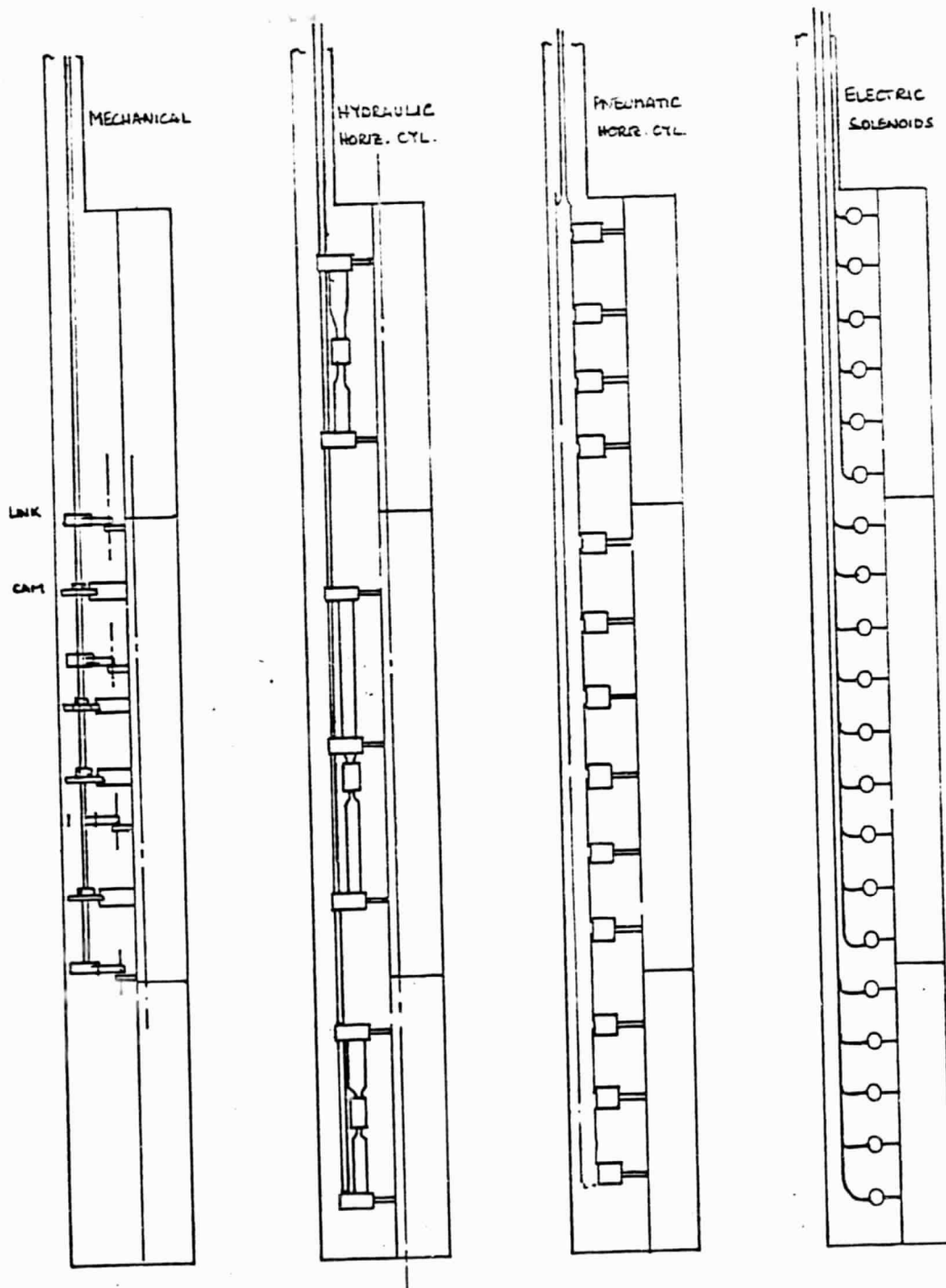
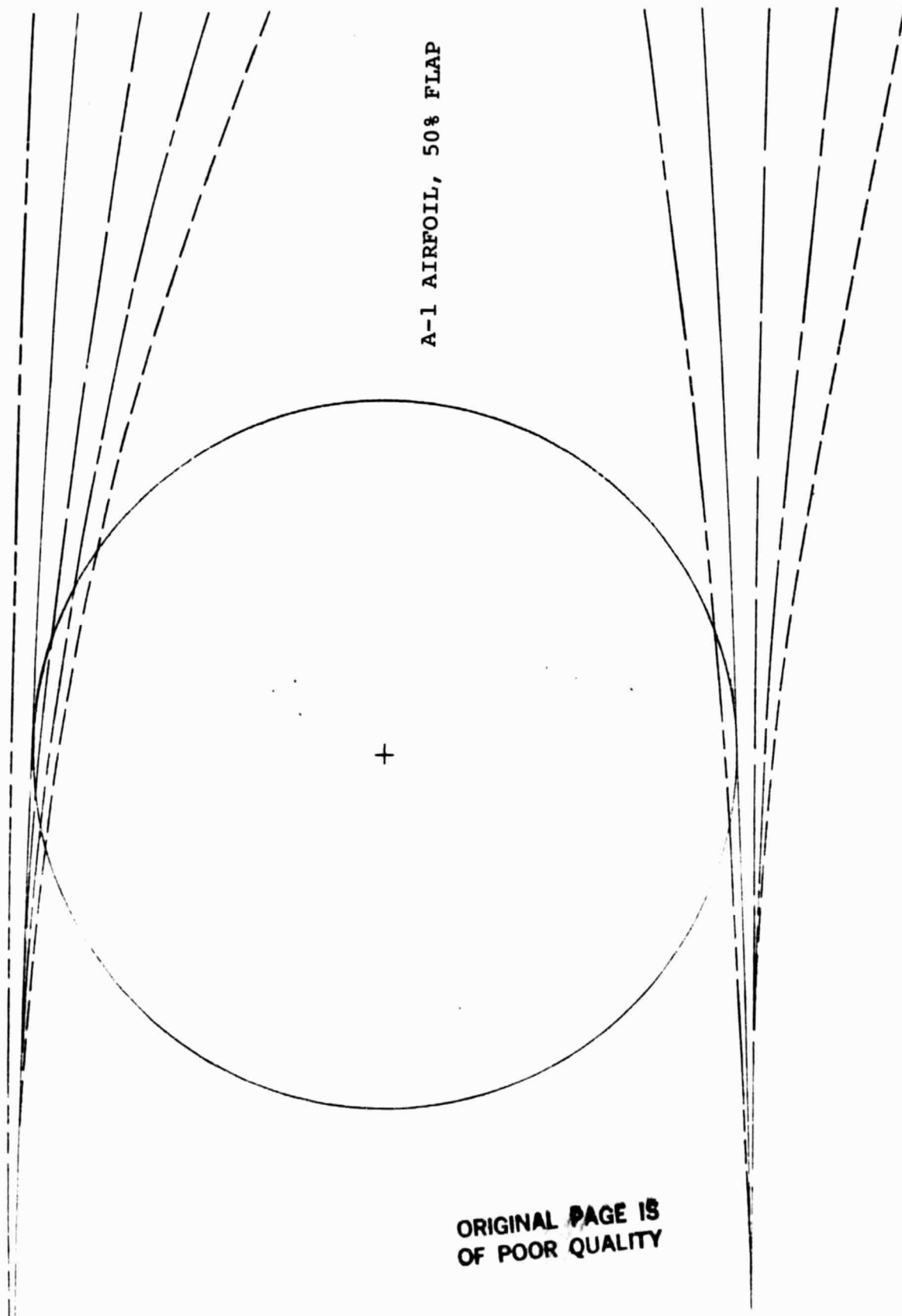


Figure 69 Examples of Variable Camber Deployment.



A-1 AIRFOIL, 50% FLAP

Figure 70 Flap Deployment Involving Flexible Skins  
at the Flap Hinge.

ORIGINAL PAGE IS  
OF POOR QUALITY

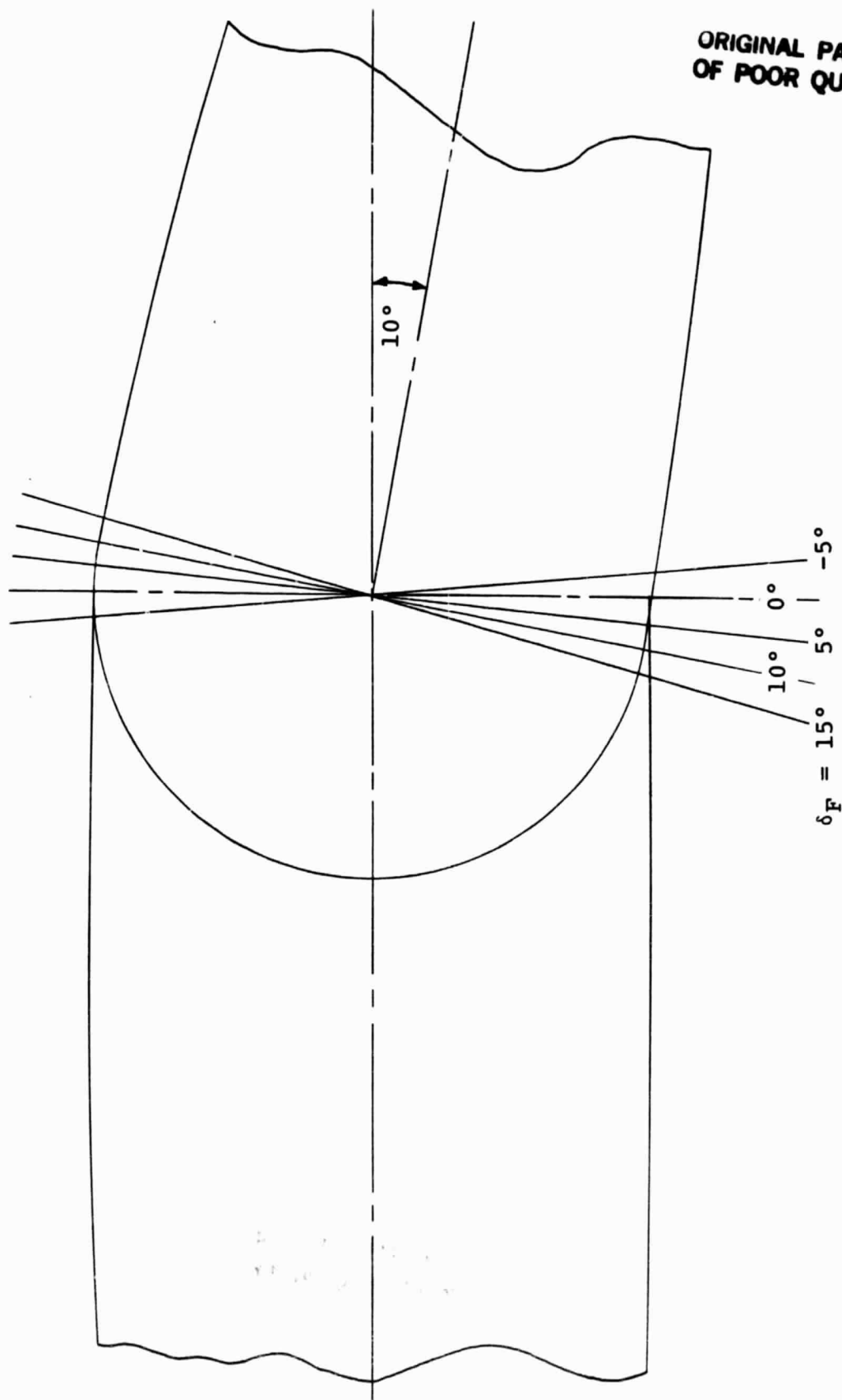


Figure 71 Rigid Flap Hinge Arrangement.

ORIGINAL PAGE IS  
OF POOR QUALITY

50% FLAP  
 $\delta_F = 10^\circ$

M	= 0.400
RN	= 3.080
XTRAN (UPPER)	= 0.200
XTRAN (LOWER)	= 0.300
ALPHA	= 3.000
CL	= 1.358517
CD	= 0.015454
CM	= -0.095008

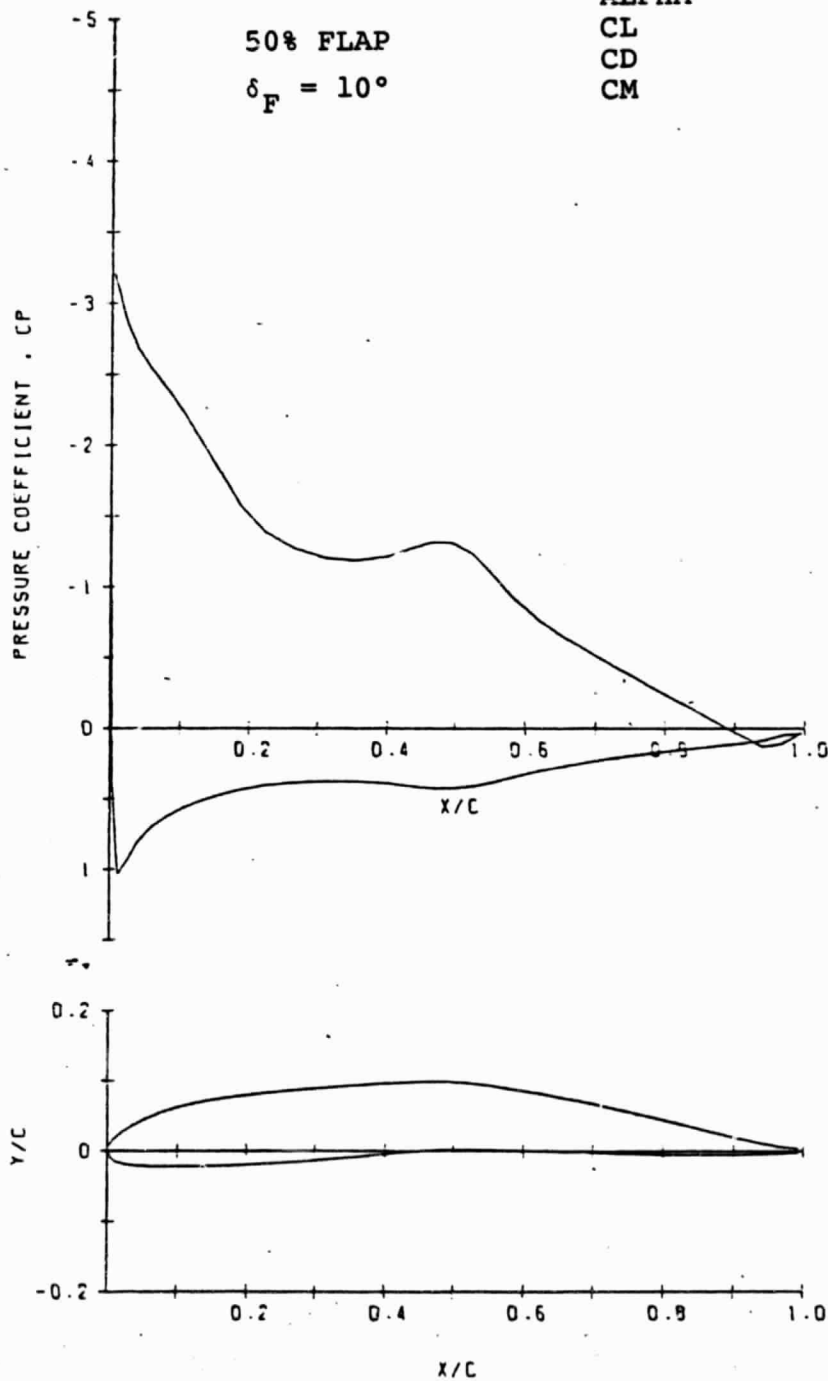


Figure 72 Example of Pressure Distributions for a Flap Configuration Utilizing Flexible Skins.

ORIGINAL PAGE IS  
OF POOR QUALITY

M	= 0.400
RN	= 3.080
XTRAN (UPPER)	= 0.200
XTRAN (LOWER)	= 0.300
ALPHA	= 3.000
CL	= 1.370767
CD	= 0.016400
CM	= -0.095987

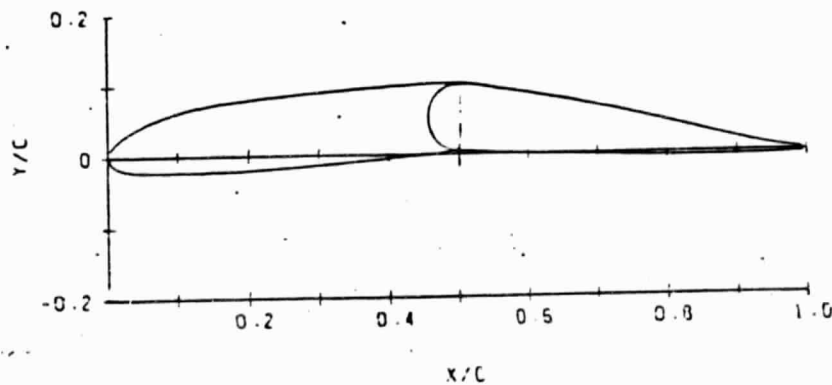
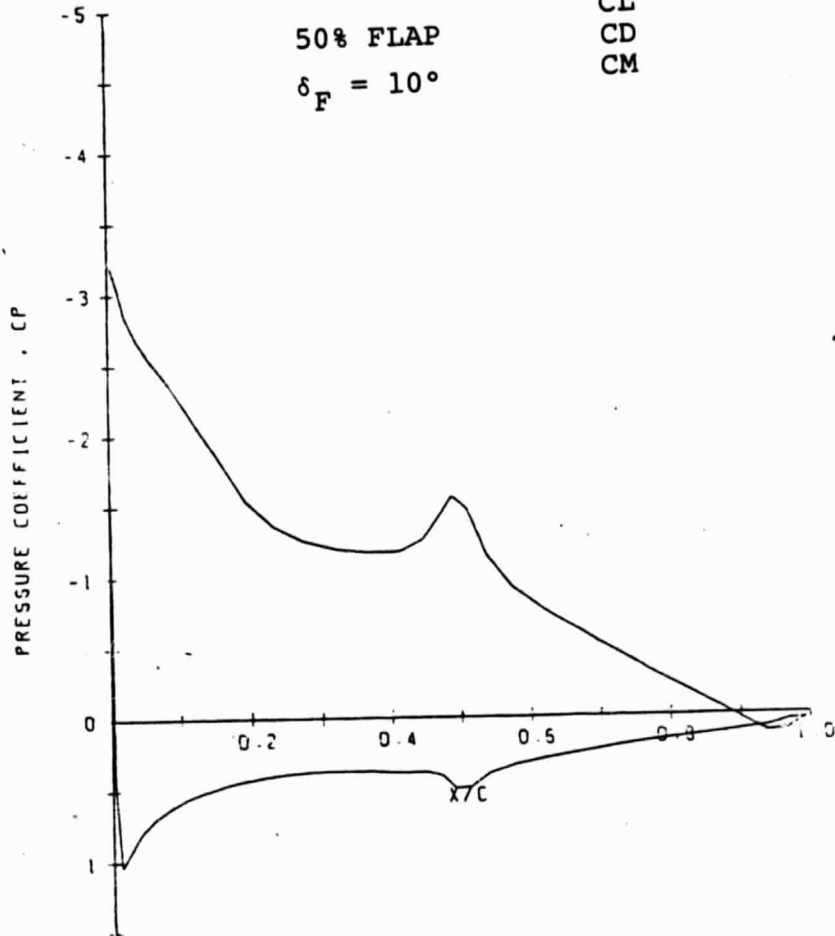


Figure 73 Example of Pressure Distributions for a Flap Configuration Utilizing a Hinge Connecting Rigid Skins.

ORIGINAL PAGE IS  
OF POOR QUALITY

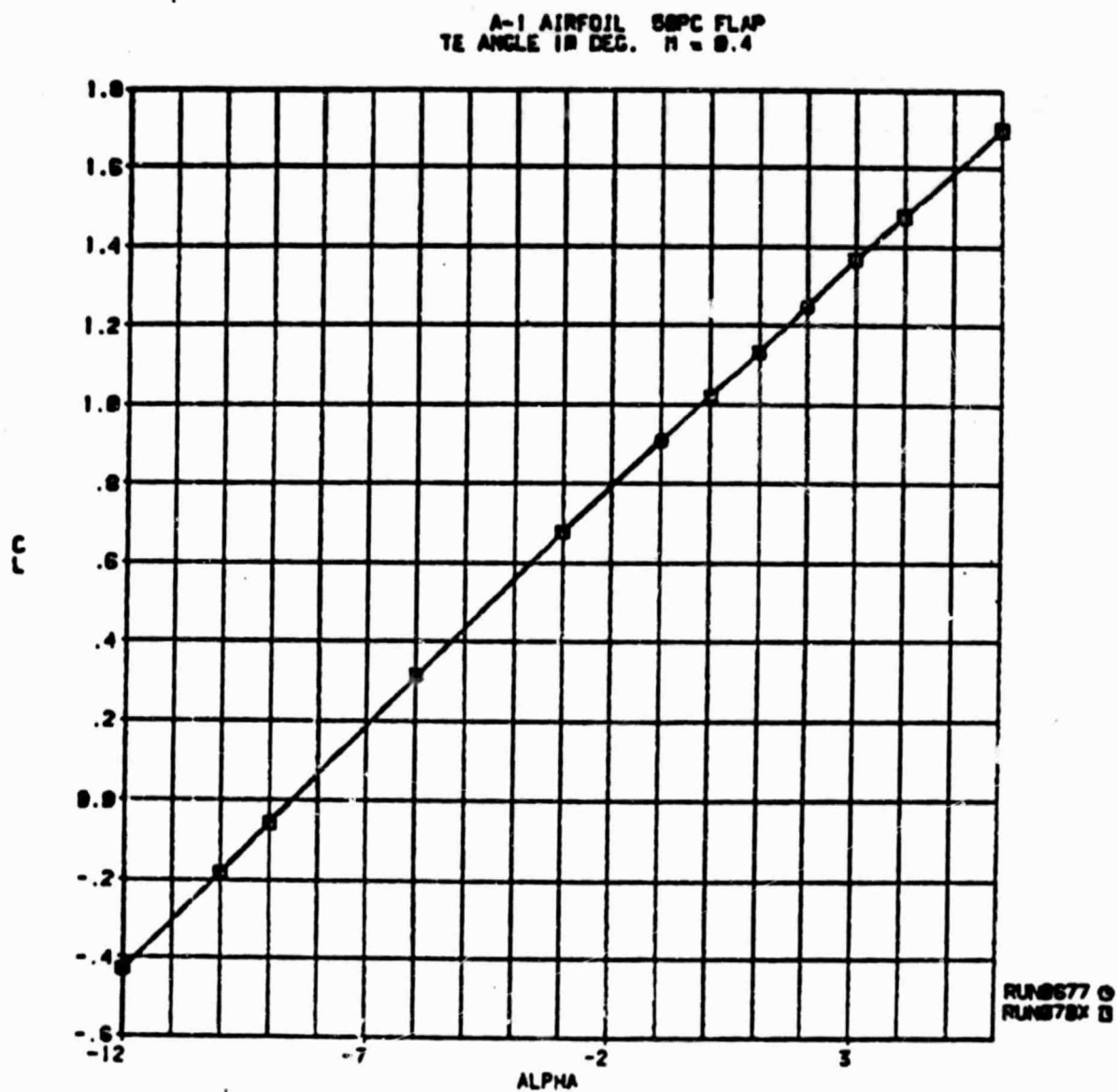


Figure 74 Rigid versus Flexible Flap Hinge. Comparison of Lift Characteristics.

ORIGINAL PAGE IS  
OF POOR QUALITY

ORIGINAL PAGE IS  
OF POOR QUALITY

A-1 AIRFOIL 50PC FLAP  
TE ANGLE 18 DEG.  $\pi = 0.4$

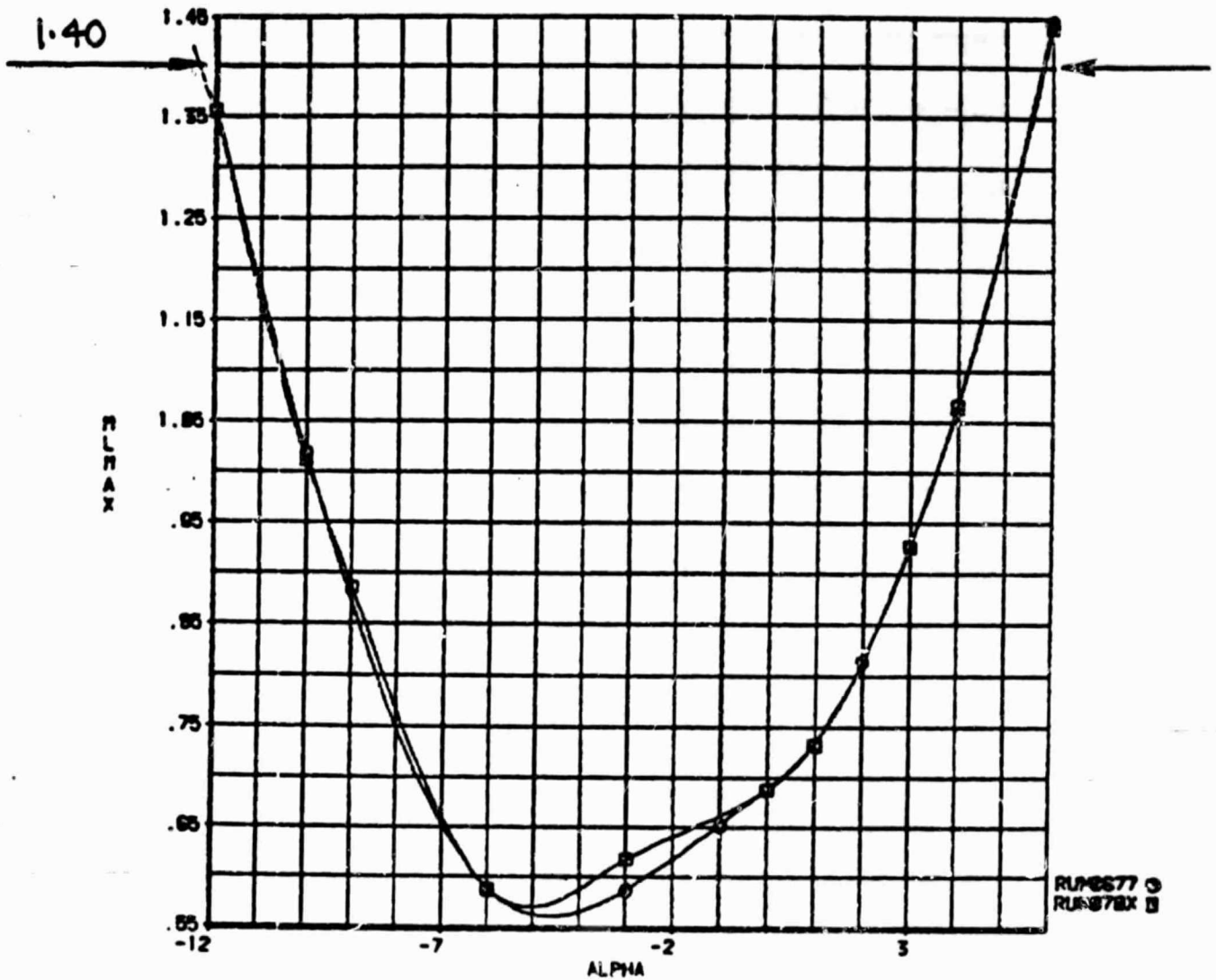


Figure 75 Rigid versus Flexible Flap Hinge. Comparison of Maximum Local Mach Number Boundaries.

ORIGINAL PAGE IS  
OF POOR QUALITY

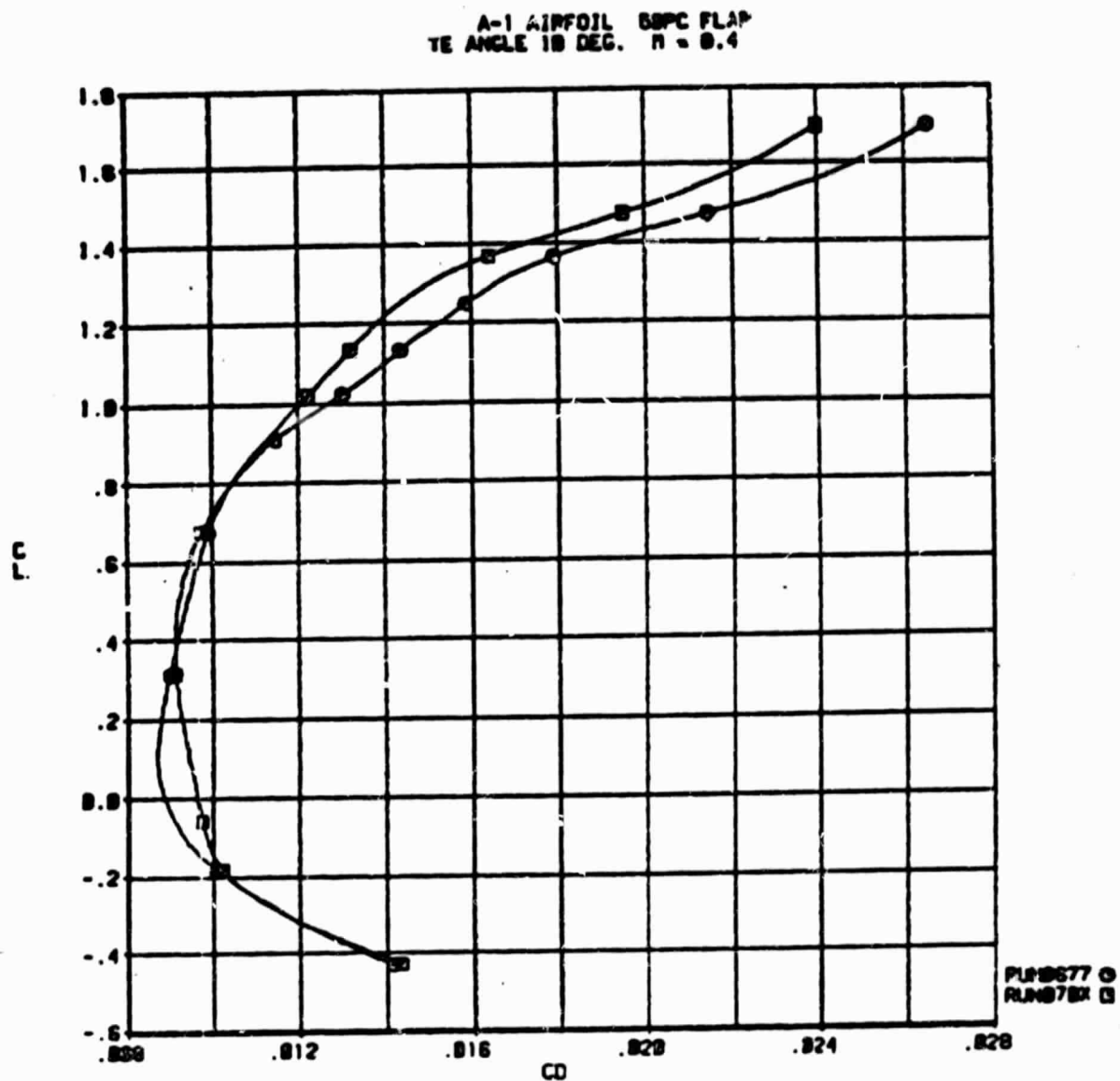


Figure 76 Rigid versus Flexible Flap Hinge. Comparison of Lift/Drag Polars.

ORIGINAL PAGE IS  
OF POOR QUALITY

ORIGINAL PAGE IS  
OF POOR QUALITY

A-1 AIRFOIL 5SPC FLAP  
TE ANGLE 18 DEG.  $M = 0.4$

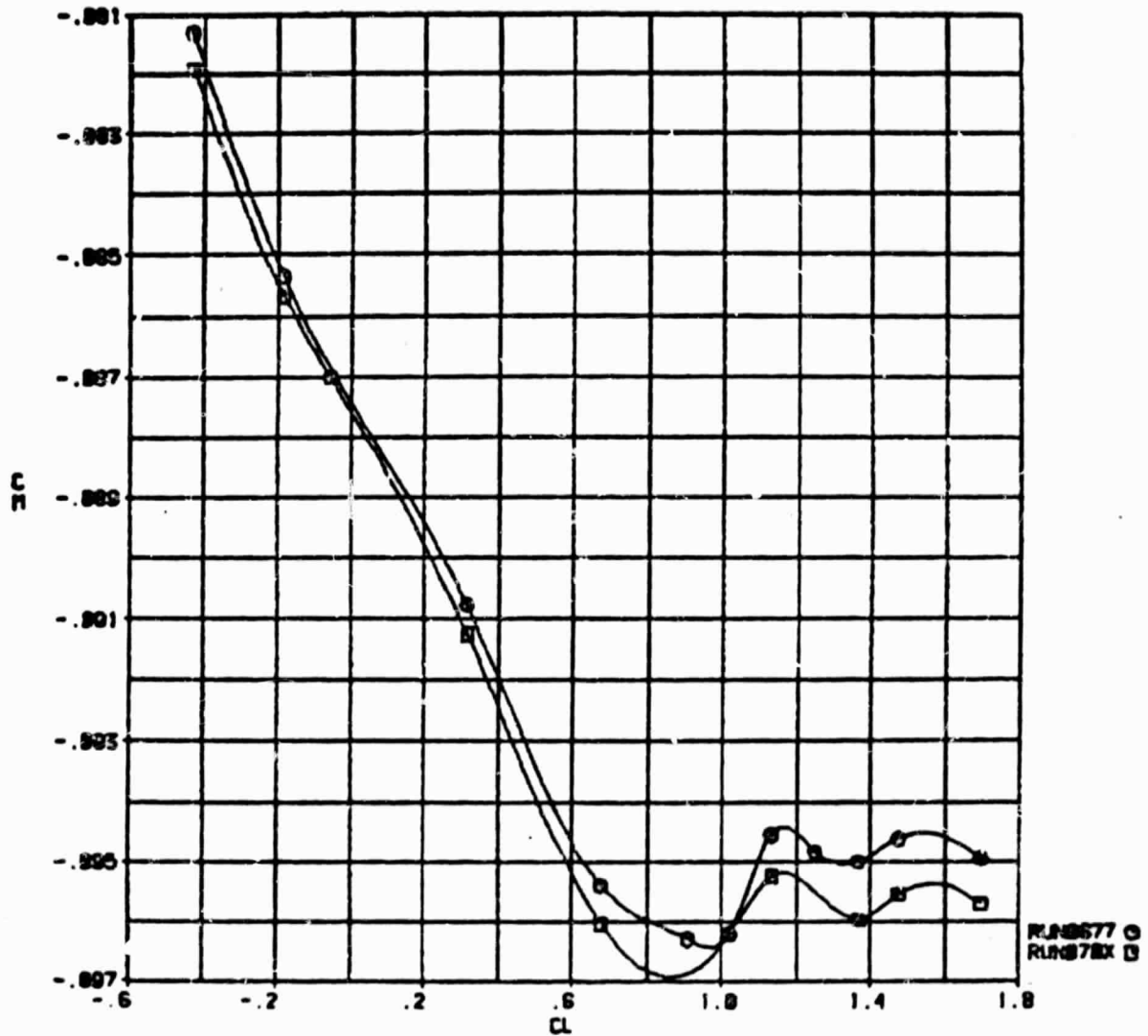


Figure 77 Rigid versus Flexible Flap Hinge. Comparison of Pitching Moments.

ORIGINAL PAGE IS  
OF POOR QUALITY

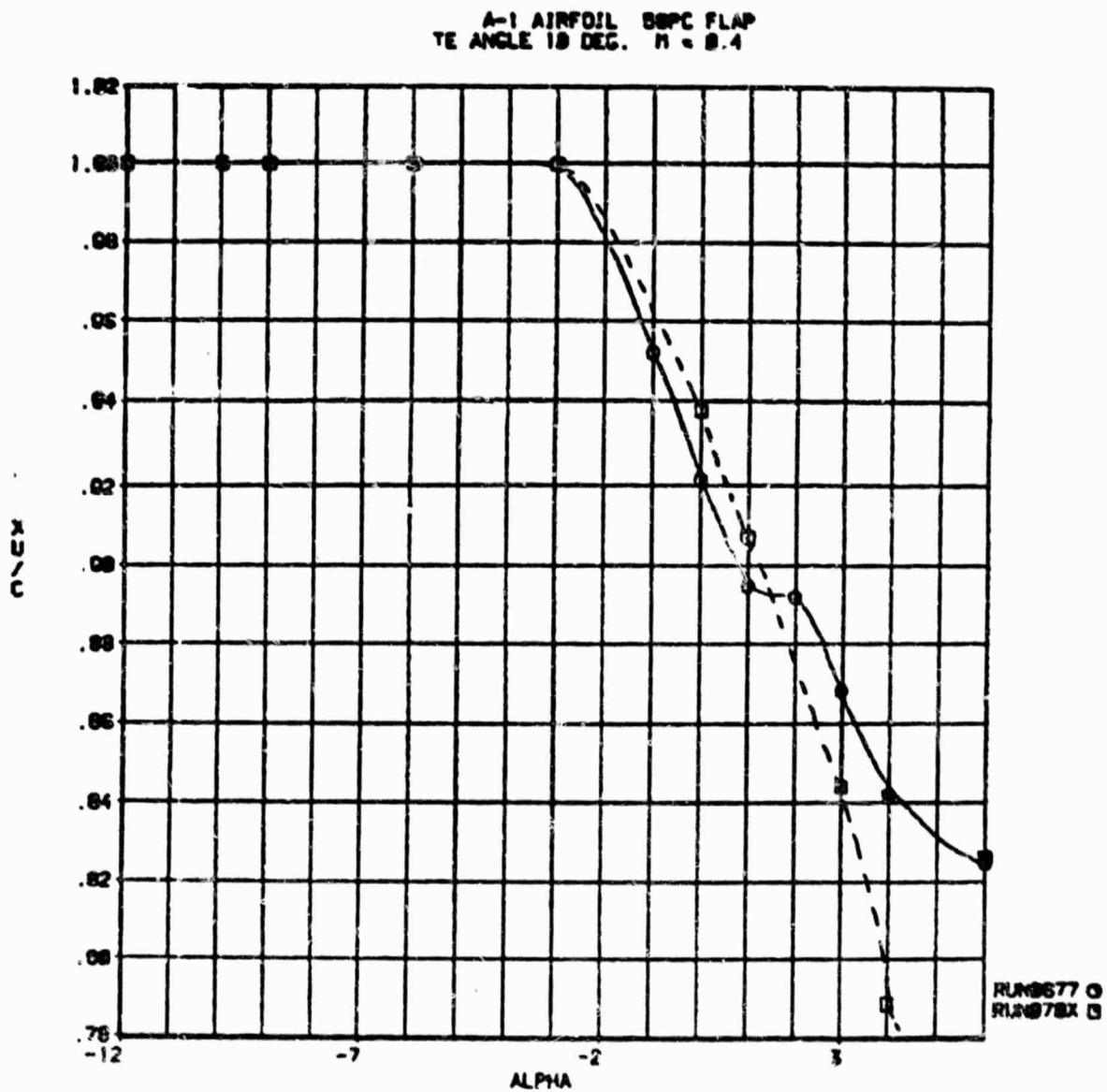


Figure 78 Rigid versus Flexible Flap Hinge. Comparison of Separation Boundaries.

ORIGINAL PAGE IS  
OF POOR QUALITY

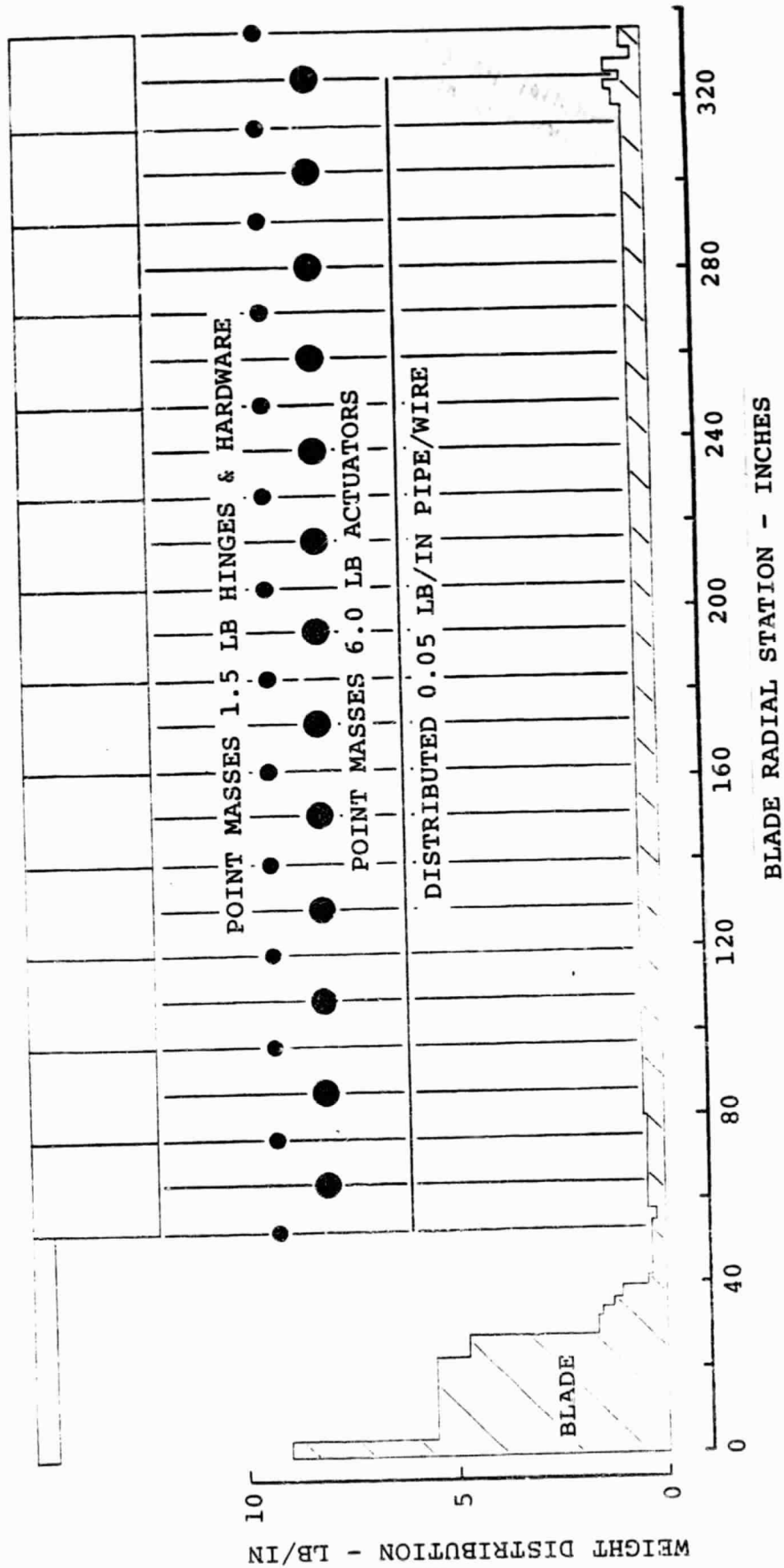


Figure 79 Approximate Weights of Variable Camber Hardware  
(28 Ft. Radius Rotor).

## 8.2 Recommendations

Since one flap deployment schedule and its derivatives decreased average rotor power for high thrust and speed flight conditions by approximately 11%, it is recommended that flight conditions beyond  $\mu = .5$  and up to  $\mu = .6$  be explored with a view toward decreasing rotor power. The exploration of high speed should be conducted at normal operating thrust levels,  $C_T/\sigma = 0.6$ , and at higher levels,  $C_T/\sigma = .09$ .

ORIGINAL PAGE IS  
OF POOR QUALITY

## REFERENCES

1. Davenport, F.J., and Front, J.V., "Airfoil Sections for Rotor Blades - A Reconsideration", presented at the 22nd Annual Forum of the American Helicopter Society, Washington, D.C., May 12, 1966.
2. Dadone, L.U., and Fukushima, T., "A Review of Design Objectives for Advanced Helicopter Rotor Airfoils", presented at the AHS Symposium on Helicopter Aerodynamic Efficiency, (Hartford, Connecticut), March 1975.
3. Sloop, J.W., Wortmann, F.X., Duhon, J.M., "The Development of Transonic Airfoils for Helicopters", presented at the 31st Annual National Forum of the American Helicopter Society, Washington, D.C., May 1975.
4. Tetervin, N., "Tests in the NACA Two-Dimensional Low Turbulence Tunnel of Airfoil Sections Designed to Have Small Pitching Moments, and High Lift-Drag Ratios", NACA Report L-452, originally issued in September 1940 as C.B. 3113.
5. Stivers, L.S., Jr., and Rice, F.J., Jr., "Aerodynamic Characteristics of Four NACA Airfoil Sections Designed for Helicopter Rotor Blades", NACA Report L-29, originally issued as R.B. L5K02, February 1946.
6. Benson, R.G., Dadone, L.U., Gormont, R.E., and Kohler, G.R., "Influence of Airfoils on Stall Flutter Boundaries of Articulated Helicopter Rotors", presented at the 28th Annual Forum of the American Helicopter Society, Washington, D.C., May 1972.
7. Wortmann, F.X., and Drees, J.M., "Design of Airfoils for Rotors", paper presented at CAL/AVLABS 1969 Symposium on Aerodynamics of Rotary Wing and VTOL Aircraft.
8. Kemp, L.D., "An Analytical Study for the Design of Advanced Rotor Airfoils", B.H.C. Report No. 299-099-635, NASA CR-112297, March 29, 1973.
9. Dadone, L., "Design and Analytical Study of a Rotor Airfoil", NASA CR 2988, 1978.
10. Blackwell, J.A., and Hinson, B.L., "The Aerodynamic Design of an Advanced Rotor Airfoil", NASA CR 2961, 1978.
11. Dadone, L., "Rotor Airfoil Optimization: An Understanding of the Physical Limits," 34th Annual AHS Forum, Wash., D.C., May 1978. Preprint 78-4.

12. Prouty, R.W., "A State-of-the-Art Survey of Two-Dimensional Airfoil Data", A.H.S. Symposium on Helicopter Aerodynamic Efficiency, March 1975.
13. Thibert, J.L., Gallot, J., "A New Airfoil Family for Rotor Blades", 3rd European Rotorcraft and Powered Lift Forum, Aix-en-Provence, France, Sept. 1977.
14. Dadone, L., "U.S. Army Helicopter Design Datcom, Volume I, Airfoils", USAAMRDL CR 76-2 (NASA CR-153247) Sept. 1976.
15. Sewell, R., Lee, S., and Fukushima, T., "Rotor Airloads and Performance Analysis with Non-Uniform Induced Inflow", Boeing Doc. D8-0312 - Original Release Dec. 1967.
16. Tarzanin, F. and Ranieri, J., "Aeroelastic Analysis Program C-60", Boeing Report D210-10371, Philadelphia, Pa. Revised 1978.
17. Gormont, R.E., "A Mathematical Model of Unsteady Aerodynamics and Radial Flow for Application to Helicopter Rotors", USAAMRDL TR72-67, May 1973.
18. LeNard, F. and Boehler, G.D., "Inclusion of Tip Relief in the Prediction of Compressibility Effects on Helicopter Rotor Performance", USAAMRDL TR73-71, Dec. 1973.
19. LeNard, J., "A Theoretical Analysis of the Tip Relief Effect on Helicopter Rotor Performance", USAAMRDL TR72-7, Aug. 1972.
20. Stevens, W.A., Goradia, S.H., Braden, J.A., "Mathematical Model for Two-Dimensional Multi-Component Airfoils in Viscous Flow", NASA CR 1843, July 1971.
21. Brune, G.W., and Manke, J.W., "An Improved Version of the NASA-Lockheed Multi-Element Airfoil Analysis Computer Program", NASA CR-145323, March 1978.
22. Bauer, F., Garabedian, P., Korn, D., Jameson, A., "Supercritical Wing Sections II", Lecture Notes in Economics and Mathematical Systems, Volume 108, Springer-Verlag (New York), 1975.
23. Henderson, M.L., "A Solution to the 2-D Separated Wake Modeling Problem and Its Use to Predict  $C_{l_{max}}$  of Arbitrary Airfoil Sections", AIAA 16th Aerospace Sciences Meeting, Huntsville, Ala., Jan. 1978.

24. Maskew, B., Dvorak, F.A., "Investigation of Separation Models for the Prediction of  $C_{l_{max}}$ ", Presented at the 33rd Annual National Forum of the American Helicopter Society, Washington, D.C., May 1977.
25. R.M. Hicks, and W.F. McCroskey; "An Experimental Evaluation of a Helicopter Rotor Section Designed by Numerical Optimization", NASA TM 78622, March 1980.
26. Lindsey, W.F., and Johnston, P.J., "Some Observations on Maximum Pressure Rise Across Shocks Without Boundary-Layer Separation on Airfoils at Transonic Speeds", NACA TN 3820, November 1956.
27. Royal Aeronautical Society Transonic Aerodynamics Committee, "A Method of Estimating Drag-Rise Mach Number for Two-Dimensional Airfoil Sections", Transonic Data Memorandum 6407, July 1964.
28. Hoerner, S.F., "Fluid Dynamic Drag", published by the Author, 1965.
29. Rabbott, J.P., Jr., Lizak A.A., and Paglino, V.M., "A Presentation of Measured and Calculated Full-Scale Rotor Blade Aerodynamic and Structural Loads", USAAVLABS Technical Report 66-31, July 1966.

APPENDIX A

# APPENDIX A

## Coordinates of the A-1 Airfoil with 35% and 50% Plain T.E. Flaps

UPPER SURFACE		LOWER SURFACE	
XU	ZU	XL	ZL
0.0	0.0	0.0	0.0
0.000200	0.002379	0.000200	-0.002228
0.000500	0.003771	0.000500	-0.003375
0.001000	0.005414	0.001000	-0.004719
0.002000	0.007656	0.002000	-0.006512
0.003500	0.010133	0.003500	-0.008436
0.005000	0.012144	0.005000	-0.009945
0.006500	0.013878	0.006500	-0.011196
0.008000	0.015434	0.008000	-0.012270
0.010000	0.017315	0.010000	-0.013503
0.012500	0.019447	0.012500	-0.014815
0.016000	0.022136	0.016000	-0.016341
0.020000	0.024901	0.020000	-0.017770
0.025000	0.028006	0.025000	-0.019223
0.035000	0.033351	0.035000	-0.021367
0.050000	0.039906	0.050000	-0.023654
0.065000	0.045233	0.065000	-0.025486
0.080000	0.049600	0.080000	-0.027101
0.100000	0.054210	0.100000	-0.029016
0.125000	0.058287	0.125000	-0.031038
0.150000	0.060977	0.150000	-0.032767
0.200000	0.063435	0.200000	-0.035505
0.250000	0.064310	0.250000	-0.037272
0.300000	0.064461	0.300000	-0.038283
0.350000	0.064089	0.350000	-0.038655
0.400000	0.063156	0.400000	-0.038481
0.450000	0.061544	0.450000	-0.037820
0.500000	0.059237	0.500000	-0.036651
0.550000	0.056234	0.550000	-0.035013
0.586000	0.053700	0.586000	-0.032800
0.616000	0.051000	0.616000	-0.030200
0.640000	0.049200	0.640000	-0.028100
0.660000	0.047900	0.660000	-0.026200
0.684000	0.046800	0.684000	-0.024000
0.714000	0.045700	0.714000	-0.020600
0.750000	0.044200	0.752543	-0.016014
0.797693	0.041602	0.802063	-0.008346
0.848197	0.038026	0.851552	-0.000325
0.898708	0.034370	0.901003	0.008135
0.923927	0.032957	0.925707	0.012609
0.949094	0.032136	0.950389	0.017333
0.974178	0.032263	0.975045	0.022355
0.989183	0.032870	0.989829	0.025476
0.999164	0.033520	0.999686	0.027545

$$C_f/C = 0.35, \delta_F = -5^\circ$$

UPPER SURFACE		LOWER SURFACE	
XU	ZU	XL	ZL
0.0	0.0	0.0	0.0
0.000200	0.002379	0.000200	-0.002228
0.000500	0.003771	0.000500	-0.003375
0.001000	0.005414	0.001000	-0.004719
0.002000	0.007656	0.002000	-0.006512
0.003500	0.010133	0.003500	-0.008436
0.005000	0.012144	0.005000	-0.009945
0.006500	0.013878	0.006500	-0.011196
0.008000	0.015434	0.008000	-0.012270
0.010000	0.017315	0.010000	-0.013503
0.012500	0.019447	0.012500	-0.014815
0.016000	0.022136	0.016000	-0.016341
0.020000	0.024901	0.020000	-0.017770
0.025000	0.028006	0.025000	-0.019223
0.035000	0.033351	0.035000	-0.021367
0.050000	0.039906	0.050000	-0.023654
0.065000	0.045233	0.065000	-0.025486
0.080000	0.049600	0.080000	-0.027101
0.100000	0.054210	0.100000	-0.029016
0.125000	0.058287	0.125000	-0.031038
0.150000	0.060977	0.150000	-0.032767
0.200000	0.063435	0.200000	-0.035505
0.250000	0.064310	0.250000	-0.037272
0.300000	0.064461	0.300000	-0.038283
0.350000	0.064089	0.350000	-0.038655
0.400000	0.063156	0.400000	-0.038481
0.450000	0.061544	0.450000	-0.037820
0.500000	0.059237	0.500000	-0.036651
0.550000	0.056234	0.550000	-0.035013
0.600000	0.052486	0.600000	-0.032965
0.650000	0.047923	0.650000	-0.030558
0.700000	0.042460	0.700000	-0.027850
0.750000	0.036002	0.750000	-0.024857
0.800000	0.028604	0.800000	-0.021534
0.850000	0.020640	0.850000	-0.017857
0.900000	0.012596	0.900000	-0.013739
0.925000	0.008990	0.925000	-0.011435
0.950000	0.005979	0.950000	-0.008881
0.975000	0.003919	0.975000	-0.006027
0.990000	0.003216	0.990000	-0.004206
1.000000	0.002994	1.000000	-0.003004

$$C_f/C = 0.35, \delta_F = 0^\circ$$

UPPER SURFACE		LOWER SURFACE	
XU	ZU	XL	ZL
0.0	0.0	0.0	0.0
0.000200	0.002379	0.000200	-0.002228
0.000500	0.003771	0.000500	-0.003375
0.001000	0.005414	0.001000	-0.004719
0.002000	0.007656	0.002000	-0.006512
0.003500	0.010133	0.003500	-0.008436
0.005000	0.012144	0.005000	-0.009945
0.006500	0.013878	0.006500	-0.011196
0.008000	0.015434	0.008000	-0.012270
0.010000	0.017315	0.010000	-0.013503
0.012500	0.019447	0.012500	-0.014815
0.016000	0.022136	0.016000	-0.016341
0.020000	0.024901	0.020000	-0.017770
0.025000	0.028006	0.025000	-0.019223
0.035000	0.033351	0.035000	-0.021367
0.050000	0.039906	0.050000	-0.023654
0.065000	0.045233	0.065000	-0.025486
0.080000	0.049600	0.080000	-0.027101
0.100000	0.054210	0.100000	-0.029016
0.125000	0.058287	0.125000	-0.031038
0.150000	0.060977	0.150000	-0.032767
0.200000	0.063435	0.200000	-0.035505
0.250000	0.064310	0.250000	-0.037272
0.300000	0.064461	0.300000	-0.038283
0.350000	0.064089	0.350000	-0.038655
0.400000	0.063156	0.400000	-0.038481
0.450000	0.061544	0.450000	-0.037820
0.500000	0.059237	0.500000	-0.036651
0.550000	0.056234	0.550000	-0.035013
0.586000	0.053900	0.586000	-0.033200
0.616000	0.050300	0.616000	-0.032400
0.640000	0.047300	0.640000	-0.032000
0.660000	0.044800	0.660000	-0.032000
0.684000	0.041000	0.684000	-0.032100
0.714000	0.035900	0.714000	-0.032600
0.752000	0.027182	0.746696	-0.033445
0.801165	0.015455	0.796796	-0.034492
0.850281	0.003163	0.846926	-0.035187
0.899390	-0.009208	0.897094	-0.035443
0.923980	-0.014979	0.922200	-0.035326
0.948623	-0.020157	0.947328	-0.034961
0.973348	-0.024388	0.972481	-0.034297
0.988230	-0.026396	0.987583	-0.033790
0.998172	-0.027489	0.997650	-0.033464

$$C_f/C = 0.35, \delta_F = 5^\circ$$

UPPER SURFACE		LOWER SURFACE	
XU	ZU	XL	ZL
0.0	0.0	0.0	0.0
0.000200	0.002379	0.000200	-0.002228
0.000500	0.003771	0.000500	-0.003375
0.001000	0.005414	0.001000	-0.004719
0.002000	0.007656	0.002000	-0.006512
0.003500	0.010133	0.003500	-0.008436
0.005000	0.012144	0.005000	-0.009945
0.006500	0.013878	0.006500	-0.011196
0.008000	0.015434	0.008000	-0.012270
0.010000	0.017315	0.010000	-0.013503
0.012500	0.019447	0.012500	-0.014815
0.016000	0.022136	0.016000	-0.016341
0.020000	0.024901	0.020000	-0.017770
0.025000	0.028006	0.025000	-0.019223
0.035000	0.033351	0.035000	-0.021367
0.050000	0.039906	0.050000	-0.023654
0.065000	0.045233	0.065000	-0.025486
0.080000	0.049600	0.080000	-0.027101
0.100000	0.054210	0.100000	-0.029016
0.125000	0.058287	0.125000	-0.031038
0.150000	0.060977	0.150000	-0.032767
0.200000	0.063435	0.200000	-0.035505
0.250000	0.064310	0.250000	-0.037272
0.300000	0.064461	0.300000	-0.038283
0.350000	0.064089	0.350000	-0.038655
0.400000	0.063156	0.400000	-0.038481
0.450000	0.061544	0.450000	-0.037820
0.500000	0.059237	0.500000	-0.036651
0.550000	0.056234	0.550000	-0.035013
0.586000	0.053800	0.586000	-0.033300
0.616000	0.050800	0.616000	-0.032600
0.640000	0.047900	0.640000	-0.032710
0.660000	0.044400	0.660000	-0.033600
0.684000	0.038900	0.684000	-0.035200
0.714000	0.030700	0.714000	-0.038100
0.753225	0.018222	0.746000	-0.042000
0.801180	0.002254	0.792474	-0.047122
0.849038	-0.014271	0.842353	-0.052183
0.896881	-0.030876	0.892308	-0.056810
0.920875	-0.038768	0.917529	-0.058883
0.944973	-0.046074	0.942392	-0.060709
0.969235	-0.052444	0.967508	-0.062239
0.983885	-0.055741	0.982596	-0.063051
0.993695	-0.057696	0.992653	-0.063603

$$C_f/C = 0.35, \delta_F = 10^\circ$$

UPPER SURFACE		LOWER SURFACE	
XU	ZU	XL	ZL
0.0	0.0	0.0	0.0
0.000200	0.002379	0.000200	-0.002228
0.000500	0.003771	0.000500	-0.003375
0.001000	0.005414	0.001000	-0.004719
0.002000	0.007656	0.002000	-0.006512
0.003500	0.010133	0.003500	-0.008436
0.005000	0.012144	0.005000	-0.009945
0.006500	0.013878	0.006500	-0.011196
0.008000	0.015434	0.008000	-0.012270
0.010000	0.017315	0.010000	-0.013503
0.012500	0.019447	0.012500	-0.014815
0.016000	0.022136	0.016000	-0.016341
0.020000	0.024901	0.020000	-0.017770
0.025000	0.028006	0.025000	-0.019223
0.035000	0.033351	0.035000	-0.021367
0.050000	0.039906	0.050000	-0.023654
0.065000	0.045233	0.065000	-0.025486
0.080000	0.049600	0.080000	-0.027101
0.100000	0.054210	0.100000	-0.029016
0.125000	0.058287	0.125000	-0.031038
0.150000	0.060977	0.150000	-0.032767
0.200000	0.063435	0.200000	-0.035505
0.250000	0.064310	0.250000	-0.037272
0.300000	0.064461	0.300000	-0.038283
0.350000	0.064089	0.350000	-0.038655
0.400000	0.063156	0.400000	-0.038481
0.450000	0.061544	0.450000	-0.037320
0.500000	0.059237	0.500000	-0.036651
0.550000	0.056234	0.550000	-0.035013
0.586000	0.053200	0.586000	-0.034700
0.616000	0.049500	0.616000	-0.034800
0.640000	0.045200	0.640000	-0.035400
0.660000	0.041100	0.660000	-0.037100
0.684000	0.035000	0.684000	-0.040200
0.714000	0.024800	0.714000	-0.045500
0.753663	0.009189	0.748000	-0.052100
0.800045	-0.010898	0.787068	-0.059327
0.846280	-0.031531	0.836316	-0.068716
0.892494	-0.052242	0.885678	-0.077680
0.915709	-0.062196	0.910423	-0.081925
0.939078	-0.071575	0.935232	-0.085928
0.962693	-0.080035	0.960119	-0.089642
0.977000	-0.084596	0.975079	-0.091765
0.986602	-0.087399	0.985049	-0.093192

$$C_f/C = 0.35, \delta_F = 15^\circ$$

UPPER SURFACE		LOWER SURFACE	
XU	ZU	XL	ZL
0.0	0.0	0.0	0.0
0.000200	0.002379	0.000200	-0.002228
0.000500	0.003771	0.000500	-0.003375
0.001000	0.005414	0.001000	-0.004719
0.002000	0.007656	0.002000	-0.006512
0.003500	0.010133	0.003500	-0.008436
0.005000	0.012144	0.005000	-0.009945
0.006500	0.013878	0.006500	-0.011196
0.008000	0.015434	0.008000	-0.012270
0.010000	0.017315	0.010000	-0.013503
0.012500	0.019447	0.012500	-0.014815
0.016000	0.022136	0.016000	-0.016341
0.020000	0.024901	0.020000	-0.017770
0.025000	0.028006	0.025000	-0.019223
0.035000	0.033351	0.035000	-0.021367
0.050000	0.039906	0.050000	-0.023654
0.065000	0.045233	0.065000	-0.025486
0.080000	0.049600	0.080000	-0.027101
0.100000	0.054210	0.100000	-0.029016
0.125000	0.058287	0.125000	-0.031038
0.150000	0.060977	0.150000	-0.032767
0.200000	0.063435	0.200000	-0.035505
0.250000	0.064310	0.250000	-0.037272
0.300000	0.064461	0.300000	-0.038283
0.350000	0.064089	0.350000	-0.038655
0.400000	0.063700	0.400000	-0.038481
0.436000	0.063300	0.436000	-0.037570
0.466000	0.062700	0.466000	-0.036550
0.490000	0.062200	0.490000	-0.035500
0.510000	0.061760	0.510000	-0.034350
0.534000	0.060900	0.534000	-0.032400
0.564000	0.060000	0.564000	-0.029320
0.598000	0.058300	0.598000	-0.025000
0.646237	0.057200	0.653077	-0.018500
0.696522	0.055500	0.702650	-0.011000
0.746895	0.053000	0.752199	-0.003500
0.797350	0.050700	0.801719	0.004700
0.847853	0.048500	0.851209	0.012760
0.898364	0.046700	0.900660	0.021220
0.923583	0.046040	0.925363	0.026000
0.948751	0.045219	0.950046	0.030700
0.973825	0.045346	0.974702	0.035450
0.988839	0.045953	0.989486	0.038559
0.998821	0.046603	0.999343	0.040628

$$C_f/C = 0.50, \delta_F = -5^\circ$$

UPPER SURFACE		LOWER SURFACE	
XU	ZU	XL	ZL
0.0	0.0	0.0	0.0
0.000200	0.002379	0.000200	-0.002228
0.000500	0.003771	0.000500	-0.003375
0.001000	0.005414	0.001000	-0.004719
0.002000	0.007656	0.002000	-0.006512
0.003500	0.010133	0.003500	-0.008436
0.005000	0.012144	0.005000	-0.009935
0.006500	0.013878	0.006500	-0.011196
0.008000	0.015434	0.008000	-0.012270
0.010000	0.017315	0.010000	-0.013503
0.012500	0.019447	0.012500	-0.014815
0.016000	0.022136	0.016000	-0.016341
0.020000	0.024901	0.020000	-0.017770
0.025000	0.028006	0.025000	-0.019223
0.035000	0.033351	0.035000	-0.021367
0.050000	0.039906	0.050000	-0.023654
0.065000	0.045233	0.065000	-0.025486
0.080000	0.049600	0.080000	-0.027101
0.100000	0.054210	0.100000	-0.029016
0.125000	0.058287	0.125000	-0.031038
0.150000	0.060977	0.150000	-0.032767
0.200000	0.063435	0.200000	-0.035505
0.250000	0.064310	0.250000	-0.037272
0.300000	0.064461	0.300000	-0.038283
0.350000	0.064089	0.350000	-0.038555
0.400000	0.063156	0.400000	-0.038481
0.436000	0.062220	0.436000	-0.038730
0.466000	0.060880	0.466000	-0.038880
0.490000	0.059600	0.490000	-0.038930
0.510000	0.057000	0.510000	-0.039170
0.534000	0.054030	0.534000	-0.039500
0.564000	0.049780	0.564000	-0.040230
0.603210	0.043614	0.598000	-0.041630
0.652622	0.034710	0.645782	-0.043472
0.701955	0.024910	0.695827	-0.045132
0.751202	0.014119	0.745898	-0.046508
0.800367	0.002391	0.795997	-0.047556
0.849483	-0.009900	0.846127	-0.048251
0.898591	-0.022271	0.896296	-0.048506
0.923182	-0.028042	0.921402	-0.048390
0.947824	-0.033221	0.946529	-0.048024
0.972550	-0.037452	0.971683	-0.047360
0.987431	-0.039460	0.986785	-0.046528
0.997374	-0.040552	0.996851	-0.046528

$$C_f/C = 0.50, \delta_F = 5^\circ$$

UPPER SURFACE		LOWER SURFACE	
XU	ZU	XL	ZL
0.0	0.0	0.0	0.0
0.000200	0.002379	0.000200	-0.002228
0.000500	0.003771	0.000500	-0.003375
0.001000	0.005414	0.001000	-0.004719
0.002000	0.007656	0.002000	-0.006512
0.003500	0.010133	0.003500	-0.008436
0.005000	0.012144	0.005000	-0.009945
0.006500	0.013878	0.006500	-0.011196
0.008000	0.015434	0.008000	-0.012270
0.010000	0.017315	0.010000	-0.013503
0.012500	0.019447	0.012500	-0.014815
0.016000	0.022136	0.016000	-0.016341
0.020000	0.024901	0.020000	-0.017770
0.025000	0.028006	0.025000	-0.019223
0.035000	0.033351	0.035000	-0.021367
0.050000	0.039906	0.050000	-0.023654
0.065000	0.045233	0.065000	-0.025486
0.080000	0.049600	0.080000	-0.027101
0.100000	0.054210	0.100000	-0.029016
0.125000	0.058287	0.125000	-0.031038
0.150000	0.060977	0.150000	-0.032767
0.200000	0.063435	0.200000	-0.035505
0.250000	0.064310	0.250000	-0.037272
0.300000	0.064461	0.300000	-0.038283
0.350000	0.064089	0.350000	-0.038655
0.400000	0.063156	0.400000	-0.038481
0.436000	0.062020	0.436000	-0.038500
0.466000	0.060250	0.466000	-0.039000
0.490000	0.058000	0.490000	-0.039880
0.510000	0.055440	0.510000	-0.041200
0.534000	0.051440	0.534000	-0.043200
0.564000	0.045030	0.564000	-0.046500
0.605634	0.034495	0.598000	-0.050750
0.654082	0.021319	0.640454	-0.055970
0.702374	0.007257	0.690164	-0.061985
0.750493	-0.007786	0.739924	-0.067720
0.798448	-0.023754	0.789742	-0.073130
0.846306	-0.040279	0.839621	-0.078191
0.894149	-0.056883	0.889576	-0.082818
0.918143	-0.064776	0.914597	-0.084890
0.942241	-0.072082	0.939660	-0.086716
0.966503	-0.078452	0.964776	-0.088247
0.981153	-0.081749	0.979864	-0.089058
0.990963	-0.083704	0.989921	-0.089611

$$C_F/C = 0.50, \delta_F = 10^\circ$$

UPPER SURFACE		LOWER SURFACE	
XU	ZU	XL	ZL
0.0	0.0	0.0	0.0
0.000200	0.002379	0.000200	-0.002228
0.000500	0.003771	0.000500	-0.003375
0.001000	0.005414	0.001000	-0.004719
0.002000	0.007656	0.002000	-0.006512
0.003500	0.010133	0.003500	-0.008436
0.005000	0.012144	0.005000	-0.009945
0.006500	0.013878	0.006500	-0.011196
0.008000	0.015434	0.008000	-0.012270
0.010000	0.017315	0.010000	-0.013503
0.012500	0.019447	0.012500	-0.014815
0.016000	0.022136	0.016000	-0.016341
0.020000	0.024901	0.020000	-0.017770
0.025000	0.028006	0.025000	-0.019223
0.035000	0.033351	0.035000	-0.021367
0.050000	0.039906	0.050000	-0.023654
0.065000	0.045233	0.065000	-0.025486
0.080000	0.049600	0.080000	-0.027101
0.100000	0.054210	0.100000	-0.029016
0.125000	0.058287	0.125000	-0.031038
0.150000	0.060977	0.150000	-0.032767
0.200000	0.063435	0.200000	-0.035505
0.250000	0.064310	0.250000	-0.037272
0.300000	0.064461	0.300000	-0.038283
0.350000	0.064089	0.350000	-0.038655
0.400000	0.063156	0.400000	-0.038481
0.436000	0.062130	0.436000	-0.038580
0.466000	0.059800	0.466000	-0.039000
0.490000	0.057000	0.490000	-0.040610
0.510000	0.053840	0.510000	-0.042640
0.534000	0.048670	0.534000	-0.045200
0.564000	0.040400	0.564000	-0.052660
0.607254	0.025200	0.585138	-0.057339
0.654369	0.007852	0.634057	-0.067995
0.701252	-0.010366	0.683054	-0.078280
0.747877	-0.029545	0.732125	-0.088330
0.794258	-0.049632	0.781281	-0.098061
0.840493	-0.070265	0.830529	-0.107450
0.886707	-0.090976	0.879891	-0.116414
0.909922	-0.100930	0.904636	-0.120659
0.933291	-0.110309	0.929445	-0.124662
0.956906	-0.118769	0.954332	-0.128376
0.971213	-0.123330	0.969292	-0.130499
0.980815	-0.126133	0.979263	-0.131926

$$C_f/C = 0.50, \delta_F = 15^\circ$$

**APPENDIX B**

# APPENDIX B

## Sectional Characteristics of the A-1 Airfoil with a 35% Plain Flap

### B.1 Sectional Characteristics in Tabular Form for $\delta_F = -5^\circ$

010 A-1 AIRFOIL WITH 0.35C FLAP (-5 DEG. FLAP ANGLE) 10/27/81

180. 180. MAX POS ALPHA, MAX NEG ALPHA

CL180	K1	K2	K3	K4	CONTROL NOS.
0.0000	1.0000	1.0000	1.0000	1.0000	

10 NO.OF MACH NUMBERS FOR CL VS ALPHA

MACH NUMBERS						
0.000	0.300	0.400	0.500	0.600	0.700	0.800
0.850	0.900	1.000				

\*\*\*\*\* LIFT TABLE \*\*\*\*\*

6	ALPHA-CL PAIRS FOR MACH NUM.= 0.000				
ALPHA	0.000	16.640	20.000	340.000	351.100 360.000
CL	-0.335000	1.540000	0.800000	-0.800000	-1.340000 -0.335000
6	ALPHA-CL PAIRS FOR MACH NUM.= 0.300				
ALPHA	0.000	16.010	20.000	340.000	351.600 360.000
CL	-0.351000	1.540000	0.800000	-0.800000	-1.340000 -0.351000
6	ALPHA-CL PAIRS FOR MACH NUM.= 0.400				
ALPHA	0.000	12.060	20.000	340.000	355.000 360.000
CL	-0.368000	1.130000	0.800000	-0.800000	-0.990000 -0.368000
6	ALPHA-CL PAIRS FOR MACH NUM.= 0.500				
ALPHA	0.000	10.410	20.000	340.000	357.400 360.000
CL	-0.392000	0.990000	0.800000	-0.800000	-0.740000 -0.392000
6	ALPHA-CL PAIRS FOR MACH NUM.= 0.600				
ALPHA	0.000	7.460	20.000	340.000	359.400 360.000
CL	-0.430000	0.660000	0.800000	-0.800000	-0.520000 -0.430000
6	ALPHA-CL PAIRS FOR MACH NUM.= 0.700				
ALPHA	0.000	0.100	5.010	20.000	340.000 360.000
CL	-0.482000	-0.480000	0.350000	0.800000	-0.800000 -0.482000
6	ALPHA-CL PAIRS FOR MACH NUM.= 0.800				
ALPHA	0.000	0.930	3.940	20.000	340.000 360.000
CL	-0.420000	-0.400000	0.210000	0.800000	-0.800000 -0.420000

6	ALPHA-CL PAIRS FOR MACH NUM.=					0.850
ALPHA	0.000	3.070	3.660	20.000	340.000	360.000
CL	-0.098000	0.010000	0.140000	0.800000	-0.800000	-0.098000
6	ALPHA-CL PAIRS FOR MACH NUM.=					0.900
ALPHA	0.000	7.640	20.000	340.000	357.700	360.000
CL	-0.435000	0.800000	0.800000	-0.800000	-0.800000	-0.435000
6	ALPHA-CL PAIRS FOR MACH NUM.=					1.000
ALPHA	0.000	10.030	20.000	340.000	354.000	360.000
CL	-0.203000	0.800000	0.800000	-0.800000	-0.800000	-0.203000

010 A-1 AIRFOIL WITH 0.35C FLAP (-5 DEG. FLAP ANGLE) 10/27/81

\*\*\*\*\* DRAG TABLE \*\*\*\*\*

MAXIMUM POS-NEG ANGLES IN CD-M TABLES

16.000 348.000

		ALPHA VALUES FOR CD VS M						
		0.000	1.000	2.000	3.000	5.000	8.000	10.000
		12.000	16.000	348.000	352.000	355.000	357.000	358.000
		359.000	360.000					
6		M-CD PAIRS FOR ALPHA = 0.000						
MACH	0.000	0.200	0.500	0.600	0.700	1.000		
CD	0.009700	0.009700	0.009200	0.009500	0.015000	0.168000		
8		M-CD PAIRS FOR ALPHA = 1.000						
MACH	0.000	0.200	0.500	0.600	0.700	0.755	0.800	
	1.000							
CD	0.009800	0.009800	0.008800	0.008800	0.011000	0.012000	0.016000	
	0.118000							
7		M-CD PAIRS FOR ALPHA = 2.000						
MACH	0.000	0.200	0.500	0.600	0.740	0.800	1.000	
CD	0.009800	0.009800	0.008600	0.008500	0.010800	0.160000	0.118000	
7		M-CD PAIRS FOR ALPHA = 3.000						
MACH	0.000	0.200	0.600	0.700	0.740	0.800	1.000	
CD	0.009800	0.009800	0.008500	0.010400	0.014000	0.023000	0.125000	
7		M-CD PAIRS FOR ALPHA = 5.000						
MACH	0.000	0.200	0.500	0.625	0.675	0.700	1.000	
CD	0.010300	0.010300	0.009000	0.009000	0.014000	0.023000	0.176000	
8		M-CD PAIRS FOR ALPHA = 8.000						
MACH	0.000	0.200	0.400	0.500	0.525	0.575	0.600	
	1.000							
CD	0.011200	0.011200	0.010800	0.010900	0.011000	0.016000	0.028750	
	0.232750							
6		M-CD PAIRS FOR ALPHA = 10.000						
MACH	0.000	0.300	0.400	0.500	0.515	1.000		
CD	0.012900	0.012900	0.013600	0.016200	0.018000	0.265350		

4		M-CD PAIRS FOR ALPHA = 12.000				
MACH	0.000	0.300	0.400	1.000		
CD	0.016900	0.016900	0.026000	0.332000		
2		M-CD PAIRS FOR ALPHA = 16.000				
MACH	0.000	1.000				
CD	0.050000	0.050000				
2		M-CD PAIRS FOR ALPHA = 348.000				
MACH	0.000	1.000				
CD	0.110000	0.110000				
3		M-CD PAIRS FOR ALPHA = 352.000				
MACH	0.000	0.310	1.000			
CD	0.025500	0.025500	0.377400			
4		M-CD PAIRS FOR ALPHA = 355.000				
MACH	0.000	0.300	0.400	1.000		
CD	0.014600	0.014600	0.022000	0.328000		
5		M-CD PAIRS FOR ALPHA = 357.000				
MACH	0.000	0.200	0.400	0.480	1.000	
CD	0.011100	0.011100	0.011700	0.016000	0.281200	
5		M-CD PAIRS FOR ALPHA = 358.000				
MACH	0.000	0.200	0.400	0.525	1.000	
CD	0.010800	0.010800	0.010600	0.015400	0.257650	
7		M-CD PAIRS FOR ALPHA = 359.000				
MACH	0.000	0.200	0.300	0.400	0.500	0.575 1.000
CD	0.010300	0.010300	0.010100	0.009800	0.010500	0.011100 0.227850
6		M-CD PAIRS FOR ALPHA = 360.000				
MACH	0.000	0.200	0.500	0.600	0.700	1.000
CD	0.009700	0.009700	0.009200	0.009500	0.015000	0.168000

010 A-1 AIRFOIL WITH 0.35C FLAP (-5 DEG. FLAP ANGLE) 10/27/81

\*\*\*\*\* PITCHING MOMENT TABLE \*\*\*\*\*

VALUES OF CM FOR MAXIMUM POS-NEG ANGLES

0.0400 0.2820

16		ALPHA VALUES FOR CM VS M						
ALPHA		0.000	0.930	3.070	3.900	5.010	7.460	10.410
		12.060	16.000	344.000	351.100	351.600	355.000	357.400
359.400		360.000						
7		M-CM PAIRS FOR ALPHA = 0.000						
MACH	0.000	0.300	0.400	0.500	0.600	0.700	1.000	
CM	0.054000	0.054000	0.055000	0.057000	0.060000	0.064000	0.064000	
8		M-CM PAIRS FOR ALPHA = 0.930						
MACH	0.000	0.300	0.400	0.500	0.600	0.700	0.800	
	1.000							
CM	0.054000	0.054000	0.055000	0.057000	0.060000	0.064000	0.073000	
	0.073000							
9		M-CM PAIRS FOR ALPHA = 3.070						
MACH	0.000	0.300	0.400	0.500	0.600	0.700	0.800	
	0.850	1.000						
CM	0.054000	0.054000	0.055000	0.057000	0.060000	0.064000	0.073000	
	0.080000	0.080000						
9		M-CM PAIRS FOR ALPHA = 3.900						
MACH	0.000	0.300	0.400	0.500	0.600	0.700	0.800	
	0.850	1.000						
CM	0.054000	0.054000	0.055000	0.057000	0.060000	0.064000	0.073000	
	0.071600	0.071600						
9		M-CM PAIRS FOR ALPHA = 5.010						
MACH	0.000	0.300	0.400	0.500	0.600	0.700	0.800	
	0.850	1.000						
CM	0.054000	0.054000	0.055000	0.057000	0.060000	0.064000	0.040900	
	0.039500	0.037000						
9		M-CM PAIRS FOR ALPHA = 7.460						
MACH	0.000	0.300	0.400	0.500	0.600	0.700	0.800	
	0.850	1.000						
CM	0.054000	0.054000	0.055000	0.057000	0.060000	0.029700	-0.032600	
	-0.044000	-0.080000						

6	M-CM PAIRS FOR ALPHA = 10.410					
MACH	0.000	0.300	0.400	0.500	0.700	1.000
CM	0.054000	0.054000	0.055000	0.057000	-0.032000	-0.095000
5	M-CM PAIRS FOR ALPHA = 12.060					
MACH	0.000	0.300	0.400	0.500	1.000	
CM	0.054000	0.054000	0.055000	0.033900	-0.140000	
2	M-CM PAIRS FOR ALPHA = 16.000					
MACH	0.000	1.000				
CM	0.040000	0.040000				
2	M-CM PAIRS FOR ALPHA = 344.000					
MACH	0.000	1.000				
CM	0.282000	0.282000				
4	M-CM PAIRS FOR ALPHA = 351.100					
MACH	0.000	0.300	0.500	1.000		
CM	0.054000	0.069000	0.246000	0.246000		
4	M-CM PAIRS FOR ALPHA = 351.600					
MACH	0.000	0.300	0.500	1.000		
CM	0.054000	0.054000	0.231000	0.231000		
7	M-CM PAIRS FOR ALPHA = 355.000					
MACH	0.000	0.300	0.400	0.500	0.600	0.700 1.000
CM	0.054000	0.054000	0.055000	0.129000	0.192000	0.214000 0.214000
7	M-CM PAIRS FOR ALPHA = 357.400					
MACH	0.000	0.300	0.400	0.500	0.600	0.700 1.000
CM	0.054000	0.054000	0.055000	0.057000	0.120000	0.142000 0.142000
7	M-CM PAIRS FOR ALPHA = 359.400					
MACH	0.000	0.300	0.400	0.500	0.600	0.700 1.000
CM	0.054000	0.054000	0.055000	0.057000	0.060000	0.082000 0.082000
7	M-CM PAIRS FOR ALPHA = 360.000					
MACH	0.000	0.300	0.400	0.500	0.600	0.700 1.000
CM	0.054000	0.054000	0.055000	0.057000	0.060000	0.064000 0.064000

B.2 Sectional Characteristics in Tabular  
Form for  $\delta_F = 0^\circ$

011 A-1 AIRFOIL WITH 0.35C F.LAP ( 0 DEG. FLAP ANGLE) 10/27/81

180. 180. MAX POS ALPHA, MAX NEG ALPHA

CL180 K1 K2 K3 K4 CONTROL NOS.  
0.0000 1.0000 1.0000 1.0000 1.0000

10 NO.OF MACH NUMBERS FOR CL VS ALPHA  
MACH NUMBERS

0.000 0.300 0.400 0.500 0.600 0.700 0.800  
0.850 0.900 1.000

\*\*\*\*\* LIFT TABLE \*\*\*\*\*

6	ALPHA-CL PAIRS FOR MACH NUM.= 0.000					
ALPHA	0.000	14.590	20.000	340.000	349.600	360.000
CL	0.051000	1.690000	0.800000	-0.800000	-1.120000	0.051000
6	ALPHA-CL PAIRS FOR MACH NUM.= 0.300					
ALPHA	0.000	13.910	20.000	340.000	350.000	360.000
CL	0.053000	1.690000	0.800000	-0.800000	-1.120000	0.053000
6	ALPHA-CL PAIRS FOR MACH NUM.= 0.400					
ALPHA	0.000	10.040	20.000	340.000	353.100	360.000
CL	0.055000	1.300000	0.800000	-0.800000	-0.800000	0.055000
6	ALPHA-CL PAIRS FOR MACH NUM.= 0.500					
ALPHA	0.000	8.560	20.000	340.000	355.400	360.000
CL	0.061000	1.200000	0.800000	-0.800000	-0.550000	0.061000
6	ALPHA-CL PAIRS FOR MACH NUM.= 0.600					
ALPHA	0.000	5.410	20.000	340.000	357.200	360.000
CL	0.067000	0.860000	0.800000	-0.800000	-0.340000	0.067000
6	ALPHA-CL PAIRS FOR MACH NUM.= 0.700					
ALPHA	0.000	3.080	20.000	340.000	358.300	360.000
CL	0.078000	0.590000	0.800000	-0.800000	-0.200000	0.078000
6	ALPHA-CL PAIRS FOR MACH NUM.= 0.800					
ALPHA	0.000	2.030	20.000	340.000	358.800	360.000
CL	0.104000	0.510000	0.800000	-0.800000	-0.140000	0.104000

6	ALPHA-CL PAIRS FOR MACH NUM.=					0.850
ALPHA	0.000	20.000	340.000	359.000	359.800	360.000
CL	0.082000	0.800000	-0.800000	-0.120000	0.075000	0.082000

6	ALPHA-CL PAIRS FOR MACH NUM.=					0.900
ALPHA	0.000	4.470	20.000	340.000	354.700	360.000
CL	0.067000	0.800000	0.800000	-0.800000	-0.800000	0.067000

6	ALPHA-CL PAIRS FOR MACH NUM.=					1.000
ALPHA	0.000	7.700	20.000	340.000	351.700	360.000
CL	0.030000	0.800000	0.800000	-0.800000	-0.800000	0.030000

011 A-1 AIRFOIL WITH 0.35C FLAP ( 0 DEG. FLAP ANGLE) 10/27/81

\*\*\*\*\* DRAG TABLE \*\*\*\*\*

MAXIMUM POS-NEG ANGLES IN CD-M TABLES

18.000 348.000

		19 ALPHA VALUES FOR CD VS M					
		ALPHA					
		0.000	1.000	2.000	3.000	4.000	5.000 8.000
		10.000	12.000	14.000	18.000	348.000	352.000
		355.000	357.000	358.000	359.000	360.000	
8		M-CD PAIRS FOR ALPHA = 0.000					
MACH		0.000	0.200	0.600	0.700	0.800	0.850 0.900
CD		0.010000	0.010000	0.008100	0.008400	0.015500	0.028000 0.054000
		0.107000					
8		M-CD PAIRS FOR ALPHA = 1.000					
MACH		0.000	0.200	0.600	0.700	0.750	0.800 0.850
CD		0.009800	0.009800	0.008300	0.009200	0.013000	0.023000 0.041000
		0.120000					
7		M-CD PAIRS FOR ALPHA = 2.000					
MACH		0.000	0.200	0.600	0.700	0.725	0.800 1.000
CD		0.009600	0.009600	0.008800	0.014000	0.016500	0.040000 0.146000
7		M-CD PAIRS FOR ALPHA = 3.000					
MACH		0.000	0.200	0.600	0.655	0.680	0.700 1.000
CD		0.009800	0.009800	0.009300	0.012000	0.014600	0.019200 0.172200
7		M-CD PAIRS FOR ALPHA = 4.000					
MACH		0.000	0.200	0.500	0.600	0.645	0.675 1.000
CD		0.010200	0.010200	0.010000	0.011000	0.015000	0.018000 0.183700
7		M-CD PAIRS FOR ALPHA = 5.000					
MACH		0.000	0.200	0.500	0.600	0.625	0.650 1.000
CD		0.010900	0.010900	0.010500	0.015400	0.017900	0.025400 0.203900
6		M-CD PAIRS FOR ALPHA = 8.000					
MACH		0.000	0.200	0.400	0.530	0.600	1.000
CD		0.011500	0.011500	0.014700	0.017900	0.045000	0.249000

5	M-CD PAIRS FOR ALPHA = 10.000				
MACH	0.000	0.200	0.430	0.500	1.000
CD	0.015500	0.015500	0.027000	0.045000	0.300000
4	M-CD PAIRS FOR ALPHA = 12.000				
MACH	0.000	0.350	0.450	1.000	
CD	0.026000	0.026000	0.056000	0.336500	
3	M-CD PAIRS FOR ALPHA = 14.000				
MACH	0.000	0.300	1.000		
CD	0.038000	0.038000	0.395000		
2	M-CD PAIRS FOR ALPHA = 18.000				
MACH	0.000	1.000			
CD	0.061000	0.061000			
2	M-CD PAIRS FOR ALPHA = 348.000				
MACH	0.000	1.000			
CD	0.075000	0.075000			
3	M-CD PAIRS FOR ALPHA = 350.000				
MACH	0.000	0.300	1.000		
CD	0.034000	0.034000	0.391000		
3	M-CD PAIRS FOR ALPHA = 352.000				
MACH	0.000	0.360	1.000		
CD	0.016800	0.016800	0.343200		
5	M-CD PAIRS FOR ALPHA = 355.000				
MACH	0.000	0.200	0.400	0.500	1.000
CD	0.012400	0.012400	0.011200	0.021200	0.276200
6	M-CD PAIRS FOR ALPHA = 357.000				
MACH	0.000	0.200	0.400	0.500	0.617 1.000
CD	0.010850	0.010850	0.009600	0.009900	0.021500 0.217200
6	M-CD PAIRS FOR ALPHA = 358.000				
MACH	0.000	0.200	0.500	0.600	0.700 1.000
CD	0.010100	0.010100	0.008900	0.009900	0.020000 0.173000

7		M-CD PAIRS FOR ALPHA = 359.000					
MACH	0.300	0.200	0.500	0.600	0.700	0.800	1.000
CD	0.010000	0.010000	0.008600	0.008400	0.009600	0.015800	0.117800
8		M-CD PAIRS FOR ALPHA = 360.000					
MACH	0.000	0.200	0.600	0.700	0.800	0.850	0.900
	1.000						
CD	0.010000	0.010000	0.008100	0.008400	0.015500	0.028000	0.054000
	0.107000						

011 A-1 AIRFOIL WITH 0.35C FLAP ( 0 DEG. FLAP ANGLE) 10/27/81

\*\*\*\*\* PITCHING MOMENT TABLE \*\*\*\*\*

VALUES OF CM FOR MAXIMUM POS-NEG ANGLES

-0.0343 0.1750

19		ALPHA VALUES FOR CM VS M					
ALPHA							
0.000	1.000	2.030	3.080	5.410	8.560	10.040	
13.910	14.590	16.000	344.000	349.600	350.000	353.100	
355.400	357.200	358.300	358.800	360.000			
8 M-CM PAIRS FOR ALPHA = 0.000							
MACH	0.000	0.400	0.500	0.600	0.700	0.800	0.850
1.000							
CM	-0.005000	-0.005000	-0.006000	-0.008500	-0.014000	-0.025500	-0.033000
	-0.052000						
8 M-CM PAIRS FOR ALPHA = 1.000							
MACH	0.000	0.400	0.500	0.600	0.700	0.800	0.850
1.000							
CM	-0.005000	-0.005000	-0.006000	-0.008500	-0.014000	-0.025500	-0.032000
	-0.050000						
8 M-CM PAIRS FOR ALPHA = 2.030							
MACH	0.000	0.400	0.500	0.600	0.700	0.800	0.850
1.000							
CM	-0.005000	-0.005000	-0.006000	-0.008500	-0.014000	-0.025500	-0.032000
	-0.050000						
8 M-CM PAIRS FOR ALPHA = 3.080							
MACH	0.000	0.400	0.500	0.600	0.700	0.800	0.850
1.000							
CM	-0.005000	-0.005000	-0.006000	-0.008500	-0.014000	-0.057000	-0.060000
	-0.070000						
7 M-CM PAIRS FOR ALPHA = 5.410							
MACH	0.000	0.400	0.500	0.600	0.700	0.800	1.000
CM	-0.005000	-0.005000	-0.006000	-0.008500	-0.048000	-0.073000	-0.120000
5 M-CM PAIRS FOR ALPHA = 8.560							
MACH	0.000	0.400	0.500	0.700	1.000		
CM	-0.005000	-0.005000	-0.006000	-0.092000	-0.200000		

4		M-CM PAIRS FOR ALPHA = 10.040				
MACH	0.000	0.450	0.700	1.000		
CM	-0.005000	-0.005000	-0.111000	-0.200000		
4		M-CM PAIRS FOR ALPHA = 13.910				
MACH	0.000	0.300	0.700	1.000		
CM	-0.005000	-0.005000	-0.165000	-0.200000		
4		M-CM PAIRS FOR ALPHA = 14.590				
MACH	0.000	0.300	0.700	1.000		
CM	-0.005000	-0.016000	-0.175000	-0.200000		
2		M-CM PAIRS FOR ALPHA = 16.000				
MACH	0.000	1.000				
CM	-0.034260	0.034260				
2		M-CM PAIRS FOR ALPHA = 344.000				
MACH	0.000	1.000				
CM	0.175000	0.175000				
8		M-CM PAIRS FOR ALPHA = 349.600				
MACH	0.000	0.300	0.400	0.500	0.600	0.700
	1.000					0.800
CM	-0.005000	0.007000	0.100000	0.168000	0.220000	0.247000
	0.250000					0.250000
8		M-CM PAIRS FOR ALPHA = 350.000				
MACH	0.000	0.300	0.400	0.500	0.600	0.700
	1.000					0.800
CM	-0.005000	-0.005000	0.088000	0.156000	0.208000	0.235000
	0.238000					0.238000
7		M-CM PAIRS FOR ALPHA = 353.100				
MACH	0.000	0.400	0.500	0.600	0.700	0.800
						1.000
CM	-0.005000	-0.005000	0.063000	0.115000	0.142000	0.145000
						0.145000
7		M-CM PAIRS FOR ALPHA = 355.400				
MACH	0.000	0.400	0.500	0.600	0.700	0.800
						1.000
CM	-0.005000	-0.005000	-0.006000	0.044000	0.073000	0.076000
						0.076000

7 M-CM PAIRS FOR ALPHA = 357.200  
MACH 0.000 0.400 0.500 0.600 0.700 0.800 1.000  
CM -0.005000 -0.005000 -0.006000 -0.008500 0.019000 0.023000 0.023000

8 M-CM PAIRS FOR ALPHA = 358.300  
MACH 0.000 0.400 0.500 0.600 0.700 0.800 0.850  
1.000  
CM -0.005000 -0.005000 -0.006000 -0.008500 -0.014000 -0.020000 -0.022000  
-0.022000

8 M-CM PAIRS FOR ALPHA = 358.800  
MACH 0.000 0.400 0.500 0.600 0.700 0.800 0.850  
1.000  
CM -0.005000 -0.005000 -0.006000 -0.008500 -0.014000 -0.025500 -0.042000  
-0.042000

8 M-CM PAIRS FOR ALPHA = 360.000  
MACH 0.000 0.400 0.500 0.600 0.700 0.800 0.850  
1.000  
CM -0.005000 -0.005000 -0.006000 -0.008500 -0.014000 -0.025500 -0.033000  
-0.052000

B.3 Sectional Characteristics in Tabular Form  
for  $\delta_F = 5^\circ$

012 A-1 AIRFOIL WITH 0.35C FLAP ( 5 DEG. FLAP ANGLE) 10/27/81

180. 180. MAX POS ALPHA, MAX NEG ALPHA

CL180 K1 K2 K3 K4 CONTROL NOS.  
0.0000 1.0000 1.0000 1.0000 1.0000

10 NO.OF MACH NUMBERS FOR CL VS ALPHA

MACH NUMBERS  
0.000 0.300 0.400 0.500 0.600 0.700 0.800  
0.825 0.900 1.000

\*\*\*\*\* LIFT TABLE \*\*\*\*\*

6		ALPHA-CL PAIRS FOR MACH NUM. = 0.000				
ALPHA	0.000	12.380	20.000	340.000	347.200	360.000
CL	0.433000	1.820000	0.800000	-0.800000	-1.000000	0.433000
6		ALPHA-CL PAIRS FOR MACH NUM. = 0.300				
ALPHA	0.000	11.640	20.000	340.000	347.600	360.000
CL	0.434000	1.820000	0.800000	-0.800000	-1.000000	0.434000
6		ALPHA-CL PAIRS FOR MACH NUM. = 0.400				
ALPHA	0.000	8.240	20.000	340.000	351.300	360.000
CL	0.479000	1.500000	0.800000	-0.800000	-0.600000	0.479000
6		ALPHA-CL PAIRS FOR MACH NUM. = 0.500				
ALPHA	0.000	6.740	20.000	340.000	353.500	360.000
CL	0.513000	1.410000	0.800000	-0.800000	-0.350000	0.513000
6		ALPHA-CL PAIRS FOR MACH NUM. = 0.600				
ALPHA	0.000	3.380	20.000	340.000	355.500	360.000
CL	0.564000	1.060000	0.800000	-0.800000	-0.100000	0.564000
6		ALPHA-CL PAIRS FOR MACH NUM. = 0.700				
ALPHA	0.000	0.970	20.000	340.000	356.500	360.000
CL	0.649000	0.810000	0.800000	-0.800000	0.070000	0.649000
6		ALPHA-CL PAIRS FOR MACH NUM. = 0.800				
ALPHA	0.000	20.000	340.000	357.100	359.200	360.000
CL	0.550000	0.800000	-0.800000	0.150000	0.540000	0.550000

6	ALPHA-CL PAIRS FOR MACH NUM.= 0.825					
ALPHA	0.000	20.000	340.000	356.900	357.600	360.000
CL	0.327000	0.800000	-0.800000	0.140000	0.270000	0.327000

6	ALPHA-CL PAIRS FOR MACH NUM.= 0.900					
ALPHA	0.000	1.500	20.000	340.000	351.900	360.000
CL	0.551000	0.800000	0.800000	-0.800000	-0.800000	0.551000

6	ALPHA-CL PAIRS FOR MACH NUM.= 1.000					
ALPHA	0.000	5.580	20.000	340.000	349.600	360.000
CL	0.242000	0.800000	0.800000	-0.800000	-0.800000	0.242000

012 A-1 AIRFOIL WITH 0.35C FLAP ( 5 DEG. FLAP ANGLE) 10/27/81

\*\*\*\*\* DRAG TABLE \*\*\*\*\*

MAXIMUM POS-NEG ANGLES IN CD-M TABLES

16.000 346.000

18 ALPHA VALUES FOR CD VS M

		0.000	1.000	2.000	3.000	5.000	8.000	10.000
		12.000	16.000	346.000	348.000	350.000	352.000	355.000
		357.000	358.000	359.000	360.000			
7 M-CD PAIRS FOR ALPHA = 0.000								
MACH	0.000	0.200	0.500	0.600	0.700	0.760	1.000	
CD	0.009800	0.009800	0.009100	0.009200	0.017000	0.023000	0.145400	
5 M-CD PAIRS FOR ALPHA = 1.000								
MACH	0.000	0.500	0.600	0.700	1.000			
CD	0.009900	0.009900	0.011500	0.025000	0.178000			
6 M-CD PAIRS FOR ALPHA = 2.000								
MACH	0.000	0.300	0.400	0.500	0.640	1.000		
CD	0.010400	0.010400	0.010700	0.011000	0.018000	0.201600		
5 M-CD PAIRS FOR ALPHA = 3.000								
MACH	0.000	0.200	0.500	0.610	1.000			
CD	0.010500	0.010500	0.012600	0.024000	0.222900			
6 M-CD PAIRS FOR ALPHA = 5.000								
MACH	0.000	0.200	0.400	0.500	0.570	1.000		
CD	0.013400	0.013400	0.015300	0.017100	0.033500	0.252800		
4 M-CD PAIRS FOR ALPHA = 8.000								
MACH	0.000	0.300	0.415	1.000				
CD	0.022500	0.022500	0.029500	0.327850				
3 M-CD PAIRS FOR ALPHA = 10.000								
MACH	0.000	0.325	1.000					
CD	0.031500	0.031500	0.375750					
3 M-CD PAIRS FOR ALPHA = 12.000								
MACH	0.000	0.250	1.000					
CD	0.058000	0.058000	0.440500					

2	M-CD PAIRS FOR ALPHA = 16.000						
MACH	0.000	1.000					
CD	0.135000	0.135000					
2	M-CD PAIRS FOR ALPHA = 346.000						
MACH	0.000	1.000					
CD	0.047500	0.047500					
3	M-CD PAIRS FOR ALPHA = 348.000						
MACH	0.000	0.300	1.000				
CD	0.024000	0.024000	0.381000				
3	M-CD PAIRS FOR ALPHA = 350.000						
MACH	0.000	0.325	1.000				
CD	0.015500	0.015500	0.359750				
4	M-CD PAIRS FOR ALPHA = 352.000						
MACH	0.000	0.300	0.400	1.000			
CD	0.011600	0.011600	0.012200	0.318200			
6	M-CD PAIRS FOR ALPHA = 355.000						
MACH	0.000	0.200	0.400	0.500	0.550	1.000	
CD	0.010400	0.010400	0.009300	0.009200	0.009200	0.238700	
6	M-CD PAIRS FOR ALPHA = 357.000						
MACH	0.000	0.200	0.600	0.700	0.800	1.000	
CD	0.009800	0.009800	0.008200	0.008200	0.021000	0.123000	
6	M-CD PAIRS FOR ALPHA = 358.000						
MACH	0.000	0.200	0.600	0.700	0.800	1.000	
CD	0.009800	0.009800	0.008200	0.008400	0.018600	0.120600	
9	M-CD PAIRS FOR ALPHA = 359.000						
MACH	0.000	0.200	0.400	0.500	0.600	0.725	0.775
	0.800	1.000					
CD	0.010000	0.010000	0.009000	0.008800	0.008700	0.008800	0.013800
	0.026550	0.128550					
7	M-CD PAIRS FOR ALPHA = 360.000						
MACH	0.000	0.200	0.500	0.600	0.700	0.760	1.000
CD	0.009800	0.009800	0.009100	0.009200	0.017000	0.023000	0.145400

012 A-1 AIRFOIL WITH 0.35C FLAP ( 5 DEG. FLAP ANGLE) 10/27/81

\*\*\*\*\* PITCHING MOMENT TABLE \*\*\*\*\*

VALUES OF CM FOR MAXIMUM POS-NEG ANGLES

-0.1260 0.0430

16 ALPHA VALUES FOR CM VS M								
ALPHA		0.000	1.000	3.400	6.700	8.240	11.640	12.400
		16.000	344.000	347.600	351.300	353.500	355.500	356.500
		359.200	360.000					
8		M-CM PAIRS FOR ALPHA = 0.000						
MACH		0.000	0.300	0.400	0.500	0.600	0.700	0.800
	1.000							
CM		-0.065000	-0.065000	-0.070000	-0.077000	-0.086000	-0.099000	-0.112000
		-0.138000						
7		M-CM PAIRS FOR ALPHA = 1.000						
MACH		0.000	0.300	0.400	0.500	0.600	0.700	1.000
CM		-0.065000	-0.065000	-0.070000	-0.077000	-0.086000	-0.099000	-0.138000
6		M-CM PAIRS FOR ALPHA = 3.400						
MACH		0.000	0.300	0.400	0.500	0.600	1.000	
CM		-0.065000	-0.065000	-0.070000	-0.077000	-0.085000	-0.180000	
7		M-CM PAIRS FOR ALPHA = 6.700						
MACH		0.000	0.300	0.400	0.500	0.600	0.700	1.000
CM		-0.065000	-0.075000	-0.070000	-0.077000	-0.135000	-0.180000	-0.280000
7		M-CM PAIRS FOR ALPHA = 8.240						
MACH		0.000	0.300	0.400	0.500	0.600	0.700	1.000
CM		-0.065000	-0.065000	-0.070000	-0.098000	-0.154000	-0.201000	-0.280000
4		M-CM PAIRS FOR ALPHA = 11.640						
MACH		0.000	0.300	0.600	1.000			
CM		-0.065000	-0.065000	-0.201000	-0.280000			
4		M-CM PAIRS FOR ALPHA = 12.400						
MACH		0.000	0.300	0.600	1.000			
CM		-0.065000	-0.075000	-0.212000	-0.280000			

2 M-CM PAIRS FOR ALPHA = 16.000

MACH 0.000 1.000

CM -0.126000 -0.126000

2 M-CM PAIRS FOR ALPHA = 344.000

MACH 0.000 1.000

CM 0.043000 0.043000

6 M-CM PAIRS FOR ALPHA = 347.600

MACH 0.000 0.300 0.400 0.500 0.600 1.000

CM -0.065000 -0.065000 0.040000 0.100000 0.150000 0.150000

7 M-CM PAIRS FOR ALPHA = 351.300

MACH 0.000 0.300 0.400 0.500 0.600 0.700 1.000

CM -0.065000 -0.065000 -0.070000 -0.011000 0.041000 0.060000 0.060000

7 M-CM PAIRS FOR ALPHA = 353.500

MACH 0.000 0.300 0.400 0.500 0.600 0.700 1.000

CM -0.065000 -0.065000 -0.070000 -0.077000 -0.024000 -0.008000 -0.008000

7 M-CM PAIRS FOR ALPHA = 355.500

MACH 0.000 0.300 0.400 0.500 0.600 0.700 1.000

CM -0.065000 -0.065000 -0.070000 -0.077000 -0.086000 -0.070000 -0.070000

7 M-CM PAIRS FOR ALPHA = 356.500

MACH 0.000 0.300 0.400 0.500 0.600 0.700 1.000

CM -0.065000 -0.065000 -0.070000 -0.077000 -0.086000 -0.099000 -0.136000

7 M-CM PAIRS FOR ALPHA = 359.200

MACH 0.000 0.300 0.400 0.500 0.600 0.700 1.000

CM -0.065000 -0.065000 -0.070000 -0.077000 -0.086000 -0.099000 -0.136000

8 M-CM PAIRS FOR ALPHA = 360.000

MACH 0.000 0.300 0.400 0.500 0.600 0.700 0.800

CM 1.000

-0.065000 -0.065000 -0.070000 -0.077000 -0.086000 -0.099000 -0.122000

-0.138000

B.4 Sectional Characteristics in Tabular Form  
for  $\delta_F = 10^\circ$

013 A-1 AIRFOIL WITH 0.35C FLAP (10 DEG. FLAP ANGLE) 10/27/81

180. 180. MAX POS ALPHA, MAX NEG ALPHA

CL180 K1 K2 K3 K4 CONTROL NOS.  
0.0000 1.0000 1.0000 1.0000 1.0000

10 NO.OF MACH NUMBERS FOR CL VS ALPHA

MACH NUMBERS  
0.000 0.300 0.400 0.500 0.600 0.650 0.700  
0.800 0.900 1.000

\*\*\*\*\* LIFT TABLE \*\*\*\*\*

6	ALPHA-CL PAIRS FOR MACH NUM.= 0.000				
ALPHA	0.000	10.200	20.000	340.000	347.200 360.000
CL	0.815000	1.960000	0.800000	-0.800000	-0.620000 0.815000
6	ALPHA-CL PAIRS FOR MACH NUM.= 0.300				
ALPHA	0.000	9.400	20.000	340.000	347.500 360.000
CL	0.854000	1.960000	0.800000	-0.800000	-0.620000 0.854000
6	ALPHA-CL PAIRS FOR MACH NUM.= 0.400				
ALPHA	0.000	3.270	20.000	340.000	349.400 360.000
CL	0.903000	1.310000	0.800000	-0.800000	-0.420000 0.903000
6	ALPHA-CL PAIRS FOR MACH NUM.= 0.500				
ALPHA	0.000	0.900	20.000	340.000	351.600 360.000
CL	0.960000	1.080000	0.800000	-0.800000	-0.160000 0.960000
6	ALPHA-CL PAIRS FOR MACH NUM.= 0.600				
ALPHA	0.000	20.000	340.000	353.400	359.200 360.000
CL	0.925000	0.800000	-0.800000	0.080000	0.930000 0.925000
6	ALPHA-CL PAIRS FOR MACH NUM.= 0.650				
ALPHA	0.000	20.000	340.000	354.200	356.800 360.000
CL	0.628000	0.800000	-0.800000	0.200000	0.600000 0.628000
6	ALPHA-CL PAIRS FOR MACH NUM.= 0.700				
ALPHA	0.000	20.000	340.000	354.800	355.100 360.000
CL	0.447000	0.800000	-0.800000	0.300000	0.360000 0.447000

6	ALPHA-CL PAIRS FOR MACH NUM.=					0.800
ALPHA	0.000	20.000	340.000	348.500	357.400	360.000
CL	0.800000	0.800000	-0.800000	-0.800000	0.800000	0.800000

6	ALPHA-CL PAIRS FOR MACH NUM.=					0.900
ALPHA	0.000	20.000	340.000	346.800	357.600	360.000
CL	0.800000	0.800000	-0.800000	-0.800000	0.800000	0.800000

6	ALPHA-CL PAIRS FOR MACH NUM.=					1.000
ALPHA	0.000	20.000	340.000	343.400	359.400	360.000
CL	0.800000	0.800000	-0.800000	-0.800000	0.800000	0.800000

013 A-1 AIRFOIL WITH 0.35C FLAP (10 DEG. FLAP ANGLE) 10/27/81

\*\*\*\*\* DRAG TABLE \*\*\*\*\*

MAXIMUM POS-NEG ANGLES IN CD-M TABLES

16.000 344.000

18 ALPHA VALUES FOR CD VS M

ALPHA	0.000	1.000	2.000	3.000	5.000	8.000	12.000
16.000	344.000	348.000	352.000	354.000	355.000	356.000	
357.000	358.000	359.000	360.000				

5 M-CD PAIRS FOR ALPHA = 0.000

MACH	0.000	0.200	0.400	0.525	1.000
CD	0.013500	0.013500	0.013900	0.016000	0.258250

4 M-CD PAIRS FOR ALPHA = 1.000

MACH	0.000	0.400	0.500	1.000
CD	0.015000	0.015000	0.024000	0.279000

4 M-CD PAIRS FOR ALPHA = 2.000

MACH	0.000	0.300	0.430	1.000
CD	0.017000	0.017000	0.018200	0.308900

4 M-CD PAIRS FOR ALPHA = 3.000

MACH	0.000	0.300	0.400	1.000
CD	0.019000	0.019000	0.026200	0.332200

3 M-CD PAIRS FOR ALPHA = 5.000

MACH	0.000	0.350	1.000
CD	0.024500	0.024500	0.356000

3 M-CD PAIRS FOR ALPHA = 8.000

MACH	0.000	0.300	1.000
CD	0.036500	0.036500	0.393500

3 M-CD PAIRS FOR ALPHA = 12.000

MACH	0.000	0.200	1.000
CD	0.072500	0.072500	0.480500

2 M-CD PAIRS FOR ALPHA = 16.000

MACH	0.000	1.000
CD	0.135000	0.135000

2	M-CD PAIRS FOR ALPHA = 344.000				
MACH	0.000	1.000			
CD	0.052500	0.052500			
3	M-CD PAIRS FOR ALPHA = 348.000				
MACH	0.000	0.300	1.000		
CD	0.017000	0.017000	0.374000		
4	M-CD PAIRS FOR ALPHA = 352.000				
MACH	0.000	0.400	0.500	1.000	
CD	0.012000	0.012000	0.016000	0.271000	
4	M-CD PAIRS FOR ALPHA = 354.000				
MACH	0.000	0.600	0.660	1.000	
CD	0.012000	0.012000	0.018000	0.191400	
4	M-CD PAIRS FOR ALPHA = 355.000				
MACH	0.000	0.655	0.700	1.000	
CD	0.012000	0.012000	0.016000	0.169000	
5	M-CD PAIRS FOR ALPHA = 356.000				
MACH	0.000	0.400	0.600	0.700	1.000
CD	0.012000	0.012000	0.011400	0.018500	0.171500
3	M-CD PAIRS FOR ALPHA = 357.000				
MACH	0.000	0.625	1.000		
CD	0.012000	0.012000	0.203250		
4	M-CD PAIRS FOR ALPHA = 358.000				
MACH	0.000	0.300	0.600	1.000	
CD	0.012100	0.012100	0.013500	0.217500	
6	M-CD PAIRS FOR ALPHA = 359.000				
MACH	0.000	0.300	0.400	0.500	0.600 1.000
CD	0.012700	0.012700	0.012900	0.013400	0.016400 0.220400
5	M-CD PAIRS FOR ALPHA = 360.000				
MACH	0.000	0.200	0.400	0.525	1.000
CD	0.013500	0.013500	0.013900	0.016000	0.258250

013 A-1 AIRFOIL WITH 0.35C FLAP (10 DEG. FLAP ANGLE) 10/27/81

\*\*\*\*\* PITCHING MOMENT TABLE \*\*\*\*\*

VALUES OF CM FOR MAXIMUM POS-NEG ANGLES

-0.2064 -0.0090

		14 ALPHA VALUES FOR CM VS M						
		ALPHA						
		0.000	0.900	3.300	9.400	16.000	344.000	347.500
		349.400	351.600	353.400	355.100	356.800	359.200	360.000
6		M-CM PAIRS FOR ALPHA = 0.000						
MACH		0.000	0.300	0.400	0.500	0.600	1.000	
CM		-0.114000	-0.114000	-0.122000	-0.132000	-0.160000	-0.160000	
6		M-CM PAIRS FOR ALPHA = 0.900						
MACH		0.000	0.300	0.400	0.500	0.600	1.000	
CM		-0.114000	-0.114000	-0.122000	-0.132000	-0.174000	-0.174000	
5		M-CM PAIRS FOR ALPHA = 3.300						
MACH		0.000	0.300	0.400	0.600	1.000		
CM		-0.114000	-0.114000	-0.122000	-0.205000	-0.205000		
5		M-CM PAIRS FOR ALPHA = 9.400						
MACH		0.000	0.300	0.400	0.600	1.000		
CM		-0.114000	-0.114000	-0.207000	-0.290000	-0.290000		
2		M-CM PAIRS FOR ALPHA = 16.000						
MACH		0.000	1.000					
CM		-0.206400	-0.206400					
2		M-CM PAIRS FOR ALPHA = 344.000						
MACH		0.000	1.000					
CM		-0.009000	-0.009000					
8		M-CM PAIRS FOR ALPHA = 347.500						
MACH		0.000	0.300	0.400	0.500	0.600	0.650	0.700
CM		-0.114000	-0.114000	-0.067000	-0.009000	0.031000	0.041000	0.045000
		0.045000						

7	M-CM PAIRS FOR ALPHA = 349.400						
MACH	0.000	0.300	0.400	0.500	0.600	0.650	1.000
CM	-0.114000	-0.114000	-0.122000	-0.067000	-0.027000	-0.015000	-0.015000
8	M-CM PAIRS FOR ALPHA = 351.600						
MACH	0.000	0.300	0.400	0.500	0.600	0.650	0.700
CM	-0.114000	-0.114000	-0.122000	-0.132000	-0.092000	-0.080000	-0.076000
8	M-CM PAIRS FOR ALPHA = 353.400						
MACH	0.000	0.300	0.400	0.500	0.600	0.650	0.700
CM	-0.114000	-0.114000	-0.122000	-0.132000	-0.147000	-0.134000	-0.131000
8	M-CM PAIRS FOR ALPHA = 355.100						
MACH	0.000	0.300	0.400	0.500	0.600	0.650	0.700
CM	-0.114000	-0.114000	-0.122000	-0.132000	-0.147000	-0.158000	-0.172000
8	M-CM PAIRS FOR ALPHA = 356.800						
MACH	0.000	0.300	0.400	0.500	0.600	0.650	0.700
CM	-0.114000	-0.114000	-0.122000	-0.132000	-0.147000	-0.158000	-0.193000
6	M-CM PAIRS FOR ALPHA = 359.200						
MACH	0.000	0.300	0.400	0.500	0.600	1.000	
CM	-0.114000	-0.114000	-0.122000	-0.132000	-0.147000	-0.147000	
6	M-CM PAIRS FOR ALPHA = 360.000						
MACH	0.000	0.300	0.400	0.500	0.600	1.000	
CM	-0.114000	-0.114000	-0.122000	-0.132000	-0.160000	-0.160000	

B.5 Sectional Characteristics in Tabular Form  
for  $\delta_F = 15^\circ$

014 A-1 AIRFOIL WITH C.35C FLAP (15 DEG. FLAP ANGLE) 10/27/81

180. 180. MAX POS ALPHA, MAX NEG ALPHA

CL180 K1 K2 K3 K4 CONTROL NOS.  
0.0000 1.0000 1.0000 1.0000 1.0000

10 NO.OF MACH NUMBERS FOR CL VS ALPHA

MACH NUMBERS  
0.000 0.300 0.400 0.500 0.550 0.600 0.700  
0.800 0.900 1.000

\*\*\*\*\* LI, T TABLE \*\*\*\*\*

6	ALPHA-CL PAIRS FOR MACH NUM.= 0.000				
ALPHA	0.000	1.910	20.000	340.000	344.600 360.000
CL	1.186000	1.400000	0.800000	-0.800000	-0.540000 1.186000
6	ALPHA-CL PAIRS FOR MACH NUM.= 0.300				
ALPHA	0.000	1.340	20.000	340.000	344.800 360.000
CL	1.243000	1.400000	0.800000	-0.800000	-0.540000 1.243000
6	ALPHA-CL PAIRS FOR MACH NUM.= 0.400				
ALPHA	0.000	20.000	340.000	347.000	357.600 360.000
CL	0.996000	0.800000	-0.800000	-0.310000	1.020000 0.996000
6	ALPHA-CL PAIRS FOR MACH NUM.= 0.500				
ALPHA	0.000	20.000	340.000	349.700	356.800 360.000
CL	0.951000	0.800000	-0.800000	0.030000	0.975000 0.951000
6	ALPHA-CL PAIRS FOR MACH NUM.= 0.550				
ALPHA	0.000	20.000	340.000	350.800	355.700 360.000
CL	0.841000	0.800000	-0.800000	0.170000	0.850000 0.841000
6	ALPHA-CL PAIRS FOR MACH NUM.= 0.600				
ALPHA	0.000	20.000	340.000	351.700	353.100 360.000
CL	0.577000	0.200000	-0.800000	0.300000	0.500000 0.577000
6	ALPHA-CL PAIRS FOR MACH NUM.= 0.700				
ALPHA	0.000	20.000	340.000	343.750	353.700 360.000
CL	0.800000	0.800000	-0.800000	-0.800000	0.800000 0.800000

6	ALPHA-CL PAIRS FOR MACH NUM.= 0.800					
ALPHA	0.000	20.000	340.000	343.000	352.800	360.000
CL	0.800000	0.800000	-0.800000	-0.800000	0.800000	0.800000

6	ALPHA-CL PAIRS FOR MACH NUM.= 0.900					
ALPHA	0.000	20.000	340.000	341.000	353.000	360.000
CL	0.800000	0.800000	-0.800000	-0.800000	0.800000	0.800000

5	ALPHA-CL PAIRS FOR MACH NUM.= 1.000					
ALPHA	0.000	20.000	340.000	354.300	360.000	
CL	0.800000	0.800000	-0.626000	0.800000	0.800000	

014 A-1 AIRFOIL WITH 0.35C FLAP (15 DEG. FLAP ANGLE) 10/27/81

\*\*\*\*\* DRAG TABLE \*\*\*\*\*

MAXIMUM POS-NEG ANGLES IN CD-M TABLES

16.000 344.000

17 ALPHA VALUES FOR CD VS M

ALPHA		0.000	1.000	4.000	8.000	16.000	344.000	345.000
		348.000	350.000	352.000	354.000	355.000	356.000	357.000
		358.000	359.000	360.000				
M-CD PAIRS FOR ALPHA = 0.000								
MACH		0.000	0.300	1.000				
CD		0.019100	0.019100	0.376100				
M-CD PAIRS FOR ALPHA = 1.000								
MACH		0.000	0.285	0.300	1.000			
CD		0.025000	0.025000	0.031000	0.388000			
M-CD PAIRS FOR ALPHA = 4.000								
MACH		0.000	0.250	1.000				
CD		0.042500	0.042500	0.425000				
M-CD PAIRS FOR ALPHA = 8.000								
MACH		0.000	0.200	1.000				
CD		0.120000	0.120000	0.528000				
M-CD PAIRS FOR ALPHA = 16.000								
MACH		0.000	1.000					
CD		0.370000	0.370000					
M-CD PAIRS FOR ALPHA = 344.000								
MACH		0.000	1.000					
CD		0.050000	0.050000					
M-CD PAIRS FOR ALPHA = 345.000								
MACH		0.000	0.300					
CD		0.028000	0.028000					
M-CD PAIRS FOR ALPHA = 348.000								
MACH		0.000	0.300	0.400	0.440	0.500	1.000	
CD		0.012500	0.012500	0.013000	0.016400	0.047000	0.302000	

5	M-CD PAIRS FOR ALPHA = 350.000						
MACH	0.000	0.300	0.400	0.500	1.000		
CD	0.011600	0.011600	0.012400	0.016000	0.271000		
7	M-CD PAIRS FOR ALPHA = 352.000						
MACH	0.000	0.300	0.400	0.525	0.590	0.615	1.000
CD	0.011200	0.011200	0.012500	0.014000	0.020500	0.033250	0.229600
6	M-CD PAIRS FOR ALPHA = 354.000						
MACH	0.000	0.300	0.400	0.550	0.600	1.000	
CD	0.011500	0.011500	0.012600	0.014300	0.039800	0.243800	
6	M-CD PAIRS FOR ALPHA = 355.000						
MACH	0.000	0.300	0.400	0.535	0.600	1.000	
CD	0.011700	0.011700	0.013000	0.014600	0.045200	0.249200	
4	M-CD PAIRS FOR ALPHA = 356.000						
MACH	0.000	0.300	0.510	1.000			
CD	0.012200	0.012200	0.017000	0.266300			
5	M-CD PAIRS FOR ALPHA = 357.000						
MACH	0.000	0.380	0.400	0.450	1.000		
CD	0.013000	0.013000	0.019000	0.022000	0.302500		
3	M-CD PAIRS FOR ALPHA = 358.000						
MACH	0.000	0.360	1.000				
CD	0.014000	0.014000	0.340400				
3	M-CD PAIRS FOR ALPHA = 359.000						
MACH	0.000	0.530	1.000				
CD	0.016000	0.016000	0.357700				
3	M-CD PAIRS FOR ALPHA = 360.000						
MACH	0.000	0.580	1.000				
CD	0.019100	0.019100	0.376100				

014 A-1 AIRFOIL WITH 0.35C FLAP (15 DEG. FLAP ANGLE) 10/27/81

\*\*\*\*\* PITCHING MOMENT TABLE \*\*\*\*\*

VALUES OF CM FOR MAXIMUM POS-NEG ANGLES

-0.3852 -0.1560

19 ALPHA VALUES FOR CM VS M							
ALPHA							
0.000	1.340	1.910	16.000	344.000	344.600	344.800	
347.000	348.000	349.000	349.700	350.800	353.100	354.000	
355.000	355.700	356.800	357.600	360.000			
4 M-CM PAIRS FOR ALPHA = 0.000							
MACH	0.000	0.300	0.550	1.000			
CM	-0.180000	-0.180000	-0.290200	-0.290200			
4 M-CM PAIRS FOR ALPHA = 1.340							
MACH	0.000	0.300	0.550	1.000			
CM	-0.180000	-0.180000	-0.308960	-0.308960			
4 M-CM PAIRS FOR ALPHA = 1.910							
MACH	0.000	0.300	0.550	1.000			
CM	-0.180000	-0.188000	-0.316940	-0.316940			
2 M-CM PAIRS FOR ALPHA = 16.000							
MACH	0.000	1.000					
CM	-0.385200	-0.385200					
2 M-CM PAIRS FOR ALPHA = 344.000							
MACH	0.000	1.000					
CM	-0.156000	-0.156000					
7 M-CM PAIRS FOR ALPHA = 344.600							
MACH	0.000	0.300	0.400	0.500	0.550	0.600	1.000
CM	-0.180000	-0.174000	-0.120000	-0.060000	-0.044000	-0.044000	-0.044000
7 M-CM PAIRS FOR ALPHA = 344.800							
MACH	0.000	0.300	0.400	0.500	0.550	0.600	1.000
CM	-0.180000	-0.180000	-0.126000	-0.066000	-0.050000	-0.050000	-0.050000
7 M-CM PAIRS FOR ALPHA = 347.000							
MACH	0.000	0.300	0.400	0.500	0.550	0.600	1.000
CM	-0.180000	-0.180000	-0.192000	-0.144000	-0.116000	0.116000	-0.116000

7	M-CM PAIRS FOR ALPHA = 348.000					
MACH	0.000	0.300	0.400	0.500	0.550	0.600 1.000
CM	-0.180000	-0.180000	-0.192000	-0.162000	-0.146000	-0.146000 -0.146000
4	M-CM PAIRS FOR ALPHA = 349.000					
MACH	0.000	0.300	0.400	1.000		
CM	-0.180000	-0.180000	-0.192000	-0.192000		
6	M-CM PAIRS FOR ALPHA = 349.700					
MACH	0.000	0.300	0.400	0.500	0.550	1.000
CM	-0.180000	-0.180000	-0.192000	-0.213000	-0.197000	-0.210000
6	M-CM PAIRS FOR ALPHA = 350.800					
MACH	0.000	0.300	0.400	0.500	0.550	1.000
CM	-0.180000	-0.180000	-0.192000	-0.213000	-0.230000	-0.243000
6	M-CM PAIRS FOR ALPHA = 353.100					
MACH	0.000	0.300	0.400	0.500	0.550	1.000
CM	-0.180000	-0.180000	-0.192000	-0.213000	-0.230000	-0.270000
6	M-CM PAIRS FOR ALPHA = 354.000					
MACH	0.000	0.300	0.400	0.500	0.550	1.000
CM	-0.180000	-0.180000	-0.192000	-0.213000	-0.230000	-0.297000
6	M-CM PAIRS FOR ALPHA = 355.000					
MACH	0.000	0.300	0.400	0.500	0.550	1.000
CM	-0.180000	-0.180000	-0.192000	-0.213000	-0.230000	-0.327000
6	M-CM PAIRS FOR ALPHA = 355.700					
MACH	0.000	0.300	0.400	0.500	0.550	1.000
CM	-0.180000	-0.180000	-0.192000	-0.213000	-0.230000	-0.348000
6	M-CM PAIRS FOR ALPHA = 356.800					
MACH	0.000	0.300	0.400	0.500	0.550	1.000
CM	-0.180000	-0.180000	-0.192000	-0.213000	-0.245400	-0.381000

6 M-CM PAIRS FOR ALPHA = 357.600  
MACH 0.000 0.300 0.400 0.500 0.550 1.000  
CM -0.180000 -0.180000 -0.192000 -0.224200 -0.256600 -0.405000

4 M-CM PAIRS FOR ALPHA = 360.000  
MACH 0.000 0.300 0.550 1.000  
CM -0.180000 -0.180000 -0.290200 -0.290200

ORIGINAL PAGE IS  
OF POOR QUALITY

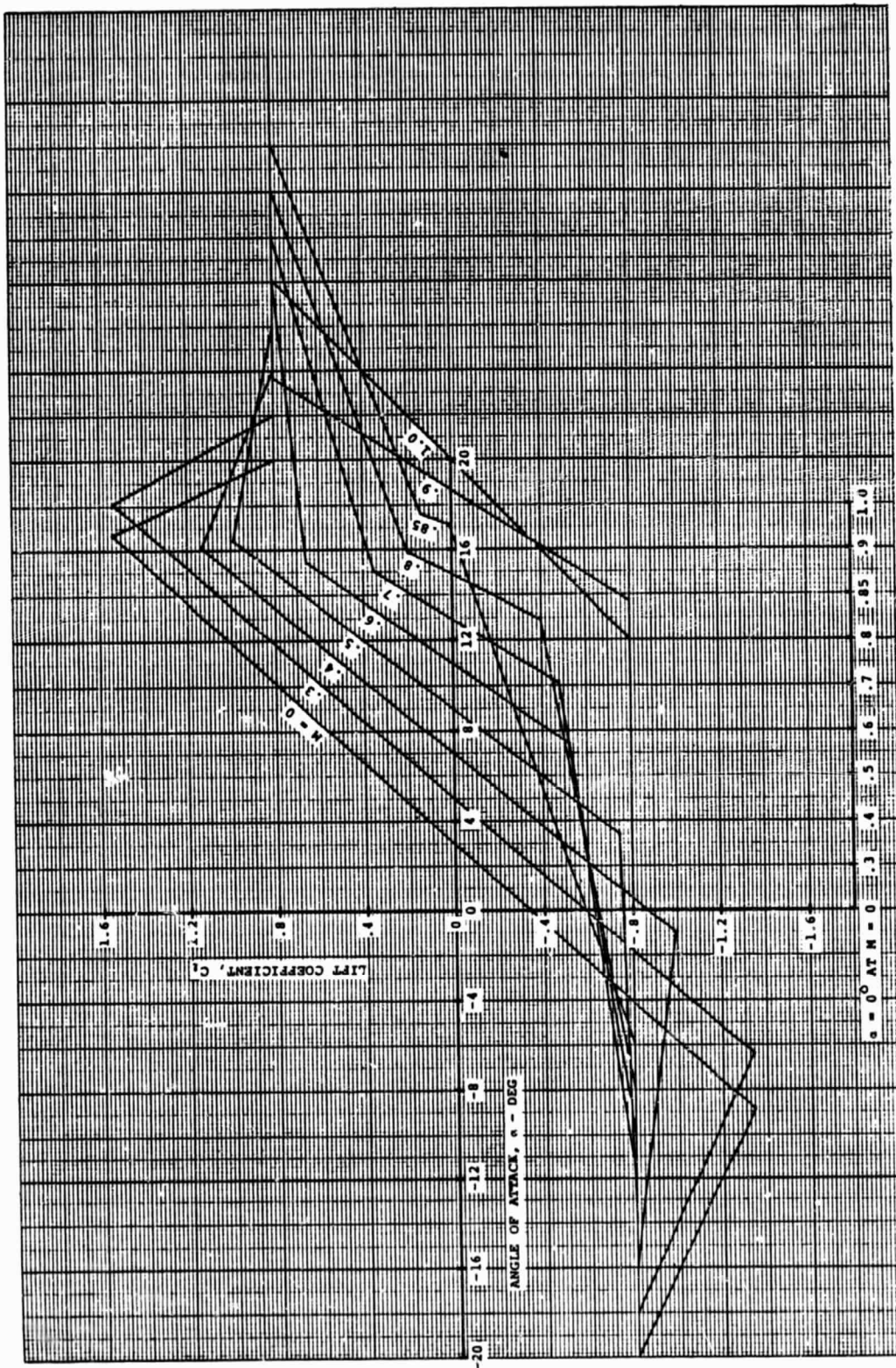


Figure B.1 Lift Coefficient for  $\delta_F = -5^\circ$

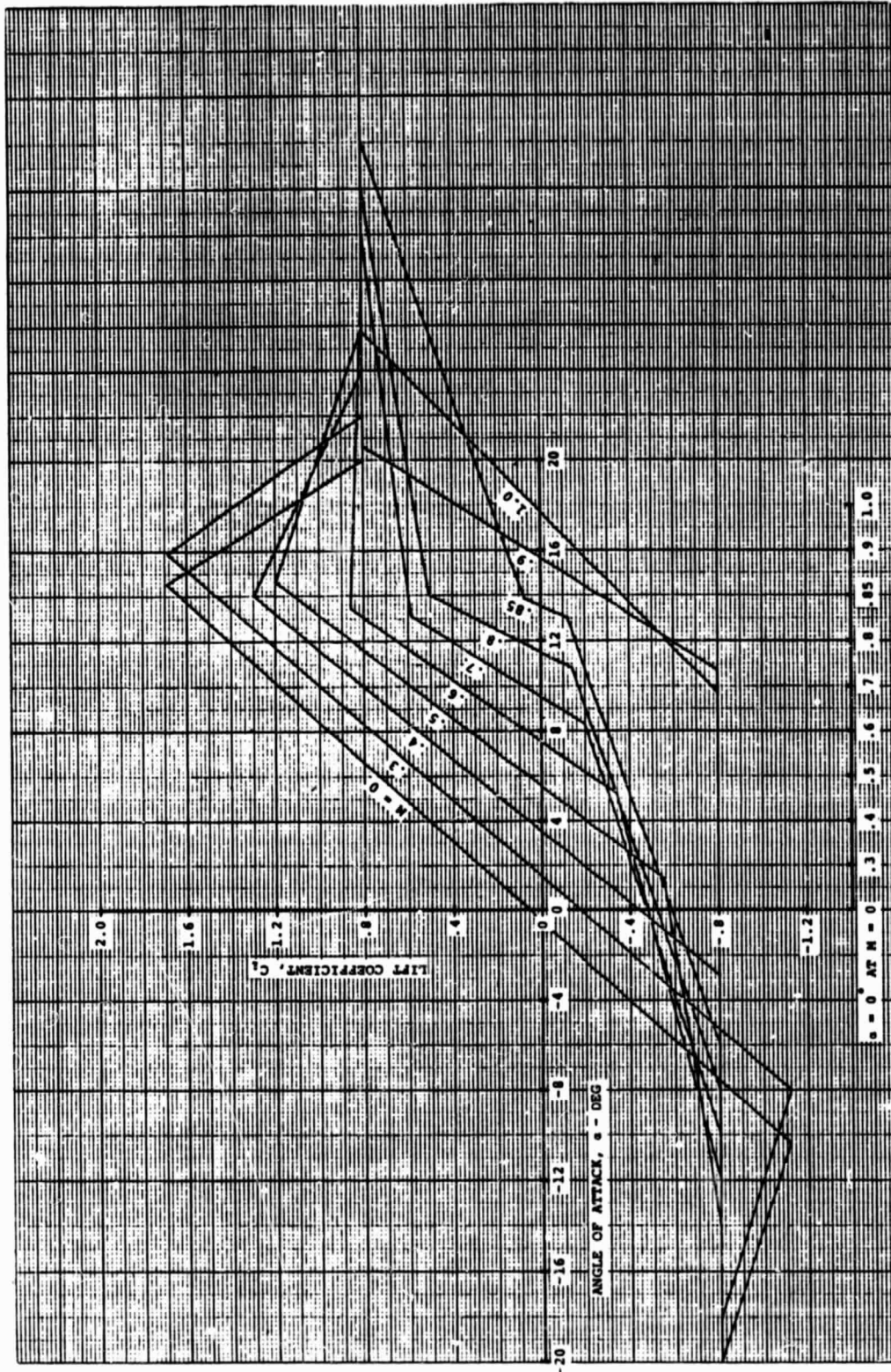


Figure B.2 Lift Coefficient for  $\delta_F = 0^\circ$

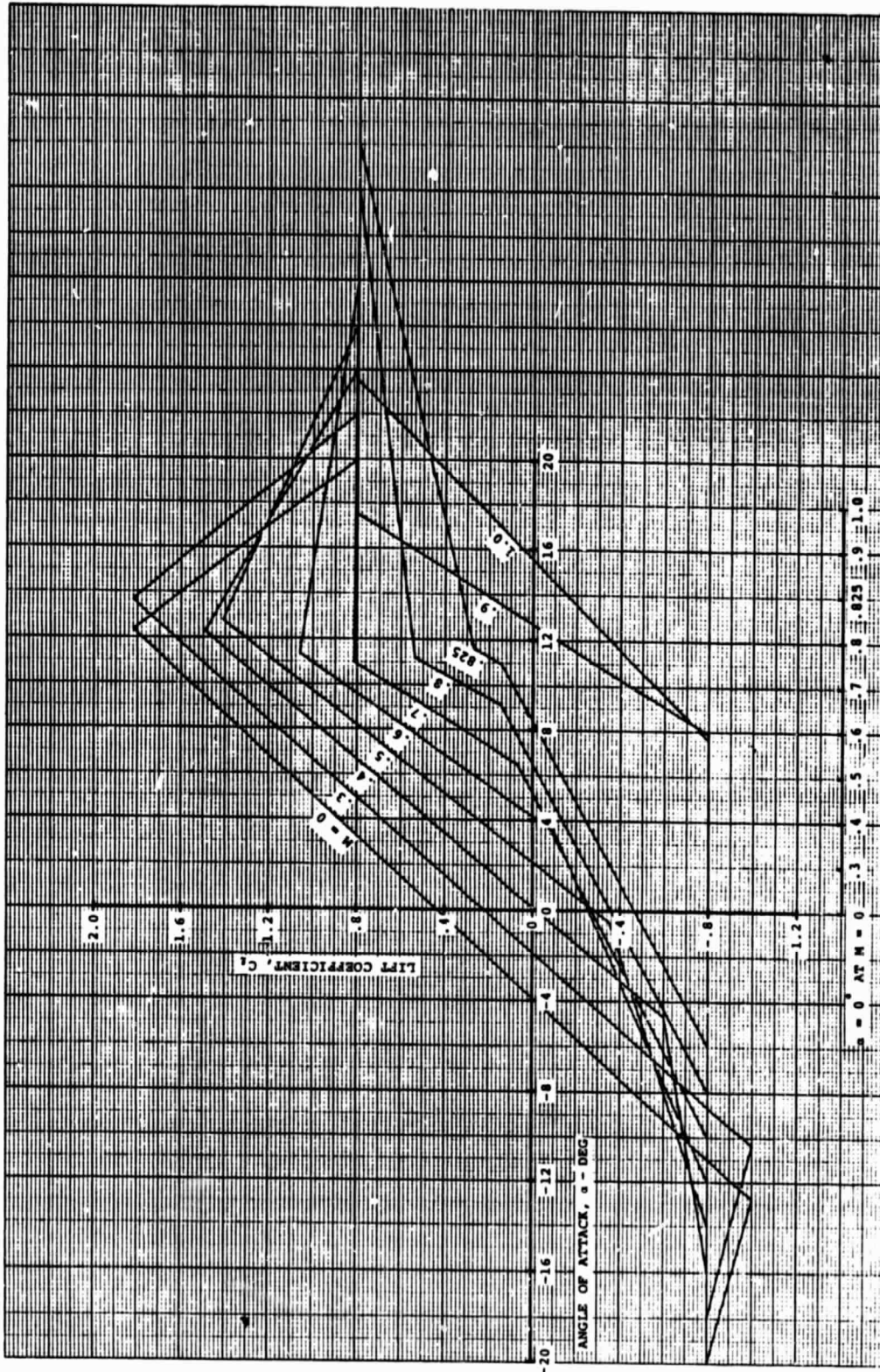


Figure B.3 Lift Coefficient for  $\delta_F = 5^\circ$

ORIGINAL PAGE IS  
OF POOR QUALITY

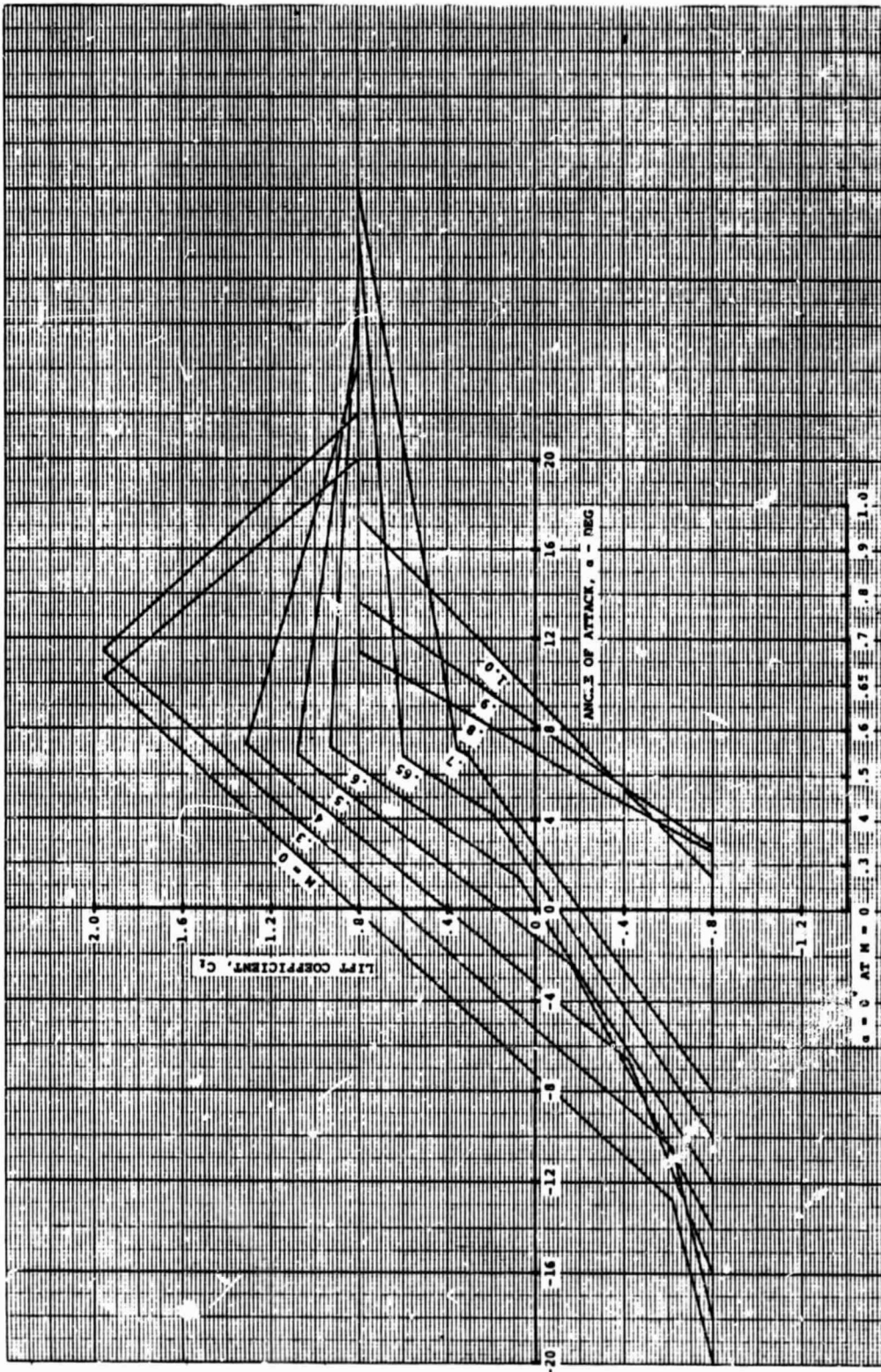


Figure B.4 Lift Coefficient for  $\delta_F = 10^\circ$

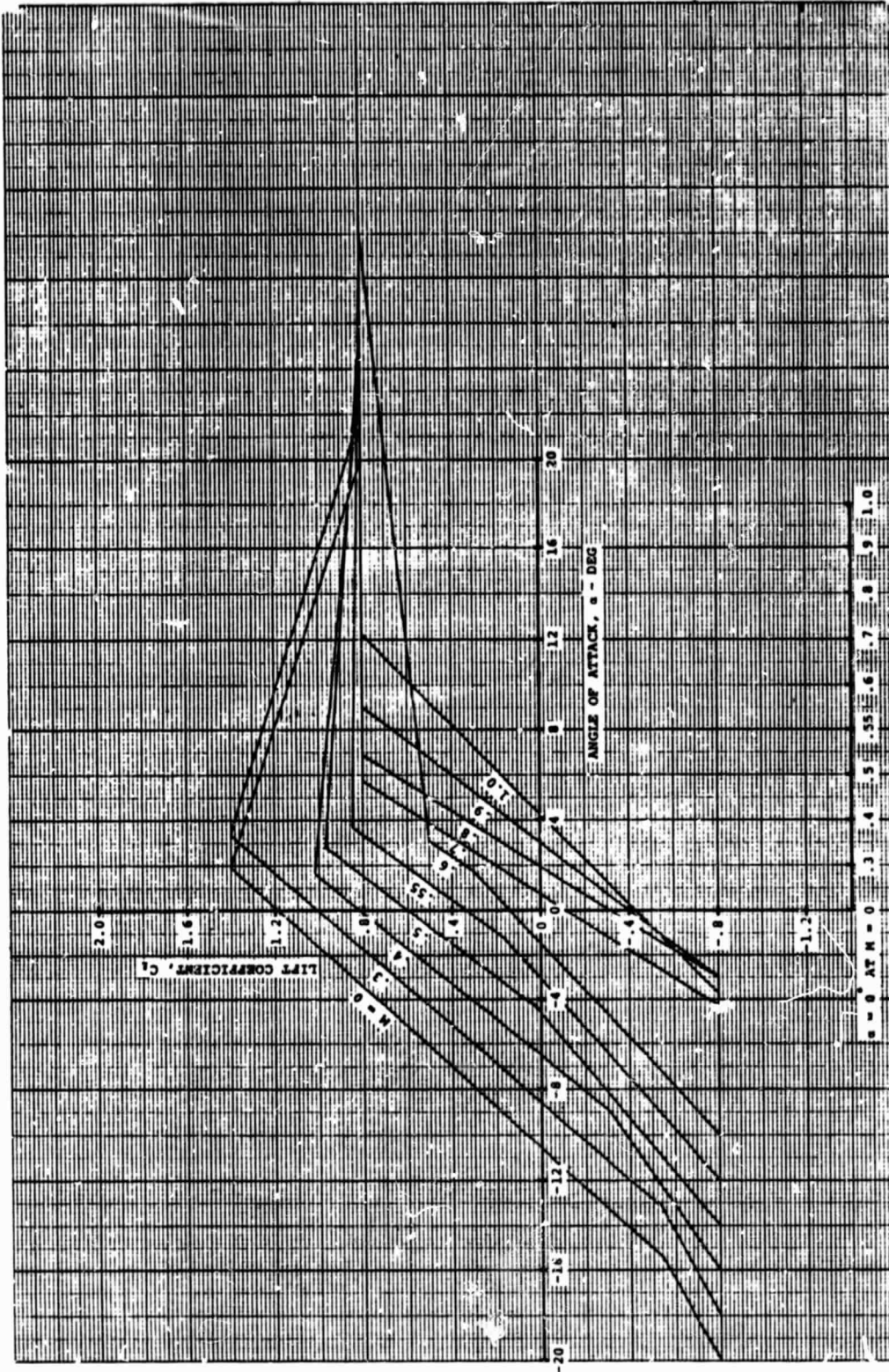


Figure B.5 Lift Coefficient for  $\delta_F = 15^\circ$

ORIGINAL PAGE IS  
OF POOR QUALITY

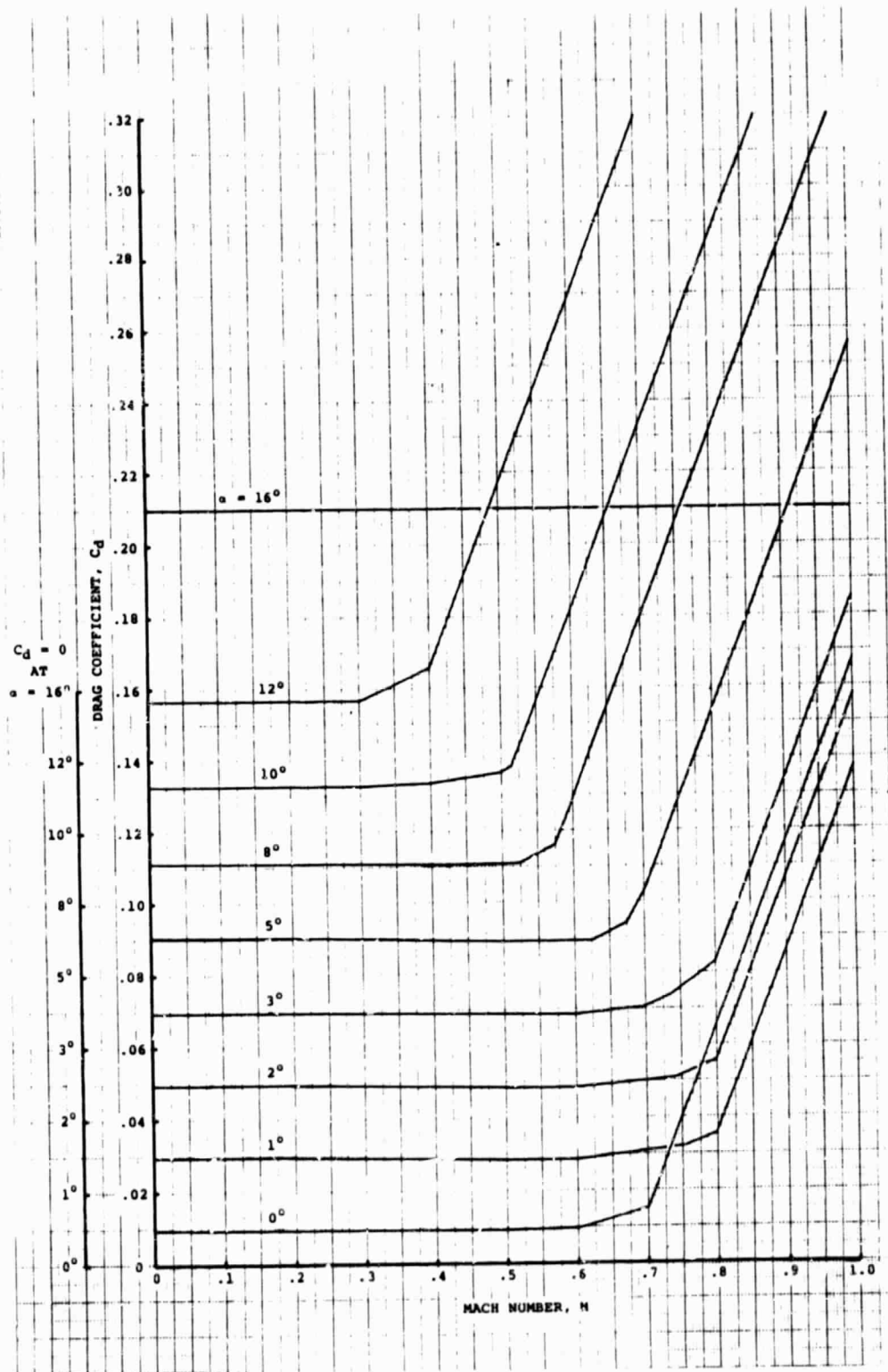


Figure B.6 Drag Coefficient for  $\delta_F = -5^\circ$  and  $\alpha \geq 0^\circ$

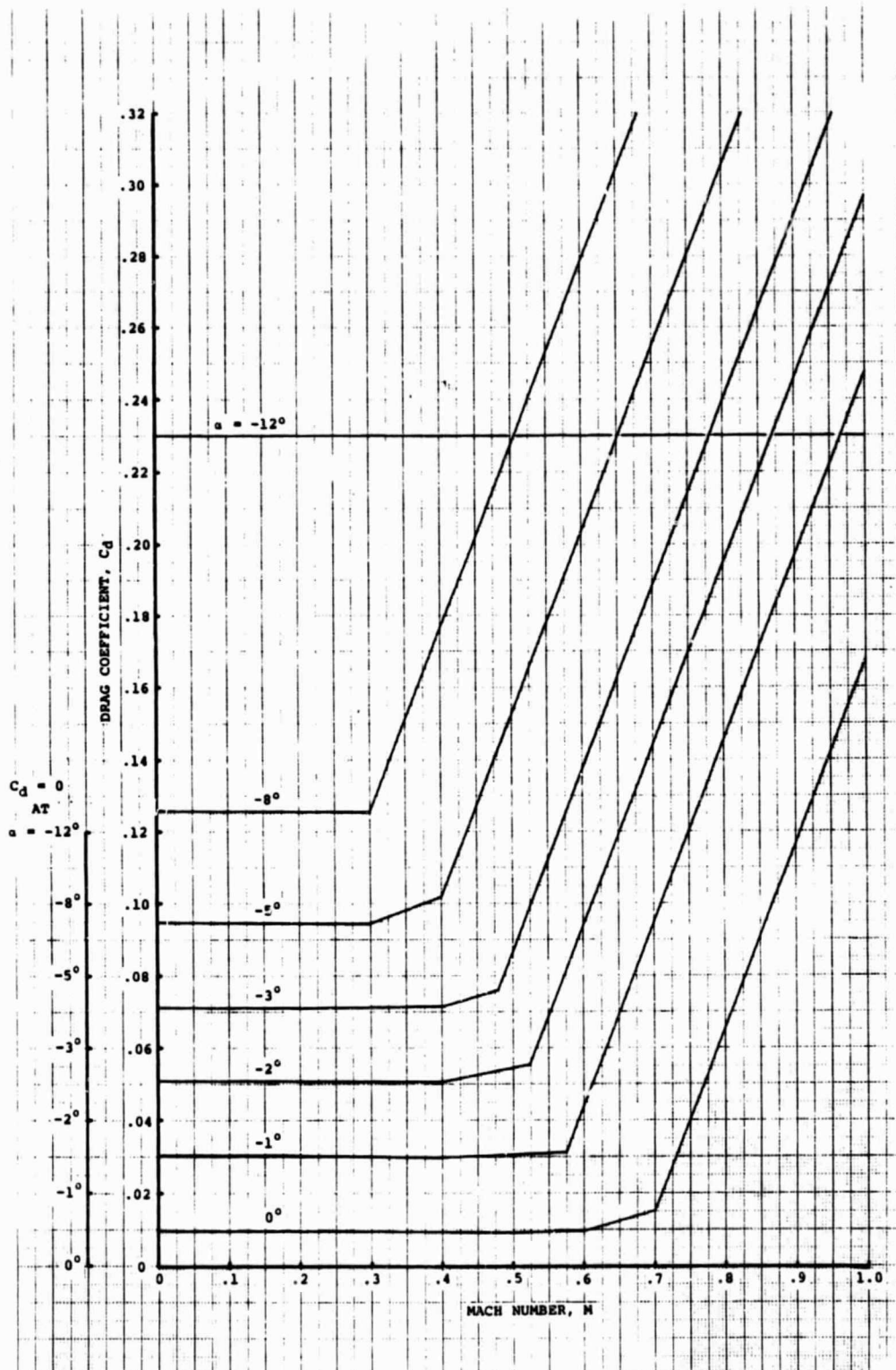


Figure B.7 Drag Coefficient for  $\delta_F = -5^\circ$  and  $\alpha \leq 0^\circ$

ORIGINAL PAGE IS  
OF POOR QUALITY

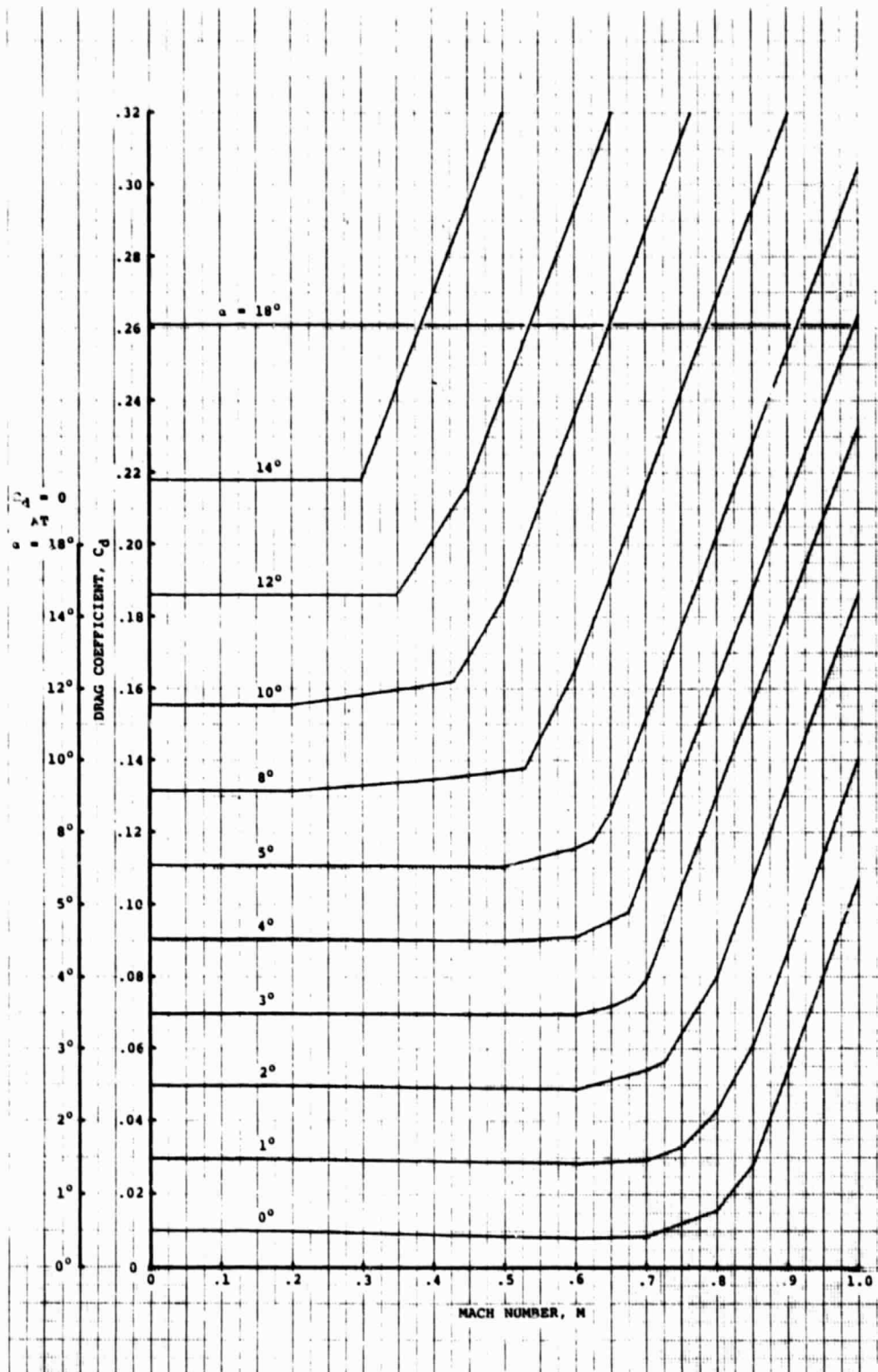


Figure B.8 Drag Coefficient for  $\delta_F = 0^\circ$  and  $\alpha \geq 0^\circ$

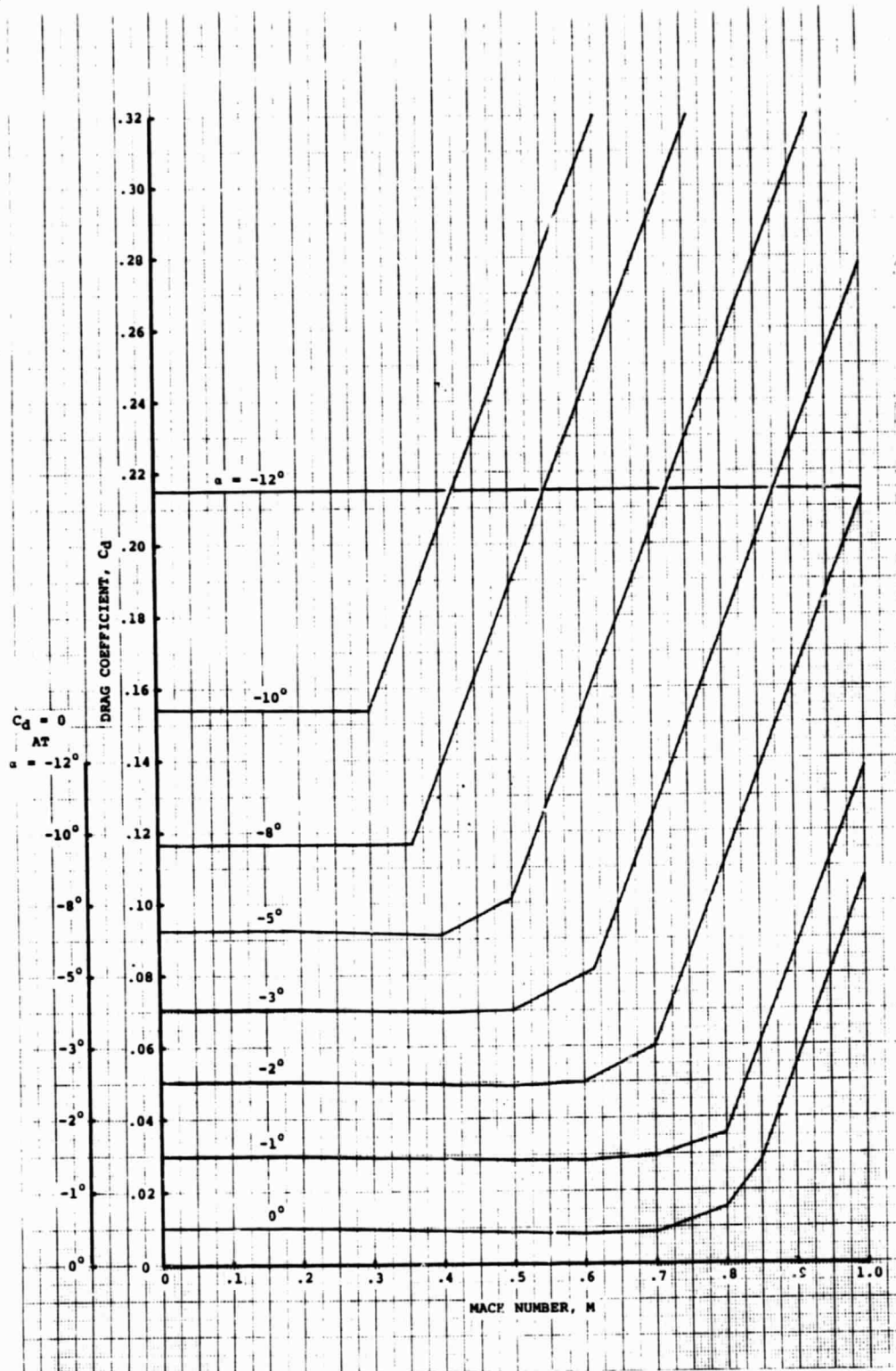


Figure B.9 Drag Coefficient for  $\delta_F = 0^\circ$  and  $\alpha \leq 0^\circ$

ORIGINAL PAGE IS  
OF POOR QUALITY

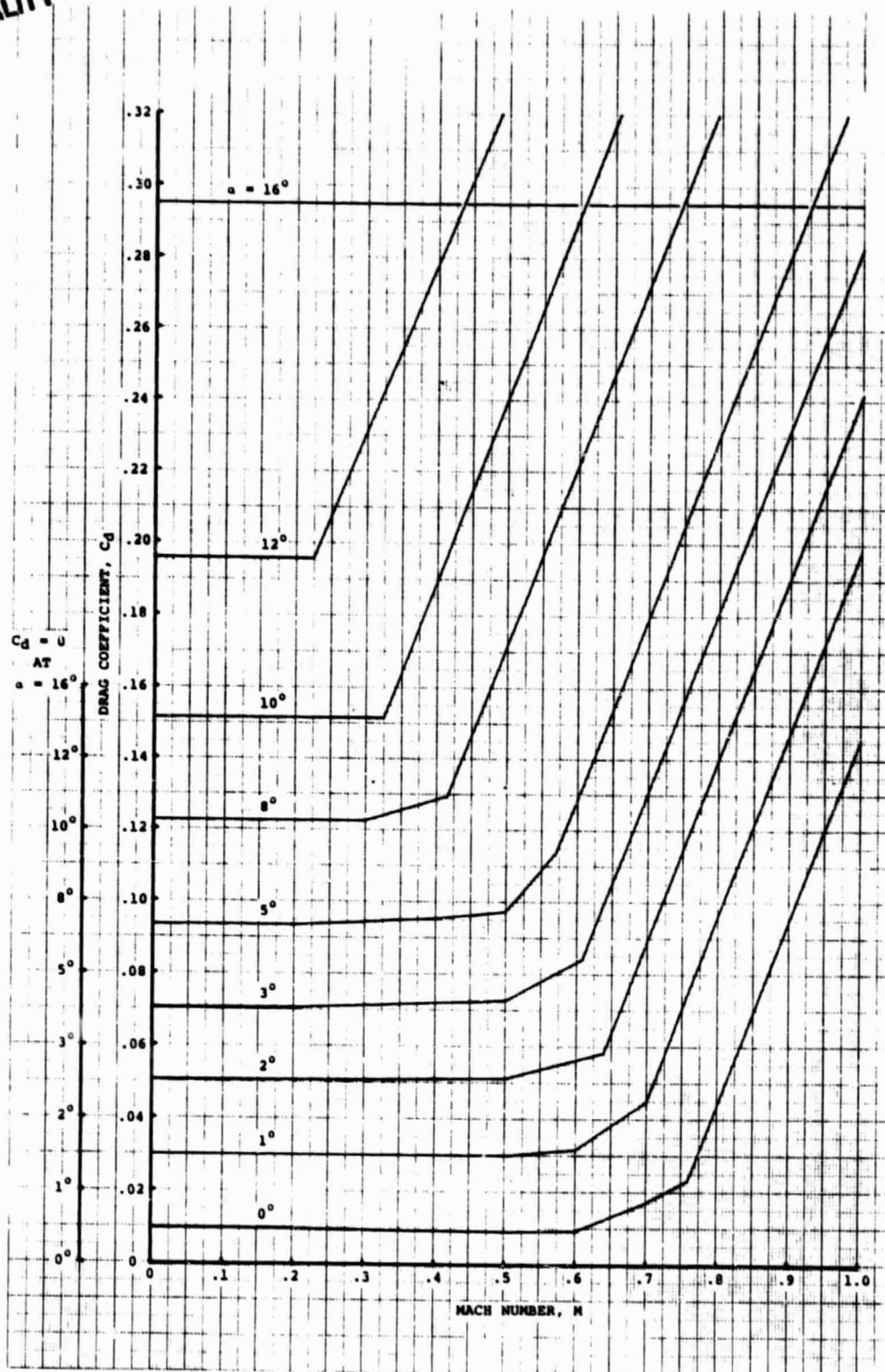


Figure B.10 Drag Coefficient for  $\delta_F = 5^\circ$  and  $\alpha \geq 0^\circ$

ORIGINAL PAGE IS  
OF POOR QUALITY

ORIGINAL PAGE IS  
OF POOR QUALITY

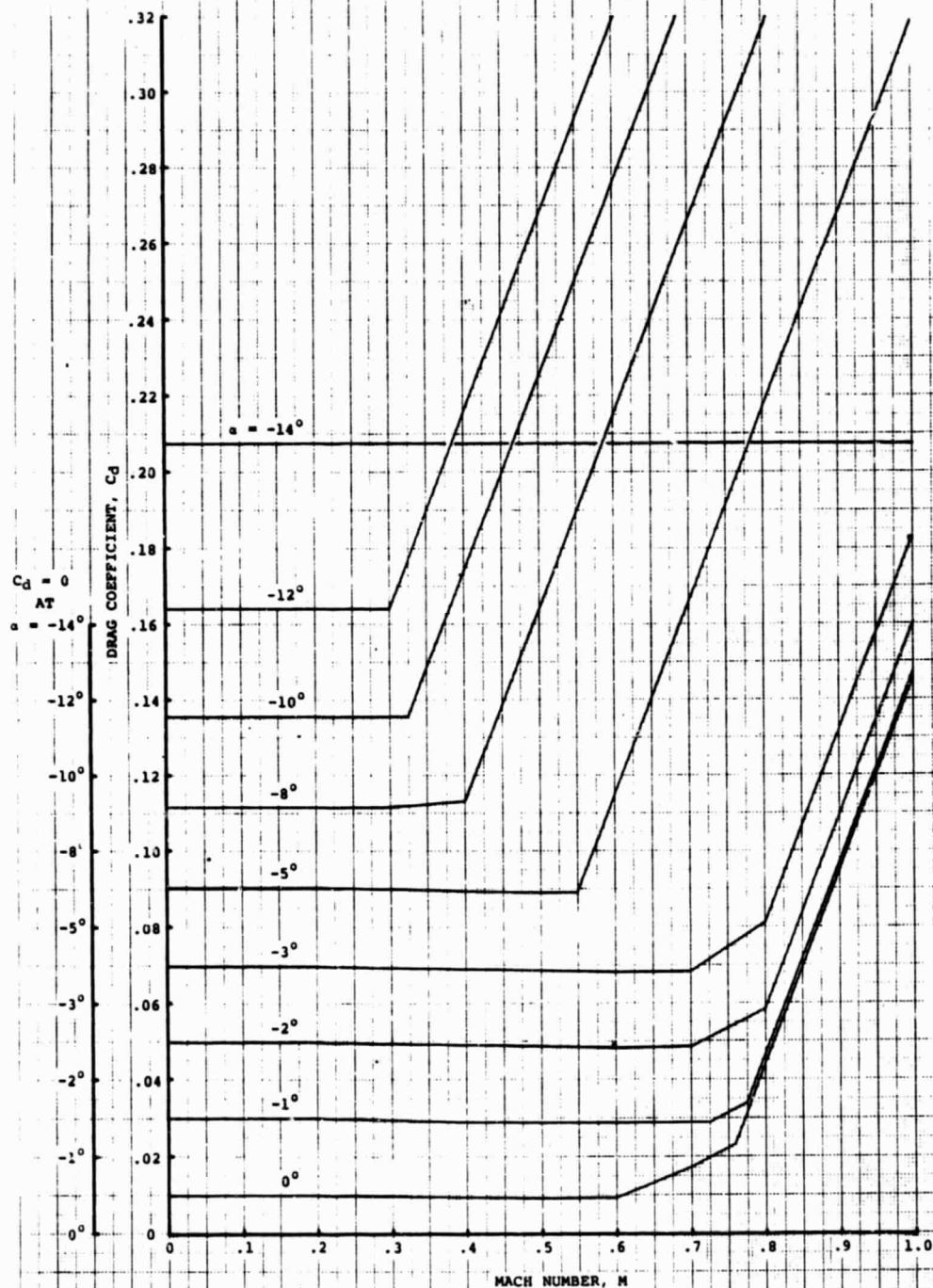


Figure B.11 Drag Coefficient for  $\delta_F = 5^\circ$  and  $\alpha \leq 0^\circ$

ORIGINAL PAGE IS  
OF POOR QUALITY

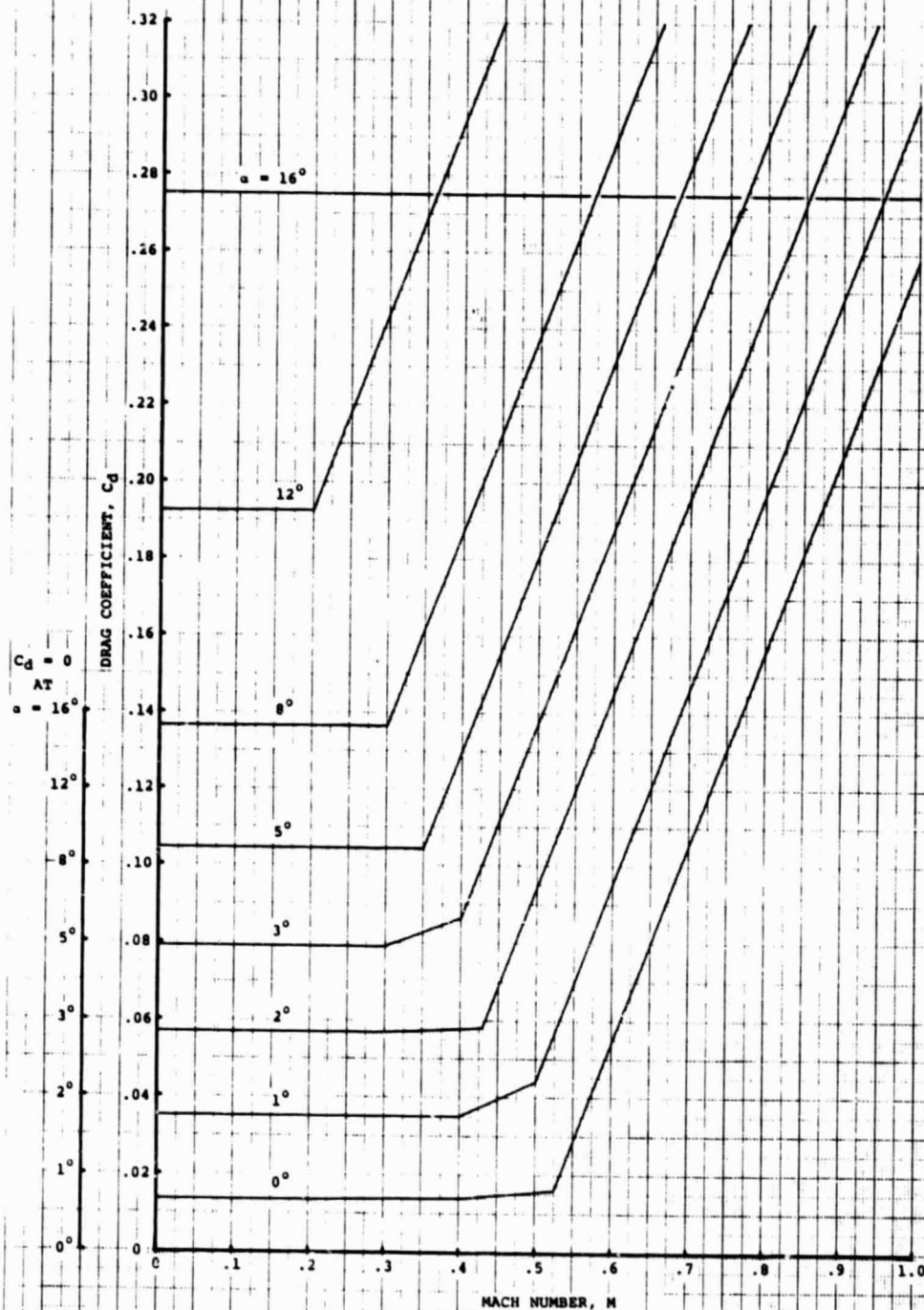


Figure B.12 Drag Coefficient for  $\delta_F = 10^\circ$  and  $\alpha \geq 0^\circ$

ORIGINAL PAGE IS  
OF POOR QUALITY

ORIGINAL PAGE IS  
OF POOR QUALITY

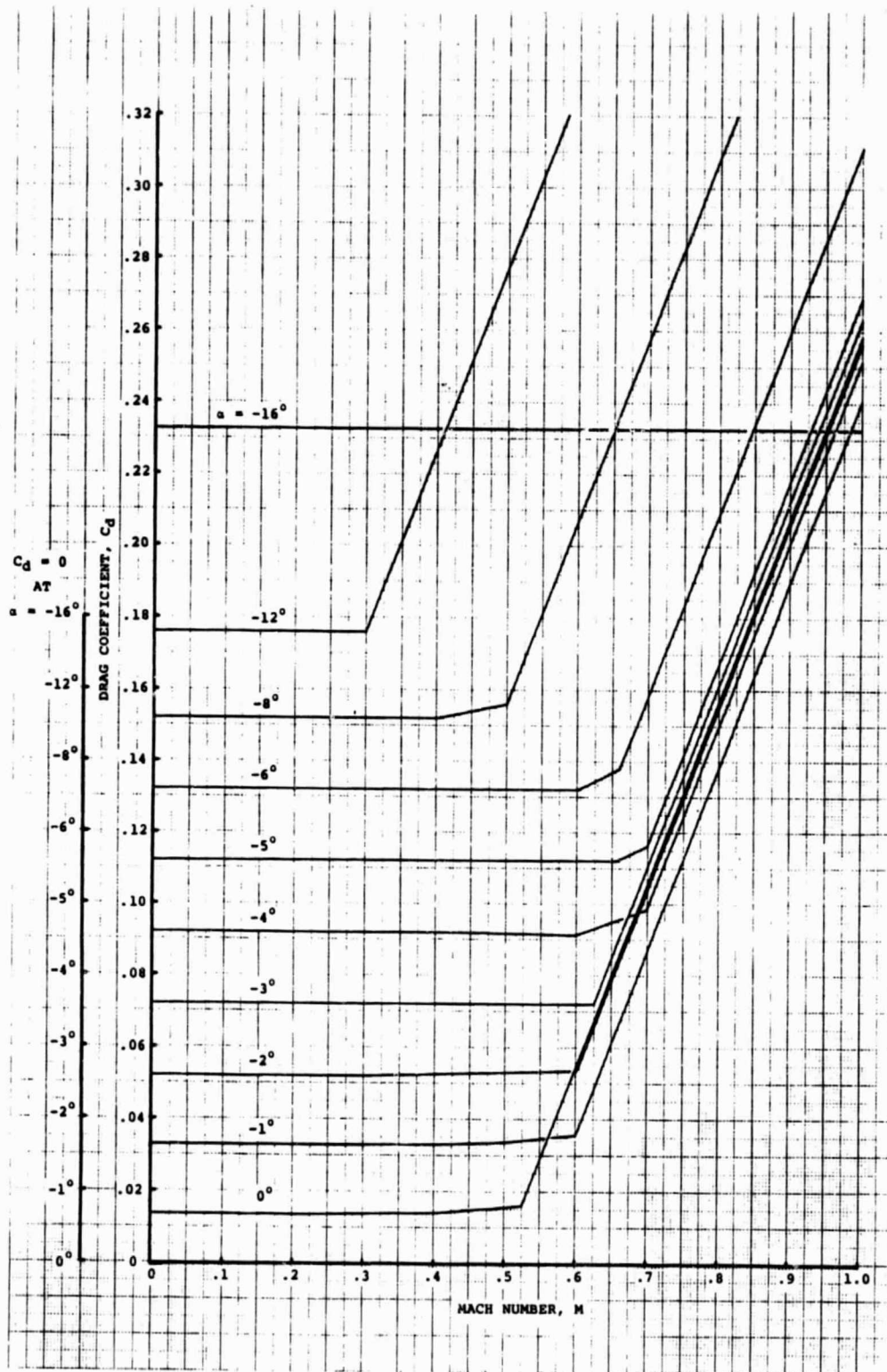


Figure B.13 Drag Coefficient for  $\delta_F = 10^\circ$  and  $\alpha \leq 0^\circ$

ORIGINAL PAGE IS  
OF POOR QUALITY

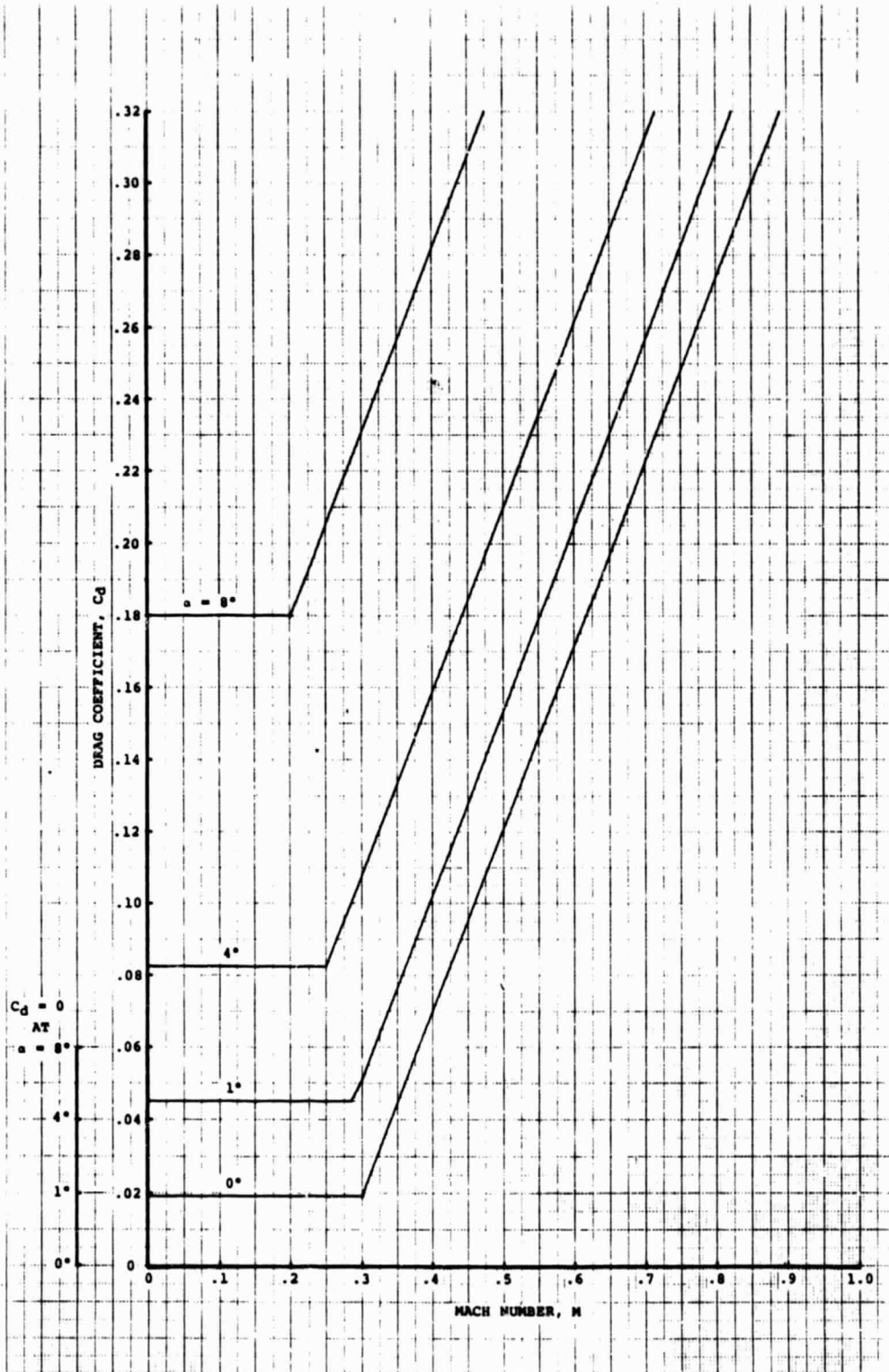


Figure B.14 Drag Coefficient for  $\delta_F \approx 15^\circ$  and  $\alpha \geq 0^\circ$

ORIGINAL PAGE IS  
OF POOR QUALITY

ORIGINAL PAGE IS  
OF POOR QUALITY

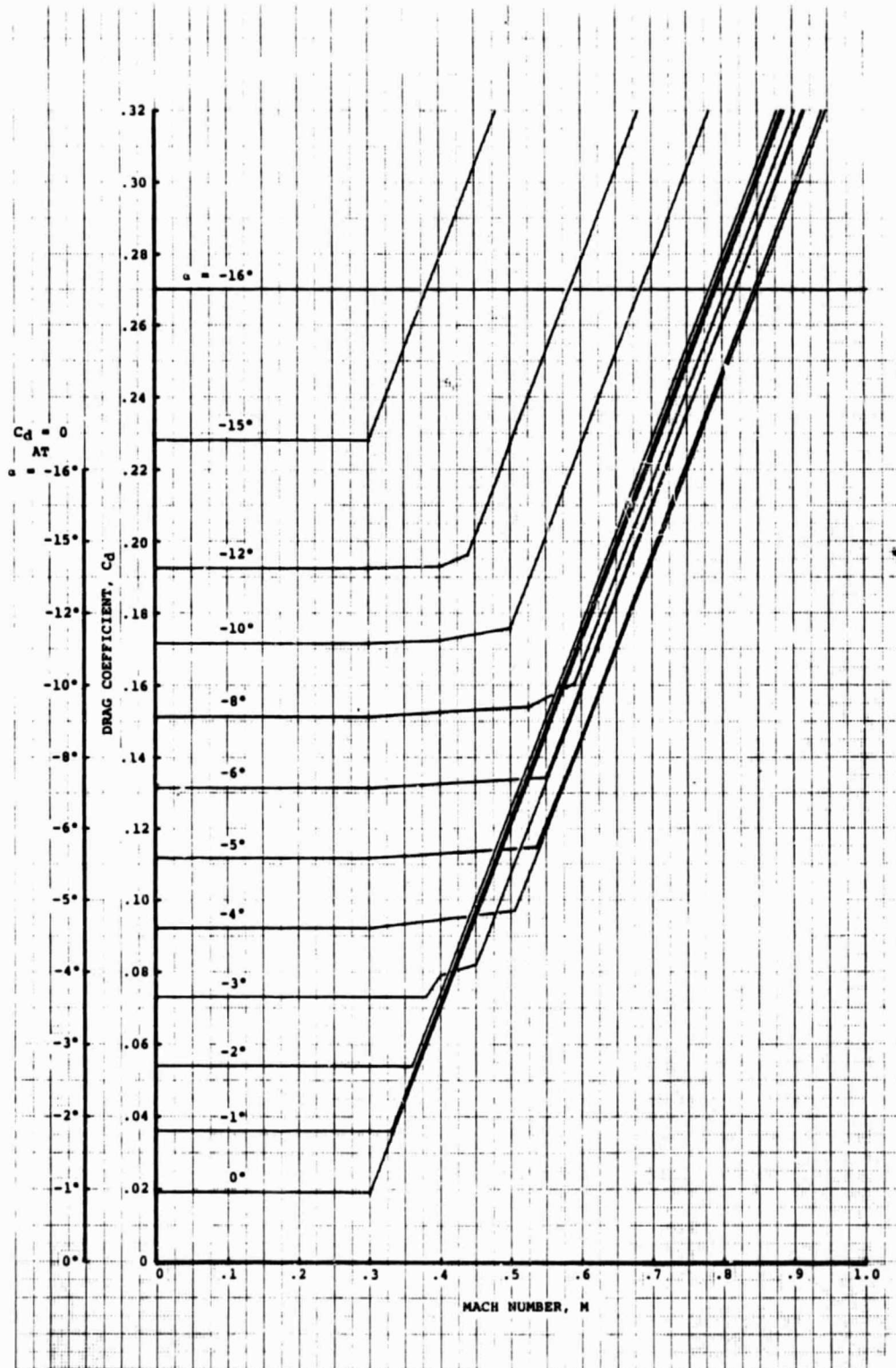


Figure B.15 Drag Coefficient for  $\delta_F = 15^\circ$  and  $\alpha \leq 0^\circ$

ORIGINAL PAGE IS  
OF POOR QUALITY

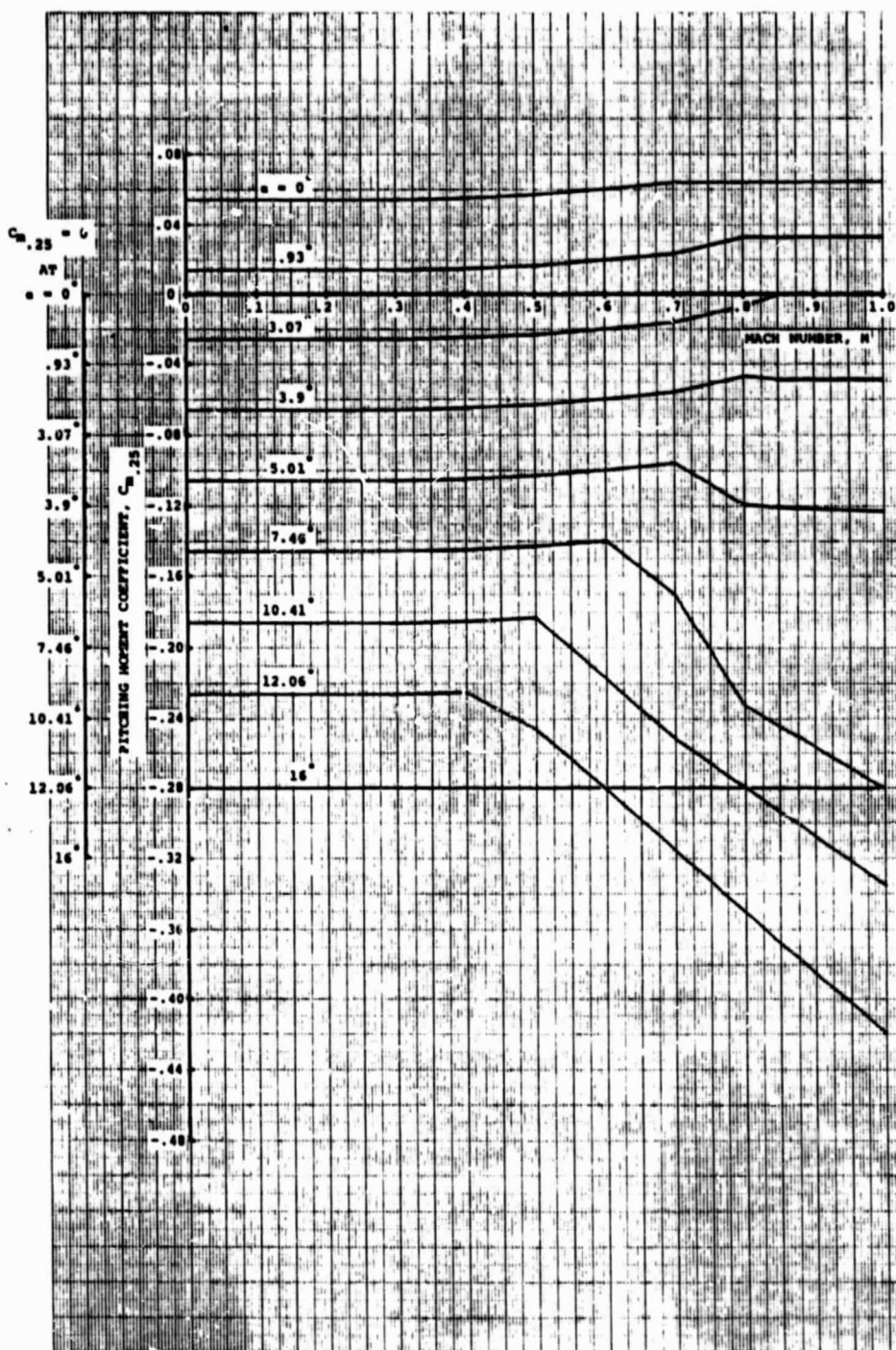


Figure B.16 Pitching Moment Coefficient for  $\delta_F = -5^\circ$  and  $\alpha \geq 0^\circ$

ORIGINAL PAGE IS  
OF POOR QUALITY

ORIGINAL PAGE IS  
OF POOR QUALITY

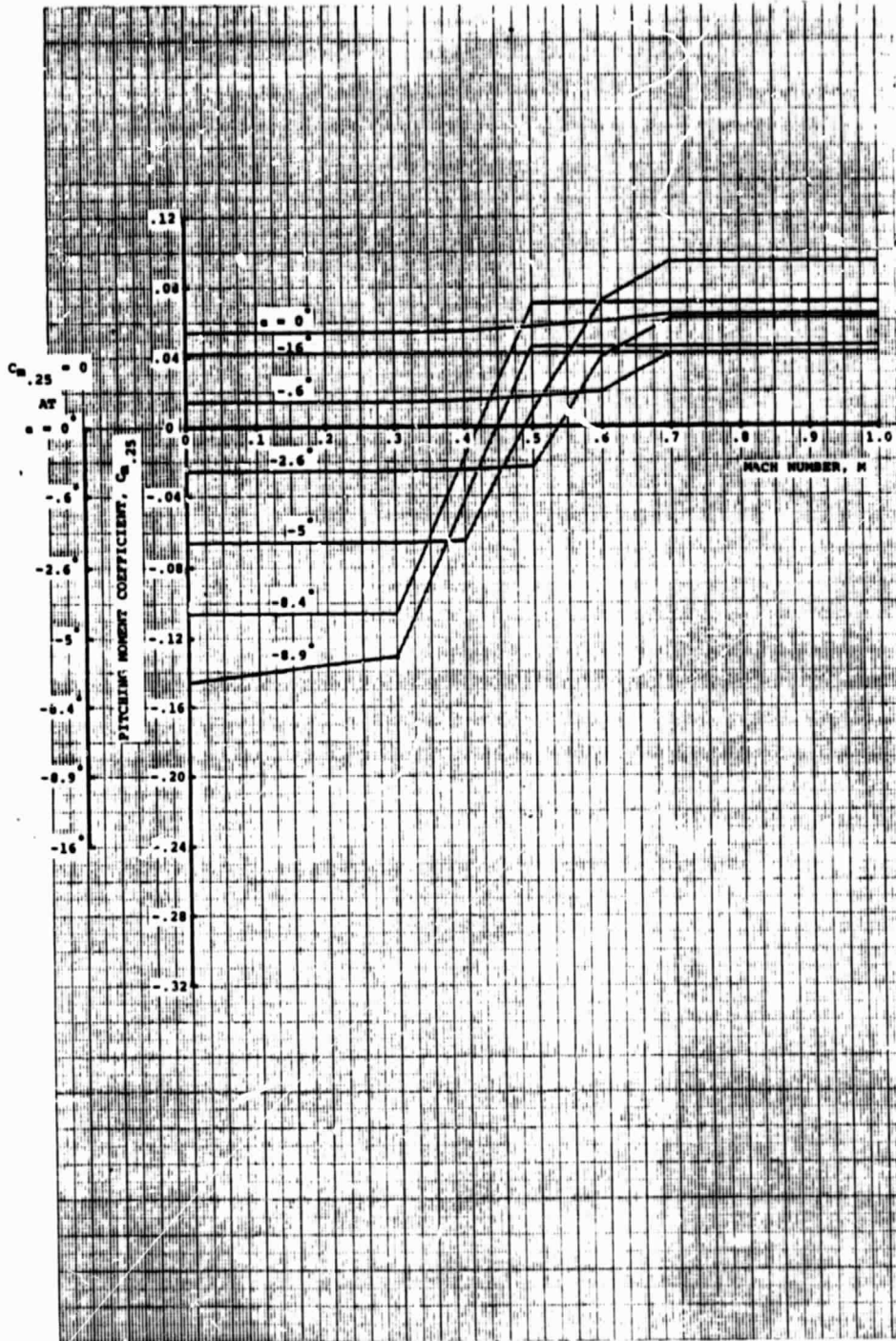


Figure B.17 Pitching Moment Coefficient for  $\delta_F = -5^\circ$  and  $\alpha \leq 0^\circ$

ORIGINAL PAGE IS  
OF POOR QUALITY

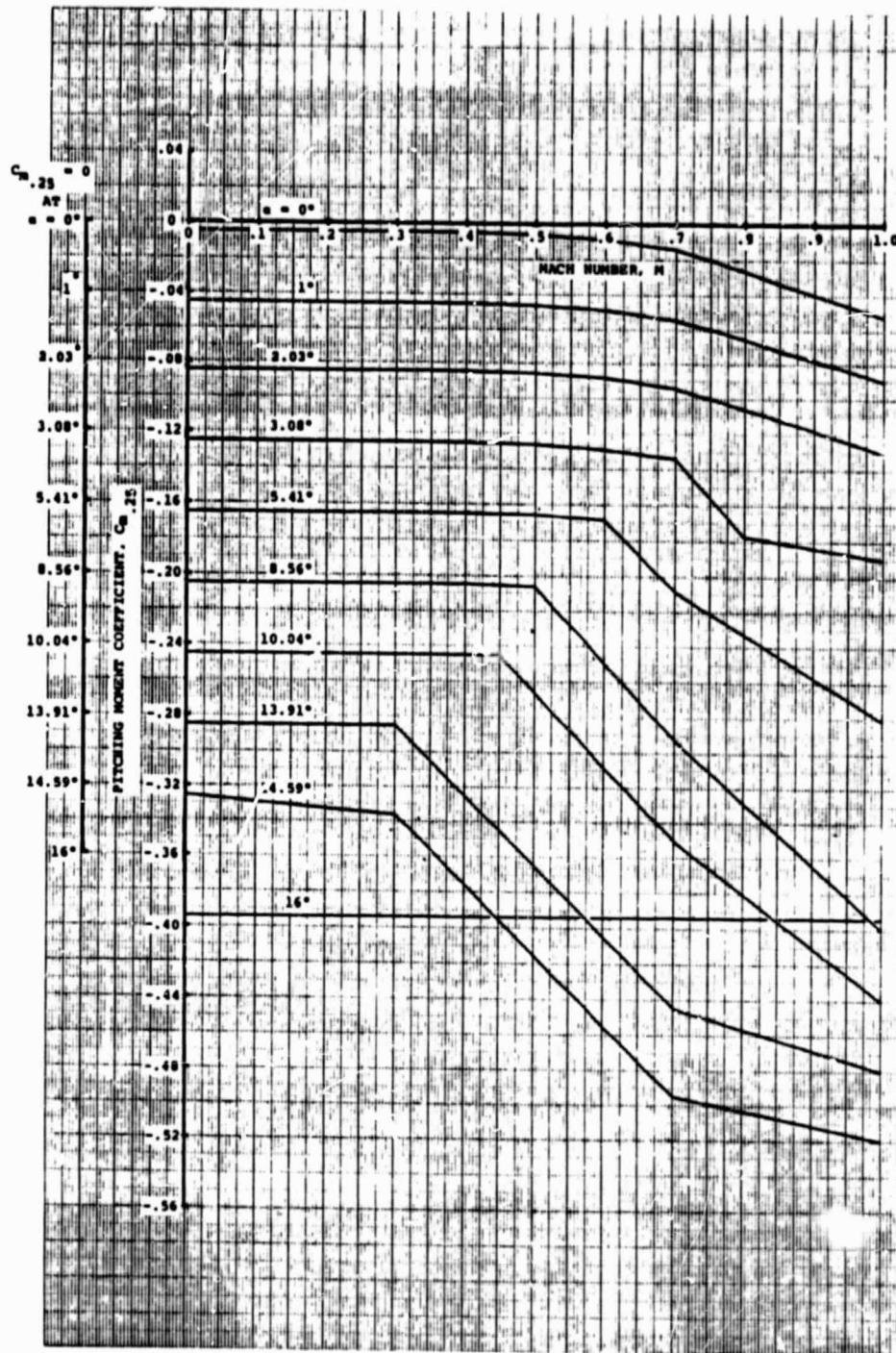


Figure B.18 Pitching Moment Coefficient for  $\delta_F = 0^\circ$  and  $\alpha \geq 0^\circ$

ORIGINAL PAGE IS  
OF POOR QUALITY

ORIGINAL PAGE IS  
OF POOR QUALITY

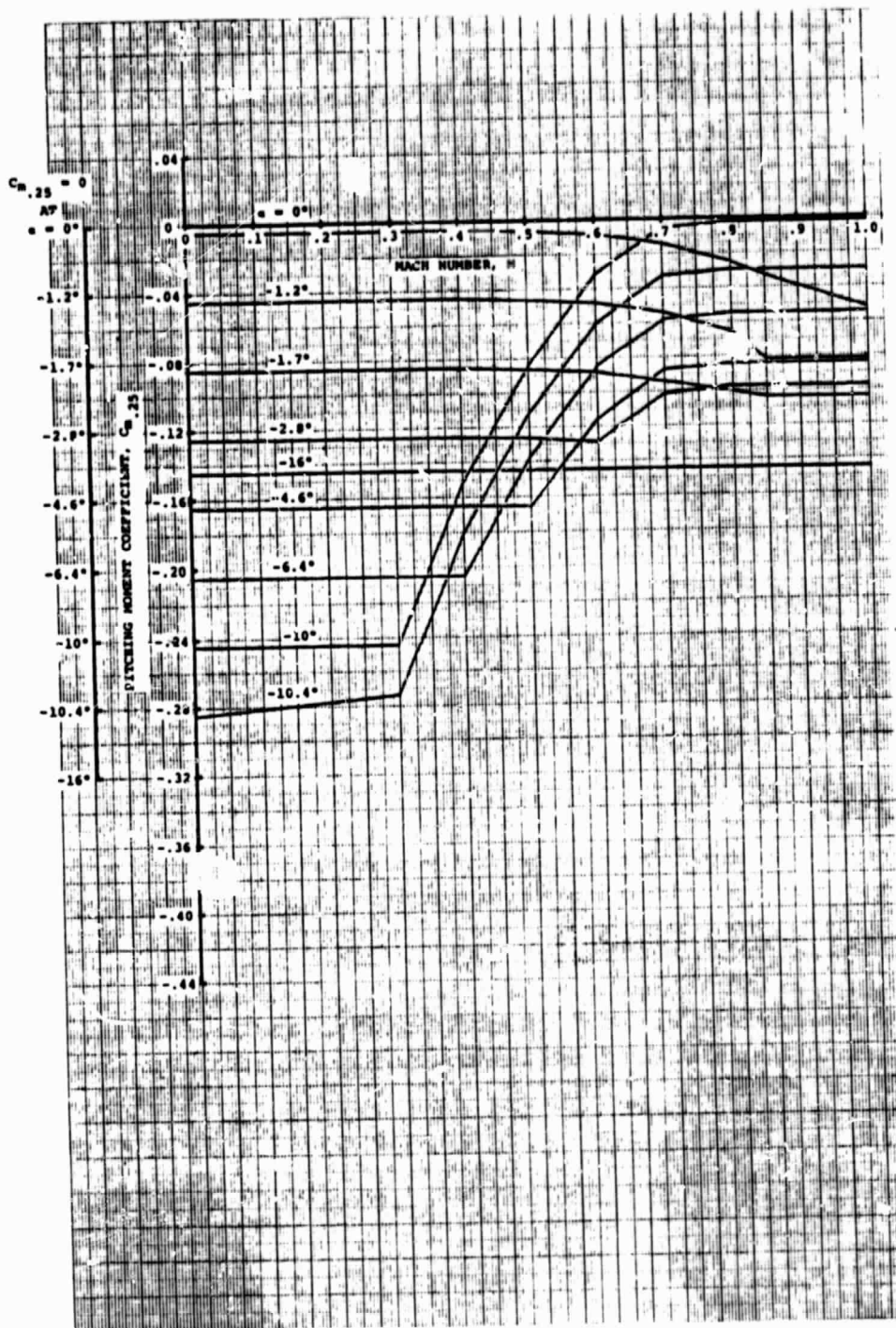


Figure B.19 Pitching Moment Coefficient for  $\delta_F = 0^\circ$  and  $\alpha \leq 0^\circ$

ORIGINAL PAGE IS  
OF POOR QUALITY

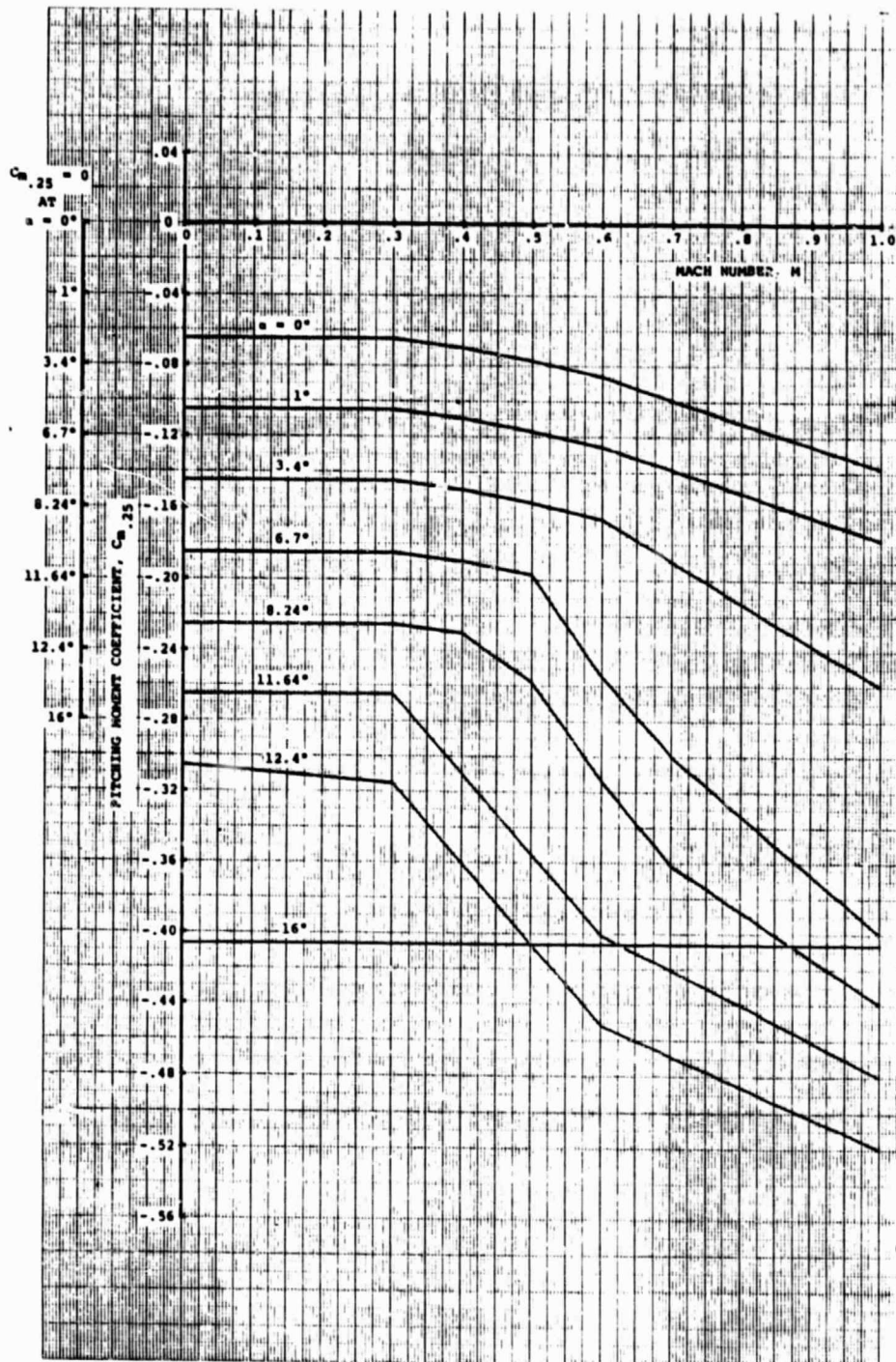


Figure L.20 Pitching Moment Coefficient for  $\delta_F = 5^\circ$  and  $\alpha \geq 0^\circ$

ORIGINAL PAGE IS  
OF POOR QUALITY

ORIGINAL PAGE IS  
OF POOR QUALITY

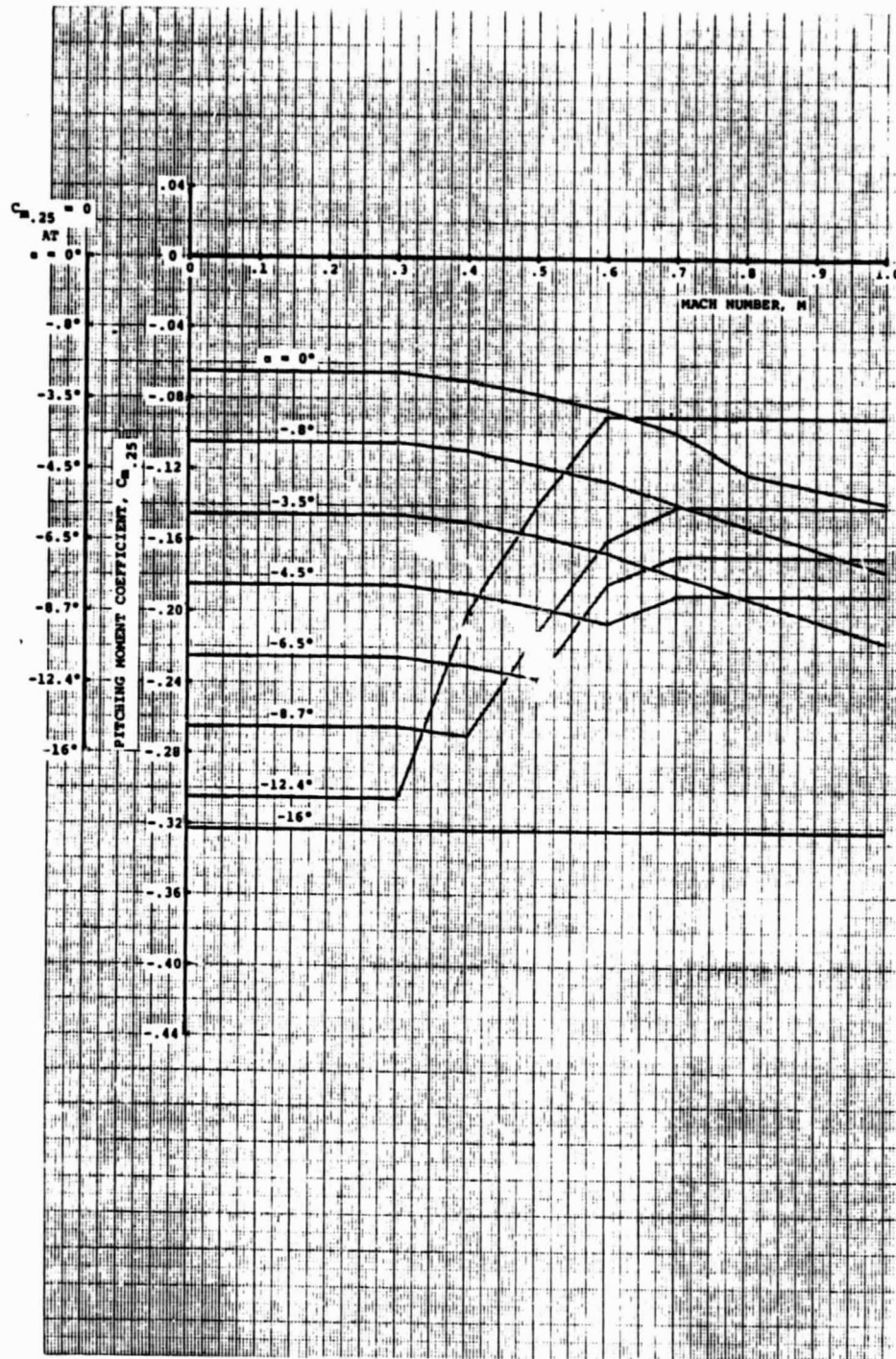


Figure B.21 Pitching Moment Coefficient for  $\delta_F = 5^\circ$  and  $\alpha \leq 0^\circ$

ORIGINAL PAGE 13  
OF POOR QUALITY

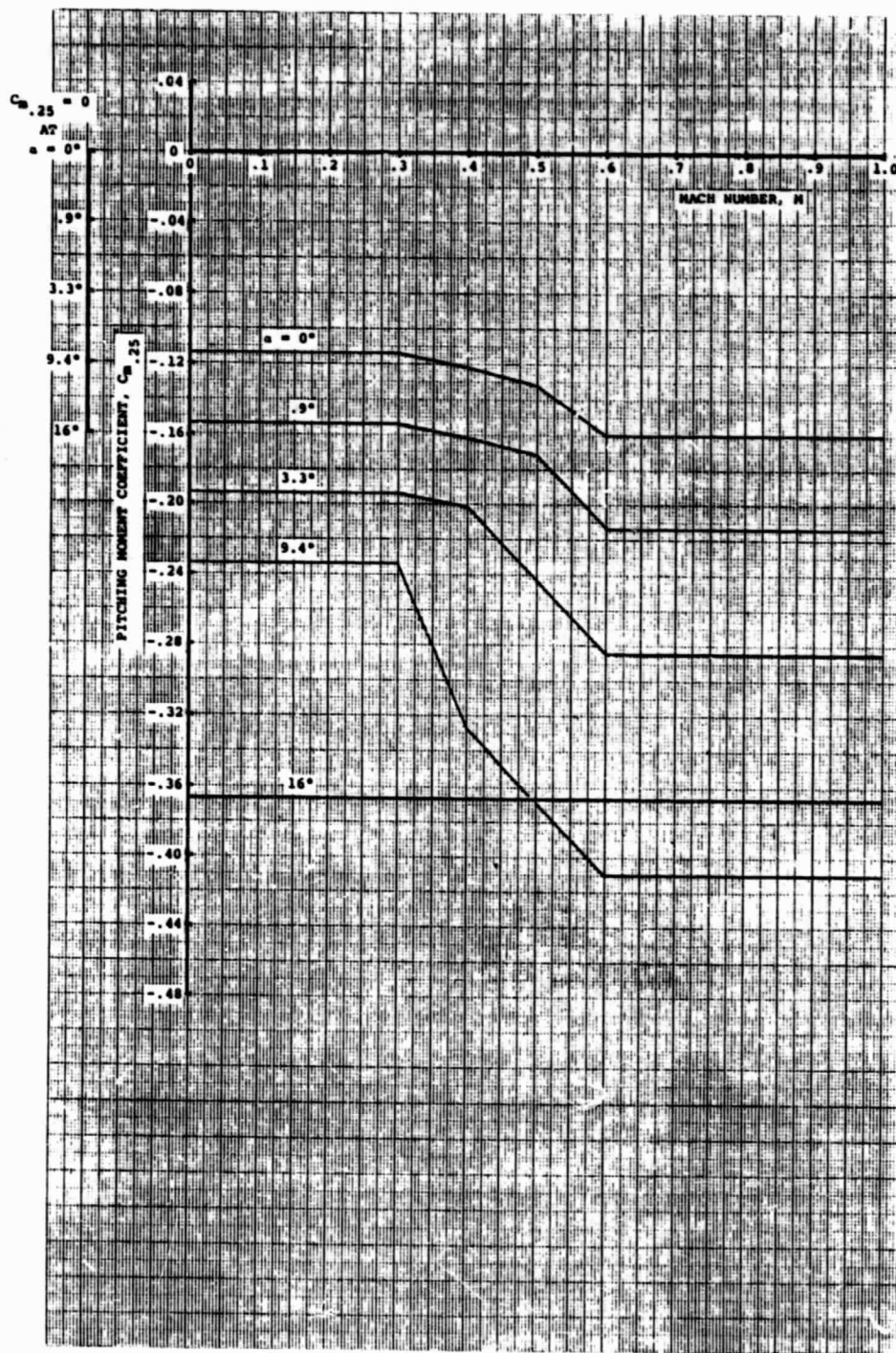


Figure B.22 Pitching Moment Coefficient for  $\delta_F = 10^\circ$  and  $\alpha \geq 0^\circ$

ORIGINAL PAGE IS  
OF POOR QUALITY

ORIGINAL PAGE IS  
OF POOR QUALITY

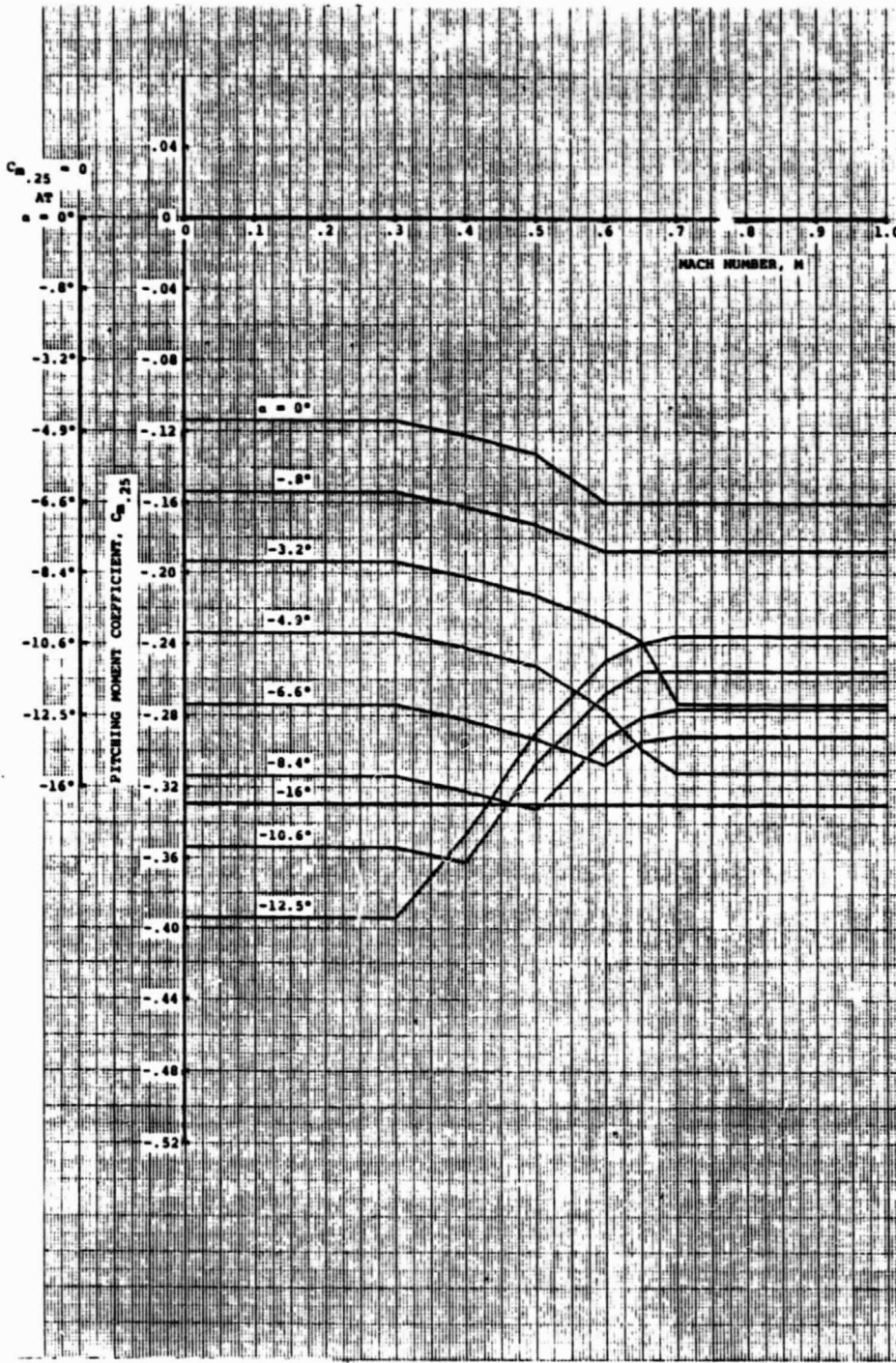


Figure B.23 Pitching Moment Coefficient for  $\delta_F = 10^\circ$  and  $\alpha \leq 0^\circ$

ORIGINAL PAGE IS  
OF POOR QUALITY

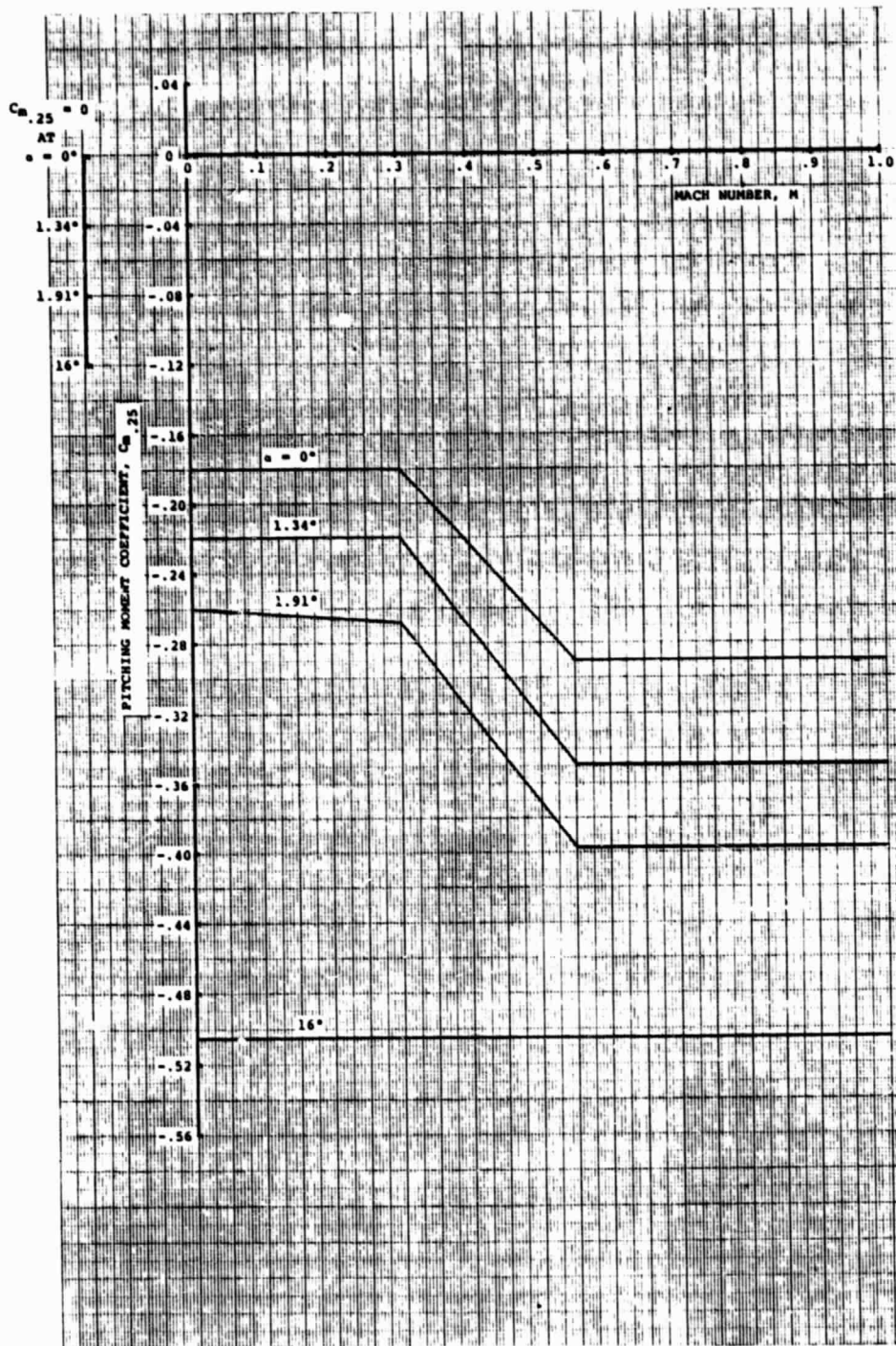


Figure B.24 Pitching Moment Coefficient for  $\delta_F = 15^\circ$  and  $\alpha \geq 0^\circ$

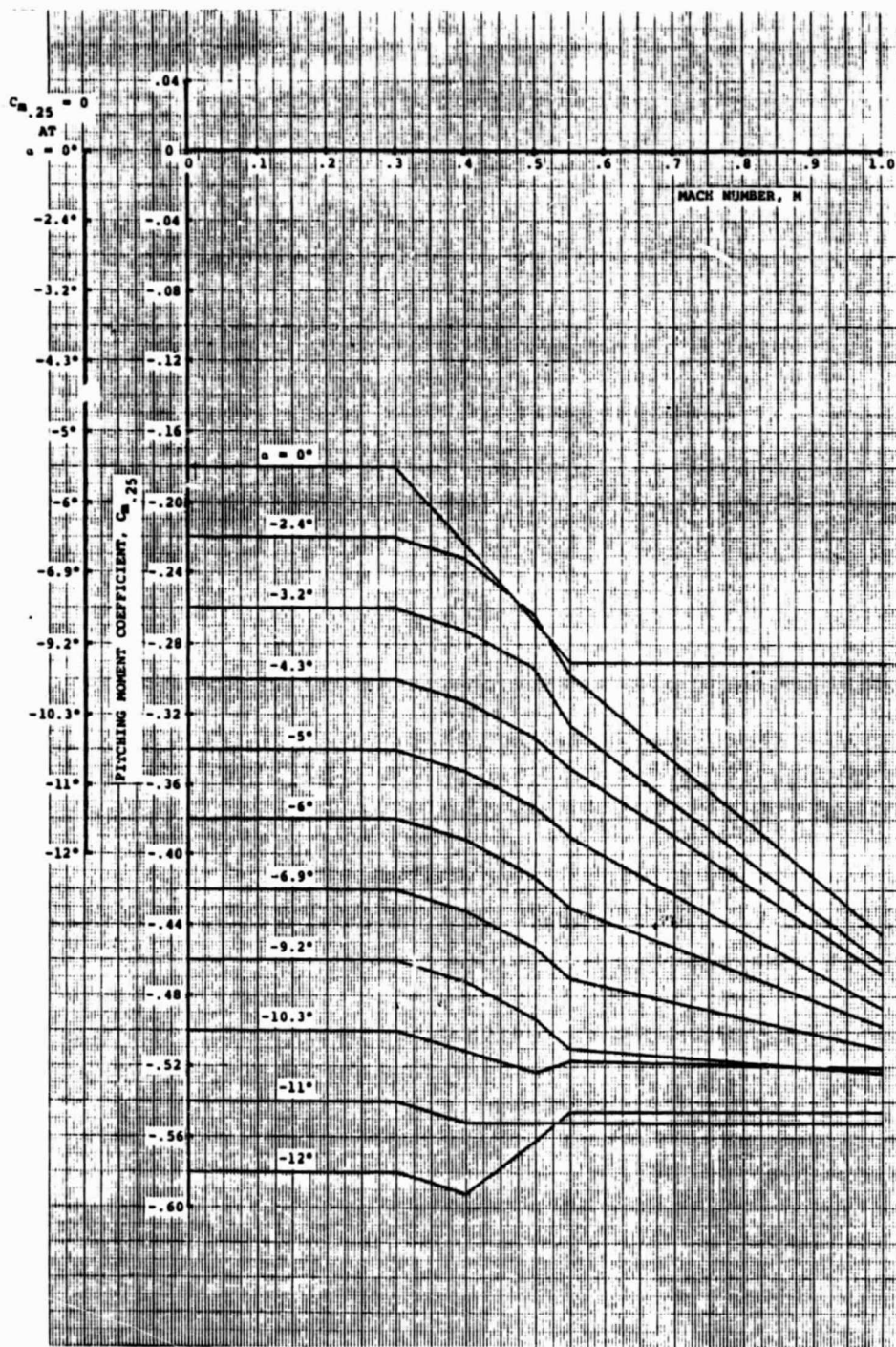


Figure B.25 Pitching Moment Coefficient for  $\delta_F = 15^\circ$  and  $0^\circ \geq \alpha \geq -12^\circ$

ORIGINAL PAGE IS  
OF POOR QUALITY

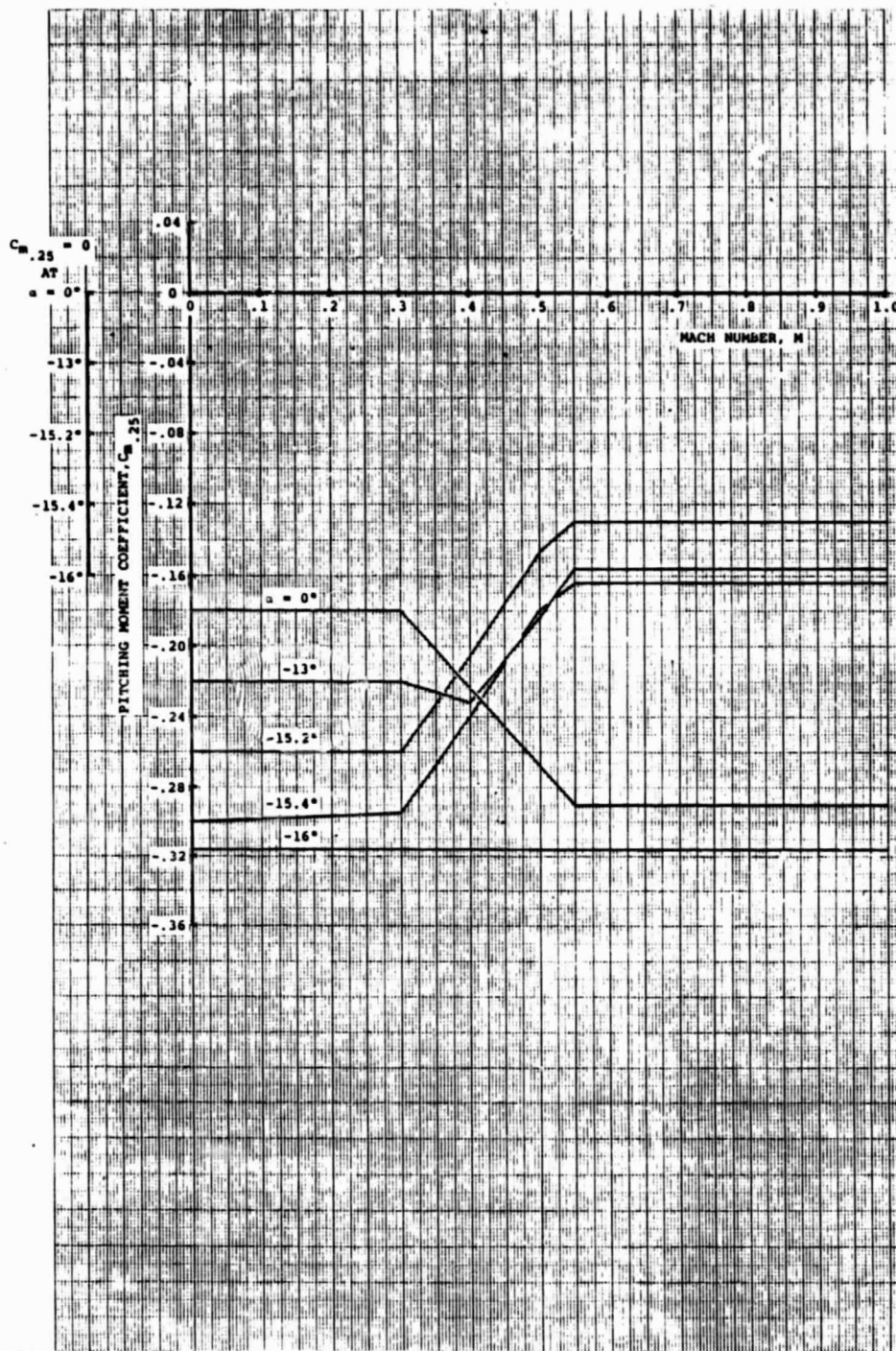


Figure B.26 Pitching Moment Coefficient for  $\delta_F = 15^\circ$  and  $\alpha \leq -13^\circ$

**APPENDIX C**

APPENDIX C

Identification of B-53 Input Variables

<u>LOCATION</u>	<u>SYMBOL</u>	<u>UNITS</u>	<u>DESCRIPTION</u>
1	V	Kt	Flight velocity.
2	$\alpha_s$	deg	Angle between the free-stream velocity direction and the disc plane (a plane normal to the rotor shaft). Positive nose-up.
3	$\theta$	deg	Pitch attitude of the helicopter fuselage at test pod, with respect to the free-stream velocity direction. Positive nose-up.
4	$\phi$	deg	Roll attitude of the helicopter fuselage or test pod, with respect to the free-stream velocity direction. Positive for clockwise roll.
5	i	deg	Shaft (incidence) angle, measured from a line perpendicular to the fuselage water line. Positive forward.
6	Aic	deg	Lateral cyclic pitch (uniform downwash).
7	Bic	deg	Longitudinal cyclic pitch (uniform downwash).
8	$\Omega R$	ft/sec	Rotor tip speed.
9	$\beta_{\mu}$	deg	Fuselage sideslip angle. Positive for nose-right.
10	$T_{DSD}$	lb	Required thrust. The analysis will update the collective pitch until the required thrust is met. If not achievable, the analysis will stop thrust convergence at the 16th iteration and continue with other convergence criteria. A warning is printed out.

<u>LOCATION</u>	<u>SYMBOL</u>	<u>UNITS</u>	<u>DESCRIPTION</u>
11	$Y_{DSD}$	lb	Required side force. For any value of $Y_{DSD}$ other than 0.0 ( $Y_{DSD} \neq 0.0$ ), the analysis will update the lateral cyclic pitch until the required side force is met. If not achievable, the analysis will stop at the 16th iteration and continue with other convergence criteria. A warning would be printed out in this case. If $Y_{DSD} = 0.0$ , the analysis will calculate the side force due to the input lateral cyclic (Loc. 6) without any iteration.
12	TEMP	°F	Air temperature.
13	$H_p$	ft	Pressure altitude.
14	$\zeta$	r/R	Flapping hinge offset, measured from the center of rotation, non-dimensionalized by rotor radius.
15	b	-	Number of blades.
16	R	ft	Radius of blade.
17	$\chi_c$	r/R	Cutout.
18	$\sigma$	-	Root chord solidity based on the entire blade having chord equal to the root chord ( $bc/\pi R$ ).
19	$\sigma_1$	-	Solidity increment from root to tip, $\Delta\sigma$ , used on blades having linear chord taper from root to tip.
20	$\theta_{TW}$	deg	Total blade twist measured from the center of rotation.
21	$\kappa_\beta$	$-\tan\delta_3$	Pitch-flap coupling.
22	$I_F$	Slug-ft <sup>2</sup>	Mass moment of inertia of the blade.
23	$M_w$	ft-lb	Weight moment of the blade.

<u>LOCATION</u>	<u>SYMBOL</u>	<u>UNITS</u>	<u>DESCRIPTION</u>
24	$N_x$	-	Number of blade data stations. The maximum number is currently 14. The blade computation points are between data stations for a maximum of 13.
25	$N_\psi$	-	Number of azimuthal increments. The analysis is currently set up for 15° azimuthal increments, and therefore, 24 azimuthal positions.
26	IDST	-	Control for solidity and twist input options:  IDST = 1.0, for solidity table and twist equation, IDST = 2.0, for solidity equation and twist table, IDST = 3.0, for solidity table and twist table, IDST = 4.0, for solidity equation and twist equation.
27	IRRA	-	Rotor interference option control:  IRRA = 0.0, front rotor IRRA = 3.0, interference velocity table.
28	XNTAB	-	Number of lift, drag and pitching moment airfoil tables.
29	$X_1$	r/R	Radial station for airfoil Table 1 starting from the inboard end and progressing towards the tip.
30	$X_2$	r/R	Radial station for airfoil Table 2.
31	$X_3$	r/R	Radial station for airfoil Table 3 (Optional).
32	$X_4$	r/R	Radial station for airfoil Table 4 (Optional).
33	$X_5$	r/R	Radial station for airfoil Table 5 (Optional).
34	$\Delta CD_1$	-	Profile drag coefficient increment to be applied at the first airfoil table station.
35	$\Delta CD_2$	-	Profile drag coefficient increment for the second data station.

<u>LOCATION</u>	<u>SYMBOL</u>	<u>UNITS</u>	<u>DESCRIPTION</u>
36	$\Delta CD_3$	-	Profile drag coefficient increment for the third data station (Optional).
37	$\Delta CD_4$	-	Profile drag coefficient increment for the fourth data station (Optional).
38	$\Delta CD_5$	-	Profile drag coefficient increment for the fifth data station (Optional).
39	PRINT	-	Printout options: Print = 1.0, azimuthal and final printout Print = 2.0, azimuthal, final and induced velocities Print = 3.0, final data only
40	CD	-	Factor on profile drag.
41	PROP	-	Propeller analysis option set to zero for articulated rotor analysis.
42	SPIR	-	Number of far-wake spirals. Generally set to two.
43		-	Airfoil table identification number for first data station.
44		-	Airfoil table identification number for second data station.
45		-	Airfoil table identification number for third data station (Optional).
46		-	Airfoil table identification number for fourth data station (Optional).
47		-	Airfoil table identification number for fifth data station (Optional).
48, 49, 50	-	-	Not used.
615	K	ft-lb/Rad	Spring constant.
616	$\delta_3$	rad	Pitch-flap coupling angle.
642	$\beta_0$	deg	Precone angle for rigid blade in propeller mode.
961	$N_\phi$	-	Number of radial locations at which flap mode shape values are specified.
962	$\phi_1$	-	First flapping mode shape value at radial station (1).

<u>LOCATION</u>	<u>SYMBOL</u>	<u>UNITS</u>	<u>DESCRIPTION</u>
963	$\phi_2$	-	First flapping mode shape value at radial station (2).
964	$\phi_3$	-	First flapping mode shape value at radial station (3).
965	$\phi_4$	-	First flapping mode shape value at radial station (4).
966	$\phi_5$	-	First flapping mode shape value at radial station (5).
967	$\phi_6$	-	First flapping mode shape value at radial station (6).
968	$\phi_7$	-	First flapping mode shape value at radial station (7).
969	$\phi_8$	-	First flapping mode shape value at radial station (8).
970	$\phi_9$	-	First flapping mode shape value at radial station (9).
971	$\phi_{10}$	-	First flapping mode shape value at radial station (10).
972	$x_{\phi_1}$	r/R	Radial station (1) for first flapping mode shape value.
973	$x_{\phi_2}$	r/R	Radial station (2) for first flapping mode shape value.
974	$x_{\phi_3}$	r/R	Radial station (3) for first flapping mode shape value.
975	$x_{\phi_4}$	r/R	Radial station (4) for first flapping mode shape value.
976	$x_{\phi_5}$	r/R	Radial station (5) for first flapping mode shape value.
977	$x_{\phi_6}$	r/R	Radial station (6) for first flapping mode shape value.
978	$x_{\phi_7}$	r/R	Radial station (7) for first flapping mode shape value.
979	$x_{\phi_8}$	r/R	Radial station (8) for first flapping mode shape value.

<u>LOCATION</u>	<u>SYMBOL</u>	<u>UNITS</u>	<u>DESCRIPTION</u>
980	$x_{\phi_9}$	r/R	Radial station (9) for first flapping mode shape value.
981	$x_{\phi_{10}}$	r/R	Radial station (10) for first flapping mode shape value.
982	$N_{\theta}$	-	Number of radial location at which torsion mode shape values are specified.
983	$\theta_1$	-	First torsion mode shape value at radial station (1).
984	$\theta_2$	-	First torsion mode shape value at radial station (2).
985	$\theta_3$	-	First torsion mode shape value at radial station (3).
986	$\theta_4$	-	First torsion mode shape value at radial station (4).
987	$\theta_5$	-	First torsion mode shape value at radial station (5).
988	$\theta_6$	-	First torsion mode shape value at radial station (6).
989	$\theta_7$	-	First torsion mode shape value at radial station (7).
990	$\theta_8$	-	First torsion mode shape value at radial station (8).
991	$\theta_9$	-	First torsion mode shape value at radial station (9).
992	$\theta_{10}$	-	First torsion mode shape value at radial station (10).
993	$x_{\theta_1}$	r/R	Radial station (1) for first torsion mode shape value.
994	$x_{\theta_2}$	r/R	Radial station (2) for first torsion mode shape value.
995	$x_{\theta_3}$	r/R	Radial station (3) for first torsion mode shape value.
996	$x_{\theta_4}$	r/R	Radial station (4) for first torsion mode shape value.

<u>LOCATION</u>	<u>SYMBOL</u>	<u>UNITS</u>	<u>DESCRIPTION</u>
997	$x_{\theta_5}$	r/R	Radial station (5) for first torsion mode shape value.
998	$x_{\theta_6}$	r/R	Radial station (6) for first torsion mode shape value.
999	$x_{\theta_7}$	r/R	Radial station (7) for first torsion mode shape value.
1000	$x_{\theta_8}$	r/R	Radial station (8) for first torsion mode shape value.
1001	$x_{\theta_9}$	r/R	Radial station (9) for first torsion mode shape value.
1002	$x_{\theta_{10}}$	r/R	Radial station (10) for first torsion mode shape value.
1003	$M_2$	Slug	Generalized mass (first flap).
1004	$I_{\theta}$	Slug-ft <sup>2</sup>	First modal inertia.
1005	$\omega_1$	cycles/rev	Modal frequency: first flap.
1006	$\omega_2$	cycles/rev	Modal frequency: second flap.
1007	$\omega_{\theta}$	cycles/rev	Modal frequency: first torsion.
1008	PA	x/c	Pitch axis, measured from the leading edge, in fraction of chord.
1009	$x_{\alpha}$	-	Factor on the $d\alpha/dt$ terms in the sectional aerodynamic coefficients.
1010	$x_{\Lambda}$	-	Factor on the sweep terms in the sectional aerodynamic coefficients.
1011	K1	-	Value of the "gamma" function for lift, $\gamma_{Cl}$ , at $M = 0.0$ .
1012	K2	-	Rate of change of the lift gamma function with Mach number, $-(d\gamma_{Cl}/dM)$ .
1013	K3	-	Value of the gamma function for the pitching moment coefficient, $\gamma_{CM}$ , at $M = 0.0$ .
1014	K4	-	Rate of change of the gamma function for the pitching moment coefficient, with Mach number, $-(d\gamma_{CM}/dM)$ .

LOCATION	SYMBOL	UNITS	DESCRIPTION
1015	DFZ11	-	Damping factors for the first flap mode. (Set to 0.1)
1016	DFZ12	-	
1017	DFZ13	-	
1018	DFZ21	-	Damping factors for the second flap mode. (Set to 0.1)
1019	DFZ22	-	
1020	DFZ23	-	
1021	DFTE1	-	Damping factors for the first torsion mode. (Set to 0.1)
1022	DFTE2	-	
1023	DFTE3	-	
1024	DFQ1	-	Damping factors for the forcing functions. (Set to 1.0).
1025	DFQ2	-	
1026	DFQ3	-	
1082	SK1	-	Factor on all gamma functions, $\gamma_{C0}$ and $\gamma_{CM}$ , for negative rates of change of the angle of attack, $d\alpha/dt < 0$ . Recommended value is SK1 = 0.5.
1083	ABPROD	-	Limiter on the maximum value of $(c\dot{\alpha}/2v)$ . The recommended value is ABPROD = 0.07.
1084	CDTRCN	-	Option to calculate three-dimensional tip relief effects on the drag coefficient by the Le Nard method. (YES = 1.0, NO = 0.0)
1085		-	Option to update the wake geometry by introducing the blade flapping motions from the non-uniform downwash (NUD) solution. (YES = 1.0, NO = 0.0)
1086		-	Control to generate a magnetic tape containing all the wake model information from the last iteration. Provisions must be made in the JCL for tape mounting instructions and output file identification. (YES = 1.0, NO = 0.0)
1101		t/c	Thickness of the airfoil specified at the first spanwise data station (LOC 29), in fraction of chord. This input is necessary only when the Le Nard 3-D relief correction on drag is required (LOC(1084) = 1.0)
1102		t/c	Thickness of the airfoil specified at the second data station (LOC 30), for the Le Nard 3-D correction.

<u>LOCATION</u>	<u>SYMBOL</u>	<u>UNITS</u>	<u>DESCRIPTION</u>
1103		t/c	Thickness of the airfoil specified at the third data station (LOC 31), for the Le Nard 3-D correction.
1104		t/c	Thickness of the airfoil specified at the fourth data station (LOC 32), for the Le Nard 3-D correction.
1105		t/c	Thickness of the airfoil specified at the fifth data station (LOC 33), for the Le Nard 3-D correction.
1109		-	Option control to carry out three-dimensional lift curve slope tip relief calculations (Levacic). (YES = 1.0, NO = 0.0)
1110	$\Delta P$	-	Constant in Dr. Levacic's lift curve slope correction for 3-D effects. The recommended value is $\Delta P = 0.1$ .
1111	XM	-	Constant in Dr. Levacic's lift curve slope correction for 3-D effects. The recommended value is $XM = 0.1$ .
1122	RV1	-	Factor on the tip vortex strength limiter. This limiter is based on Dr. N. Ham's observation that an individual vortex cannot induce a local lift coefficient increment larger than $\Delta C_l = 0.3$ .  Use RV1 = 1.0 unless there are reasons to alter Ham's limit.
1123	RV2	-	Factor on the vortex limiter as applied to the root vortex. The value currently recommended for the B-65 and B-53 codes is $RV2 = 0.01$ .
1124	RVLIM	X/R	Proximity limiter in the Biot subroutine. The default value built into the codes is 0.04 (4% of blade radius). The recommended value is $RVLIM = C_{.75R}$ .
1125	WDF	-	Near wake damping. This quantity controls how much of the near-wake induced velocity calculated in any iteration is to be used, on the basis of the following formula:

$$V_{IND} = (WDF)(V_{IND})_{NEW} + (1-WDF)(V_{IND})_{OLD}$$

<u>LOCATION</u>	<u>SYMBOL</u>	<u>UNITS</u>	<u>DESCRIPTION</u>
1126	FLAGAB	-	Non-uniform downwash cyclic option. By setting FLAGAB = 1.0, the analysis will require and use separate cyclic pitch controls for the uniform and non-uniform calculations. This allows the separate trimming of UD and NUD solutions.
1127	A1C2D	deg.	<p>Lateral cyclic pitch input for the non-uniform downwash (NUD) solution.</p> <p>Necessary when LOC(1126) = 1.0. The uniform downwash counterpart of this input is LOC(6). When the required side force (LOC 11) is set to 0.0 the analysis will bypass any side force convergence calculations and print out the side force values due to the lateral cyclic levels of LOC(6) and LOC(1126). Whenever the required side force is a value <math>\neq</math> 0.0, side force iteration will take place.</p>
1128	B1C2D	deg.	<p>Longitudinal cyclic pitch input for the non-uniform downwash (NUD) solution. Necessary when LOC(1126) = 1.0. Note: The propulsive force is not iterated on in the current B-65, B-66, B-67 and B-53 codes.</p>
1160		-	Near wake limiter. The default value is (-0.98). The currently recommended value is 0.9.
1161	UD	-	<p>Option to run uniform or both uniform and non-uniform downwash calculations.</p> <p>(a) Uniform only      UD = 1.0  (b) UD and NUD      UD = 0.0 (Default value)</p>
1162		-	Option to calculate dynamic stall delay effects on the pitching moment coefficient by a procedure similar to the C-60 loads analysis formulation. For "C-60" formulation use LOC(1162) = 1.0. The default value is 0.0.

<u>LOCATION</u>	<u>SYMBOL</u>	<u>UNITS</u>	<u>DESCRIPTION</u>
1163		-	Factor on the $\Delta Z$ vertical displacement component due to induced effects (uniform downwash approximation), used in constructing the tip vortex structure of the far wake model. This factor can be used to move the tip vortices closer to or away from the blades. Set LOC(1163) = 1.0 when variation is not needed.
1164		-	Factor on the $\Delta Z$ vertical displacement component due to induced effects on the root vortex components of the far wake model. Set LOC(1164) = 1.0.
1165		-	Control to generate a TSO data file for computer assisted graphic display of calculated flow characteristics. (YES = 1.0, NO = 0.0).
1166			Factor on the vortex strength limiter (N. Ham) as applied to the near wake vortex segments. Generally set LOC(1166) = 1.0.
1167		-	Factor on the vortex strength limiter (N. Ham) as applied to the mid-wake vortex segments. Generally set LOC(1167) = 1.0.
1168		-	Option to include in the unsteady aero formulation the derivatives of externally input local pitch angles. (YES = 0.0)
1169		-	Wake geometry skew angle option. (YES = 0.0)